

***Pharmacological interactions between phenylbenzothiazoles
and Aryl Hydrocarbon Receptor (AhR)***

by

Rana Bazzi, B.Sc, M.Sc

Thesis submitted to The University of Nottingham

for the degree of Doctor of Philosophy

June 2008

Abstract

The aryl hydrocarbon receptor is a ligand-dependent transcription factor that induces expression of a number of genes encoding drug metabolizing enzymes, such as CYP1A1, CYP1A2 and CYP1B1. Recently, it was suggested that the AhR signaling pathway may be involved in mediating the anticancer activity of novel 2-(4-aminophenyl) benzothiazole drugs in MCF-7 breast cancer cells. There is no direct proof of direct binding between these drugs and AhR, and it is also unclear how AhR signaling per se plays a role in the activity of these drugs. This study investigates the role of AhR in the mechanism of action of the benzothiazole drugs by determining the ability of these drugs to bind to the rat hepatic AhR, to induce *CYP1A1* mRNA and to inhibit cell growth in rat hepatoma H4-II-E cells.

The apparent binding kinetics of [³H]-TCDD to AhR in rat liver cytosol were, $K_D = 0.37$ nM and $B_{max} = 40$ fmol/mg cytosolic protein. Using the standard assay conditions, 18 compounds competitively displaced [³H]-TCDD from specific sites, and are ligands for AhR. Induction of *CYP1A1* mRNA by 5 compounds was determined in H4-II-E cells. The highest affinity ligand, IH445, was the most potent with an $EC_{50} \sim 80$ -fold lower than that of TCDD (60 pM) with no detectable antagonistic activity in H4-II-E cells. The other high-affinity benzothiazoles tested were (30-100) $\times 10^3$ -fold less potent for inducing CYP1A1 mRNA than TCDD. The binding affinities of these compounds were 200-1000-fold higher than induction potency. For example, 5F 203 has a K_i value of 2.8 nM, induced *CYP1A1* mRNA to similar maximal levels as seen with TCDD, and has an EC_{50} of 3 μ M. The 1000-fold difference for 5F 203 between binding and CYP1A1 RNA induction was suggested to be a result of metabolism or that 5F 203 exhibits partial AhR antagonist activity. The time course effect on the *CYP1A1*/ β -actin mRNA ratios by 5F 203 revealed that the response was increasing linearly in response to 5F 203 at 4 h treatment, indicating that the former possibility is less likely to be a major factor. To address the second

possibility, the antagonistic activity of 5F 203 on TCDD-induced *CYP1A1* mRNA was investigated. H4-II-E cells were treated with increasing concentrations of TCDD \pm 1 μ M 5F 203. The results demonstrated that 5F 203 shifted the EC₅₀ of TCDD 100-fold to the right. Schild analysis on the antagonism of TCDD-induced *CYP1A1* mRNA by different concentrations of 5F 203 provided a quantitative explanation for the 1000-fold difference between binding and induction for 5F 203. In contrast, the EC₅₀ of 5F 203 in human MCF-7 cells was 2 nM, which is \sim 10-fold less potent than TCDD. Moreover, 5F 203 had no detectable antagonistic activity on TCDD-induced *CYP1A1* mRNA. When 5F 203 was assessed for cell growth inhibition by MTT assay, it was found active in MCF-7 cells with a GI₅₀ of 18 nM, but failed to elicit the same effect in H4-II-E cells.

These results prove that 5F 203 is a potent agonist in MCF-7 cells, but a partial agonist in H4-II-E cells. The partial agonism observed with 5F 203 is a compound-specific property given that another analogue, IH 445, was found potent inducer of *CYP1A1* mRNA with no antagonistic activity. The results of this study reveal species-specific partial agonism of the AhR. The potency of the cytostatic effect of 5F 203 parallel potency for inducing *CYP1A1* mRNA in both cells. Moreover, both, the cytostatic effect of 5F 203 and partial agonism of AhR for inducing *CYP1A1* mRNA is species-specific. Whether agonism/antagonism for the induction of *CYP1A1* mRNA is related to the anticancer activity of 5F 203 remains to be elucidated.

Acknowledgements

I wish to express my sincere gratitude to my supervisor Dr David Bell for his encouragement, openness to discussion, and for his continuous guidance for my development as a toxicologist. I am also thankful to Dr Tracey Bradshaw for moral and academic supports and to my advisor Professor David Archer for his general advices.

I would like to thank the members of the Molecular Toxicology laboratory, former postdoctors as well as students for their support and encouragement. I would also like especially to thank Dr Tao Jiang for her assistance and advices. A special thanks goes to mister Declan Brady, he was always around when needed.

I am indebted to my relatives and friends for their consistent care and support. Any source of advice and guidance is greatly appreciated.

This work would not have been done without the financial support provided from Al Tajir Trust to which I am gratefully indebted.

My dear parents, sisters and brothers, i thank God for having such a great family, thank you for your constant support, encouragment, understanding and love. Thank you for allowing me to live such a wonderful experience. Thank you for being proud of me. I would not have succeeded without you. All my gratitude my lovely parents.

Dedication

To my mother

To my father,

To my sisters and brothers

This thesis is dedicated to the memories of my sister Fatima,

To Fatima

Declaration

The work presented in this thesis is my own unless otherwise stated. Information from other sources has been fully acknowledged. No part of this thesis has been previously submitted for examination leading to the award of a degree.

Rana Bazzi

June 2008

TABLE OF CONTENTS

Abstract	2
Acknowledgements	4
Dedication	5
Declaration	6
Abbreviations	14
1 Introduction	18
1.1 The aryl hydrocarbon receptor (AhR)	18
1.1.1 Identification of the Ah receptor	18
1.1.2 Expression of the Ah receptor	18
1.1.3 The Ah receptor structural domains	19
1.1.3.1 The AhR ligand binding domain	22
1.1.4 AhR and associated proteins	24
1.1.5 Ah receptor ligands	25
1.1.5.1 Halogenated Aromatic Hydrocarbons (HAHs)	26
1.1.5.1.1 2,3,7,8-Tetrachlorodibenzo-p-dioxin (TCDD)	27
1.1.5.1.2 The 3,4,3',4'-Tetrachloroazoxybenzene (TCAOB)	27
1.1.5.2 Polycyclic Aromatic hydrocarbons (PAHs)	28
1.1.5.3 Natural ligands	28
1.1.6 The AhR signaling pathway	29
1.1.6.1 Binding and translocation to nucleus	29
1.1.6.2 Dimerisation of AhR with Arnt	30
1.1.6.3 Transcriptional activation	31
1.1.6.4 Ligand binding-independent activation of the AhR	34
1.2 Regulation of AhR and crosstalk	35
1.3 AhR functions	36
1.3.1 Regulation of xenobiotic metabolism	36
1.3.2 Mediation of HAH toxicity	36
1.3.3 Vascular development	37
1.4 The AhR and anticancer therapy	38
1.5 AhR and drug metabolism	39
1.5.1 Phase I enzymes:	39
1.5.1.1 Nomenclature	40
1.5.1.2 CYP1 family	40
1.5.2 Phase II reactions:	41
1.6 Phenylbenzothiazoles	41
1.6.1 2-(4-aminophenyl)benzothiazoles (series 1)	41
1.6.1.1 Discovery of non-fluorinated 2-(4-aminophenyl)benzothiazole analogues	41
1.6.1.2 Discovery of fluorinated 2-(4-aminophenyl)benzothiazole analogues	42
1.6.1.3 Mechanistic investigations	42
1.6.1.4 Structure-Activity Relationships (SARs)	45
1.6.2 2-(3,4-Dimethoxyphenyl)benzothiazoles (series 2)	46
1.6.2.1 Background	46
1.6.2.2 Mechanistic investigation	46
1.6.2.3 Structure-Activity Relationships (SARs)	46
2 Materials and Methods	49
2.1 Materials	49
2.1.1 Animals	49
2.1.2 Cell lines and cell culture chemicals	49

2.1.3 Kits and reagents	50
2.1.4 Compounds.....	50
2.1.5 Buffers.....	56
2.1.6 Solutions.....	58
2.1.7 Gels.....	60
2.1.8 Real-time RT-PCR primers and probes	61
2.2 General laboratory methodology.....	62
2.2.1 Receptor preparation	62
2.2.2 Determination of protein concentrations.....	63
2.2.3 [³ H]-TCDD Binding assay	63
2.2.3.1 Principle	63
2.2.3.2 Methodology	64
2.2.3.3 [³ H]-TCDD standard binding assay	65
2.2.3.4 [³ H]-TCDD competition assay.....	65
2.2.3.4.1 Principle	65
2.2.3.4.2 Methodology:	66
2.2.4 Cell cultures.....	67
2.2.5 Cell growth curves	67
2.2.6 Chemical treatment for the induction assay	68
2.2.7 Preparing H4-II-E and MCF-7 cells before total RNA isolation	69
2.2.8 RNA isolation.....	69
2.2.9 Quantitation of total RNA	71
2.2.10 cDNA synthesis.....	71
2.2.11 Quantitation of cDNA	72
2.2.12 Polymerase Chain Reaction PCR.....	73
2.2.13 Quantitative Real-Time RT-PCR using TaqMan [®] probes.....	74
2.2.13.1 Principle	74
2.2.13.2 Analysis.....	74
2.2.13.3 Quantification by real-time RT-PCR	75
2.2.13.4 qRT-PCR standard curves.....	76
2.2.14 Induction protocol	77
2.2.15 Growth inhibitory assay: MTT assay	78
2.2.16 Curve modelling and statistical analysis	79
3 Results	80
3.1 Characterization of the binding to the rat hepatic Ah receptor	80
3.1.1 Incubation time.....	80
3.1.2 Dextran-coated charcoal (DCC).....	82
3.1.3 TCAOB concentration.....	84
3.1.4 Cytosolic protein concentration	86
3.1.4.1 Effect of cytosolic protein concentration on [³ H]-TCDD specific binding	86
3.1.4.2 Effect of cytosolic protein concentration on [³ H]-TCDD in solution.....	87
3.1.5 Effect of [³ H]-TCDD concentration on [³ H]-TCDD in solution	89
3.1.6 Binding assay standard.....	91
3.1.7 Displacement of [³ H]-TCDD by cold TCDD	94
3.1.8 Displacement of [³ H]-TCDD by test competitors.....	96
3.1.9 Structure-Activity Relationships (SARs).....	102
3.2 Characterization of CYP1A1 induction	104
3.2.1 Cell growth curves	104
3.2.2 Testing the primers and probes for specificity	105

3.2.3 Assessment of RNA quality	105
3.2.4 qRT-PCR probe/ primer efficiency	106
3.2.5 CYP1A1 induction assay in H4-II-E cells	109
3.2.5.1 Effect of confluence	109
3.2.5.2 Effect of varying the treatment time	113
3.2.5.3 Effect of medium on CYP1A1 mRNA induction	116
3.2.6 Effect of time on the dose response curves for TCDD	120
3.2.7 Induction of CYP1A1 mRNA by 3-methylcholanthrene (MC)	122
3.2.8 Induction of CYP1A1 mRNA by 5F 203	125
3.2.9 Induction of CYP1A1 mRNA by IH 445, DF 203, GW 610, AW 892 and IH 318 ...	127
3.2.10 Estimation of intrinsic efficacy and fractional receptor occupancy	131
3.2.11 Inhibition of TCDD-induced CYP1A1 mRNA by 5F 203	133
3.2.12 Competitive antagonism of 5F 203 on TCDD-induced <i>CYP1A1</i> mRNA	137
3.2.13 Effect of IH 445 on TCDD-induced <i>CYP1A1</i> mRNA	140
3.2.14 CYP1A1 induction assay in MCF-7 cells	143
3.2.14.1 Concentration-response curves of TCDD	143
3.2.14.2 Induction of CYP1A1 mRNA by 5F 203	146
3.2.14.3 Effect of 5F 203 on TCDD-induced <i>CYP1A1</i> mRNA	149
3.2.14.4 Induction of CYP1A1 mRNA by CH-223191	151
3.3 Growth inhibitory activity in H4-II-E cells	153
3.3.1 Growth inhibitory activity of 5F 203 in H4-II-E cells	153
3.3.2 Effect of TCDD on 5F 203 cytostatic effect in H4-II-E cells	156
3.3.3 Growth inhibitory activity of 5F 203 in MCF-7 cells	157
3.3.4 Effect of TCDD on 5F 203 and CH-223191 growth inhibitory activity in MCF-7 cells	159
4 Discussion	162
4.1 The [³ H]-TCDD radioactive binding assay	162
4.1.1 Validation of the [³ H]-TCDD radioactive binding assay	162
4.1.2 Characterization of the binding of phenylbenzothiazoles to AhR	166
4.1.3 Structure-Activity Relationships (SARs)	167
4.1.3.1 Structure-activity relationships for binding AhR	167
4.2 CYP1A1 induction assay using TaqMan real-time RT-PCR	169
4.2.1 The choice of the cell cultures	169
4.2.2 qRT-PCR analysis	169
4.2.3 Normalisation to housekeeping genes	170
4.2.4 Factors affecting <i>CYP1A1</i> RNA induction in H4-II-E cells	171
4.2.5 Validation of the induction assay in H4-II-E cells using TCDD	172
4.2.6 5F 203, DF 203, GW 610 and AW 892 but not IH 445: low potent agonists for inducing <i>CYP1A1</i> mRNA in H4-II-E cells	174
4.2.7 Interpretation of difference in potency between binding affinity and <i>CYP1A1</i> induction: partial agonism	175
4.2.8 TCDD and 5F 203: potent agonists in human MCF-7 cells	181
4.2.9 Agonism/antagonism species-specific differences	182
4.3 AhR, a target for anticancer phenylbenzothiazole analogues: mechanistic investigations	185
4.3.1 Correlation between SARs for binding and anticancer activity	186
4.3.2 Correlation between SARs for inducing <i>CYP1A1</i> RNA and anticancer activity	188
4.3.3 Investigating the effect of AhR agonism on cell growth	189
4.3.4 Investigating the effect of AhR antagonism on cell growth	190

4.3.5	Mechanism of action of 5F 203: relevance of the mechanism of Genotoxicity?.....	192
4.3.6	Relevance of partial agonism in risk assessment	193
4.3.7	Concluding remarks	193
	Appendix - Pharmacological background	197
	References	201

LIST OF FIGURES

Figure 1.1 Domain structure of AhR.....	20
Figure 1.2 Alignment of PAS domain amino acid sequences of vertebrate AHRs and a possible invertebrate AHR homolog.	21
Figure 1.3 Cartoon representation of the three modeled structures of the mAHR LBD.....	24
Figure 1.4 Structures for representative AhR ligands.	26
Figure 1.5 Structure of 3,4,3',4'-tetrachloroazoxybenzene (TCAOB)	28
Figure 1.6 The AhR/Arnt heterodimer.	31
Figure 1.7 Description of AhR signaling pathway.....	32
Figure 1.8 Mode of action of Phortress.....	44
Figure 3.1 Effect of incubation time on [³ H]-TCDD specific binding to rat cytosolic protein.....	81
Figure 3.2 Effect of charcoal on [³ H]-TCDD binding to rat cytosolic and BSA proteins. ..	83
Figure 3.3 Effect of TCAOB concentration on [³ H]-TCDD binding to rat cytosolic proteins.	85
Figure 3.4 Effect of cytosolic protein concentration on [³ H]-TCDD specific binding to rat cytosolic protein.....	87
Figure 3.5 Effect of cytosolic protein concentration on [³ H]-TCDD solubility.	89
Figure 3.6 Concentration of [³ H]-TCDD in solution.	90
Figure 3.7 The binding standard of [³ H]-TCDD to rat liver cytosol.....	92
Figure 3.8 Competitive displacement of hot TCDD by cold TCDD.....	95
Figure 3.9 Competitive displacement of [³ H]-TCDD by 5F 203.....	96
Figure 3.10 Growth curves of H4-II-E and MCF-7 cells.....	104
Figure 3.11 An agarose gel showing the integrity of the total RNA as assessed by the relative intensities of the 28S and 18S RNA bands.....	106
Figure 3.12 Amplification efficiencies for <i>CYP1A1</i> , <i>b-actin</i> and <i>AhR</i>	108
Figure 3.13 Effect of cell density on CYP1A1 mRNA in H4-II-E cells over time course. ..	111
Figure 3.14 Time course of induction of CYP1A1 mRNA by 5F 203 in H4-II-E cells.	114
Figure 3.15 Effect of medium change on CYP1A1 mRNA expression in H4-II-E cells: ...	117
Figure 3.16 Effect of time on the concentration-response curves for CYP1A1 mRNA induction by TCDD in H4-II-E cells.	121
Figure 3.17 Effect of TCDD and MC on CYP1A1 mRNA in H4-II-E cells.	124
Figure 3.18 Concentration-response curves for CYP1A1 mRNA induction by TCDD and 5F 203 in H4-II-E cells.....	126
Figure 3.19 Concentration-response curves for the induction of CYP1A1 mRNA by TCDD, IH 445, DF 203, GW 610, AW 892 and IH 318 in H4-II-E cells.....	128
Figure 3.20 Inhibition of TCDD-induced CYP1A1 mRNA by 5F 203 in H4-II-E cells.	136
Figure 3.21 Competitive inhibition of TCDD-induced <i>CYP1A1</i> mRNA by 5F 203 in H4-II-E cells.....	138
Figure 3.22 Schild regression.....	139
Figure 3.23 Effect of IH 445 on TCDD response in H4-II-E cells.	142
Figure 3.24 Comparison between the log concentration-response curves for CYP1A1 mRNA induction by TCDD in H4-II-E and MCF-7 cells.....	144
Figure 3.25 Induction of CYP1A1 mRNA by TCDD and 5F 203 in MCF-7 cells.....	148
Figure 3.26 Comparison between the log concentration-response curves for CYP1A1 mRNA induction by 5F 203 in H4-II-E and MCF-7 cells.....	149
Figure 3.27 Effect of 5F 203 on TCDD response in MCF-7 cells.	151
Figure 3.28 Studies on CYP1A1 mRNA induction by CH-223191 in MCF-7 cells.	152
Figure 3.29 Growth inhibitory activity of 5F 203, IH 445 and TCDD in H4-II-E cells.	154

Figure 3.30 Effect of TCDD on the growth inhibitory activity of 5F 203 against H4-II-E cells.....	157
Figure 3.31 Growth inhibitory activity of 5F 203, CH-223191 and TCDD against MCF-7 cells.	158
Figure 3.32 Growth inhibitory activity of TCDD \pm 5F 203 or \pm CH-223191 against MCF-7 cells.	160

LIST OF TABLES

Table 2.1 RT-PCR oligonucleotides primers for rat genes	61
Table 2.2 RT-PCR oligonucleotides primers for human genes.....	62
Table 2.3 PCR experimental reaction.....	73
Table 2.4 PCR thermal cycler programme	73
Table 2.5 qRT-PCR cycling protocol.....	76
Table 2.6 Multiplex real-time RT-PCR experimental reaction.	76
Table 3.1 Summary of binding kinetics of [³ H]-TCDD to rat hepatic cytosol from three independent experimental trials.	93
Table 3.2 Comparison with literature for binding kinetics of TCDD for AhR.	94
Table 3.3 Binding affinities of TCDD, TCAOB, TCDF, TCPT, astrazeneca compound 1c and benzothiazole analogues in rat liver cytosol.	98
Table 3.4 Quantitation data of qRT-PCR for rat genes.	109
Table 3.5 Quantitation data of qRT-PCR for human genes.	109
Table 3.6 Summary for the EC ₅₀ values of TCDD for the induction of CYP1A1 mRNA in H4-II-E cells.	125
Table 3.7 Control levels for <i>CYP1A1/b-actin</i> mRNA ratios by phenylbenzothiazole compounds in H4-II-E cultures.	130
Table 3.8 CYP1A1 mRNA induction by IH 445, DF 203, GW 610, AW 892 and IH 318.	130
Table 3.9 Data for CYP1A1 mRNA induction and AhR binding in rat.....	132
Table 3.10 Intrinsic efficacy and fractional receptor occupancy at 50% of AhR ligands in H4-II-E cells.....	132
Table 3.11 EC ₅₀ values for the induction of CYP1A1 mRNA by TCDD in MCF-7 cells. .	146
Table 3.12 Literature values for the EC ₅₀ of TCDD for inducing ethoxyresorufin <i>O</i> -deethylase (EROD) and aryl hydrocarbon hydroxylase (AHH) at in H4-II-E and MCF-7 cells.	146
Table 3.13 Summary for binding to AhR (rat cytosol), <i>CYP1A1</i> mRNA induction and growth inhibitory potency of compounds in H4-II-E cells	155

Abbreviations

A549	Human lung cancer cell lines
AH ^{R100}	AhR-deficient
AHH	Aromatic hydrocarbon hydroxylase
AhR	Aryl hydrocarbon receptor
AhRC	Aryl hydrocarbon receptor complex
Aldh3A1	Aldehyde reductase 3A1
Arnt	Aryl hydrocarbon receptor nuclear translocator
bHLH	basic helix-loop-helix proteins
B _{max}	Concentration of receptor
BSA	Bovine serum albumin
C57BL/6	Prototype responsive mice strain
CP	Cytosolic protein
CYP	Cytochrome P450
DBA/2	Prototype non-responsive mice strain
DCC	Dextran-coated charcoal
DMSO	Dimethyl Sulfoxide

dpm	Desintegration per minute
DRE	Dioxin responsive element
DTT	Dithiothreitol
DV	Ductus venous
EC ₅₀	Ligand concentration that produces 50% response
E2	17 β -Estradiol
EDTA	(Ethylenedinitrilo)- tetraacetic acid)
ER α	Oestrogen receptor
EROD	7-ethoxyresofurin-O-deethylase (EROD)
GI ₅₀	Concentration of compound needed to cause 50% growth inhibition
GSTA1-1	Glutathione S-transferase A1
HAH	Halogenated aromatic hydrocarbon
HIF-1 α	Hypoxia-inducible factor 1 alpha
Hsp90	90 kDa Heat shock protein
[³ H]-TCDD	Tritium labelled 2,3,7,8-tetrachlorodibenzo-para-dioxin
IC ₅₀	Competing ligand concentration that produces 50% reduction in specif
ic binding	

I3C	Indole-3-carbinol
KCl	Potassium Chloride
K _D	Equilibrium dissociation constant
K _i	Equilibrium inhibition constant
LBD	Ligand binding domain
LC ₅₀	Concentration of compound needed to cause 50% cell death
MC	3-Methylchloranthrene
MCF-7 cells	Human breast carcinoma cells
MDA-MB	Human breast carcinoma cells
MOPS	3-(N-morpholino) propanesulfonic acid
NES	Nuclear export
NF-κB	Necrosis factor proteins
NLS	Nuclear localization sequence
NQ01	NAD(P)H:quinone oxidoreductase
NSB	Non specific binding
PAH	Planar aromatic hydrocarbon
PAS	PER, Arnt, AhR, SIM

PBT	Phenylbenzothiazole
PCR	Polymerase chain reaction
PER	Drosophila circadian rhythm protein
RT	Reverse transcriptase
Real time RT-PCR	Real time reverse transcriptase polymerase chain reaction
RT-PCR	Reverse transcriptase polymerase chain reaction
SA	Specific activity
SAR	Structure-activity relationship
SB	Specific binding
SIM	Drosophila neurogenic protein
TB	Total binding
TCAOB	3,4,3',4'-TetrachloroAzoxybenzene
TCDD	2,3,7,8-tetrachlorodibenzo-para-dioxin
TGF- β 1	Tumour growth factor
TL	Total ligand
UGT1A6	Glucuronosyl transferase 1A6
XRE	Xenobiotic responsive element

Chapter 1 Introduction

Section 1.1 The aryl hydrocarbon receptor (AhR)

Section 1.1.1 Identification of the Ah receptor

In 1972, two different laboratories were working on the genetics of aryl hydrocarbon hydroxylase (AHH) induction in mice in response to polycyclic hydrocarbons. They found that the difference in responsiveness to AHH induction between the sensitive strain (prototype C57BL/6 carrying the *Ah^b* allele) and the relatively nonresponsive strain (prototype DBA/2 carrying the *Ah^d* allele) is controlled by a single autosomal locus, termed Ah (for aryl hydrocarbon responsiveness) [4]. Structure-activity relationships study performed by Poland and Glover (1973) on the chlorinated dibenzo-*p*-dioxins and AHH induction showed good correlation between the toxicity of these compounds and their inducing capacity, with halogenated aromatic compounds such as dioxin being more potent agonists as AHH inducers than were the PAHs. This finding led the researchers to hypothesize the existence of an Ah-encoded receptor, the aryl hydrocarbon receptor (AhR) [5]. In 1976, the hypothesis was confirmed and the receptor designated AhR was identified using radiolabelled TCDD that exhibited specific, saturable and high-affinity to the protein [6]. The protein is designated as the “Ah receptor”, because it binds and mediates the response to aromatic hydrocarbons.

Section 1.1.2 Expression of the Ah receptor

The AhR was found in the tissues from several mammalian and non-mammalian species. In humans, it is expressed in placenta at the highest levels, also highly expressed in lung, heart, pancreas, and liver, and less expressed in brain, kidney, and skeletal muscles [7]. In rodents, it is expressed in liver, lung, thymus, and kidney with much lower concentrations in testis, brain, and skeletal muscles [251]. The expression of the AhR was confirmed in cultured cells, including

rat hepatoma H4-II-E [7] [9] and human breast carcinoma MCF-7 cells [10] [11] [7] [253] [12] [13] [14].

AhR is well conserved from invertebrates like *Caenorhabditis elegans* and *Drosophila melanogaster* to vertebrates [15]. In mammalian species, only one AhR has been identified, AhR1. Its molecular mass varies from 95 to 110 kDa [16] [17]. Recently, two AhR isoforms (AhR1 and AhR2) from two bird species have been isolated, the black-footed albatross (*Phoebastria nigripes*) and common cormorant (*Phalacrocorax carbo*) [18]. The Ah locus, which encodes the AhR, was found on mouse chromosome 12 [4] and human chromosome 7p21 [19].

Section 1.1.3 The Ah receptor structural domains

The AhR contains several structural domains revealed from the amino acid sequence deduced from its cDNA [20]. AhR structural domains are represented in Figure 1.1. The molecular cloning of the Ah receptor revealed that it was a member of a basic helix-loop-helix (bHLH) protein family which includes PAS proteins: mammalian Per (a *Drosophila* protein involved in the circadian rhythm), Aryl hydrocarbon receptor nuclear translocator (Arnt) protein, and Sim (a *Drosophila* CNS developmental protein) [21] and the hypoxia-inducible factor 1 alpha (HIF-1 α) [22].

The AhR has a bHLH region located at the amino terminus required for DNA binding [23] and contains sequences important for nuclear localization (NLS) [24] and nuclear export (NES) [25]. The nuclear export sequence (NES), is responsible for the cytoplasmic shuttling of nuclear AhR and leads to its ubiquitination and degradation [26]. The bHLH region also contains a domain of about 300 amino acids (non polar residues) situated next to the bHLH domain. This domain has homology with the PAS sequence motif. This PAS region contains two subdomains of 110 amino acids, PAS A and PAS B domains, separated by a sequence of ~50 amino acids

[27]. The PAS domain plays a role in AhR/Arnt dimerisation (PAS A) and ligand binding as well as hsp90 binding (PAS B) [28], but it seems from deletion mutagenesis experiments on both PAS A and PAS B that PAS B seems to be more important in ligand binding than PAS A [29]. Moreover, PAS B is very important for stabilization of a functional AhR-Arnt conformation [30].

The transactivation domain (TA), situated at the carboxy terminal region is rich in glutamine residues, and is responsible for the interactions with the general transcription machinery [31].

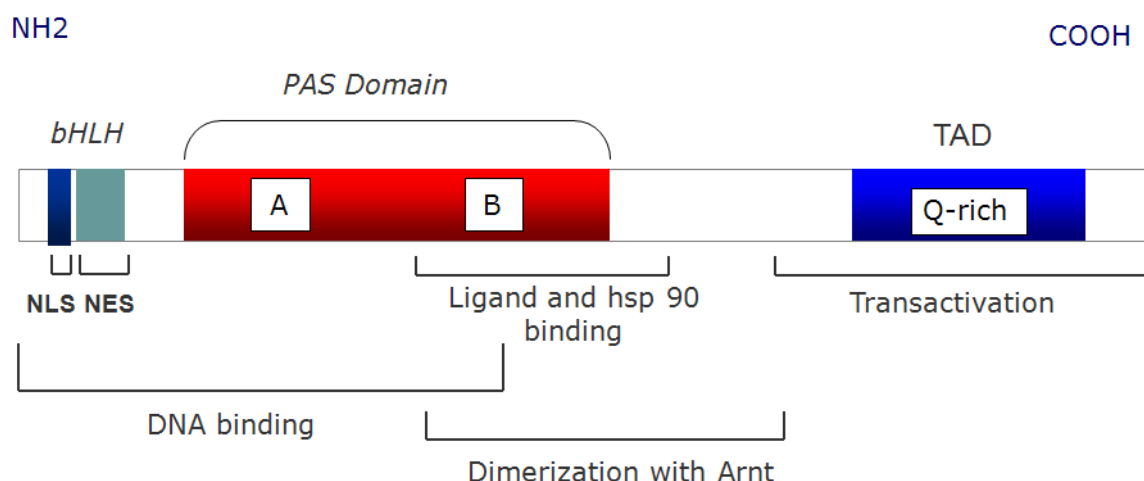


Figure 1.1 Domain structure of AhR. bHLH: basic-helix-loop-helix, NLS: nuclear localization sequence, NES: nuclear export sequence, PAS: Per, Arnt and Sim, Arnt: aryl hydrocarbon receptor nuclear translocator protein, hsp90: heat-shock protein 90, TAD: transactivation domain. (Adapted from [2]).

Comparison of the rat, human and mouse AhR revealed that the amino terminal domain of the AhR is highly conserved with 100% identity between the rat and mouse receptors and 98% between the rat and human receptors in the bHLH. The amino acid sequences in the PAS domain was 96% identical between rat and mouse but only 86% between rat and human AhR. In contrast, the C-terminal domain sequence was less well conserved between the three species, with

79% identical amino acids between rat and mouse and only 61% between rat and human [32]. Another study showed that the alignment of the PAS domain sequences of all vertebrate AhRs revealed 82 residues (41%) are conserved in the PAS domains of all these AhRs [261] (Figure 1.2). C-terminal variation explains why the molecular weight of Ah receptor is variable within and across species (95 to 145 kDa) [33].

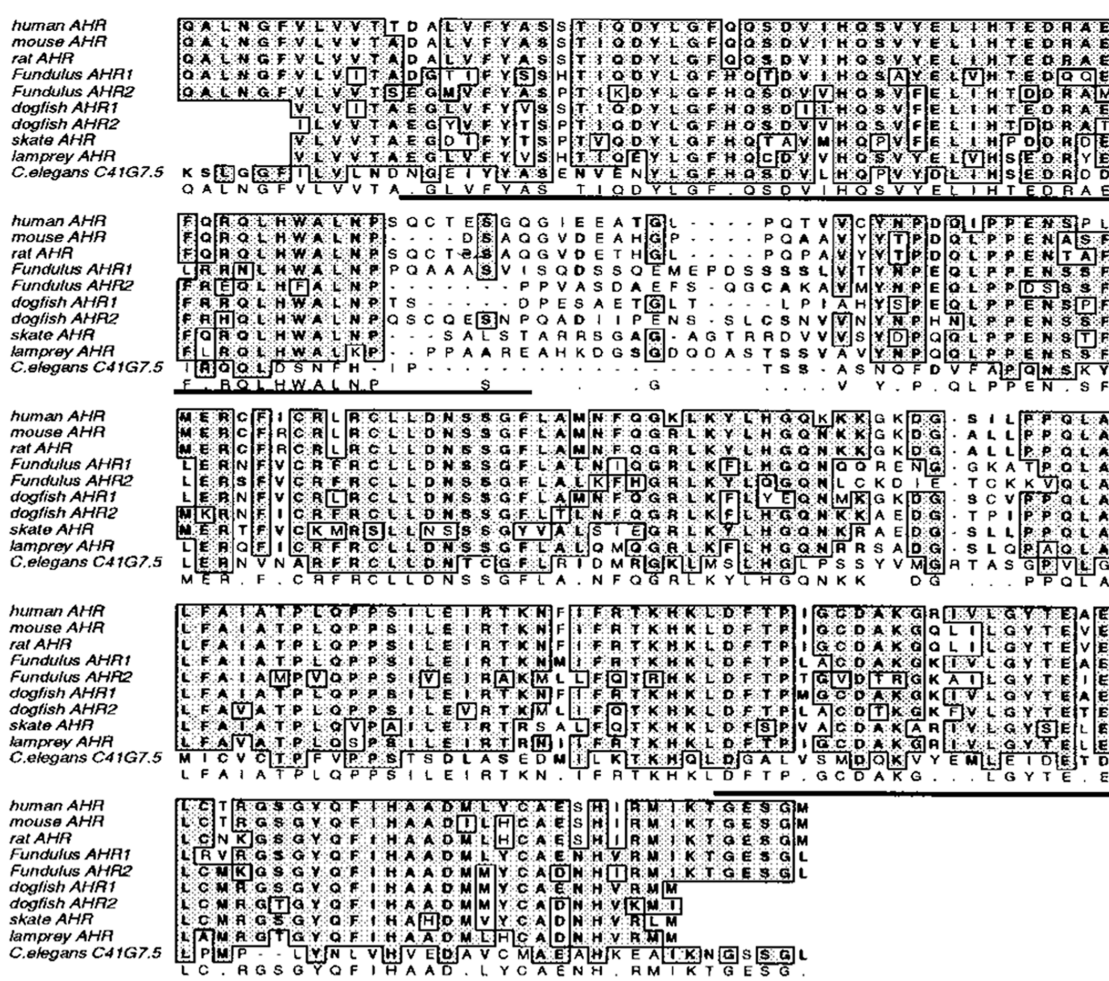


Figure 1.2 Alignment of PAS domain amino acid sequences of vertebrate AHRs and a possible invertebrate AHR homolog. (See text for discussion. Adapted from [261]).

Section 1.1.3.1 The AhR ligand binding domain

Although the AhR was identified 34 years ago, its tertiary structure is yet to be determined. The crystallization of this receptor was hampered by low levels of expression (100-1000 fmol/mg protein) and the instability of the receptor [34] which made work with it technically difficult.

As mentioned in Section 1.1.3, the ligand binding domain (LBD) amino acid sequence comparison among species demonstrated a high degree of identity [35]. This observation motivated researchers to investigate the importance of this domain. The murine LBD was mapped between amino acids 230 and 421 [36]. It was shown that the affinity of this LBD for TCDD is similar to that of the full-length AhR [36], hence it contains all the information necessary for ligand binding. Based on that, successful transfection of this LBD into an expression system could be a useful tool. Compared with the rat or mouse AhR, the human AhR appears to have lower affinity for TCDD; the K_D in human was determined to be 1.6 nM, whereas it is about 0.27 nM in mouse [35].

Site-directed mutagenesis was used to identify key ligand-binding residues. It was demonstrated that the residue that influences the ligand binding affinity of the human AhR is a valine 381 (equivalent to the valine 375 of the mouse AhR), whereas this residue is alanine 375 in C57BL/6 mice [35]. This difference in ligand-binding residues between the mouse and the human AhR was shown to be the cause for the lower binding affinity of the human receptor [35] [37]. For instance, replacing the valine 381 residue with an Alanine in the human LBD enhanced TCDD-induced activity, whereas replacing valine 381 with an aspartate abolished completely TCDD binding [35]. A recent study using mutated residues in the LBD of Gal4-AhR revealed that ligands with low-or high- affinity do not interact with the same residues of the AhR ligand-binding pocket [9].

Some trials in our laboratory were done with the aim of cloning large amounts of functional AhR LBD for crystallography study. Therefore, a Histidine-tag truncated AhR LBD was expressed in *Spodoptera frugiperda* insect cells (sf9) using a baculovirus expression system. The system yield soluble AhR LBD protein at ~ 0.15% of cytosol protein with full ligand binding activity. The study refined the minimal LBD to a region of 125 amino acids [38]. Microgram-milligram quantities of the human AhR and the ARNT proteins were expressed using a baculovirus system [39]. To facilitate purification with Ni-NTA chromatography, a polyhistidine tag was cloned at the C-termini. The results revealed that approximately 23% of the over-expressed AhR was soluble whereas 77% formed insoluble aggregates. It was suggested that cellular factors were required for AhR/Arnt/DRE interactions and that these factors were removed during purification.

Waller and McKinney (1995) described a model for the ligand- binding site based on structure-activity relationship studies with a significant number of AhR ligands. The model suggests that the ligand-binding site is hydrophobic and AhR ligands are generally planar non-polar with maximal dimensions of (14 x 12 x 5) Å [40] [41]. The structural diversity among AhR ligands suggests that this receptor has a promiscuity of the ligand binding activity of the AhR [42].

Very recently, three different models for the mouse (mAhR) PAS B LBD were developed by Pandini et al (2007) [260] based on the sequence identity and similarity of the residues among mAhR, HIF-2 α and ARNT. These models identified a cavity within the core of the LBD of the mAhR PAS B domain with an internal space sufficient for ligands as opposed to the well packed cavity in HIF-2 α and ARNT PAS structures (Figure 1.3).

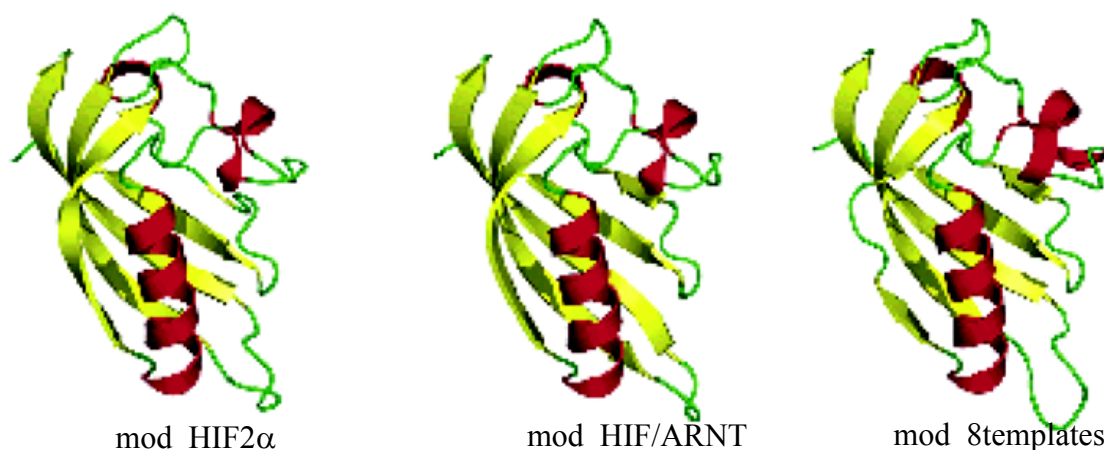


Figure 1.3 Cartoon representation of the three modeled structures of the mAhR LBD. mod_HIF-2 α : model using only the HIF-2 α template, mod_HIF/ARNT: model based on the HIF-2 α and ARNT template structures. mod_8templates: model using eight of the PAS structures. (The models were derived by MODELLER). (See text for discussion. Adapted from [260]).

As a summary, the three-dimensional structure of the LBD is yet to be defined. Once the LBD structure is determined, further analysis could be carried out in order to elucidate how ligands bind and activate AhR LBD.

Section 1.1.4 AhR and associated proteins

Different laboratories have conducted proteomic studies on AhR. Some of the proteins bound to AhR have been identified whereas others are still unknown. The receptor is found to be constitutively present in the cytosol as an inactive complex with two molecules of 90-kDa heat shock protein hsp90 [43], a 43-kDa protein known as Aryl hydrocarbon interacting protein (AIP) [44], XAP2 [45] [46] or ARA9 [47] and a 23-kDa co-chaperone protein p23 [48].

hsp90 is one of the chaperone proteins that binds AhR. The role of this protein in the receptor signaling is still unclear. It was postulated that the role of the protein is to repress receptor function given that the receptor bound to hsp90 did not dimerise with the Arnt protein [28]. It was also suggested that hsp90 may be important for proper folding of AhR LBD, maintaining lig-

and-free AhR in a configuration that facilitates ligand binding and for the regulation of the nuclear localization of the AhR complex [49]. Moreover, hsp90 was found to be implicated in the regulation of AhR function *in vivo* [49].

AIP appears to increase ligand-induced signaling through AhR; it binds to both AhR and hsp90 and it stabilizes the AIP-hsp90-AhR complex [50]. Recent work reported that AIP repressed the transactivation potential of the AhR [51]. P23 appears to play a role in release of AhR from hsp90 after ligand binding [48].

The Ah receptor nuclear translocator (Arnt) was cloned and identified as a component of the nuclear form of the Ah receptor complex. The human Arnt-protein amino acid sequence is about 87 kDa. The protein is not a part of the ligand-binding subunit of the receptor. It was thought that it is a factor required for the AhR complex to translocate from the cytosol to the nucleus to bind the Dioxin Response Element (DRE) after binding ligand, a reason for the mis designation of Arnt as a translocator [52]. It was found later on that Arnt is not involved in transport of the Ah receptor into the nucleus, instead it dimerises with the ligand-bound AhR already translocated in the nucleus [53]. It was shown also that this protein is required to direct the ligand-activated AhR to enhancer elements upstream of the genomic target [21]. It has been demonstrated that Arnt can bind to E-box motifs as a homodimer [54] and can form complexes with the HLH proteins SIM and HIF-1 to mediate their biological responses [55]. A second form of Arnt from rat termed Arnt2 has been described [56]. Furthermore, Arnt-nullizygous mice are lethal [57]. Arnt shares with AhR a structural organization in that it also has a bHLH domain, PAS domains and a TA domain. However, the Arnt does not bind ligand nor hsp90.

Section 1.1.5 Ah receptor ligands

AhR ligands can be either xenobiotics (xenos=foreign and bios=life) or endogenous. Typical

exogenous ligands for the cytosolic Ah receptor include planar halogenated aromatic amines (HAHs), polyaromatic hydrocarbons (PAHs) and their halogenated derivatives polychlorinated biphenyls. These are synthetic chemicals and are either present in the environment or are produced during industrial processes. On the other hand, natural ligands that are formed in biological systems are also identified. Structures of some AhR ligands are displayed in Figure 1.4.

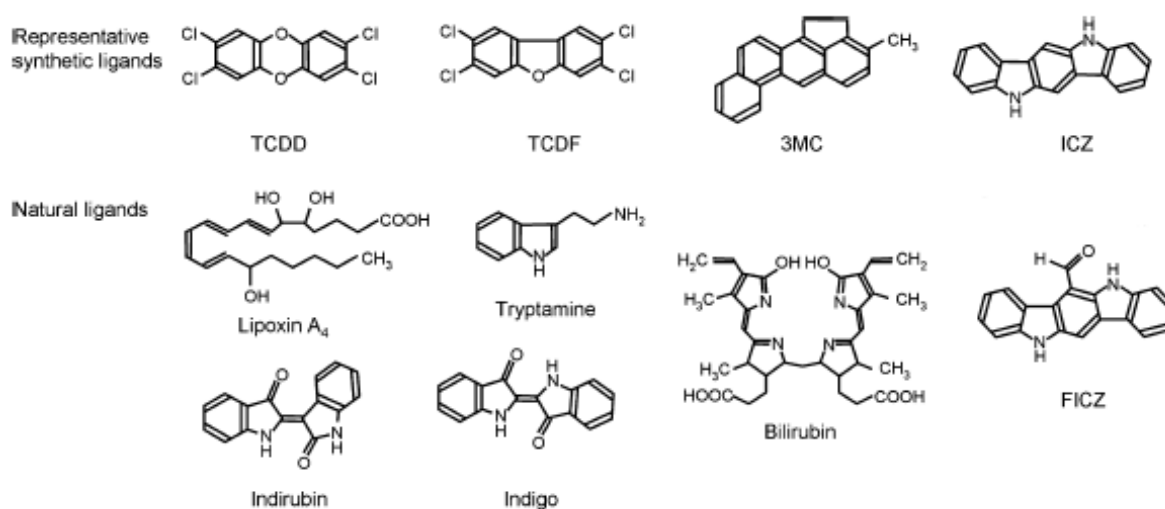


Figure 1.4 Structures for representative AhR ligands. TCDD: 2,3,7,8-tetrachlorodibenzo-*p*-dioxin, TCDF: 2,3,7,8-tetrachlorodibenzofuran, 3MC: 3-methylcholanthrene, ICZ: indolo[3,2-*b*]carbazole, FICZ: 6-formylindolo[3,2-*b*]carbazole. (Adapted from [252]).

Section 1.1.5.1 Halogenated Aromatic Hydrocarbons (HAHs)

These include the polychlorinated dibenzo-*p*-dioxins (PCDDs), dibenzofurans and biphenyls and related chemicals [58]. They represent a class of toxic environmental chemicals. These chemicals are extremely dangerous and can have a significant impact on the health and well being of humans and animals because of their ubiquitous distribution, fat solubility, resistance to biological and chemical degradation and potential for bioaccumulation [58]. The prototype, 2,3,7,8-Tetrachlorodibenzo-*p*-dioxin, (TCDD, dioxin), binds strongly to AhR and exhibits most

of its known functions via this receptor [254]. It was observed by competition binding studies with congeners of TCDD that high-affinity ligands bind stereospecifically to AhR, *i.e* these ligands are planar and contained halogen atoms in at least three of the four lateral positions [59].

Section 1.1.5.1.1 2,3,7,8-Tetrachlorodibenzo-*p*-dioxin (TCDD)

The term "dioxin" refers to a group of chemicals, the polychlorinated dibenzo-*p*-dioxins (PCDD). There are 75 possible congeners, one of them is 2,3,7,8-tetrachlorodibenzo-*p*-dioxin (TCDD), a potent toxic compound in animals and humans [59]. It can be formed as a contaminant in the commercial herbicide 2,4,5-trichlorophenoxyacetic acid (2,4,5-T), a component of Agent Orange and in other industrial chlorine processes such as waste incineration, chemical and pesticide manufacturing and pulp and paper bleaching. Because of their solubility in lipids and chemical stability, dioxins are concentrated along the food chain, and food has become the major exposure pathway for humans. This lipophilic character enables them to cross cell membranes and accumulate in the fatty tissue of the organism.

The toxicity of TCDD (measured as oral LD₅₀) varies considerably among species. Classic examples are the guinea pig, where the LD₅₀ is ~ 1 µg/kg [154] and hamster ~ 5000 µg/kg [60].

The potency of TCDD is partially attributable to its resistance to metabolism [61] and high solubility in lipids [62]. The many toxic effects of TCDD and other HAHs include body weight loss, thymic atrophy, hepatotoxicity and porphyria, carcinogenesis, teratogenesis, suppression of the immune system, and reproductive toxicity [59] [63] [20]. These toxic effects depend on the species, age and sex (reviewed in [58]). TCDD is classified as a "human carcinogen" [64].

Section 1.1.5.1.2 The 3,4,3',4'-Tetrachloroazoxybenzene (TCAOB)

TCAOB is a member of the halogenated aromatic hydrocarbons (HAH) family. It can be formed

as an unwanted contaminant during the synthesis of 3,4-dichloroaniline and in the degradation of herbicides in soil and was responsible for three outbreaks of acne (Chloracne) among chemical workers [65].

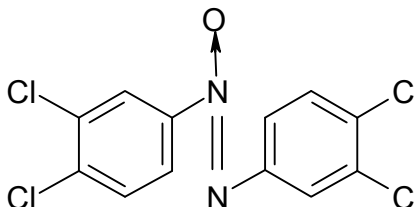


Figure 1.5 Structure of 3,4,3',4'-tetrachloroazoxybenzene (TCAOB).

It has typical dioxin-like effects, including thymic atrophy, increased liver weights, induction of hepatic cytochrome P4501A, and decreased mean body weight gains [66].

TCAOB is a potent inducer of hepatic aryl hydrocarbon hydroxylase activity and competes for stereospecific binding sites in mouse hepatic cytosol, (K_D of TCAOB = 0.93 nM compared to that of TCDD = 0.27 nM) [66], therefore, TCAOB was used as an unlabelled competitor for dioxin in binding assays [66].

Section 1.1.5.2 Polycyclic Aromatic hydrocarbons (PAHs)

Typical PAH ligands are benzo(a)pyrene, 3-methylcholanthrene (3MC), aromatic amines and other related chemicals [59]. Polynuclear aromatic hydrocarbons (PAHs) also bind and activate the AhR [67]. These chemicals are also toxic but less potent than HAHs. They are generated from incomplete carbon combustion, high temperature cooking, diesel exhaust and cigarette smoke [68]. Compared to the HAHs, the PAHs have lower binding affinity to the AhR (reviewed in [2]).

Section 1.1.5.3 Natural ligands

In addition to synthetic and environmental chemicals, numerous naturally occurring dietary and

endogenous ligands have been identified.

AhR ligands were isolated from different vegetables, fruits, herbs and teas (reviewed in [2]). These can be agonists such as quercetin [69], or antagonists as flavonoids [70]. Flavonoids represent the largest group of naturally occurring dietary AhR ligands. The indolo-[3,2-b]-carbazole (ICZ), an acidic condensation product formed from indole-3-carbinol (13C), has the most highest-affinity natural AhR ligand identified to date [71] and is an agonist for AhR [72].

Many endogenous physiological chemicals have been isolated as candidate natural ligands for AhR, such as endogenous tryptophan-derived natural chemicals, indirubin, indigo [73] and 6-formylindolo[3,2-b]carbazole (FICZ), a tryptophan photoproduct [74]. Other ligands include tryptamine [255], bilirubin [75] and lipoxin A4 [76].

Finally, AhR is still considered as an 'orphan receptor', for the lack of knowledge of its physiological ligand. Extending the broad of knowledge of AhR ligands facilitates the prediction of the properties of its endogenous ligand.

Section 1.1.6 The AhR signaling pathway

Section 1.1.6.1 Binding and translocation to nucleus

The AhR ligands, by the virtue of their lipophilicity, diffuse across the plasma membrane and bind to AhR associated with hsp90 and other proteins. It is presumed that following ligand binding, the AhR undergoes conformational change that exposes a nuclear localization sequence (s) [24] [30] that allows translocation to the nucleus [77]. This is a rapid process that occurs shortly after ligand binding [78].

Section 1.1.6.2 Dimerisation of AhR with Arnt

In the nucleus, the AhR dissociates from the complex and dimerises with Arnt [68]. This heterodimerisation enables AhR to bind DNA (Xenobiotic Response Elements, XRE of target promoters) [77]. Arnt was initially discovered as a necessary component of the AhR signal transduction pathway, where it dimerises with the AhR to mediate many of the biological responses to halogenated aromatic hydrocarbons [79] [20] [80] [81]. The AhR/Arnt heterodimer is depicted in Figure 1.6.

AhR heterodimerises with Arnt at the bHLH and the PAS domains and this heterodimerisation is essential for DNA recognition [79] [28]. Dimerisation of AhR with Arnt converts the AhR into its high affinity DNA binding form [20] [30]. Selective deletion analysis identified a DNA sequence, containing the core consensus sequence 5'-TNGCGTG-3', the core binding motif of the dioxin or xenobiotic responsive element (DRE or XRE) to which AhR and Arnt bind directly [82]. It was reported that AhR/Arnt heterodimerisation and/or XRE binding is regulated by phosphorylation by a protein Kinase C (PKC) [83].

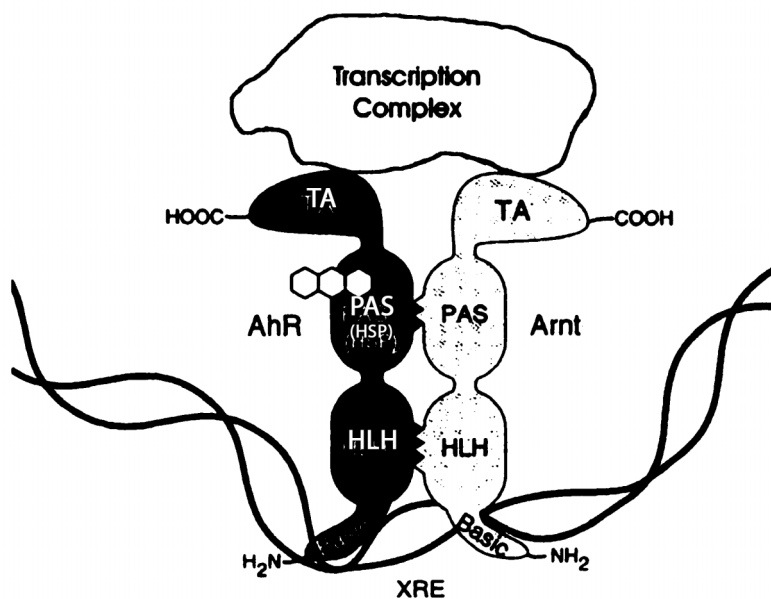


Figure 1.6 The AhR/Arnt heterodimer. Each protein contains a transactivation region (TA), a Per-AhR (Arnt)-Sim (PAS) region, a helix-loop-helix (HLH) region and a basic region that binds XRE on DNA. In addition, AhR contains a ligand binding region (PAS B) and a region that binds hsp90 (HSP) when AhR is a monomer (unliganded). (see text for discussion) (adapted from [3]).

Section 1.1.6.3 Transcriptional activation

The AhR/Arnt heterodimer is recruited with its associated factors to the enhancer and TATA box regions of the XRE of the CYP1A1 promoter and other responsive genes [84] [85] [249]. Both, enhancer and promoter are required to mediate the induction of CYP1A1 by TCDD [86]. As a result, there is stimulation of transcription initiation of genes known as the (AhR) gene-battery. It was found that, in Ah receptor- and Arnt- defective cells, TCDD fails to induce the activation response [81]. This finding gives evidence that AhR together with Arnt are required for CYP1A1 transcription activation. The general model for CYP1A1 induction is depicted in Figure 1.7.

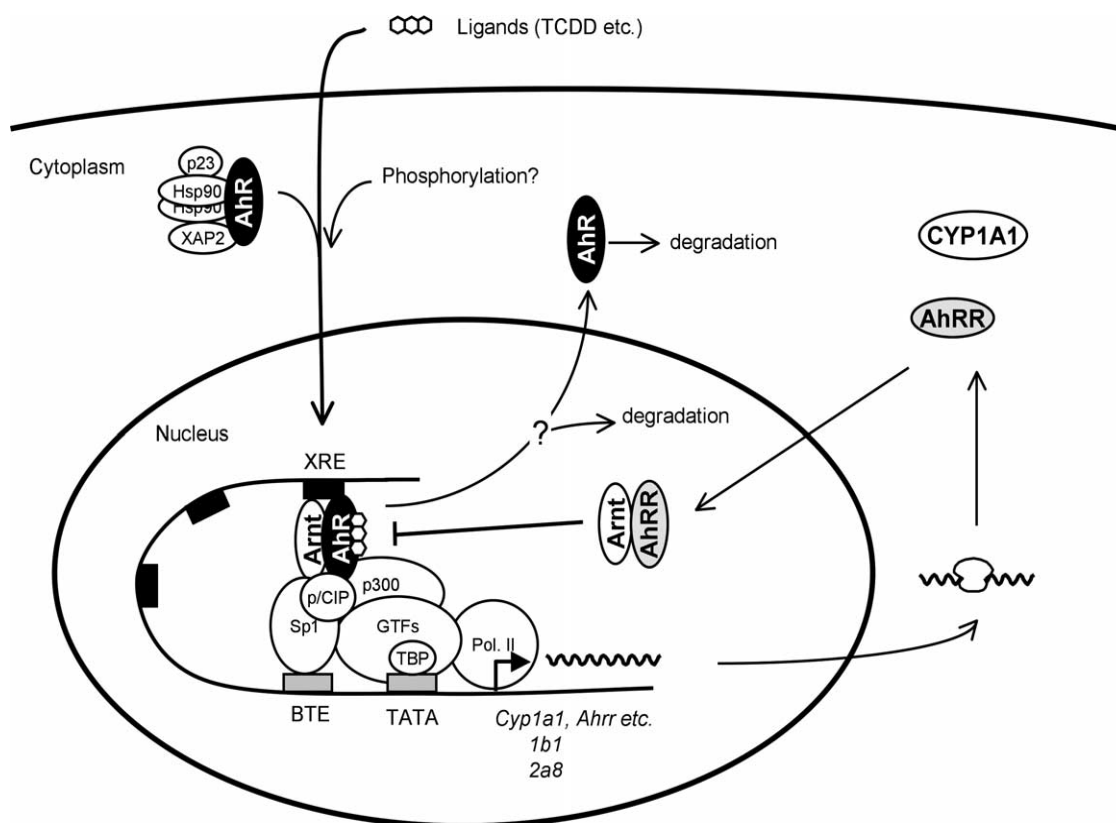


Figure 1.7 Description of AhR signaling pathway. (See text for discussion. Adapted from [252]).

Another sequence, the BTE (basic transcription element) or the GC box sequence, localized in the proximal promoter of *CYP1A1*, is also important for CYP1A1 induction. *CYP1A1* gene expression is enhanced by Sp1 binding to the BTE which in turn, facilitates the binding of AhR/Arnt to the XRE and vice versa. Binding of the AhR/Arnt heterodimer recruits P300, a histone acetyl transferase (HAT) coactivator to the C-terminus of Arnt and several other coactivators, such as, but not exclusively, SRC-1, NCoA-2 and p/CIP to the *CYP1A1* enhancer region. Binding of PolIII to the promoter enhances gene expression (reviewed in [252]).

It was reported that chromatin structure has a important role in the regulation of gene transcription [87] [88]. Whitlock JP et al., 1996 [3], proposed a model describing the role of chromatin

remodeling in the transcription of CYP1A1. In their model, the induction in response to drug is associated with chromosome remodelling. So in the presence of inducers, AhR/Arnt heterodimer binds the enhancer and the enhancer/promoter region undergoes a change in structure. Subsequently, the nucleosomes in the promoter region are disrupted then the transcription binding protein (TBP) and other transcription factors occupy their cognate binding sites and initiate transcription of *CYP1A1* into mRNA. These mRNAs then get translated into CYP1A1 proteins in the cytoplasm. In the absence of inducers, nucleosomes in the regulatory region are positioned to prevent any transcription occurring (reviewed in [3]).

TCDD binding to the AhR activates the receptor and as result, an array of genes are transcriptionally activated or repressed [89]. The genes that are directly activated by AhR include some phase I and phase II drug-metabolizing enzymes such as cytochrome P450 CYP1A1, CYP1A2, CYP1B1, aldehyde dehydrogenase (ADH), NADPH-quinone-oxidoreductase (NQO1), glutathione S-transferase (GST) Ya (GST1), uridine diphosphate glucosyltransferase 1 family polypeptide A1 (UGT1A1) [90] [89], p27^{kip1} [91] and N-myristoyl-transferase 2 [92]. Recently, microarray analysis showed that AhR can regulate the expression of some genes indirectly by binding to a factor (AHRE II) that binds DNA. In this case, AhR acts as a co-activator rather than a transcription factor [93].

Overall, the activation of AhR signaling pathway is made of several steps starting from the ligand binding followed by translocation to the nucleus, binding with nuclear factors, transactivation of gene transcription and degradation [53]. These steps are differentially regulated in different species.

However, the molecular mechanism by which the AhR signaling pathway is activated is still not fully elucidated. As mentioned previously, this lack of information is attributed to the lack of

structural information about AhR LBD.

The induction of *CYP1A1* gene expression is considered one of the most sensitive indicators of exposure of AhR agonists [94]. Moreover, the induction of expression of CYP1A1 is maintained in most species [33], therefore, induction of CYP1A1 has been used as a model system to define the mechanism of action of AhR ligands. Based on CYP1A1 induction, several AhR ligands were identified as agonists, partial agonists [95] [96] [97] and antagonists [98] [69] [41] [99].

Section 1.1.6.4 Ligand binding-independent activation of the AhR

Generally, AhR activation is mediated by AhR ligands, however it was shown that activation of AhR signal transduction could be mediated via a ligand-independent mechanism. In a study conducted by Ma and Whitlock (1996), omeprazole (OME), a gastric anti-ulcer drug, induced CYP1A1 but was not affected by 3'-methoxy-4'-aminoflavone that was able to antagonize TCDD-mediated CYP1A1 induction [100]. Later, Backlund and collaborators (1997), compared OME with TCDD for binding (rat cytosol) and activating the Ah receptors in H4-II-E cells [101]. Omeprazole and TCDD induced CYP1A1 gene (northern blot analysis) and protein expression (western blot analysis) but OME, unlike TCDD, did not bind specifically rat AhR as demonstrated by [³H]-TCDD competitive assay nor activated cytosolic AhR to an XRE-binding form as shown by EMSA. However, both OME and TCDD recruited AhR and Arnt nuclear protein complex to XRE as shown by EMSA on nuclear extracts treated with both compounds. Tyrosine kinase inhibitors inhibited OME- but not TCDD-mediated CYP1A1 induction (mRNA and protein) as well as AhR-induced binding to XRE indicating that OME activates AhR via intracellular signal transduction which is tyrosine kinase-dependent, that is different from the induction mediated by TCDD.

Section 1.2 Regulation of AhR and crosstalk

The AhR signal transduction pathway is controlled by regulatory mechanisms. It was shown that degradation of AhR is necessary for proper activation. AhR degradation involves ubiquitination [102] and it occurs shortly (1-2 hours) after TCDD binding [103].

A nuclear protein that acts as a negative regulator of the AhR, the AhRR, has been identified [104]. This protein is induced by AhR and binds to Arnt inhibiting the formation of the transcriptionally active AhR/Arnt complex.

The AhR interacts with other pathways involving the oestrogen receptor (ER) and androgen receptor. The cross talk between AhR and ER was supported with the observations that female rats chronically treated with TCDD developed less mammary and uterine tumors [105]. The cross-talk between AhR and ER is complex and it was shown that the AhR downregulates the ER-mediated effects through multiple mechanisms, such as rapid metabolism of oestrogen by CYP1A1 [106] [107], ER degradation by proteasomes through AhR [14], sharing common co-factors, such as Arnt [108]. Recently, using Chromatin Immunoprecipitation (ChIP) assays, TCDD was shown to recruit ER α to the CYP1A1 promoter which is enhanced by estradiol (E2) [85].

In the case of the androgen receptor, exposure to TCDD inhibits androgen-mediated cell proliferation through modulation of retinoblastoma protein (pRb) phosphorylation [256]. Finally, inhibition of AhR-mediated responses by hypoxic conditions have been demonstrated in mouse Hepa-1 cells [109].

The regulation of AhR function appears to be tissue/cell-specific. One of the aspects of the species-specific differences in AhR regulation is the interaction of AhR with nuclear proteins including activators and co-repressors that are species/cell-specific [110].

Section 1.3 AhR functions

Section 1.3.1 Regulation of xenobiotic metabolism

In general, several AhR ligands form highly reactive intermediates during metabolism by cytochrome P450 which results ultimately in adduct formation. This is the case for PAHs that are metabolized by several phase 1 enzymes, such as cytochrome P450s, CYP1A1 and CYP1B1 to electrophilic derivatives that can mutate DNA [20] [59], whereas most of the HAHs are more resistant to metabolic degradation and have higher binding affinity (in the pM range for HAHs, compared to nM range for PAHs) which results in continuous activation of AhR and thus persistent activation of gene expression [111]. This could explain the lesser potency of PAHs compared to HAHs.

Section 1.3.2 Mediation of HAH toxicity

In addition to its role in modulating the induction of gene expression, numerous studies also support a role of AhR in mediating toxicity. Previously, Poland and Glover have shown that the potency of various halogenated dibenzo-*p*-dioxins at inducing the aryl hydrocarbon hydroxylase AHH activity closely parallels their toxic potency (*e.g.* their potency to elicit acne) [5]. Structure-activity relationship (SAR) analysis on a variety of inbred strains of mice with different functional AhR and HAH responsiveness confirmed the correlation of the structure-activity relationship for receptor binding with toxic potency [58] [112]. For example, an addition of non-lateral chlorines or removal of lateral chlorines from these planar structures decreases toxicity. These findings were confirmed when Fernandez-Salguero and his collaborators administered TCDD to AhR-knock-out mice and found that these mice were resistant to TCDD-induced biochemical or toxic effects [257]. Combined together, these data support the hypothesis that AhR mediates HAHs toxic effects [59]. Another study was done on AhR expression in transgenic mice revealed that the constitutively active AhR protein reduced the life span of the mice and

induced tumours in the glandular part of the stomach. These results demonstrated the involvement of the receptor in cancer and regulation of cell proliferation [113].

PAHs and HAHs are all toxic but they exhibit differences in toxic potency. The toxic and biological responses mediated by AhR are species-, tissue- and ligand-specific. Moreover, they are dependent on the dose, length of exposure, strain, age and sex of animals [59].

Unlike the PAHs, TCDD is not genotoxic (does not bind covalently to DNA to form DNA adducts), but it is a very powerful tumour promoter [114]. It induces tumours in rodent models. The pattern of these tumours varies among species. However, the mechanism(s) whereby HAHs cause cancer are not known. Besides tumour promotion, exposure to TCDD results in several toxicological effects, including chloracne, liver disorders, adverse effects on the immune system, and reproductive and teratogenic defects [115].

What is known is that AhR-dependent transcription is required for dioxin toxicity [116] but it is unknown how the activation of the AhR-dependent genes produces the multiplicity of toxic responses characteristic of dioxin exposure.

Section 1.3.3 Vascular development

In addition to its role in the adaptive metabolism of xenobiotics and in the toxic events that follow exposure to TCDD [59], AhR seems to play a developmental role. Recent studies on the phenotype of AhR null mice [68] [257] [117] [118], revealed that these mice display smaller livers, reduced fecundity, and decreased body weights. This phenotype is presumed to result from loss of AhR activation by endogenous ligand(s), although the identity of the responsible chemical(s) remains elusive.

A recent study investigated the mechanism of DV closure which is the closure of a hepatic vas-

cular shunt known as the ductus venous (DV). Previously, Walisser et al (2004) demonstrated that AhR together with its heterodimeric partner, Arnt, plays a role in this vascular defect. Using hypomorphic models of AhR and Arnt, it was demonstrated that these two proteins localize to the nucleus and are required for normal DV closure, suggesting that AhR-Arnt heterodimerisation is essential for normal vascular development [119] [116].

Strikingly, the environmental pollutant TCDD has found to correct this physiological defect. This suggests that chemicals of this class could have therapeutic applications in particular for diagnosis developmental vascular defects [120]. This is consistent with the idea that an unknown endogenous activator ligand participates in normal developmental signaling [119], which can give insight for more research on a possible physiological role of AhR in this area.

Overall, AhR signaling can govern three distinct biological functions, up-regulation of xenobiotic metabolism, dioxin toxicity, and normal vascular development.

Section 1.4 The AhR and anticancer therapy

The AhR is gaining increasing attention as a potential target for anticancer therapy. Since AhR signaling is known to play a role in carcinogenesis by activating some procarcinogens into their genotoxic forms by CYP1A1 and other phase I metabolizing enzymes [59] [20], research on AhR antagonism as a chemopreventative strategy seems to be a promising area. For instance, Safe and collaborators have focused on identifying selective AhR modulators (SAhRMs) that are AhR agonists but with reduced ability to induce DRE responsive genes and exhibit antioestrogenic and antitumorigenic activity [121] [122]. Such SAhRMs, but not limited to, 6-methyl-1,3,8-triCDF (6-MCDF) [94] and diindolylmethane (DIM) [123], which are AhR ligands and partially inhibit TCDD-induced CYP1A1. These compounds were found to be highly effective in inhibiting mammary tumour growth in Sprague-Dawley rats with induced cancers [94] [124].

Also, several structurally-diverse natural products that exhibit chemoprotective anti-tumorigenic properties have been characterized as AhR agonists/antagonists. These include flavonoids, carotenoids, indole-3-carbinol (13C) and related compounds, and the antioxidant resveratrol. All these compounds inhibit formation and/or growth of tumours in animal models, and their mode of anti-carcinogenic action may, in part, be AhR-mediated [106].

Research on phenylbenzothiazoles has recently focused on AhR agonism in anticancer therapy. Generally, these chemicals induce drug metabolizing enzymes (CYP1A1 for example) and get biotransformed into activated forms leading to genotoxic effects. This is the case of some anti-cancer phenylbenzothiazole derivatives [126] [128], with a selective and potent anticancer profile *in vivo* against some human xenograft models and *in vitro* against some human cancer cells [128] [130] [131]. This class of drugs will be covered later in this chapter.

Section 1.5 AhR and drug metabolism

Humans are exposed daily to xenobiotics. Most of these chemicals are insoluble in water, but soluble in fats and thus tend to accumulate in the body. In order to avoid their accumulation, these chemicals must be rendered more polar and therefore more water soluble to facilitate their excretion in the urine. This metabolism is due, by and large, to enzymes with broad substrate specificity including the cytochrome P450 enzymes in the liver. In general, drugs undergo metabolism reaction known as phase I and phase II metabolism.

Section 1.5.1 Phase I enzymes:

They involve oxidation (the P450 enzymes), reduction and hydrolysis. Most of these reactions occur in the liver but some of them occur in the gut wall, plasma and the lung.

The hepatic microsomal cytochrome P450s are members of a superfamily of monooxygenases

that catalyse metabolism of xenobiotics, the initial step in the biotransformation and elimination of a wide variety of substrates, from endogenous steroids to environmental pollutants. There are 57 known P450s in humans, among which 15 are involved in metabolizing xenobiotics, including drugs. P450s are located primarily in the endoplasmic reticulum of liver tissue. The cytochrome CYP 450 or P450 (P for pigment) owes its nomenclature to its characteristic absorption maximum at 450 nm of carbon monoxide adduct. The enzyme exists as multiple forms, each has different physiochemical properties [265]. Among multiple functions, P450s are responsible for metabolic activation of procarcinogens, detoxification of xenobiotics and drugs biotransformation and metabolism. Several cytochrome P450 enzymes are inducible by xenobiotics [131].

Section 1.5.1.1 Nomenclature

The system is based on amino acid sequence homologies. The prefix CYP is followed by a number indicating families, then a capital letter indicating subgroups, and then a number defining an individual isoform [132].

Section 1.5.1.2 CYP1 family

The P450s of this family are CYP1A1, CYP1A2 and CYP1B1. These enzymes are inducible by many xenobiotics, including planar polycyclic aromatic hydrocarbons (PAHs) and 2,3,7,8-tetrachlorodibenzo-*p*-dioxin (TCDD) which is a highly potent inducer of CYP1A1 in particular [133]. As mentioned earlier, it is well documented that regulation of the CYP1 family is mediated by the AhR and its nuclear translocator Arnt [3] [134] [20] [135]. Although the AhR is involved in the regulation of all three CYP1 enzymes, it has been reported [96] that CYP1A1 is significantly more inducible by TCDD than CYP1A2. Essentially, substrates of CYP1A1 are hydrophobic and characterized as relatively planar PAH molecules comprised of two to four fused aromatic

rings, which also tend to be rectangular in shape [136] [137].

The levels of these enzymes in the liver and other organs are variable and subject to chemical induction, genetic variation and other factors relating to lifestyle, diet, age, sex and medical conditions [138]. In humans, CYP1A2 is mainly expressed in liver, whereas CYP1A1 and CYP1B1 are expressed extrahepatically. In rodents, CYP1A1 is expressed in the liver [125].

Section 1.5.2 Phase II reactions:

The oxidized products of phase I are made more polar by enzymes in phase II. All of them are conjugation reactions which add various highly polar groups such as glucuronic acid and glutathione. They also occur mainly in the liver.

Section 1.6 Phenylbenzothiazoles

Section 1.6.1 2-(4-aminophenyl)benzothiazoles (series 1)

Section 1.6.1.1 Discovery of non-fluorinated 2-(4-aminophenyl)benzothiazole analogues

Originally, the compound 2-(4-aminophenyl)benzothiazole CJM126 was discovered as an intermediate during the synthesis of hydroxylated 2-phenylbenzothiazoles as potential tyrosine kinase inhibitors [139]. CJM126 exhibited a selective *in vitro* activity in MCF-7 (ER+) breast carcinoma cell lines ($GI_{50} < 0.001 \mu M$). However, the growth curve displayed an unusual biphasic dose response where the drug killed the cells at sub-nanomolar concentrations but was inactive in the micromolar range [128].

Among the 3'-substituted congeners, 2-(4-aminophenyl-3-methylphenyl)benzothiazole (DF 203; NSC 674495) was originally selected as the lead compound for its superior *in vivo* activity in human xenograft models and *in vitro* activity in specific breast, ovarian, renal, colon, melano-

ma and non small cell lung cell lines [128] [129].

Section 1.6.1.2 Discovery of fluorinated 2-(4-aminophenyl)benzothiazole analogues

Metabolic studies on DF 203 showed that it was biotransformed by the drug metabolizing enzyme cytochrome P450 (CYP) 1A1 to 2-(4-aminophenyl-3-methylphenyl)-6-hydroxybenzothiazole (6-OH 203) in sensitive cells. 6-OH 203 (IH 130) was devoid of antitumour activity [140] and reversibly inhibited CYP1A1 [141].

In attempts to overcome the metabolism of non-fluorinated analogues, the 5-fluoro isomer (5F 203) was synthesized. It was found to block selectively oxidative metabolism of the non-fluorinated counterpart DF 203 and restored the conventional dose-response curve [126]. Similar to DF 203, 5F 203 potently and selectively inhibited the growth of renal, breast, and ovarian cancer cell lines [141]. The prodrug, lysylamide dihydrochloride salt of 5F 203 (Phortress, NSC 710305) is in Phase I clinical trials under the auspices of Cancer Research UK [127].

Section 1.6.1.3 Mechanistic investigations

2-(4-aminophenyl)benzothiazoles showed a potent and selective antitumour profile, for instance, MCF-7 and T-47 D breast carcinoma cells were sensitive and renal TK-10 or ovarian IGROV1 cells had intermediate sensitivity, breast MDA-MB-435, ovarian SK-OV-3, and renal CAKI I, were insensitive [128] [126]. It was reported that phenylbenzothiazole compounds may modulate the activity of more than one receptor and may display cross-talk between pathways [84]. The MCF-7 cells express both ER α and AhR [142] [143]. However, 5F 203 and DF 203 had cell growth inhibitory potency in human breast cancer cells irrespectively of the ER or growth factor receptor status [128].

It was postulated that the selectivity is due to metabolism of the drugs, where drug uptake and biotransformation were observed only in sensitive cell lines, in contrast to little or no metabolism in resistant cell lines [140]. Chua and colleagues (2000) reported that DF 203 induced and was metabolized by CYP1A1 only in sensitive cell lines [141]. The major metabolite reported is 6-OH 203 [140], whereas lysates prepared from untreated MCF-7 cells failed to catalyse the 6-hydroxylation of DF 203. Because CYP1A1 activity is known to be induced by AhR signal transduction pathway, it was postulated that the receptor may mediate DF 203 action. Loaiza-Perez and collaborators (2002) demonstrated that the AhR pathway was activated in MCF-7 cell lines but not in MDA-MB-435 cells, resulting in *CYP1A1* mRNA induction [253]. Moreover, DF 203 binds to DNA and forms DNA adducts in sensitive but not resistant cells [140].

It was reported that the differential capacity of AhR to regulate CYP1A1 expression in different cell types may underlie the sensitivity to DF 203. For instance, in DF 203-sensitive cells, AhR translocation to the nucleus and binding to XRE sequences seems to occur after treatment, whereas, in DF 203-resistant cells, AhR was found in cytoplasm and nucleus before and after treatment with DF 203. Furthermore, protein complexes bound to XRE were not observed in resistant cells and CYP1A1 expression was not detected at the mRNA nor the protein levels and finally, adduct formation is negligible [253].

The general proposed mechanism of action of 5F 203 was described by Bradshaw and Westwell (2004) [145]:

Water soluble Phortress is rapidly reverted to its hydrophobic parent 5F 203 drug that is readily sequestered by sensitive cell lines only. Subsequently, 5F 203 binds cytosolic AhR and then translocates to the nucleus. Like any classical mechanism of AhR activation, the complex AhR-benzothiazole dimerizes with Arnt and complexes with XRE on the CYP1A1 promoter and ac-

tivates gene transcription. 5F 203 then binds to CYP1A1 and gets metabolized to reactive intermediate(s). Highly electrophilic, intermediate(s) bind(s) DNA and form(s) DNA adducts and single strands breaks leading ultimately to the cell death *in vitro* and *in vivo*. It appears from this model that metabolism is essential for 5F 203 antiproliferative activity through DNA adduct formation [253] [141] [146].

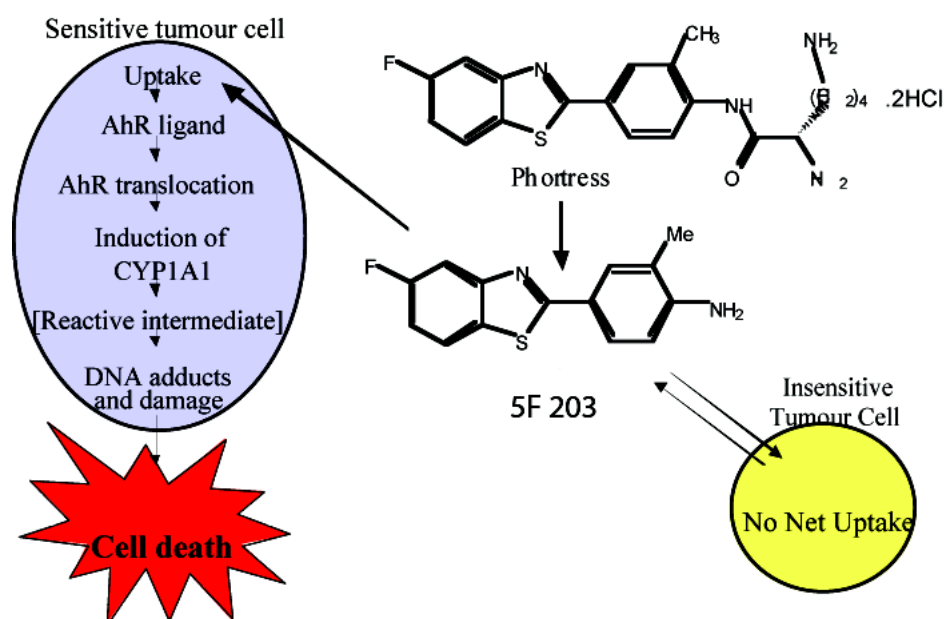


Figure 1.8 Mode of action of Phortress. (Adapted from [248]). See text for discussion.

DNA adducts accumulated in MCF-7 cells treated with 1 μ M 5F 203 within 2 h and attained saturation levels at 24 h. At concentrations > 100 nM, adducts were detected in DNA of MCF-7 cells treated with 5F 203. At 1 μ M 5F 203, one major adduct and few minor adducts were formed. Increasing the concentration to 10 μ M led to the formation of a new dominant adduct in MCF-7 cells [146].

Engagement of apoptotic machinery (CD95/FAS1, upregulation of P53 and P21, downregulation of Bcl-2)[147] and detection of single-strand breaks has been observed in responsive mammary carcinoma cells following treatment with benzothiazole analogues [148]. The drug candidate 5F 203 also induced mRNA levels of IL-6, an NF-kappaB-responsive gene, in MCF-

7 cells, but not in MDA-MB-435 cells, as determined by quantitative RT-PCR. Based on that, it was suggested that 5F 203 activation of the NF-kappaB signaling cascade may contribute to 5F 203-mediated anticancer activity in human breast cancer MCF-7 cells [149]. Recently, with the aim of characterising the pathways involved in 5F 203 toxicity, cDNA microarrays were used to determine gene expression changes in both sensitive MCF-7 cells and resistant MDA-MB-435 after treatment with 1 μ M 5F 203 [150]. The results revealed that AhR-regulated genes, DNA-damage responsible genes, and a PLAcental Bone morphogenetic (PLAB) gene (a gene encoding for a member of TGF- β superfamily and encoding a proapoptotic protein) were induced in MCF-7 but not in MDA-MB-435 cells. 5F 203 accumulates human breast cancer MCF-7 cells in G1 and S phase, and induces the formation of DNA adducts.

Overall, AhR pathway activation then subsequently CYP1A1 induction seems to be essential for 5F 203 metabolism. But whether metabolism and/or AhR activation are prerequisites for 5F 203 antitumour activity will be the subject for future studies.

Section 1.6.1.4 Structure-Activity Relationships (SARs)

Benzothiazole molecules contain a benzene ring fused to a thiazole ring [128]. Their optimised structure is planar. Their antitumour profile is modulated by substitutions at specific positions on the benzothiazole pharmacophore [140] [126]. Structure-activity relationships revealed that compounds with a methyl group (DF 203) or halogen group (Cl, Br, or I) in the 3' position were relatively potent with a selective antitumour activity in MCF-7 and MDA 468 cell lines.

Section 1.6.2 2-(3,4-Dimethoxyphenyl)benzothiazoles (series 2)

Section 1.6.2.1 Background

A new series of 2-phenylbenzothiazoles, the dimethoxyphenylbenzothiazoles, bearing oxygenated substituents on the phenyl ring has been synthesized. The lead compound 2-(3,4-dimethoxyphenyl)-5-fluorobenzothiazole (GW 610; NSC 721648) elicited superior antitumour activity against a range of breast (*e.g.* MCF-7, MDA 468), colon (*e.g.* HCC2998, KM12), non-small cell lung, ovarian and renal cell lines (GI_{50} values < 1 nM) [151].

Section 1.6.2.2 Mechanistic investigation

Mechanistically, like the series (1), activity of series (2) seems to be AhR-mediated. However, their antitumour activity is not restricted to cell lines with inducible CYP1A1.

GW 610 induced CYP1A1 transcription and protein expression in MCF-7 and MDA 468. Importantly, this compound was found active in both CYP1A1 inducible and non-inducible cells (*e.g.* colon cell line HCC2998). In comparison with DF 203 from series (1), GW 610 is active in breast MCF-7 and MDA 468 variant cell lines with acquired resistance to DF 203, however, MCF-7 and MDA 468 variant lines exhibiting acquired resistance to GW 610 displayed cross resistance to DF 230 [151]. Exclusively in sensitive cell lines, GW 610 is rapidly depleted from nutrient media, induces G2/M cell cycle arrest and DNA adducts. Overall, the activity of the GW 610 is not CYP1A1-dependent [262].

Section 1.6.2.3 Structure-Activity Relationships (SARs)

Structure-activity relationships revealed that, unlike the series (1), the presence of a fluorine atom, at the position 5 in the benzothiazole ring, is essential for antitumour activity. For instance,

its removal yields the inactive compound (AW 892). Moreover, shifting the fluorine atom from position 5 to the position 4 or 6, resulted in an attenuated activity in colon cell lines but not in breast and lung cancer cell lines. In the phenyl ring, the dimethoxy moiety was found essential for activity in positions 3 and 4. For instance, an introduction of a methylenedioxy bridge at this position, inactivates the compound (JMB 81). Finally, it seems that the compounds of this series are very sensitive to substituent modifications [151].

AIMS

The study described here was undertaken to establish the correlation between binding, induction and growth inhibitory potency of the phenylbenzothiazoles (series 1 and 2) in rat and generate a QSAR model on the binding affinity and the induction potency of the phenylbenzothiazoles in order to elucidate the mechanism of action of these compounds.

The specific objectives were to:

- Characterize the binding (derived as inhibition constants K_i) of the phenylbenzothiazoles (series 1 and 2) to the AhR by means of a radioactive competitive binding assay in rat cytosol.
- Characterize the induction potency of the phenylbenzothiazoles (series 1 and 2) (EC_{50}) for *CYP1A1* mRNA in rat H4-II-E cells.
- Characterize the growth inhibitory potency (GI_{50}) of the phenylbenzothiazoles (series 1 and 2) in H4-II-E cells.

Chapter 2 Materials and Methods

Section 2.1 Materials

Section 2.1.1 Animals

Male Wistar rats CRL:WI (2-3 weeks, 200-250g) were purchased from Life Sciences, Charles River laboratories (251 Ballardvale Street, Wilmington, MA 01887-1000). The animals were housed in cages under standard laboratory conditions (24°C, 60% humidity, 12 hours dark/light cycle) and had access to standard laboratory chow and water *ad lib*. The animals were given 3 days to adapt to the standard laboratory conditions. These animals were used for cytosol preparation following liver perfusion.

Section 2.1.2 Cell lines and cell culture chemicals

Human Caucasian breast adenocarcinoma MCF-7	cat.no 86012803
Rat hepatoma H4-II-E	cat.no 85061112
Minimum essential medium eagle (MEM) 100x	cat.noM2279
Non essential amino acid solution (MEM) 100x	cat.noM7145
Dulbecco's phosphate buffered saline	cat.noD8537
Fetal bovine serum	cat.no F7524
L-Glutamine-penicillin-streptomycin 100x solution	cat.noG1146
Trypsin-EDTA solution 10x	cat.noT4174

Both cell lines were purchased from Sigma Ecacc and culture chemicals were purchased from

Sigma (The Old Brickyard, New Road, Gillingham, SP8 4XT Dorset).

Section 2.1.3 Kits and reagents

Absolutely RNA® Miniprep kit (cat.no 400800), Affinity Script QPCR cDNA synthesis kit (cat.no 600559) and Brilliant® multiplex QPCR Master Mix (cat.no 600553) were purchased from Stratagene (Gebouw California, Hogehilweg 15, 1101 CB Amsterdam Zuidoost, The Netherlands).

Quanti-iT™ Ribogreen® RNA assay kit (cat.no R11490), Quanti-iT™ Pibogreen® dsDNA assay kit (cat.no P7589) and DNA ladder 1kb plus (cat. no10488-085) were purchased from Invitrogen Molecular Probes (3 Fountain Drive, Inchinnan Business Park, Paisely, UK PA4 9RF).

ReddyMix PCR Master Mix conc.1.1x (cat.no AB-0575/LD/A) was purchased from ABgene (ABgene House, Blenheim Road, Epsom KT19 9AP, UK).

Section 2.1.4 Compounds

CH-223191 (purity 95.71%) (cat.no 182705) was purchased from Calbiochem (or MERCK, Padge Road, Beeston, Nottingham NG9 2JR, UK).

3-Methylcholanthrene (MC) (purity 98%) (cat.no 213942) was purchased from Aldrich.

Tetrachlorodibenzo-*p*-dioxin (TCDD) (purity 99%) (cat.no ED-901-B) and Tetrachlorodibenzofuran (TCDF) (purity 98%) (cat.no EF-903-C) were purchased from Cerilliant Cambridge isotope laboratories (LGC Promochem, Queens Road, Teddington Middlesex TW11 OLY, UK).

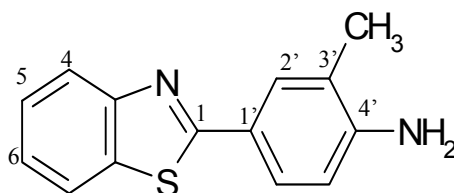
Benzothiazole test chemicals were synthesized by the Cancer Research Laboratories at the University of Nottingham, UK and the Drug Synthesis and Chemistry Branch, NCI, following pub-

lished methods [126]. Benzothiazole test chemicals and Camptothecin were kindly provided by Dr Tracey Bradshaw.

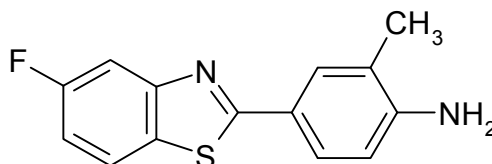
TCAOB was a gift from Dr. Andy Smith (MRC Toxicology Unit, Leicester). The compound 1c was kindly provided by Astrazeneca and was synthesized following published methods [152]. Tetrachlorophenothiazine (TCPT) compound was provided by Dr.Kristian Fried [196].

Compound structures were drawn using CDS/ISIS DRAW Program:

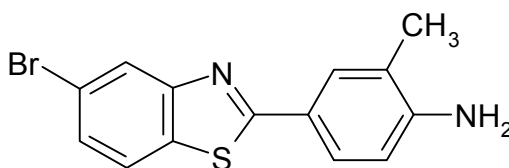
A- 2-(4-aminophenyl)benzothiazoles (series 1):



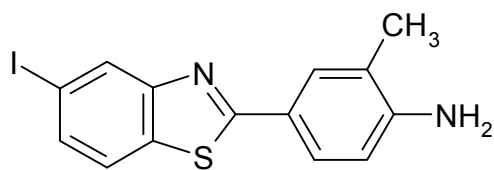
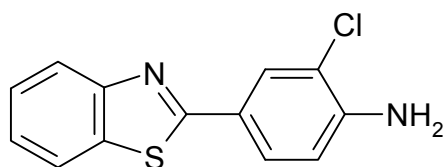
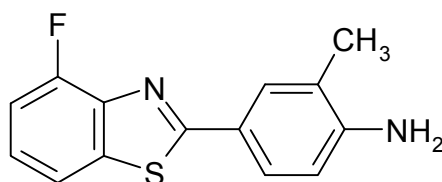
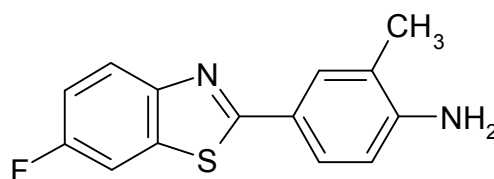
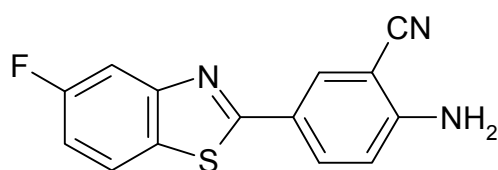
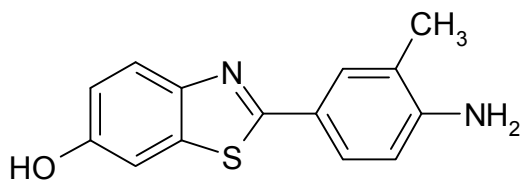
2-(4-amino-3-methylphenyl)benzothiazole [**DF 203**]

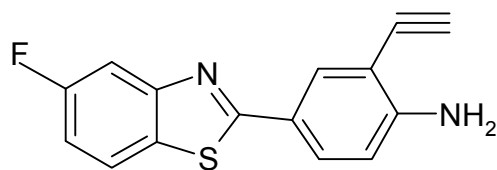


2-(4-amino-3-methylphenyl)-5-fluorobenzothiazole [**5F 203**]

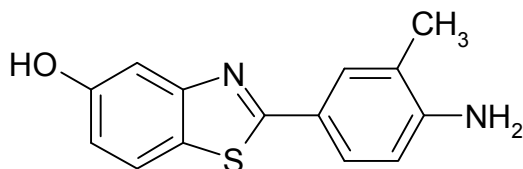


2-(4-amino-3-methylphenyl)-5-bromobenzothiazole [**IH 318**]

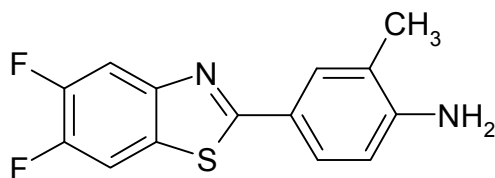
2-(4-amino-3-methylphenyl)-5-iodobenzothiazole [**IH 278**]2-(4-amino-3-chlorophenyl)benzothiazole [**DF 229**]2-(4-amino-3-methylphenyl)-4-fluorobenzothiazole [**IH 220**]2-(4-amino-3-methylphenyl)-6-fluorobenzothiazole [**IH 168**]2-(4-amino-3-cyanophenyl)-5-fluorobenzothiazole [**IH 352**]2-(4-amino-3-methylphenyl)-5-hydroxybenzothiazole [**IH 130**]



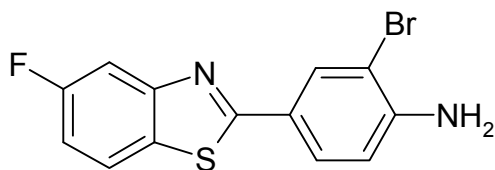
2-(4-amino-3-acetylphenyl)-5-fluorobenzothiazole [IH 445]



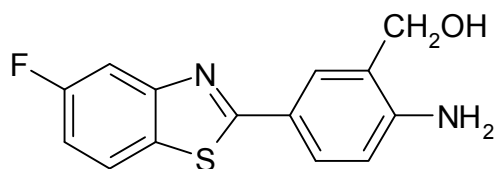
2-(4-amino-3-methylphenyl)-5-hydroxybenzothiazole [IH 186]



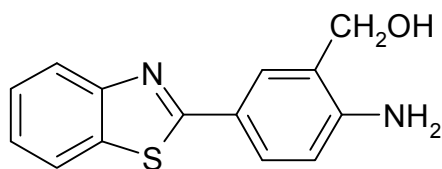
2-(4-amino-3-methylphenyl)-5,6-difluorobenzothiazole [IH 321]



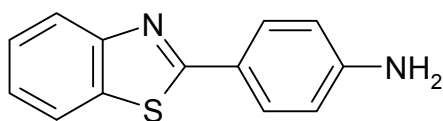
2-(4-amino-3-bromophenyl)-5-fluorobenzothiazole [IH 277]



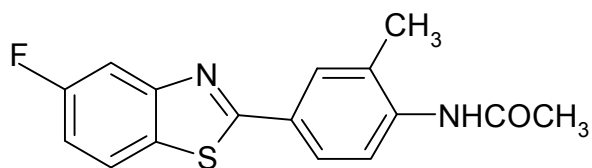
2-(4-amino-3-hydroxymethylphenyl)-5-fluorobenzothiazole [IH 353]



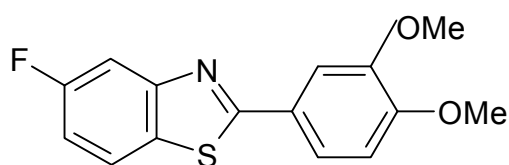
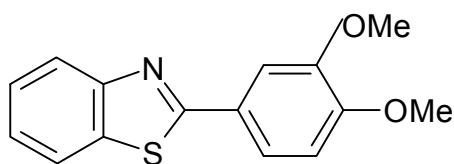
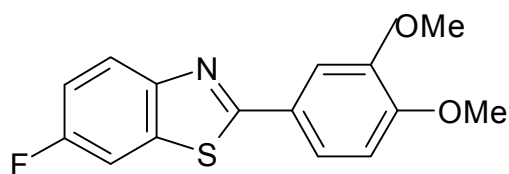
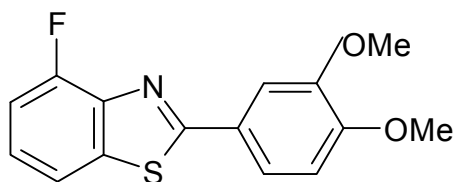
2-(4-amino-3-hydroxymethylphenyl)benzothiazole [IH 224]

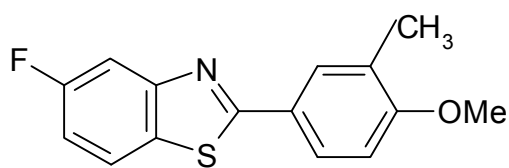
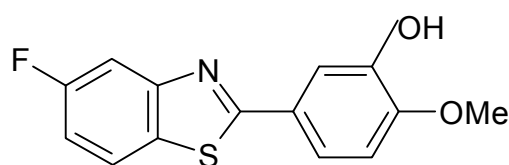
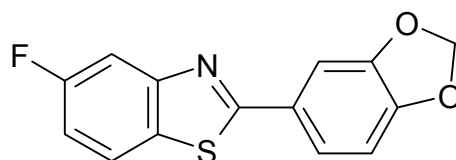


2-(4-aminophenyl)benzothiazole [CJM 126]

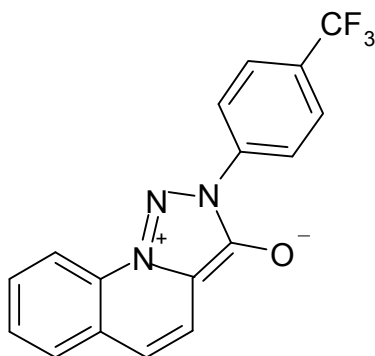
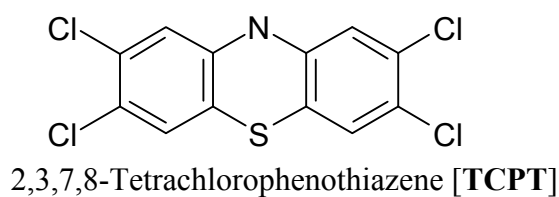
2-(4-aminocarbonylmethyl-3-methylphenyl)-5-fluorobenzothiazole[**IH 128**]

B- 2-(3,4-Dimethoxyphenyl)benzothiazoles (series 2):

2-(3,4-dimethoxyphenyl)-5-fluorobenzothiazole [**GW 610**]2-(3,4-dimethoxyphenyl)benzothiazole [**AW 892**]2-(3,4-dimethoxyphenyl)-6-fluorobenzothiazole [**AW 898**]2-(3,4-dimethoxyphenyl)-4-fluorobenzothiazole [**4F 610**]

2-(3-methylphenyl-4-methoxy)-5-fluorobenzothiazole [**JP-1**]2-(3-hydroxyphenyl-4-methoxy)-5-fluorobenzothiazole [**JP-2**]2-(3,4-methylenedioxyphenyl)-5-fluorobenzothiazole [**JMB 81**]

C-Miscellaneous:



Compound **1c** from Astrazaneca

3-Hydroxy-2-[4-(trifluoromethyl)phenyl]-[1,2,3]-triazolo[1,5-a]quinolinium hydroxide.

Section 2.1.5 Buffers

MN stock buffer (pH 7.5 at 4°C) : 25 mM MOPS + 0.02 % Sodium Azide.

MEN stock buffer (pH 7.5 at 4°C) : MN buffer + 1 mM EDTA.

MDENG stock buffer (pH 7.5 at 4°C) : MEN buffer + 10 % (w/v) glycerol + 1 mM dithiothreitol (DTT). (DTT is freshly supplemented to the buffer before the protein preparation).

TE buffer: 10 mM Tris-HCl, 1 mM EDTA, pH 7.5.

5x TBE buffer

0.45 M Tris-Borate (pH 8.3)

0.01 M EDTA

10x Loading dye

50 % glycerol

0.25 % bromophenol blue

0.25 % xylene cyanol FF

1 mM ethylenediaminetetraacetic acid (EDTA)

10x DNase I Buffer

500 mM Tris-HCl (pH 7.5)

100 mM MgCl₂

0.5 mg/ml nuclease-free bovine serum albumin (BSA)

10x MOPS buffer (pH 7.0):

0.2 M MOPS (3-[N-morpholino] propanesulfonic acid

0.05 M sodium acetate

0.01 M (EDTA)

Loading buffer (100µl total volume)

10 µl 10x MOPS buffer

11.5 µl RNase-free water

50 µl of deionized formamide

17.5 µl 37% formaldehyde solution

10 µl 10x loading dye

1 µl 10 mg/ml ethidium bromide

Lysis buffer- β -ME: 7 μ l of β -ME to each 1 ml of Lysis Buffer (provided with Absolutely RNA® Miniprep kit).

Section 2.1.6 Solutions

[³H]-TCDD

The radioligand [³H]-TCDD (specific activity 34.7 Ci/mmol, 0.929 mCi/ml in toluene/CH₃OH, 1 x 500 mCi) was from ChemSyn Laboratories (13605 W. 96th Terr, Lenexa, Kansas, U.S.A., 66215-1297). The concentration of [³H]-TCDD was calculated 26 μ M (SA = 29,77 Ci /mmole). From this stock, a 535 nM top stock was prepared by diluting with *p*-Dioxane and stored at -20°C. The radioligand was diluted to the working concentration (200 nM) immediately prior to use.

Cold TCDD

The top stock solution of TCDD (155 μ M) was prepared in DMSO and stored at room temperature protected from light.

TCAOB

It was prepared as 3 mM top stock dissolved in *p*-dioxane and stored at room temperature protected from light, and diluted to the working concentration (20 μ M) for experimental procedures.

Phenylbenzothiazoles (PBT)

Stock solutions (20 mM) of phenylbenzothiazoles compounds were prepared in DMSO, and stored protected from light at -20°C. Prior to experimentation, these test agents were diluted to the desired working concentrations.

TCDF

Stock solution (20 mM) of TCDF compounds was dissolved in *p*-dioxane and stored at room temperature protected from light. Prior to experimentation, TCDF was diluted to the desired working concentrations.

Astrazeneca compound 1c and MC

Stock solutions (20 mM) of TCDF and MC compounds was dissolved in *p*-dioxane and stored at -20°C protected from light. Prior to experimentation, these drugs were diluted to the desired working concentrations.

TCPT

Stock solution (1 mM) of TCPT was prepared in DMSO, and stored protected from light at -20°C. Prior to experimentation, TCPT was diluted to the desired working concentrations

MTT solution

Thiazolyl Blue Tetrazolium Bromide, MTT chemical, (purity 98%), was purchased from Sigma (cat.no M5655-1G). MTT stock solution was prepared in water at 2 mg/ml and stored at 4°C, protected from light.

Dextran-coated charcoal (DCC) stock suspension

DCC was purchased from Sigma (cat no. C-6241). It was prepared as follows: 0.67 g of charcoal-dextran coated powder was resuspended in 10 ml of ice-cold MDENG for a final concentration of 10 mg/ml (2 mg of charcoal /mg cytosolic protein) and stored at 4°C, wrapped with aluminium foil, at least one day prior to experiment.

DNase solution

50 µl of DNase Digestion Buffer + 5 µl of reconstituted RNase-Free DNase I (prepared according to Stratagene's instructions).

Abgene's PCR readyMix (1.3x) (per final 1x reaction)

0.625 units ThermoPrime Taq DNA polymerase

75 mM Tris-HCl (pH 8.8 at 25°C)

20 mM (NH₄)₂SO₄

1.5 mM MgCl₂

0.01% (v/v) Tween[®] 20

0.2 mM each of dATP, dCTP, dGTP and dTTP

Section 2.1.7 Gels**1% agarose gel (100 ml)**

1 g agarose

88 ml RNase-free water

10 ml 10x MOPS buffer

2.7 ml 37% formaldehyde

8% TBE gel (100 ml)

26.6 ml 30% Acrylamide

52.7 ml water

20 ml 1x TBE

0.7 µl 10% APS

50 µl TEMED

Section 2.1.8 Real-time RT-PCR primers and probes

Real-time RT-PCR primers and probes for human genes were designed using primer 3 (<http://frodo.wi.mit.edu/>) and synthesized by the genomic company Eurofins MWG Operon for primers and probes synthesis. The rat primers and probes were designed by Dr Tao Jiang [153]. The primer and probe sequences, the gene accession numbers, and the probe labels for rat and human are listed in (Table 2.1 & Table 2.2) respectively.

To avoid amplification from traces of possible contaminating DNA in the RNA isolation, one of the two primers was placed at the junction between two exons (for rat, *CYP1A1*, β -actin and *AhR* genes and human β -actin and *AhR* genes). Except for the human *CYP1A1* gene, the probe was designed to span the junction between two exons. Primers were checked for specificity by Blast search using the relative NCI BLAST search. The human primer pairs give rise to PCR products of 122 bp, 139 bp and 150 bp for *CYP1A1*, β -actin and *AhR* respectively.

Rat Gene	Oligonucleotide sequence	Genebank accession No	Labels
<i>CYP1A1</i> F R P	CCA CAG CAC CAT AAG AGA TAC AAG CCG GAA CTC GTT TGG ATC AC ATA GTT CCT GGT CAT GGT TAA CCT GCC AC	X00469	FAM-BH1
<i>AhR</i> F R P	GCA GCT TAT TCT GGG CTA CA CAT GCC ACT TTC TCC AGT CTT A TAT CAG TTT ATC CAC GCC GCT GAC ATG	Af082124	HEX-BH2

Table 2.1 RT-PCR oligonucleotides primers for rat genes. The primers and probes are identified by letters designating the forward (F) and, reverse (R) primer or the probe (P), and a number corresponding to the position of the base at the 5' end of the positive strand of primer or probe in the reference sequence, according to gene bank accession number. Sequences are given from 5'→3'. The reporter dye is at the 5' end of the oligonucleotide, and the quencher dye Black-Hole-1 or -2 is at the 3' end; FAM, iscarboxy fluorescein; Hex, hexachlorofluorescein; ROX, 5(6)-carboxy-X-rhodamine.

Rat Gene	Oligonucleotide sequence	Genebank accession No	Labels
<i>β-Actin</i> F R P	CTG ACA GGA TGC AGA AGG AG GAT AGA GCC ACC AAT CCA CA CAA GAT CAT TGC TCC TCC TGA GCG	V01217	ROX-BH1

Table 2.1 RT-PCR oligonucleotides primers for rat genes. The primers and probes are identified by letters designating the forward (F) and, reverse (R) primer or the probe (P), and a number corresponding to the position of the base at the 5' end of the positive strand of primer or probe in the reference sequence, according to gene bank accession number. Sequences are given from 5'→3'. The reporter dye is at the 5' end of the oligonucleotide, and the quencher dye Black-Hole-1 or -2 is at the 3' end; FAM, iscarboxy fluorescein; Hex, hexachlorofluorescein; ROX, 5(6)-carboxy-X-rhodamine.

Human Gene	Oligonucleotide sequence	Genebank accession No	Labels
<i>CYP1A1</i> F R P	GTT GTG TCT TTG TAA ACC AGT G CTC ACT TAA CAC CTT GTC GAT A CAA CCA TGA CCA GAA GCT ATG GGT	NC_000015	FAM-BH1
<i>AhR</i> F R P	ATA CAG AGT TGG ACC GTT TG CTT TCA GTA GGG GAG GAT TT TCA GCG TCA GTT ACC TGA GAG CCA	NC_000007.12	HEX-BH2
<i>β-Actin</i> F R P	GAC ATG GAG AAA ATC TGG C AGG TCT CAA ACA TGA TCT GG ACA CCT TCT ACA ATG AGC TGC GTG T	NC_000007	ROX-BH1

Table 2.2 RT-PCR oligonucleotides primers for human genes. The primers and probes are identified by letters designating the forward (F), and reverse (R) primer or the probe (P), and a number corresponding to the position of the base at the 5' end of the positive strand of primer or probe in the reference sequence, according to gene bank accession number. Sequences are given from 5'→3'. The Reporter dye is at 5' end of the oligonucleotide, and the quencher dye Black-Hole-1 or -2 is at 3' end. FAM, iscarboxy fluorescein; Hex, hexachlorofluorescein; ROX, 5(6)-carboxy-X-rhodamine

Section 2.2 General laboratory methodology

Section 2.2.1 Receptor preparation

AhR was prepared from rat liver cytosol given it is rich in AhR proteins. The preparation requires that all materials should be autoclaved and all work carried on ice. The rats were first administered a single intra-peritoneal dose of 0.3 ml Dolethal (200 mg/ml) (purchased from Vetoquinol Company) and then death confirmed by cervical dislocation. The livers were perfused immediately with cold 150 mM KCl, pH 7.4 via the hepatic portal vein. While perfusing, the inferior vena cava was cut to discard blood. It is essential to perfuse efficiently with cold

buffer in attempts to minimize contamination by endogenous proteases. Livers were quickly removed, weighed, minced on a dish placed on ice with scissors in cold MDENG buffer, decanted and homogenized in 5-volumes of MDENG (v/w) at 0°C in a Potter-Elvehjem glass homogenizer fitted with a Teflon pestle. The homogenate was centrifuged at 12,000 x g for 20 min at 4°C in a Beckman J21-21 centrifuge. The supernatant was removed avoiding lipid layers on top and subjected to ultracentrifugation at 440,000 x g for 25 min at 4°C. Aliquots of this supernatant, referred as hepatic cytosol, were stored at -80°C until use.

Section 2.2.2 Determination of protein concentrations

Protein concentration was determined using the Bradford method using Bio-Rad reagents with bovine serum albumin as the standard [155].

Section 2.2.3 [³H]-TCDD Binding assay

Section 2.2.3.1 Principle

The binding assay using radiolabeled [³H]-TCDD in liver cytosol was extensively used to determine the binding affinities of several compounds relative to the TCDD's K_D [164] [66] [157] [158] [67] [159]. The radioligand [³H]-TCDD and non radioligand competitor (TCAOB) are equilibrated with a preparation containing AhR receptor (hepatic cytosolic protein) for a certain time sufficient to reach the binding equilibrium. Parallel experiments were run with an unlabeled competitor (TCAOB) known to bind to the same receptor population. TCAOB was added in excess concentration to define the non-specific binding of [³H]-TCDD.

The unbound radioligand was removed by adsorption to dextran-coated charcoal solution. The assay is terminated by this step, and the radioactivity quantified. [³H]-TCDD remaining in the cytosol after adsorption represents the total binding ("specific" and "nonspecific"). The sub-

straction of the nonspecific binding from the total binding defines the specific binding of the preparation. The radioactive signal corresponds to the concentration of radioligand bound to the receptor.

Section 2.2.3.2 Methodology

The radioligand binding assay described in this work is slightly modified from the classic assay. The conditions of the binding assay were as described [164], except using tetrachloroazoxybenzene (TCAOB) [66] as a competitor.

The frozen cytosolic aliquots from rat liver protein preparation were diluted in ice-cold MDENG buffer to a concentration of 5 mg of protein /ml prior to each experiment. The general procedure in binding assays consists of adding 1 μ l of 200 nM [3 H]-TCDD in *p*-dioxane to the solution of proteins (rat liver cytosolic preparation or bovine serum albumin) to a final concentration of 1 nM in 200 μ l total volume, unless indicated differently in the individual figure legends. In order to define the non specific binding (NSB) of [3 H]- TCDD, the same experiment was run in parallel with 1 μ l of unlabeled TCAOB (200-fold molar excess of [3 H]-TCDD concentration). The tubes were incubated at 4°C for 16 h. Each sample was analyzed in triplicate.

After the 16-18 h incubation, tubes were vortexed thoroughly (~ 30 seconds) then centrifuged at 1000 x g briefly to collect the solution from the top and the edges of the tubes. The assay was terminated by the addition of 30 μ l dextran-coated charcoal (10 mg/ml in MDENG buffer), unless indicated differently in the individual figure legends, to remove unbound [3 H]-TCDD. Samples were vortexed vigorously and incubated on ice for 10 minutes, followed by centrifugation at 20,000 x g at 4°C for 10 min. A volume of 150 μ l of supernatant were transferred to scintillation vials containing 5 ml scintillation fluid and mixed vigorously before counting.

Parallel to each experiment, the total [^3H]-TCDD in solution, was determined by the transfer of a 30 μl of aliquot to scintillation vials after the 16-h incubation (no charcoal-dextran is added to these tubes). This step is an important control, for total radioactivity in solution.

Radioactivity was determined by liquid scintillation counting using a Packard Tri-carb Model 2100 TR Liquid Scintillation analyser. Data were collected as d.p.m values, then, converted to nM as follows [160]:

$$\text{RL}^* = B / (V \times \text{SA} \times 2220) \text{ nM.}$$

Where B is the radioligand bound (d.p.m) corrected for counter background, V is the volume of radioligand assayed (ml), SA is the specific activity of the radioligand (Curies /mmole), and 2220 is the conversion factor from d.p.m to nanocuries.

Given the high [^3H]-TCDD toxicity, a swipe test was performed regularly, to detect [^3H]-TCDD contamination.

Section 2.2.3.3 [^3H]-TCDD standard binding assay

The standard binding assays were processed essentially as described in binding assay methodology except with incubating 200 μl of aliquots containing receptor preparation with a range of concentration of [^3H]-TCDD \pm TCAOB (200-fold molar excess) for 16 h at 4°C.

Section 2.2.3.4 [^3H]-TCDD competition assay

Section 2.2.3.4.1 Principle

The binding affinity constant of the radioligand [^3H]-TCDD was determined from the saturation experiment. The relative binding affinities, (or inhibition constant K_i) of the test compounds

were calculated from the IC_{50} , the concentration of the test compound which inhibits 50 % of the specific binding of [3H]-TCDD in the absence of the competitor. K_i of test compounds are calculated by GraphPad Prism 5.0 Software using the equation derived by Cheng and Prusoff [161]:

$$K_i = (IC_{50}) / (1 + [L] / (KL))$$

Where, L is the concentration of the radioligand and KL is the IC_{50} value for [3H]-TCDD.

Section 2.2.3.4.2 Methodology:

The competitive assays were run essentially under the same conditions as for [3H]-TCDD binding standard assay. In order to determine the IC_{50} of the competitor that displaces [3H]-TCDD from specific sites, four experiments were run in triplicate, each using 200 μ l cytosol and 1 μ l of either TCDD, TCAOB or test competitor, to define:

- a) Total binding of [3H]-TCDD in the absence of test competitor: cytosols + 1 nM [3H]-TCDD.
- b) Non-specific binding of [3H]-TCDD in the absence of test competitor: a) + 200 nM TCAOB.
- c) Specific binding of [3H]-TCDD in the absence of competitor: a) - b).
- d) Total binding of [3H]-TCDD in the presence of test competitor: a) + increasing concentrations of competitor.
- e) Non specific binding of [3H]-TCDD in the presence of competitor: b) + increasing concentrations of competitor.
- f) Specific binding of [3H]-TCDD displaced from AhR by test competitor: d) - e).

[³H]-TCDD (1 nM) was added to 200 µl cytosolic preparations ± TCAOB (200 nM) ± varying concentration of unlabeled competitor dissolved in DMSO. Competitors were added first from 10-30 minutes to allow equilibrium before the addition of [³H]-TCDD. Steps a), b) and c) are positive controls. Step e) was performed only once for each test competitor with the aim of verifying that the amount of [³H]-TCDD NSB is unchanged in the presence of increasing concentrations of test competitor and to test whether the test competitor and [³H]-TCDD are competing for NSB sites. After validating that the NSB of [³H]-TCDD in the presence of test competitor is similar to that in the absence of the test competitor, the step e) was replaced with step b). Other controls are:

(a) Assay tubes were incubated with 1 µl [³H]-TCDD + 1 µl DMSO (0.5%).

(b) 30 µl of triplicate samples were subjected to counting before treatment with charcoal to assess the concentration of [³H]-TCDD in incubations. All the samples were performed in triplicate. The assay was terminated by the charcoal adsorption as described in binding assay methodology.

Section 2.2.4 Cell cultures

The H4-II-E and MCF-7 cells were cultured in modified Eagle's medium (MEM) containing sodium bicarbonate and supplemented with 10% fetal bovine serum, 1% (200 mM L-glutamine, 10,000 U penicillin and 10 mg/ml Streptomycin) solution 100x, 1% MEM nonessential amino acid solution 100x. The cells were cultured in a humidified atmosphere with 5 % CO₂ at 37°C.

Section 2.2.5 Cell growth curves

MCF-7 and H4-II-E cells were plated in triplicate in 96 well plates at the densities of 2.5×10^3 and 5×10^3 cells in 180 µl per well of medium respectively for 7 consecutive days at 37°C/5 %

CO₂ to reach 90-95% confluence. On the third day, the old medium in cultures was replaced by fresh medium. Each day, medium was removed, cells were washed with 150 µl PBS, trypsinized with 60 µl Trypsin/EDTA and subjected to counting by hemocytometer.

Section 2.2.6 Chemical treatment for the induction assay

Benzothiazole test chemicals and TCDD were prepared in dimethyl sulfoxide (DMSO) at 20 mM and 10 µM top stock solutions respectively. Prior to each experiment, concentrations were prepared in DMSO then further diluted with fresh (first two experiments) or incubation medium (all subsequent experiments) into the working concentrations at the final concentration of 0.1% or 0.5 % immediately before use.

The solubility of the top stock solutions and the incubation concentrations was assessed visually by examining precipitation formation and solution turbidity. None of the chemicals used were found insoluble at the concentrations mentioned above. However, that was not confirmed analytically.

All experiments were conducted using the same source of each benzothiazole test chemicals and one top stock solution of TCDD that was aliquoted in Eppendorf tubes and stored at -20°C till further use.

H4-II-E and MCF-7 cell cultures (90-95% confluent) were treated with 20 µl of incubation medium containing the test chemical and TCDD or vehicle DMSO. For experiments on TCDD and test chemicals with 10 µM as the highest concentration, the final concentration of DMSO in the cultures was 0.1%, whereas for experiments on test chemicals with 30 µM as the highest concentration, the DMSO final concentration was 0.15%. At these concentrations, DMSO was not found toxic and did not increase the *CYP1A1* expression above the constitutive basal levels. MCF-7 and H4-II-E cultures were seeded in triplicate in 96 well plates at a cell density of 5 x

10^4 and 1×10^5 cells per well respectively and incubated for 24 h at $37^\circ\text{C}/5\% \text{ CO}_2$ to reach 90-95% confluency. Cell confluence was assessed visually at 24 h and the incubation medium was replaced with the incubation medium containing the test chemical (indicated concentrations), the positive control (TCDD 10 nM) or negative control (DMSO 0.1%) for 4 h. Untreated cells were included as a negative control in all experiments. To compare the maximal inducing effect for *CYP1A1* mRNA for each chemical with that of TCDD, the concentration response curves for all test-chemicals were generated relative to the maximally inducing concentration of TCDD (10 nM) unless indicated differently in the individual figure legends.

Section 2.2.7 Preparing H4-II-E and MCF-7 cells before total RNA isolation

Following incubation with the indicated chemical(s), medium containing the test chemical was removed and cultures were washed with 100 μl of phosphate buffered saline (PBS). The PBS was then replaced with 60 μl Trypsin/EDTA. When cells were detached, they were resuspended in 120 μl CMEM, then transferred to microcentrifuge tubes and centrifuged at $5000 \times g$ for 5 min at 4°C . Cell pellets were resuspended in phosphate buffer saline and centrifuged for another 5 min at $5000 \times g$ at 4°C . Cell pellets were frozen at -20°C until ready for total RNA isolation.

Section 2.2.8 RNA isolation

Total RNA from H4-II-E cells was isolated according to the Absolutely RNA protocol (Stratagene), with minor modifications.

The optimized protocol is the following:

1. For low-density cells (1×10^4 - 1×10^5 cell number), add 100 μl Lysis buffer- β -ME mixture to the cell pellet and vortex to homogenise. For high-density cells (1×10^5 - 1×10^6 cell number), lyse with 200 μl Lysis buffer- β -ME (prepared freshly).

2. Add an equal amount of 70% ethanol to the lysates and vortex the tubes well.
3. Transfer the lysates in ethanol to an RNA binding spin cup and spin in a microcentrifuge at maximum speed for 1 minute at room temperature.
4. Discard the filtrate and add 400 μ l of 1x Low-Salt Wash Buffer and spin in a microcentrifuge at maximum speed for 1 minute at room temperature.
5. Add 50 μ l of DNase I solution (prepared freshly) onto the fiber matrix and incubate the samples at 37°C for 15 minutes in a water incubator.
6. Add 400 μ l of 1x High-Salt Wash Buffer and spin in a microcentrifuge at maximum speed for 1 minute at room temperature.
7. Discard the filtrate and add 400 μ l of 1x Low-Salt Wash Buffer and spin in a microcentrifuge at maximum speed for 1 minute at room temperature.
8. Discard the filtrate and add 200 μ l of 1x Low-Salt Wash Buffer and spin in a microcentrifuge at maximum speed for 2 minutes at room temperature.
9. Transfer the spin cup to a 1.5 ml microcentrifuge tube and discard the receptacle tube.
10. Add 30 μ l of Elution Buffer directly onto the centre of the fiber matrix inside the spin cup and cap the spin cup. Incubate at room temperature. Spin the tube in a microcentrifuge at maximum speed for 2 minutes at room temperature.
11. Store RNA in the Elution Buffer at -80°C.

Section 2.2.9 Quantitation of total RNA

The quantity of total RNA was determined using a RiboGreen RNA quantitation kit (Molecular Probes, Eugene, OR). It consists on measuring the fluorescence of RiboGreen, a fluorescent RNA-binding probe, against a standard. The RiboGreen assay was prepared using high range ribosomal RNA (rRNA) standard curve. The standard was generated from 2 µg/ml rRNA using five concentrations including the blank sample (final concentrations ranging from 10 to 500 ng/ml) in a 200 µl volume. 2 µl of each RNA sample was diluted 50-fold with TE buffer. The RiboGreen was diluted 200-fold before performing each standard and 100 µl was added to both the RNA standards and isolated samples. The concentration of total RNA in the samples was extrapolated from the standard curve. The fluorescence was measured using a Wallac Victor² plate reader (Perkin Elmer) instrument set at 485 nm excitation and 510 nm emission. Once the concentration of RNA was determined, the quality of RNA was assessed by the relative intensities of the 28S and 18S rRNA bands visualized by electrophoresis on 1% denaturing agarose gel after ethidium bromide staining.

Section 2.2.10 cDNA synthesis

Total RNA was reverse-transcribed into first strand cDNA using AffinityScript QPCR cDNA synthesis kit. The reverse transcription reaction was prepared from 50 ng total RNA as follows:

In 20 µl total volume:

10 µl of 2x cDNA synthesis master mix.

1 µl of random primers (~100 ng).

1 µl of oligo d(T) (~100 ng).

1 µl of Reverse transcriptase (RT).

x µl of RNase free water.

x μ l of total RNA (50 ng).

In addition, under the same conditions described above, a sample with no RT was run as a negative control for genomic DNA contamination. DEPC-treated water was substituted for RT.

The reverse transcription reaction was initiated by running the samples under the following program:

- 25 °C for 5 minutes.
- 42°C for 45 minutes.
- 95°C for 10 minutes.

Section 2.2.11 Quantitation of cDNA

The quantity of cDNA was determined using a picogreen DNA quantitation kit (Molecular Probes, Eugene, OR). It consists of measuring the fluorescence of PicoGreen, a fluorescent DNA-binding probe relative to a λ DNA standard curve. The standard was generated from 2 μ g/ml λ DNA using five concentrations including the blank sample (final concentration ranging from 10 to 200 ng/ml) in a 200 μ l volume. A volume of 5 μ l of each RNA sample was diluted 20-fold with TE buffer. The Picogreen was diluted 200-fold before performing each standard and 100 μ l was added to both the DNA standards and cDNA samples. Concentration of unknown cDNA in the samples was extrapolated from the standard curve. The fluorescence was measured using Wallac Victor² plate reader (Perkin Elmer) set at 485 nm excitation and 510 nm emission.

Section 2.2.12 Polymerase Chain Reaction PCR

Before running the qRT-PCR on the cDNA samples, each set of primers and probes for individual genes were tested on the cDNA samples by amplification with a ordinary PCR reaction then run on an 8% acrylamide TBE gel to test for the specificity of the primers and for genomic contamination in the samples.

	Volume	Final Concentration 1X
ReddyMix PCR Master Mix	22.6 μ l	1X
Primer forward (12.5 μ M each)	0.7 μ l	0.35 μ M
Primer reverse (12.5 μ M each)	0.7 μ l	0.35 μ M
Nuclease-free water	variable	
DNA template	1 μ l	1 ng
Total volume	25 μ l	

Table 2.3 PCR experimental reaction.

	Temperature	Time	Number of cycle
Initial denaturation	94°C	2 min	1 cycle
Denaturation	94°C	1 min	35 cycles
Annealing	58 °C	30 sec	
Extension	70°C	30 sec	
Final extension	70°C	10 min	1 cycle

Table 2.4 PCR thermal cycler programme.

A negative control consists of substituting the DNA template with 1 μ l Nuclease-free water. PCR products were then analyzed on a 8% TBE gel electrophoresis along with a DNA ladder.

Section 2.2.13 Quantitative Real-Time RT-PCR using TaqMan[®] probes

Section 2.2.13.1 Principle

TaqMan real-time PCR provides a fluorescence measurement of mRNA expression during each cycle of a PCR protocol. It is a quantitative analysis of mRNA expression based on PCR cycling threshold (Ct) values using MX4000 software. The TaqMan RT-PCR was used to assess the inducibility of *CYP1A1* and the expression of *AhR* and β -*actin*. It allows study of changes in gene expression by measuring messenger RNA (mRNA) levels in total RNA extracted from rat H4-II-E and human MCF-7 cells.

The Stratagene's Brilliant[®] multiplex QPCR master mix allows more targets (up to four) to be amplified with a normalizing gene in the same reaction by using probes with spectrally different fluorophores for the detection of each amplicon. *CYP1A1*, *AhR* and β -*actin* mRNA were run simultaneously in the same qRT-PCR reaction. *CYP1A1*, and *AhR* mRNA expression was quantitated by performing comparative Ct method for relative quantitation of gene expression using TaqMan real-time Multiplex quantitative PCR technology with β -*actin* as the endogenous control. The use of β -*actin* as reference RNA, was based on the fact that β -*actin* RNA measurements in both H4-II-E and MCF-7 cells were unchanged at all treatment concentrations (finding proven in the actual study in Chapter 3). The first step consists of evaluating the protocol by administering TCDD to the H4-II-E cells. Once evaluated, the protocol was used for the rest of the test compounds.

Section 2.2.13.2 Analysis

Gene expression analysis was performed using the relative quantitation method by Pfaffl (2001) [162]. Quantitation of RNA copy number of the target gene was calculated from the experimen-

tal Ct values. The threshold Ct value for each DNA was adjusted so that the Ct value is in the exponential phase of the PCR reaction. The threshold was kept constant throughout the analysis for all the experiments. That is for *CYP1A1*, *β-actin* and *AhR* 2000, 200 and 200 respectively. In each experiment, an independent control sample was included and run along with the samples. The Ct of this external control was used as a calibrator. Negative controls were run side by side with samples for each RT-PCR reaction. These were no-RT and no-RNA samples.

First, the Ct of the target gene was normalized to that of the external control (RNA from rat tissue liver homogenate treated with dioxin), for both treated (test) and vehicle (DMSO) samples: $\Delta Ct = Ct_{(target)} - Ct_{(external\ control)}$. The copy number of the test chemical, vehicle and untreated samples was normalized to that of internal control (*β-Actin*) as target/ *β-actin* ratio. Then, the $\Delta\Delta Ct$ was converted to copy number after correcting for qRT-PCR efficiency for each target according to the equation $= E^{-\Delta\Delta Ct}$. Finally, the ratio was normalized to control untreated cells, vehicle treated cells or 10 nM TCDD-treated cells according to the experiment.

Section 2.2.13.3 Quantification by real-time RT-PCR

Once the quantity of cDNA was determined, 2 ng of cDNA was subjected to qRT-PCR amplification. Briefly, the Multiplex qRT-PCR reaction was set up using Brilliant[®] Multiplex QPCR Master Mix (refer to Table 2.6) and amplified using a TaqMan thermal cycler (Mx4000). The Multiplex real-time (RT-PCR) reactions were run under the conditions cited in Table 2.5.

Number of cycles	Time	Temperature
1	10 min	95°C
40	20 sec 1 min; 30 sec	95°C 58°C

Table 2.5 qRT-PCR cycling protocol. The conditions for the multiplex real-time PCR reactions were one cycle at 95 °C for 10 min, followed by 40 cycles at 95°C for 20 s, and 58°C for 90 s

qRT-PCR experimental reaction (12.5µl rxn)
2.375 µl Nuclease-free PCR-grade water H2O
5.25 µl of 2x master mix
2 µl cDNA
<i>CYP1A1</i>
0.25 µl of FAM
0.125 µl of reverse primer
0.125 µl of forward primer
<i>β-Actin</i>
0.5 µl of ROX
0.25 µl of reverse primer
0.25 µl of forward primer
<i>AhR</i>
0.75 µl of HEX
0.25 µl of reverse primer
0.375 µl of forward primer

Table 2.6 Multiplex real-time RT-PCR experimental reaction. The volume of master mix, water, the pair of primers and the probes as indicated for each gene in 12.5 µl of buffer solution qRT-PCR experimental reaction.

Section 2.2.13.4 qRT-PCR standard curves

To define the QPCR efficiency (E), a standard curve of the three genes, *CYP1A1*, *β-actin* and

AhR was generated by stepwise dilutions of cDNA in both human and rat cell lines. Human and rat cDNA samples used to generate the standard curves were prepared from MCF-7 and H4-II-E cells treated with TCDD (10 nM) for 4 h respectively. cDNA at 2 ng/μl initial concentration was further diluted 5-fold to the final concentration of 16 pg/μl. A duplicate of the four samples (2000, 400, 80 and 16 pg/μl) was subjected to Multiplex real time RT-PCR reaction.

The standard curves for each dye were generated using the least mean squares curve fitting logarithm by MX4000. The R Squared (RSq) or regression value is determined for each standard from the equation for the line [$y = m \log x + b$, where m is the slope of the line]. The RSq value is an indicator of the quality of the fit of the standard curve to the Standard data points plotted. The value will always be between 0 and 1. The closer the value is to 1, the better the fit of the line. The slope of the curve is directly related to the average amplification efficiency throughout the cycling reaction. The equation that relates the slope to amplification efficiency is according to Pfaffl [162]:

$$\text{PCR Efficiency} = 10^{(-1/\text{slope})}.$$

where PCR Efficiency corresponds to the proportion of template molecules that are doubled every cycle. From this equation it follows that a reaction with 100% efficiency will result in a slope of -3.322.

As negative controls, no RT and no template reactions were run in parallel. A sample of cDNA from rat liver chronically treated with dioxin was included as a positive control. Amplification efficiency was used to determine gene copy number as described in Section 2.2.13.2.

Section 2.2.14 Induction protocol

The general conditions consist of incubating H4-II-E cells and MCF-7 cells at 1×10^5 cells and

5×10^4 cells per 180 μ l in 96 well plates respectively. The following day, cultures were treated with vehicle control 0.1% DMSO as a negative control, TCDD (10 nM) as a positive control and the test inducer at the indicated concentrations for 4 h. In the first two experiments, chemical treatment consisted of diluting DMSO, TCDD or the test inducer in a fresh medium prior to addition. In all subsequent experiments, chemicals were diluted into 200 μ l of incubation medium, then 20 μ l of incubation medium containing the chemical was added into the well for a total volume of 200 μ l. Untreated cultures were included as a negative control in all experiments except for the first experiment (Section 3.2.5.1).

Section 2.2.15 Growth inhibitory assay: MTT assay

MTT assay measures the antiproliferative activity of test compounds. The general procedure is essentially as described by [250]. MCF-7 and H4-II-E cells were seeded in triplicate into 96-well microliter plates at a density of 2.5×10^3 cells /180 μ l and 5×10^3 /180 μ l respectively and allowed 24 h to adhere before drugs were introduced (final concentration 0.1nM to 10 μ M, n = 9). In parallel to each treatment, control triplicate cultures were seeded to assess the number of viable cells at the time of the addition of the drugs (time zero, T0). Serial drug dilutions were prepared in medium immediately prior to each assay. The following day, cultures were treated with 20 μ l of the test drugs and 3-(4,5-dimethylthiazol-2-yl)-2,5-diphenyltetrazolium bromide (MTT) was added to the T0 cultures. Cell viability was measured at the time of the drug addition (time zero) and following 72 h exposure by MTT reduction. A volume of 50 μ l MTT was added to each well (final concentration 400 μ g/ml). Incubation at 37°C for 4 h allowed reduction of MTT by mitochondrial dehydrogenase to an insoluble formazan product. Well contents were aspirated and formazan solubilized by addition of 150 μ l DMSO. Absorbance was read on Wallac Victor² plate reader (Perkin Elmer) instrument at 590 nm as a measure of cell viability. Cell viability was assessed using DMSO treated cells as the 100% viable control.

Camptothecin, a known toxic compound [163], was included as a positive control at varying concentrations.

Section 2.2.16 Curve modelling and statistical analysis

All data are represented as mean \pm SD. Statistical significance is tested by Student's *t*-test, paired *t*-test, or one-way analysis of variance (ANOVA) followed by Dunnett's Multiple Range Test. Groups were considered significantly different if $p < 0.05$.

K_D and B_{max} were determined from non linear regression for single site binding hyperbola analysis by GraphPad Prism 5.0 Software (GraphPad Software Inc, San Diego, CA).

[3H]-TCDD log concentration competition curves were fitted using non linear regression for single site competitive binding analysis, IC_{50} values represent the concentrations of test compound required to displace 50% of [3H]-TCDD specifically bound the Ah receptor. IC_{50} values were determined using GraphPad Prism 5.0 Software (GraphPad Software Inc, San Diego, CA).

The concentration-response curves for the *CYP1A1* mRNA induction were modelled using the variable slope sigmoid Hill equation (GraphPad Prism 5.0 Software). The *CYP1A1* mRNA EC_{50} is the concentration at which the induced gene is halfway between the calculated bottom and the top of each concentration-response curve.

Chapter 3

Results

Section 3.1 Characterization of the binding to the rat hepatic Ah receptor

This chapter aims to quantitate the binding of phenylbenzothiazole analogues to the AhR by virtue of a [^3H]-TCDD competitive binding assay. A conventional representation of the binding affinity is the reciprocal of the ligand-receptor complex dissociation constant, and denoted K_D . In this work, the binding affinities will be indirectly presented as the equilibrium dissociation constants for direct binding measurements or inhibition constants K_i for displacement measurements. All experiments were carried - out assuming:

- A single binding site between the drug and the receptor.
- The experiment has reached equilibrium.
- A stable concentration of drug/receptor.
- The binding is reversible and follows the law of mass action.
- There is no cooperativity.
- Receptors are either free or bound to ligand. No partial binding.
- The binding does not alter the ligand or receptor.
- Only a small fraction of ligand binds to the receptor to approximate the free concentration with the added concentration

The binding assay was developed as described [164], except using tetrachloroazoxybenzene (TCAOB) [66] as a competitor. It was essential to optimise several aspects of the assay.

Section 3.1.1 Incubation time

It is essential to determine whether the binding of [^3H]-TCDD to the AhR has reached equilibrium. To investigate this, the time course of specific binding of [^3H]-TCDD to rat liver cytosol was measured.

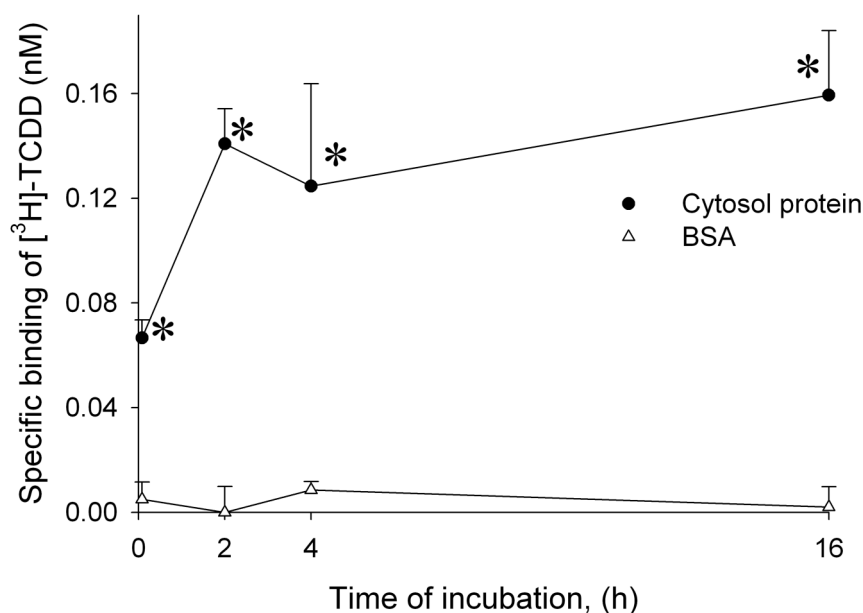


Figure 3.1 Effect of incubation time on $[^3\text{H}]$ -TCDD specific binding to rat cytosolic protein. Rat liver cytosol [●] and bovine serum albumin [Δ] proteins were incubated at 4°C with 1 nM $[^3\text{H}]$ -TCDD \pm 200 nM unlabeled TCAOB at varying times of incubation. At the specified time point, charcoal was added to remove unbound ligand and terminate the assay and radioactivity in the resultant supernatant measured by liquid scintillation spectrometry. The radioactivity remaining in the solution after adsorption with charcoal represents the total binding (“specific and “non specific”). The non specific binding is defined by the radioactivity remaining in solution in the tubes with TCAOB. The specific binding is calculated by subtracting the non specific binding from the total binding. Radioactivity was converted to nanomolar concentrations. Each point represents the average of mean \pm S.D for triplicate samples, and is representative of results obtained from three experiments. (* asterisk; $p < 0.01$, t -test, $n=3$, $[^3\text{H}]$ -TCDD specific binding in CP compared to BSA for each time point). Ordinate: specific binding of $[^3\text{H}]$ -TCDD (nanomolar concentration). Abscissa: Incubation time (0, 2, 4 and 16 h).

Cytosolic protein preparations were incubated with $[^3\text{H}]$ -TCDD (1 nM) \pm TCAOB (200 nM) for different incubation times (0, 2, 4 and 16 h) (time zero does not correspond really to time zero, but it is estimated to be very few minutes). Charcoal was added to terminate the assay and radioactivity measured as described in Materials and Methods (Section 2.2.3.2). BSA was used in place of cytosolic protein as a negative control.

In Figure 3.1 is shown the effect of time on $[^3\text{H}]$ -TCDD specific binding. The results show that $[^3\text{H}]$ -TCDD binds specifically to rat liver cytosol quickly after addition of the radioligand (Figure 3.1). Maximal specific binding of $[^3\text{H}]$ -TCDD to rat cytosolic protein was detected after 2

h of incubation and remained unchanged after that time (Figure 3.1). [^3H]-TCDD specific binding to BSA was negligible, whereas [^3H]-TCDD specific binding to rat cytosolic protein was found to be high in three experimental repeats. The high specific binding of [^3H]-TCDD to the rat cytosolic proteins and the negligible binding to the BSA confirms that the [^3H]-TCDD binds specifically to a cytosolic protein, which has previously been shown to be the AhR [66], and the specific binding protein will henceforth be referred to as the AhR. The time of incubation was selected to be 16 h following the protocol described by Bradfield and Poland (1988) [164].

Section 3.1.2 Dextran-coated charcoal (DCC)

The Dextran-coated charcoal was used to separate the bound from the free ligand. So, it is essential to have enough charcoal to adsorb loosely bound radioligand and free radioligand remaining in solution. However, a high amount of charcoal could also adsorb the specifically bound radioligand. So it was important to optimise the amount of charcoal for a balance between decreasing [^3H]-TCDD nonspecific binding and loss of specific binding to the receptor.

Cytosolic proteins (or BSA as a negative control) were incubated with [^3H]-TCDD (1nM) \pm TCAOB (200 nM) and incubated at 4°C for 16 h. After the 16 h-incubation, protein samples were incubated with 30 μl of different amounts of charcoal in suspension (0.06, 0.2, 0.6, 2 and 6 mg /mg protein) and the charcoal removed by centrifugation. Radioactivity in the resultant supernatants was measured as described in Materials and Methods (Section 2.2.3.2). Figure 3.2 shows the effect of charcoal amount on the total, nonspecific and specific binding of [^3H]-TCDD to cytosol and BSA proteins. Figure 3.2 B reveals high nonspecific binding of [^3H]-

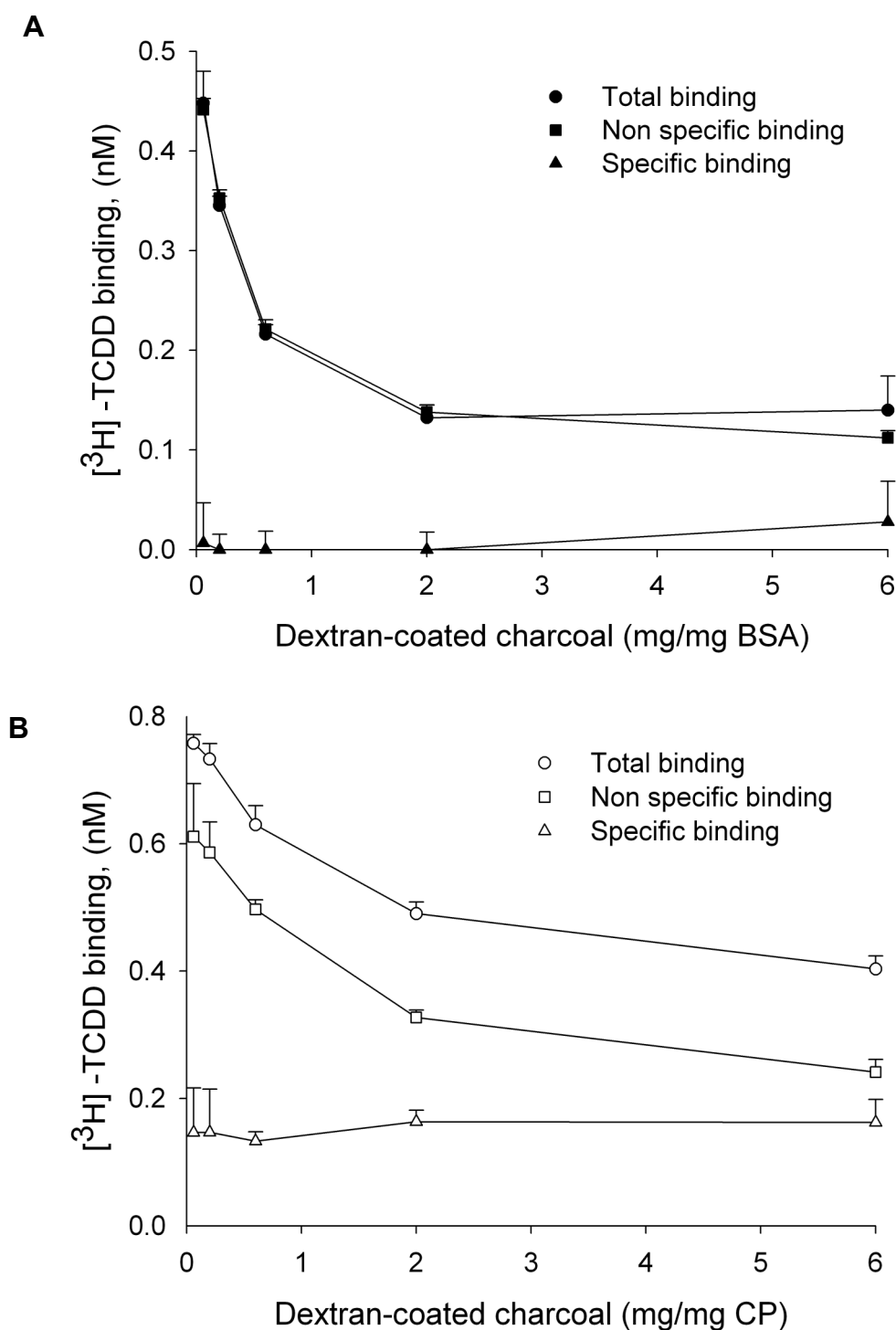


Figure 3.2 Effect of charcoal on $[^3\text{H}]$ -TCDD binding to rat cytosolic and BSA proteins. $[^3\text{H}]$ -TCDD binding to BSA (A) and rat cytosol (B). Aliquots of cytosolic (CP) and bovine serum albumin (BSA) proteins (5 mg/ml, prepared in MDENG buffer) were incubated with 1nM $[^3\text{H}]$ -TCDD \pm 200 nM TCAOB for 16 h at 4°C. Varied amounts of charcoal-dextran in MDENG buffer (0.06, 0.2, 0.6, 2 and 6 mg/mg cytosolic protein) were then added to samples and incubated on ice for 10 min. Charcoal-dextran was removed by centrifugation at 20,000 \times g for 10 min, and the radioactivity measured. Total and non-specific were measured and specific binding calculated as described in Figure 3.1 legend. Each point represents the mean \pm S.D for triplicate samples, and is representative of results obtained from three experiments. Ordinate: total, non-specific and specific binding of $[^3\text{H}]$ -TCDD to rat hepatic cytosolic and BSA (nanomolar). Abscissa: varying amount of charcoal (mg/mg protein).

TCDD to cytosolic proteins compared to the specific, particularly at low amounts of charcoal (< 2mg/mg protein). It has been reported that this is partly due to the use of relatively high concentration of [^3H]-TCDD (1 nM) which enhances [^3H]-TCDD binding to non receptor compartments [165]. Increasing amounts of charcoal decreased [^3H]-TCDD non specific binding to both cytosol and BSA. However, [^3H]-TCDD specific binding was not affected with increasing charcoal amount up to the amount tested (6 mg /mg protein). When BSA protein was used as a negative control, no statistically significant specific binding of [^3H]-TCDD was measured for all charcoal amounts. Charcoal concentrations ≥ 2 mg/mg cytosolic protein did not alter the specific binding levels of [^3H]-TCDD and further decreased the nonspecific binding of [^3H]-TCDD to cytosolic protein, therefore, a concentration of 2 mg of charcoal /mg cytosolic protein was used in subsequent experiments.

Section 3.1.3 TCAOB concentration

The unlabelled competitor, TCAOB, was used to determine the non-specific binding of [^3H]-TCDD. In principle, the competitor is added in excess and will compete with [^3H]-TCDD for the high-affinity and saturable binding sites. However, at sufficiently high concentrations, it is a possibility that the TCAOB could compete with [^3H]-TCDD at non-specific sites [166]. Therefore, it was essential to optimise the concentration to be used throughout the binding assay. The experiment was conducted essentially as described in Materials and Methods (Section 2.2.3.2), except with a range of TCAOB concentrations (0-50-100-200-400 and 800 nM) for 16 h at 4°C. The same experiment was run on BSA as negative control. After the 16-h incubation charcoal was added and radioactivity measured as described in Materials and Methods (Section 2.2.3.2). Figure 3.3 shows the total, non specific and specific binding of [^3H]-TCDD to rat cytosolic proteins and to BSA used as a negative control. The results show that the [^3H]-TCDD binds specifically to the cytosolic protein but does not specifically bind BSA. [^3H]-TCDD spe-

cific binding remains unchanged with increasing TCAOB concentrations for cytosolic protein preparations (Figure 3.3). This experiment shows that the non-specific binding of [3 H]-TCDD to cytosolic proteins and BSA was unchanged up to the highest concentration tested (800 nM), which proves that TCAOB is not competing with [3 H]-TCDD at non specific sites. The TCAOB concentration selected for the assay was 200 nM consistent with the literature [66].

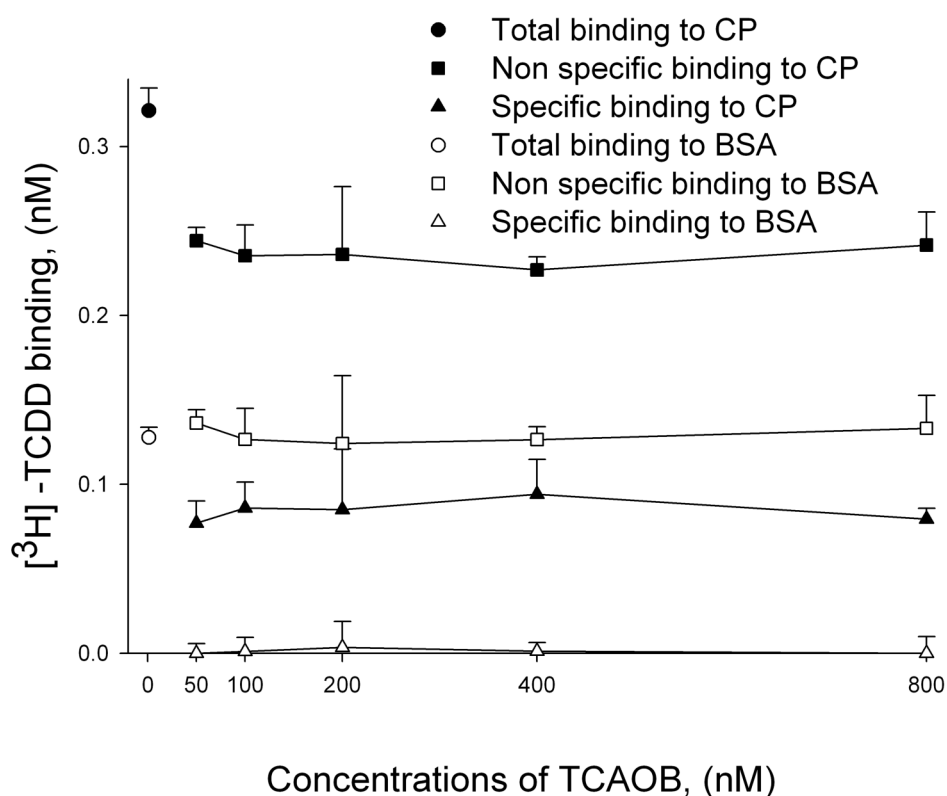


Figure 3.3 Effect of TCAOB concentration on [3 H]-TCDD binding to rat cytosolic proteins. [3 H]-TCDD total, non specific and specific binding was measured in rat liver cytosolic (CP) and bovine serum albumin (BSA) proteins after incubating [3 H]-TCDD (1 nM) \pm varying concentration of the unlabeled competitor TCAOB (0-50-100-200-400 and 800 nM) for 16 h at 4°C as as described in Figure 3.1 legend. Each bar represents the mean \pm S.D for triplicate samples, and is representative of results obtained from three experiments. Ordinate: total, non-specific and specific binding of [3 H]-TCDD to rat hepatic cytosolic and bovine serum albumin proteins (nanomolar). Abscissa: unlabeled TCAOB (nanomolar).

Section 3.1.4 Cytosolic protein concentration

Section 3.1.4.1 Effect of cytosolic protein concentration on [^3H]-TCDD specific binding

One of the important parameters that could affect the specific binding of [^3H]-TCDD is the protein concentration. It is known that at high receptor number, the ligand could be depleted by binding to the receptors. As mentioned earlier in the introduction of this chapter, only a small fraction of the [^3H]-TCDD should bind to the receptor so that the system is not facing ligand depletion by binding to receptors and thus the binding obeys to the law of mass action. Therefore, it was important to investigate the effect of protein concentration on the specific binding of [^3H]-TCDD as well as the free concentration in solution. Initially, all experiments were conducted using 5 mg/ml protein concentration [38] [67].

The experiment conducted here investigates the effect of a range of rat liver cytosolic protein concentration on [^3H]-TCDD specific binding. Therefore, 200 μl cytosolic protein preparations at different protein concentrations (0, 1, 3, 5 and 8 mg/ml) were incubated with [^3H]-TCDD (1 nM) \pm TCAOB (200 nM) at 4°C for 16 h.

Figure 3.4 shows the effect of protein concentration on [^3H]-TCDD specific binding. As seen in Figure 3.4, as protein concentration increases, the specific binding of [^3H]-TCDD increases in a linear way up to 5 mg/ml protein concentration. Above 5 mg/ml, [^3H]-TCDD specific binding deviates from linearity. At 5 mg/ml, only around 20% of [^3H]-TCDD is specifically bound to the AhR. As the aim is to select conditions for high [^3H]-TCDD specific binding (high signal-to-noise ratio) while the response is still in the linear part, a protein concentration of 5 mg/ml protein was within these criteria, thus subsequent work will be carried out, as previously, using this protein concentration.

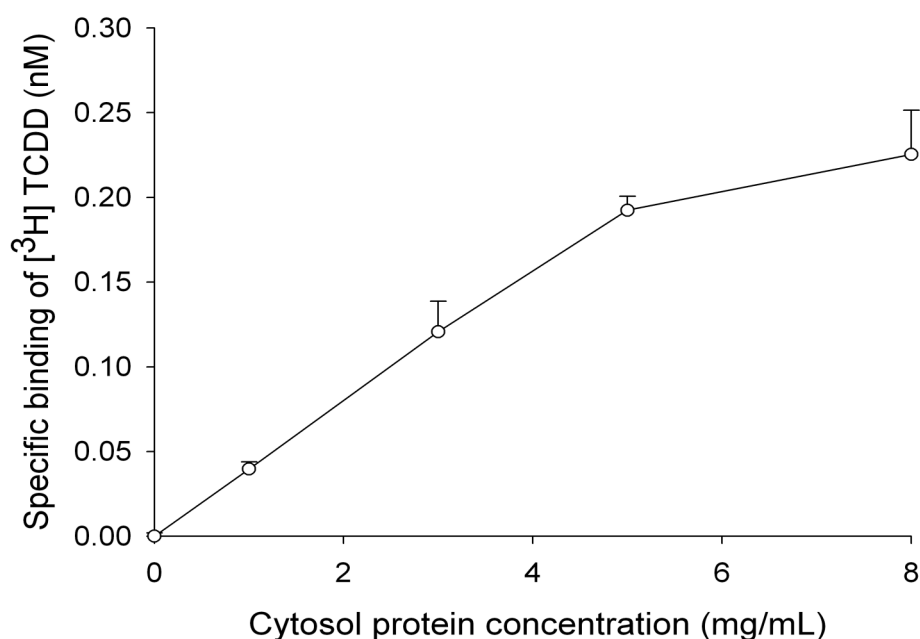


Figure 3.4 Effect of cytosolic protein concentration on $[^3\text{H}]$ -TCDD specific binding to rat cytosolic protein. $[^3\text{H}]$ -TCDD (1 nM) was incubated with 200 μl of varying concentrations of cytosolic protein (0, 1, 3, 5 and 8 mg/ml prepared in MDENG buffer) \pm 200 nM TCAOB for 16 h at 4°C. After 16 h, total and non specific binding were determined after washing with charcoal and specific binding of $[^3\text{H}]$ -TCDD was calculated as described described in Figure 3.1 legend. Each point represents the average of mean \pm S.D for triplicate samples, and is representative of results obtained from three experiments. Ordinate: specific binding of $[^3\text{H}]$ -TCDD (nanomolar). Abscissa: cytosolic protein concentration (mg/ml).

Section 3.1.4.2 Effect of cytosolic protein concentration on $[^3\text{H}]$ -TCDD in solution

A technical problem is the limited solubility of TCDD in aqueous solutions [167]. This experiment was conducted to examine the effect of protein concentration on $[^3\text{H}]$ -TCDD actual concentrations in the solutions. The best conditions consist of selecting the protein concentration at which more $[^3\text{H}]$ -TCDD is retained in solution.

The concentration of $[^3\text{H}]$ -TCDD that remained in solution was examined, before and after a 16-h incubation, as a function of a range of concentrations of the cytosolic protein preparation, and is shown in Figure 3.5. No charcoal was added in this experiment as the aim is to assess the total (free), but not bound, radioligand concentration.

As shown in Figure 3.5, in preparations containing no protein, ~ 50 % of free [^3H]-TCDD was depleted from solution immediately after the addition [^3H]-TCDD (no incubation time) and ~ 86% was depleted after 16-h incubation. The addition of protein retains more total [^3H]-TCDD in solution with and without 16-h incubation \pm 200 nM TCAOB. [^3H]-TCDD concentration was significantly higher in protein incubations than observed in no protein incubations ($p < 0.01$, t -test, $n=3$). At protein concentrations of 3 mg/ml or greater, more total [^3H]-TCDD was found in solution before (~ 99%) and after incubation (78%), and these concentrations were significantly different from no-protein incubations ($p < 0.01$, One-way ANOVA followed by Dunnett's Multiple Comparison test, $n=3$). That is true for samples with or without 200 nM TCAOB. The lower value of [^3H]-TCDD concentration in solution after the 16-h incubation is not surprising, a similar depletion of ligand has been reported [164]. Although maximum solubility was achieved at a cytosolic protein concentration of 3 mg/ml, at 5 mg/ml higher specific binding of [^3H]-TCDD was observed (Figure 3.4), moreover, it seems to increase the solubility of competing ligands when performing competition assays. In the light of these results, we confirmed that under the conditions of incubating cytosolic proteins (5 mg/ml) with 1 nM [^3H]-TCDD and 200 nM TCAOB for 16-h incubation at 4°C, ~ 20% of ligand is depleted from solutions. This was not considered problematic, since ligand depletion within this limit is acceptable and does not affect the displacement curves when performing competition studies [165].

Taken together, the results of the two experiments shown in Figure 3.4 & Figure 3.5, the concentration of 5 mg/ml cytosolic protein was used for subsequent experiments.

In parallel, TCAOB (200 nM) was added to test its effect on [^3H]-TCDD solubility. The values in the absence of TCAOB are very similar to those with TCAOB, which shows that TCAOB has no effect on [^3H]-TCDD solubility.

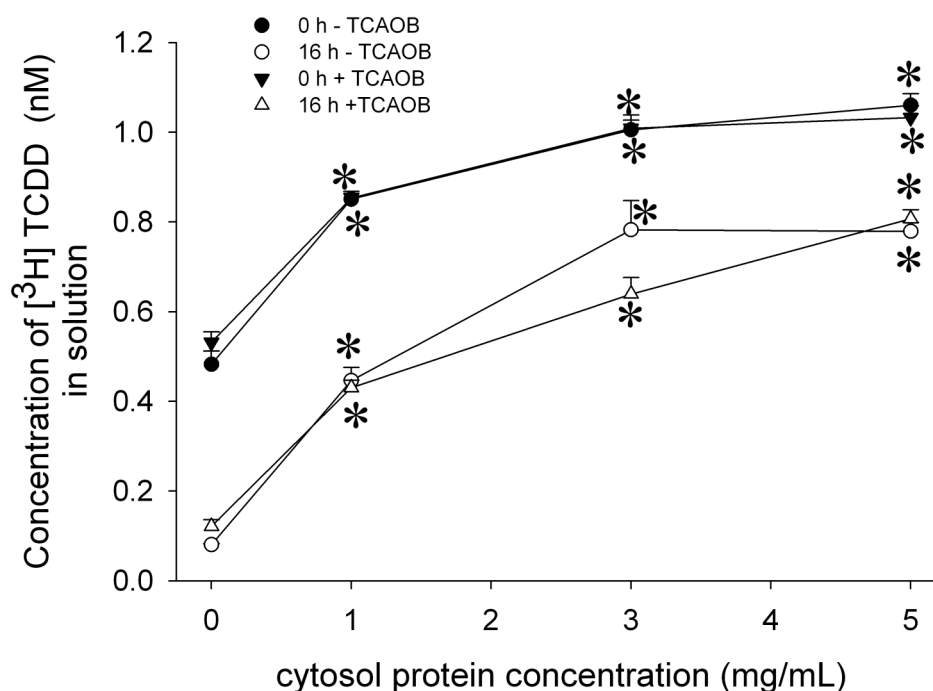


Figure 3.5 Effect of cytosolic protein concentration on $[^3\text{H}]$ -TCDD solubility. $[^3\text{H}]$ -TCDD (1 nM) was incubated for 16 h at 4°C with varying concentrations of the receptor preparation (0, 1, 3 and 5 mg/ml cytosolic protein prepared in MDENG buffer) in the presence (Δ) or absence (\circ) of the non-radioligand TCAOB (200 nM). In parallel, the same experiment was run without incubation in the presence (\blacktriangledown) or absence (\bullet) of TCAOB (200 nM). Before and after the 16-h incubation, the total $[^3\text{H}]$ -TCDD in solution was measured by counting radioactivity in 150 μl of samples with no charcoal added. Radioactivity data was converted into nanomolar concentrations. Each point represents the average of mean \pm S.D for triplicate samples, and is representative of results obtained from three experiments. (*; asterisk; $p < 0.01$; one-way ANOVA followed by Dunnett's Multiple Comparison test; $n=3$, $[^3\text{H}]$ -TCDD concentrations in solution of protein incubations compared to no protein incubations at the specified concentrations). Ordinate: total $[^3\text{H}]$ -TCDD in solution (nanomolar). Abscissa: cytosolic protein concentration (mg/ml).

Section 3.1.5 Effect of $[^3\text{H}]$ -TCDD concentration on $[^3\text{H}]$ -TCDD in solution

As for Section 3.1.4.2, the concern is the limited solubility of $[^3\text{H}]$ -TCDD in aqueous solutions. The aim is to select the concentration of $[^3\text{H}]$ -TCDD added at which $[^3\text{H}]$ -TCDD remains in solution after 16-h incubation. The experiment investigates the concentration of $[^3\text{H}]$ -TCDD that remains in solution, after the 16-h incubation, as a function of a range of $[^3\text{H}]$ -TCDD concentrations added in solution and is presented in Figure 3.6. The experiment was performed by incubating 200 μl of cytosolic protein with varying concentrations of $[^3\text{H}]$ -TCDD \pm 200-fold molar excess of TCAOB for each $[^3\text{H}]$ -TCDD concentration. No charcoal was added. The assay

was terminated by transferring 150 μ l for liquid scintillation counting.

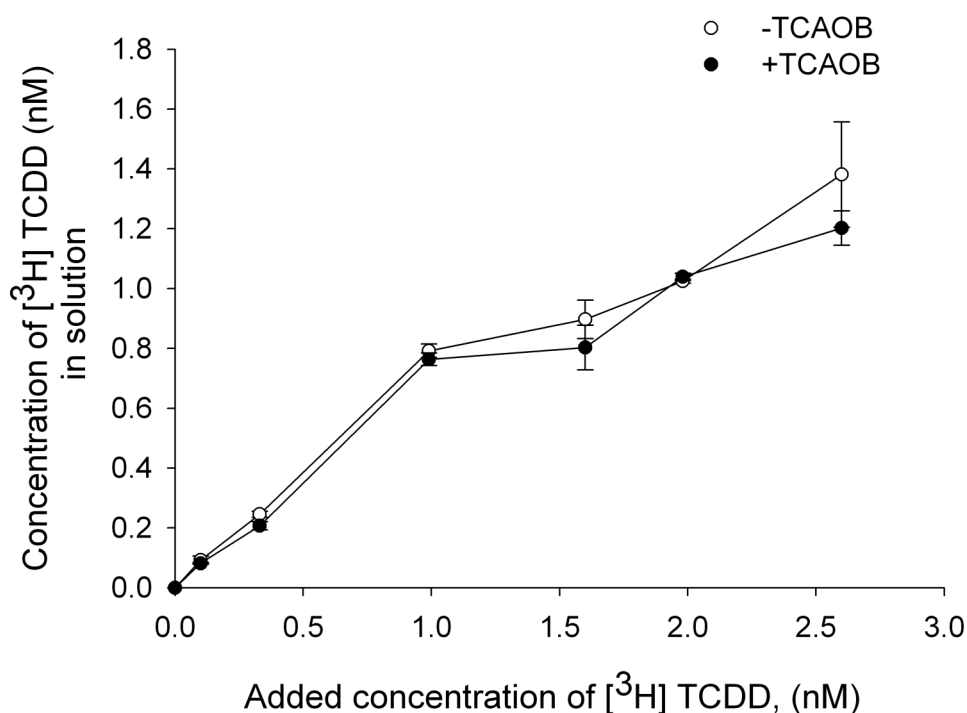


Figure 3.6 Concentration of [3 H]-TCDD in solution. Aliquots of 200 μ l cytosolic protein was incubated with a range of increasing concentrations (0-2.6 nM) of [3 H]-TCDD in the presence [●] or absence [○] of 200-fold molar excess unlabeled TCAOB for 16 h at 4°C. The concentration of [3 H]-TCDD in solution was measured after the 16-h incubation by transferring 150 μ l for liquid scintillation counting. Radioactivity data was converted into nanomolar concentration. Each point represents the average of mean \pm S.D for triplicate samples, and is representative of results obtained from three experiments. Ordinate: [3 H]-TCDD in solution (nanomolar). Abscissa: added [3 H]-TCDD (nanomolar).

As seen in Figure 3.6, the concentration of [3 H]-TCDD remaining in solution after incubation versus the initial concentration added was almost linear up to 1 nM [3 H]-TCDD, at which \sim 20% of the [3 H]-TCDD was depleted from solutions. Above 1 nM [3 H]-TCDD, much less [3 H]-TCDD remains in solution after incubation. This could be problematic for analyzing binding assays under these conditions, since above 1 nM, the concentration of TCDD varies by two-fold over the course of the 16-h incubation. This experiment was repeated three times with consistent results.

To rule out the possibility of TCAOB affecting the [3 H]-TCDD solubility at high concentra-

tions, in each experiment, samples were incubated for 16 h with and without 200-fold excess molar TCAOB with varying concentration of the [^3H]-TCDD (0, 0.1, 0.33, 0.99, 1.6, 1.98 and 2.6 nM). The results showed no effect of TCAOB addition on [^3H]-TCDD solubility in *p*-dioxane for all [^3H]-TCDD initially added concentrations, which is consistent with previous finding (Figure 3.5). In all experiments, the final [^3H]-TCDD concentration used was 1 nM, and as the Figure 3.6 shows, at this concentration, most of the radioligand was in solution.

Section 3.1.6 Binding assay standard

Saturation analysis of [^3H]-TCDD binding experiments to rat liver cytosol was used to characterize the binding of [^3H]-TCDD quantitatively and determine the apparent affinity constant (K_D) and the maximum concentration of specific binding sites, B_{\max} .

[^3H]-TCDD standard binding assay was performed by incubating aliquots of cytosolic protein with several concentrations of [^3H]-TCDD (0-2.6 nM) with and without 200-fold molar excess TCAOB for 16-h incubation at 4°C. The assay was terminated by addition of charcoal (2 mg/mg protein) after the 16-h incubation and radioactivity measured as described previously.

The simultaneous measurement of [^3H]-TCDD binding in the presence of excess TCAOB permits experimental estimation of the nonspecific binding. The binding parameters were determined from nonlinear regression for single site binding hyperbola analysis using GraphPad Prism version 5. The saturation binding isotherm of [^3H]-TCDD to the preparation of liver cytosol is shown in Figure 3.7 A. [^3H]-TCDD specific binding to rat cytosol was saturable at ≥ 1 nM. The data in Figure 3.7 B shows that the non specific binding of [^3H]-TCDD is linear with increasing concentrations of [^3H]-TCDD (as indicated in Figure 3.7 B legend). The apparent K_D for specific binding of [^3H]-TCDD to rat liver cytosol and the concentration of binding sites, B_{\max} were 0.37 ± 0.08 nM (74 fmol/mg) and 0.19 ± 0.01 nM (~40 fmol/mg) respectively. The

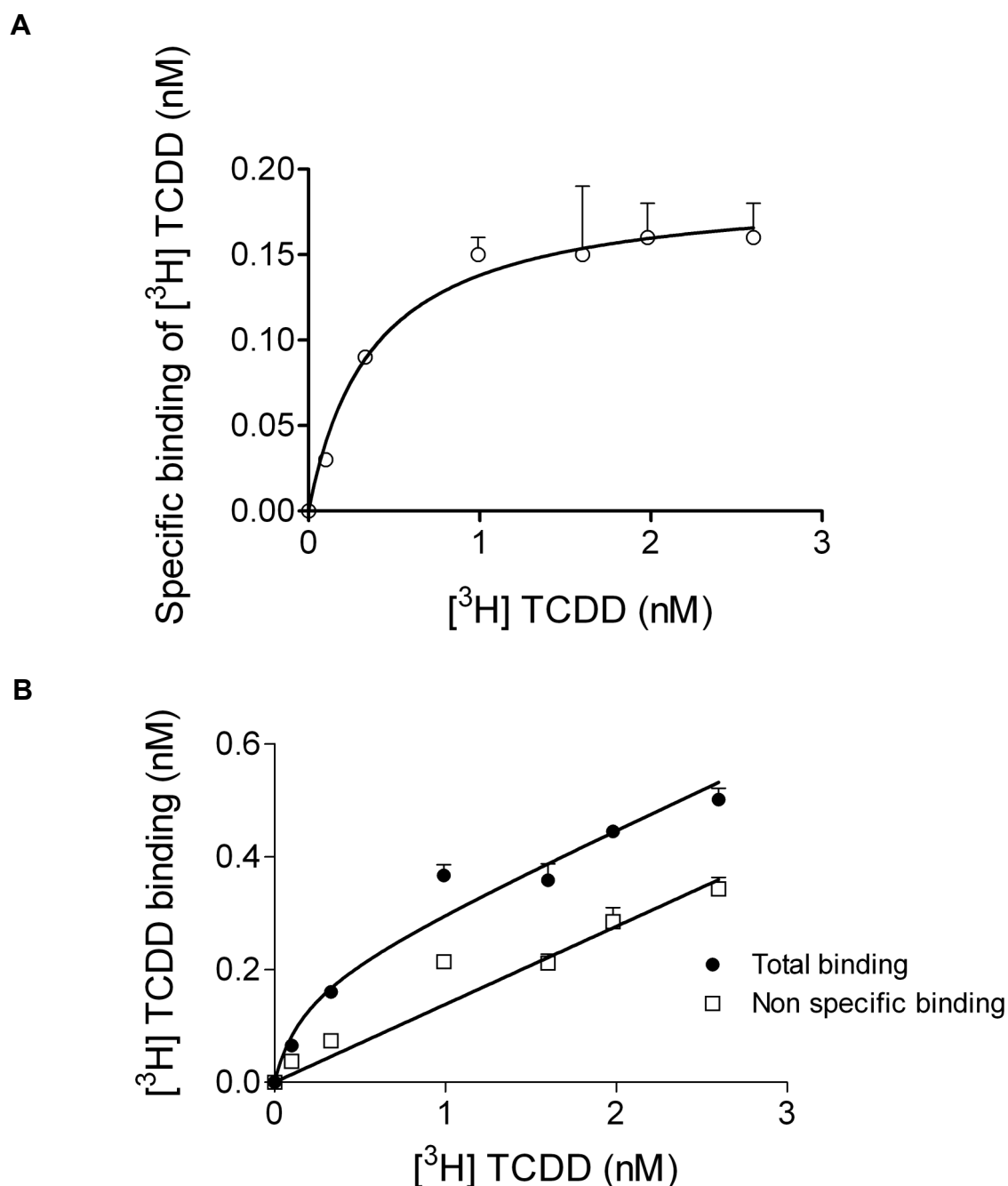


Figure 3.7 The binding standard of $[^3\text{H}]$ -TCDD to rat liver cytosol. **A.** Radioactivity for total [●] and non-specific binding [□] of $[^3\text{H}]$ -TCDD was determined for each sample and $[^3\text{H}]$ -TCDD specific binding was calculated as described in (Figure 3.1) legend. **B.** The standard binding curve for $[^3\text{H}]$ -TCDD specific binding [○] generated from subtracting non-specific from total binding in curves in (A). 200 μl aliquots cytosolic protein (5mg/ml) were incubated with varying concentrations of $[^3\text{H}]$ -TCDD (0, 0.1, 0.33, 0.99, 1.6, 1.98 and 2.6 nM) \pm 200-fold molar excess TCAOB for 16 h at 4°C. The assay was terminated by the addition of charcoal-dextran (2 mg/mg protein). The standard assay was analyzed for one site binding by using GraphPad Prism version 5.00 for windows. Each point represents the average of mean \pm S.D for triplicate samples, and is representative of results obtained from three experiments. Ordinates: binding of $[^3\text{H}]$ -TCDD (nanomolar). Abscissa: added $[^3\text{H}]$ -TCDD (nanomolar).

standard binding assay was repeated three times with increasing numbers of $[^3\text{H}]$ -TCDD con-

centrations, each in triplicate, and the average of the apparent K_D and the concentration of binding sites, B_{max} were 0.37 ± 0.06 nM (74 fmol/mg) and 0.23 ± 0.06 nM (~40 fmol/mg) respectively (Table 3.1). These data show reproducibility of the binding assay with the coefficients of variation of assay K_i and B_{max} values are 16% and 26% respectively. The results of the current binding assay are in good agreement with earlier results where apparent dissociation constants for TCDD AhR were determined (Table 3.2).

Experiments	K_D [nM] (95% confidence intervals)	B_{max} [nM] (95% confidence intervals)
(1)	0.37 (0.1-0.9)	0.19 (0.2-0.4)
(2)	0.45 (0.2-0.6)	0.3 (0.17-0.2)
(3)	0.33 (0.1-1)	0.2 (0.1-0.3)
Average \pm S.D	0.37 ± 0.06	0.23 ± 0.06

Table 3.1 Summary of binding kinetics of [3 H]-TCDD to rat hepatic cytosol from three independent experimental trials. K_D and B_{max} were determined from three standard binding assays using non linear regression for one site binding equation (GraphPad Prism 5.0). Each standard assay was performed on different concentrations of [3 H]-TCDD conducted in triplicates. The average and S.D values represent the mean and the standard deviations of binding kinetics from three trials.

The binding assay was generated successfully and proves saturable and high-affinity specific binding of [3 H]-TCDD to the Ah receptor, and thus the K_D of [3 H]-TCDD will be used in the competitive binding assays to determine the binding affinities of the test compounds.

Table 3.2 Comparison with literature for binding kinetics of TCDD for AhR. These data, along with those reported from this study, were generated from different binding assays in Wistar rat, Sprague-Dawley rat and C57BL/6J mice liver cytosols. K_D is the dissociation constant and the value is inversely proportional to binding affinity. K_D values from literature were determined using Scatchard analysis, whereas the K_D value determined in the present study was determined using one site binding analysis by Prism 5.0.

Species	Protein concentration (mg/ml)	Radioligand and SA (Ci/mmol)	TCDD K_D (nM)	B_{max} (fmole/mg)	References
C57BL/6J mice	2	[3H]-TCDD; 52.5	0.27	84	[164]
C57BL/6J mice	0.145	[^{125}I]2-Iodo-7,8-dibromo-dibenzo- <i>p</i> -dioxin; 2176	0.006	120	[156]
Sprague Dawley rat	2	[3H]-TCDD; 55	2.4	187	[168]
Sprague Dawley rat	2	[3H]-TCDD; 52	0.22	89	[169]
Sprague Dawley rat	5	[3H]-TCDD; 50-52	1.2	34	[67]
Wistar rat	6	[3H]-TCDD; 50-52	1.25	100	[170]
Wistar rat	5	[3H]-TCDD; 34.7	1.45	40.6	[38]
Wistar rat	5	[3H]-TCDD; 29.77	0.37	40	current study

Section 3.1.7 Displacement of [3H]-TCDD by cold TCDD

In order to validate the [3H]-TCDD binding assay, [3H]-TCDD binding was assessed by the ability of the unlabelled TCDD to displace [3H]-TCDD from specific sites via a competitive binding assay. Therefore, 200 μ l cytosolic protein (5 mg/ml) was incubated with 1 nM [3H]-TCDD \pm 200 nM TCAOB \pm a range of nine concentrations of cold TCDD for 16 h at 4°C and

specific binding of [^3H]-TCDD displaced by competitor was calculated as described in Materials and Methods (Section 2.2.3.4.2).

The aim is to determine the concentration of TCDD at which 50% of [^3H]-TCDD (IC_{50}) is displaced from the specific binding sites. Figure 3.8 shows the log concentration-curve for [^3H]-TCDD against unlabelled TCDD. From Figure 3.8, the IC_{50} value extrapolated from the competitive displacement curve was 1.65 nM (95% CI, 0.66 - 4.1), and thus calculated K_i for cold TCDD was 0.44 nM (95% CI, 0.18-11.1).

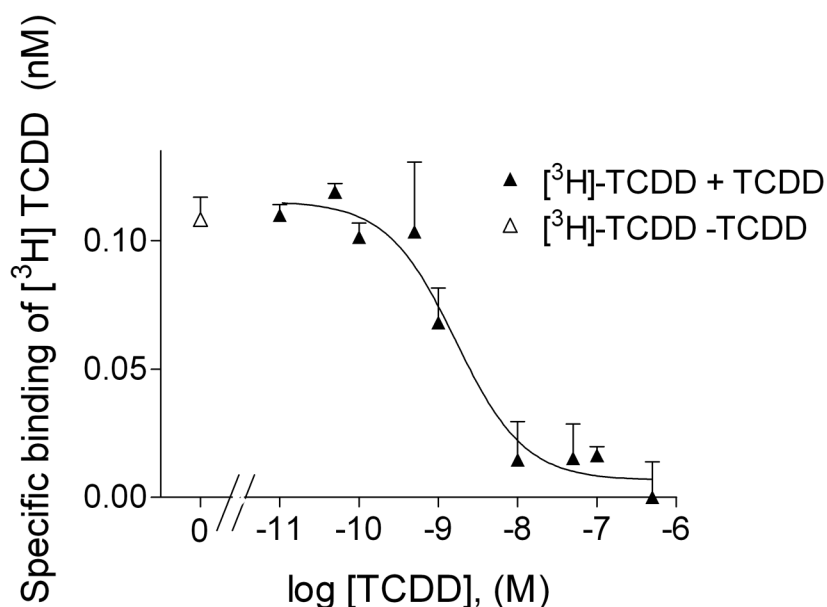


Figure 3.8 Competitive displacement of hot TCDD by cold TCDD. Cytosolic protein (5 mg/ml) was incubated for 16 h at 4°C with 1nM [^3H]-TCDD \pm increasing concentration of TCDD \pm (200 nM) TCAOB. At each specified TCDD concentration, [^3H]-TCDD total binding and non specific binding was measured experimentally and specific binding of [^3H]-TCDD displaced by cold TCDD (▲) was calculated as described in Section 2.2.3.4.2. The specific binding of [^3H]-TCDD in the absence of cold TCDD (Δ) was included as a positive control. The competitive binding curve was analyzed for one site competition by using GraphPad Prism version 5.00 for windows. Each point represents the average of mean \pm S.D for triplicate samples, and is representative of results obtained from one single experiment. Ordinate: specific binding of [^3H]-TCDD to cytosolic protein (nanomolar). Abscissa: logarithms of molar concentrations of unlabeled TCDD.

This is in agreement with the results of the saturation binding assay (K_D 0.37 nM). This finding

confirms that the conditions under which the displacement experiment is conducted are stable and yield reproducible results as compared to the standard binding assay.

Section 3.1.8 Displacement of [^3H]-TCDD by test competitors

To investigate the strength of the interactions between the test compounds and the AhR, competitive assays were conducted as described in Materials and Methods (Section 2.2.3.4.2).

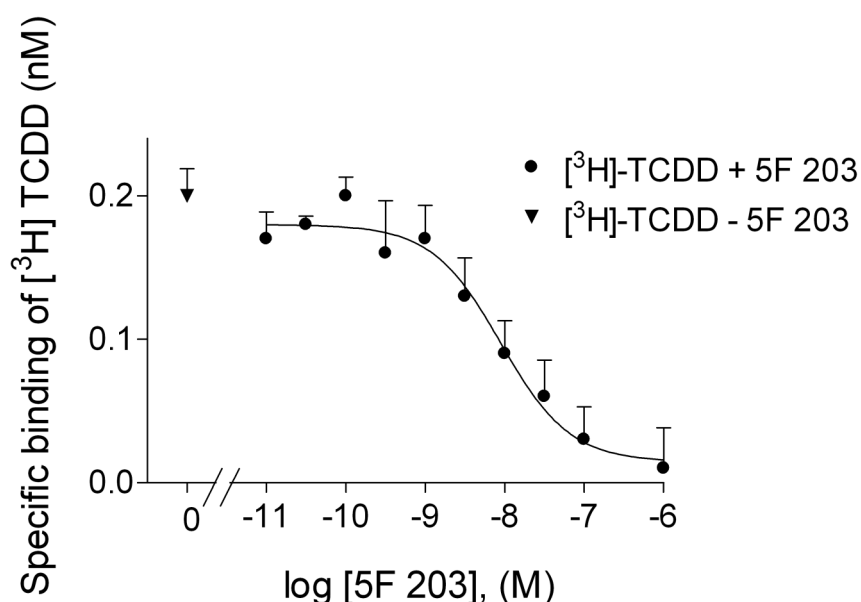


Figure 3.9 Competitive displacement of [^3H]-TCDD by 5F 203. Cytosolic protein (5 mg/ml) was incubated with 1nM [^3H]-TCDD and increasing concentrations of 5F 203 \pm (200nM) TCAOB for 16 h at 4°C. At each specified 5F 203 concentration, [^3H]-TCDD total binding and non specific binding was measured experimentally and specific binding of [^3H]-TCDD displaced 5F 203 was calculated as described in Section 2.2.3.4.2. The specific binding of [^3H]-TCDD in the absence of 5F 203 (\blacktriangledown) was included as a positive control. The competitive binding curve was analyzed for one site competition by using GraphPad Prism version 5.00 for windows. Each point represents the average of mean \pm S.D for triplicate samples, and is representative of results obtained from three experiments. Ordinate: specific binding of [^3H]-TCDD to cytosolic protein (nanomolar). Abscissa: logarithms of molar concentrations of 5F 203.

The binding of 5F 203 was determined by adding different concentrations of 5F 203 to a 1 nM solution of [^3H]-TCDD in rat liver cytosol \pm 200 nM TCAOB. Figure 3.9 shows the log concentration curve for [^3H]-TCDD displacement by 5F 203. The concentration of 5F 203 that displaced 50% of [^3H]-TCDD, IC_{50} was 9 nM (95% CI, 4.6-17.3). Given that the [^3H]-TCDD

concentration utilized is 1nM and the apparent K_D 0.37nM, the K_i of 5F 203 was calculated as described in Materials and Methods (Section 2.2.3.4.2) to be 2.4 nM (95% CI, 1.3-4.7). Thus, this study identifies 5F 203 as a new potent high-affinity ligand for AhR.

Competitive displacement curves for a variety of phenylbenzothiazole analogues were generated under the same conditions. The 5F 203 K_i value represents the average of three separate experiments. Nanomolar concentrations of K_i and their 95% confidence intervals for phenylbenzothiazole analogues, TCDD, TCAOB, TCDF, TCPT and compound 1c are displayed in (Table 3.3).

The binding affinities for TCAOB and TCDF, two PAHs known to potent ligands for AhR, are very similar to literature reports [66] [6], which further validates the [^3H]-TCDD competitive assay .

Of the 24 compounds tested for their binding avidity to the AhR, 22 were found to be ligands for AhR with low nanomolar K_i values. 2-(4-amino-3-methylphenyl)-6-hydroxybenzothiazole, (IH 130) and 2-(3-hydroxy-methoxyphenyl)-5- fluorobenzothiazole (JP-2) were low-affinity ligands, with K_i value $> 1\mu\text{M}$. Interestingly, the tetrachlorophenothiazine (TCPT) and the compound 1c from Astrazeneca were found high-affinity ligands for the AhR ligands with potency similar to (TCPT, $K_i = 400\text{ pM}$) or greater (1c, $K_i = 40\text{ pM}$) than TCDD's (Table 3.3).

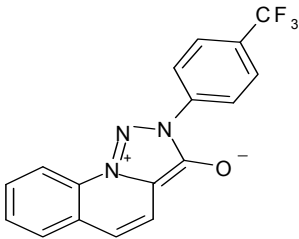
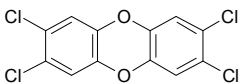
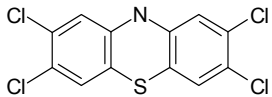
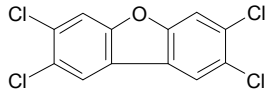
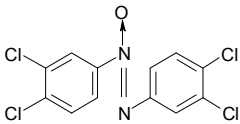
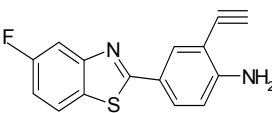
Nomenclature	Compound	K _i [nM] (95% confidence intervals)	Chemical structures
3-Hydroxy-2-[4-(trifluoromethyl)phenyl]-[1,2,3]-triazolo[1,5-a]quinolinium hydroxide	1c★	0.04 (0.01-0.1)	
2,3,7,8- Tetrachlorodibenzo-p-dioxin	TCDD	0.44 (0.18-1)	
Tetrachlorophenothiazine	TCPT	0.4 (0.08-2.2)	
Tetrachlorodibenzofuran	TCDF	0.5 (0.2-1.6)	
Tetrachloroazoxybenzene	TCAOB	0.8 (0.3-2.5)	
(Aminomethylphenyl)benzothiazoles (series 1)			
2-(4-amino-3-ethynylphenyl)-5- fluoro-benzothiazole	IH 445*	0.9 (0.05-16.9)	

Table 3.3 Binding affinities of TCDD, TCAOB, TCDF, TCPT, astraZeneca compound 1c and benzothiazole analogues in rat liver cytosol. The affinity of the test compounds for the Ah receptor was measured by their ability to compete with the specific binding of [³H]-TCDD. Concentrations of compounds that inhibited 50% of [³H]-TCDD specific binding (IC₅₀) from Ah receptor, were determined (by Prism 5.0) from the curves and their relative inhibition constants (K_i) were calculated according to [³H]-TCDD's K_D. All values reported are the average of two independent experiments, except for 5F 203, the data are the average of three independent trials, each conducted in triplicate. (*) to represent compounds with only one trial conducted in triplicate. (★) [152]. Compound structures were drawn using ISIS DRAW Program.

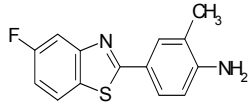
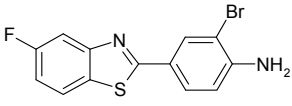
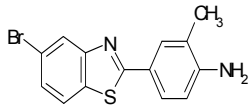
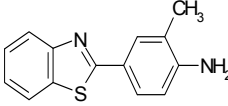
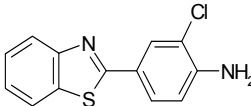
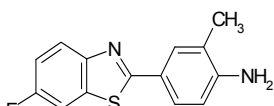
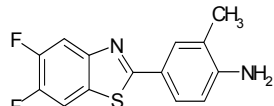
Nomenclature	Compound	K_i [nM] (95% confidence intervals)	Chemical structures
2-(4-amino-3-methylphenyl)-5-fluorobenzothiazole	5F 203	2.8 (2-5)	
2-(4-amino-3-bromophenyl)-5-fluorobenzothiazole	IH 277*	2.8 (1.4-5.5)	
2-(4-amino-3-methylphenyl)-5-bromobenzothiazole	IH 318	8 (5.5-12)	
2-(4-amino-3-methylphenyl) benzothiazole	DF 203	9.9 (5.3-18.7)	
2-(4-amino-3-chlorophenyl) benzothiazole	DF 229*	10 (1.6-68)	
2-(4-amino-3-methylphenyl)-6-fluorobenzothiazole	IH 168	13 (3-59)	
2-(4-amino-3-methylphenyl)-5,6-difluorobenzothiazole	IH 321	16 (3.5-75.5)	

Table 3.3 Binding affinities of TCDD, TCAOB, TCDF, TCPT, astrazeneca compound 1c and benzothiazole analogues in rat liver cytosol. The affinity of the test compounds for the Ah receptor was measured by their ability to compete with the specific binding of [3 H]-TCDD. Concentrations of compounds that inhibited 50% of [3 H]-TCDD specific binding (IC_{50}) from Ah receptor, were determined (by Prism 5.0) from the curves and their relative inhibition constants (K_i) were calculated according to [3 H]-TCDD's K_D . All values reported are the average of two independent experiments, except for 5F 203, the data are the average of three independent trials, each conducted in triplicate. (*) to represent compounds with only one trial conducted in triplicate. (★) [152]. Compound structures were drawn using ISIS DRAW Program.

Nomenclature	Compound	K_i [nM] (95% confidence intervals)	Chemical structures
2-(4-amino-3-methylphenyl)-4-fluorobenzothiazole	IH 220	30 (3-300)	
2-(4-amino-3-methylphenyl)-5-iodobenzothiazole	IH 278*	32 (11-95)	
2-(4-amino-3-cyanophenyl)-5-fluorobenzothiazole	IH 352	36.6 (11-119)	
2-(4-amino-3-hydroxymethylphenyl)-5-fluorobenzothiazole	IH 353*	98 (48.3-199)	
2-(4-amino-3-hydroxymethylphenyl)benzothiazole	IH 224*	149 (123-182)	
2-(4-amino-3-methylphenyl)-5-hydroxybenzothiazole	IH 186*	175 (54-571)	
2-(4-aminophenyl) benzothiazole	CJM 126*	265 (98-715)	

Table 3.3 Binding affinities of TCDD, TCAOB, TCDF, TCPT, astrazeneca compound 1c and benzothiazole analogues in rat liver cytosol. The affinity of the test compounds for the Ah receptor was measured by their ability to compete with the specific binding of [3 H]-TCDD. Concentrations of compounds that inhibited 50% of [3 H]-TCDD specific binding (IC_{50}) from Ah receptor, were determined (by Prism 5.0) from the curves and their relative inhibition constants (K_i) were calculated according to [3 H]-TCDD's K_D . All values reported are the average of two independent experiments, except for 5F 203, the data are the average of three independent trials, each conducted in triplicate. (*) to represent compounds with only one trial conducted in triplicate. (★) [152]. Compound structures were drawn using ISIS DRAW Program.

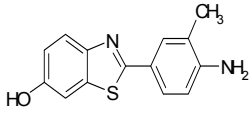
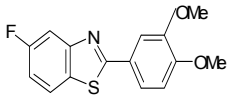
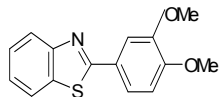
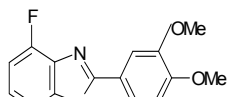
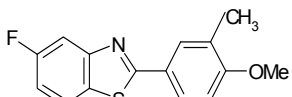
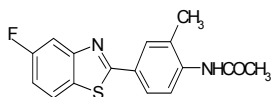
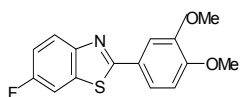
Nomenclature	Compound	K_i [nM] (95% confidence intervals)	Chemical structures
2-(4-amino-3-methylphenyl)-6-hydroxybenzothiazole	IH 130	1462 (800.7 to 2670)	
(Dimethoxyphenyl)benzothiazoles (series 2)			
2-(3,4-dimethoxyphenyl)-5-fluorobenzothiazole	GW 610	6.8 (1.5-30)	
2-(3,4-dimethoxyphenyl) benzothiazole	AW 892	9.8 (4.4-22)	
2-(3,4-dimethoxyphenyl)-4-fluorobenzothiazole	4F 610	14 (3.2-62)	
2-(3-methyl-4-methoxyphenyl)-5-fluorobenzothiazole	JP-1	26 (2.3-284)	
2-(4-aminocarboxymethoxy-3-methylphenyl)-5-fluorobenzothiazole	IH 128*	47 (37-61)	
2-(3,4-dimethoxyphenyl)-6-fluorobenzothiazole	AW 898	185 (18-182)	

Table 3.3 Binding affinities of TCDD, TCAOB, TCDF, TCPT, astraZeneca compound 1c and benzothiazole analogues in rat liver cytosol. The affinity of the test compounds for the Ah receptor was measured by their ability to compete with the specific binding of [3 H]-TCDD. Concentrations of compounds that inhibited 50% of [3 H]-TCDD specific binding (IC_{50}) from Ah receptor, were determined (by Prism 5.0) from the curves and their relative inhibition constants (K_i) were calculated according to [3 H]-TCDD's K_D . All values reported are the average of two independent experiments, except for 5F 203, the data are the average of three independent trials, each conducted in triplicate. (*) to represent compounds with only one trial conducted in triplicate. (★) [152]. Compound structures were drawn using ISIS DRAW Program.

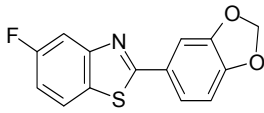
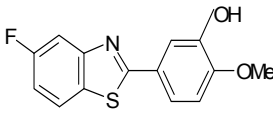
Nomenclature	Compound	K _i [nM] (95% confidence intervals)	Chemical structures
2-(3,4-methylenedioxyphenyl)-5- fluoro-benzothiazole	JMB 81	613 (195-1932)	
2-(3-hydroxy-4-methoxyphenyl)-5- fluoro-benzothiazole	JP-2*	5000 (185.5 to 125500)	

Table 3.3 Binding affinities of TCDD, TCAOB, TCDF, TCPT, astrazeneca compound 1c and benzothiazole analogues in rat liver cytosol. The affinity of the test compounds for the Ah receptor was measured by their ability to compete with the specific binding of [³H]-TCDD. Concentrations of compounds that inhibited 50% of [³H]-TCDD specific binding (IC₅₀) from Ah receptor, were determined (by Prism 5.0) from the curves and their relative inhibition constants (K_i) were calculated according to [³H]-TCDD's K_D. All values reported are the average of two independent experiments, except for 5F 203, the data are the average of three independent trials, each conducted in triplicate. (*) to represent compounds with only one trial conducted in triplicate. (★) [152]. Compound structures were drawn using ISIS DRAW Program.

Section 3.1.9 Structure-Activity Relationships (SARs)

The structures of the compounds tested are displayed in Section 2.1.4 under Materials and Methods. The results from the binding data show differences in binding potency between compounds. Structure-activity relationship analysis for binding of these test compounds revealed that the binding affinities were substituent-dependent and varied over 3 orders of magnitude. AhR binding was weakened by polar groups, such as hydroxyl- or methylenedioxy-significantly reduced the binding. Importantly, the effect of hydroxylation was position-dependent. For example, the 3'-hydroxylation in the phenyl ring (IH 224) or the 6-hydroxylation in the benzothiazole ring (IH 130) inhibited the binding affinity whereas the 5-hydroxylation in the benzothiazole ring (IH 186) only decreased the binding but retained nanomolar values.

The 5-fluorination in the phenyl ring was not essential for the binding activity, as the fluorinated-(5F 230) and the non-fluorinated (DF 203) analogues have binding affinities within ~3-fold for the AhR. Importantly, the 3' position in the phenyl moiety seems to be required for binding,

as the CMJ 126 has 33-fold lower K_i than that of 5F 203. Furthermore, it was observed that the presence of a hydrophobic group on this position enhanced the binding. This is the case when the carbon at the 3' position is occupied by a bromine atom > acetylene group > chlorine atom or methylene group > methoxy or cyanide compared to the hydrogen atom at this position (CJM 126).

Under the conditions of the current binding assay, two compounds emerged as AhR high-affinity ligands with potency similar to TCDD's (TCPT, $K_i = 400$ pM) or greater (1c, $K_i = 40$ pM) (Table 3.3). These compounds bear some structural similarities to TCDD, in that they have polycyclic aromatic structures. Interestingly, the compound 1c, in contrast to TCPT, does not fit the classic model for the ligand binding pocket of a rectangle with a maximal dimension of (14 x 12 x 5 Å) generally described for AhR ligands [40]. Moreover, both compounds are not planar like TCDD.

The data for the compound 1c, along with the phenylbenzothiazole analogue structures, seems to suggest that there is promiscuity of the binding domain of this receptor that deviates from the known ligand binding model [9].

Originally, the aim of quantifying the interactions of the phenylbenzothiazole analogues with the AhR was to establish a quantitative structure activity relationship (QSAR) analysis and generate a model for their binding. However, such quantitative analysis requires a significant number of compounds (at least 50), and this study was constrained by the limited number of the compounds available, the lack of some substituent groups essential for elucidating the QSAR and the time involved in generating the data.

Section 3.2 Characterization of CYP1A1 induction

Section 3.2.1 Cell growth curves

It is essential to characterize the growth of the cells, and to determine accurately the characteristic growth rate for each cell line and when exactly the cells reach high confluence. Therefore, growth curves for both cell lines were generated.

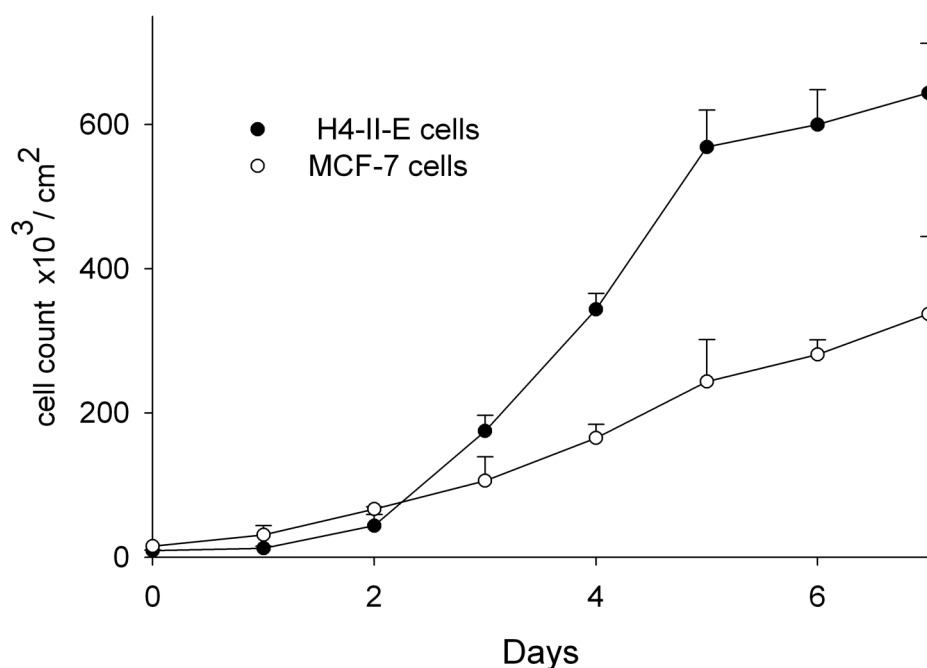


Figure 3.10 Growth curves of H4-II-E and MCF-7 cells. H4-II-E and MCF-7 cells were cultured respectively in triplicate in 96 well plates initially at a density of 3×10^3 and 2.5×10^3 cells/well in $180 \mu\text{l}$ culture medium and cultured for 7 days at 37°C . The old medium was replaced with a fresh medium every three days. At each time point, cells were washed with PBS, trypsinized and counted by hemocytometer as described under Materials and Methods Section 2.2.5. Each point represents the average of mean \pm S.D for triplicate samples, and is representative of results obtained from three experiments. Ordinate: cell count $\times 10^3 / \text{cm}^2$. Abscissa: time (days).

Figure 3.10 shows growth curves for H4-II-E and MCF-7 cell lines over seven days of culture. 90-95% cell confluence was achieved at concentrations of $\sim 2 \times 10^5$ cells / well or 6.25×10^5 cells / cm^2 and $\sim 1 \times 10^5$ cells / well or 3×10^5 cells / cm^2 (96 well plates, $0.32 \text{cm}^2/\text{well}$) for H4-II-E and MCF-7 cells respectively. H4-II-E cells grow twice as fast as MCF-7 cells, but the latter cells reach confluence at lower density. These growth characteristics were similar to the literature in that H4-II-E cells had a doubling time between 18 and 24 h [171]. From these growth

curves, the concentrations for which high confluence will be achieved after 24 h for MCF-7 and H4-II-E cells were 5×10^4 cells/well and 1×10^5 cells/well respectively.

Section 3.2.2 Testing the primers and probes for specificity

It was important to test the primers and probes for specificity and susceptibility to any genomic contamination.

For the human and rat *CYP1A1*, *β -actin* and *AhR* genes, the primers were tested on cDNA samples from 4-h-TCDD-treated H4-II-E and MCF-7 cells by performing firstly endpoint PCR analysis and then by real-time PCR. One single band of the expected size was found for each gene with no additional bands showing genomic contamination, except for the human *CYP1A1*, where genomic contamination was found (data not shown). For this gene, the probe, but not primers, was designed to span the junction between two exons as described in Materials and Methods (Section 2.1.8). As expected, when tested by real-time qRT-PCR this genomic contamination was not detected, as shown in no reverse transcriptase controls. No signal was detected in no template controls (no Ct), indicating no contamination of any assay reagents (data not shown). The results revealed no primer-dimers or genomic amplification and that all amplicons were at the expected size. Thus, the specificity of the primers and probes was confirmed, and found suitable for use in qRT-PCR measurements.

Section 3.2.3 Assessment of RNA quality

The quality of RNA was assessed by the relative intensities of the 28S and 18S rRNA bands visualized by electrophoresis on 1% denaturing agarose gel after ethidium bromide staining. The results in Figure 3.11 show that the RNA extracted were of a high quality with two distinct bands corresponding to the 28S and 18S rRNA. .

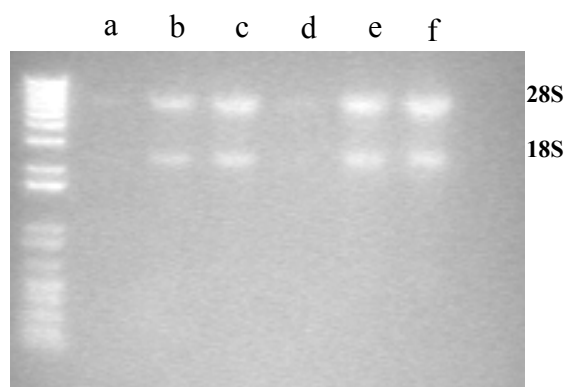


Figure 3.11 An agarose gel showing the integrity of the total RNA as assessed by the relative intensities of the 28S and 18S RNA bands. RNA were randomly selected from different experiments and were loaded on the gel. The first lane at the left represents DNA ladder (1kb+). Lanes a, b and c: 100 ng, 300 ng, and 600 ng respectively of total RNA extracted from high-confluent H4-II-E cells treated with 10 nM TCDD for 4 h. Lanes d, e and f: 100 ng, 1 μ g and 2 μ g respectively of total RNA extracted from tissue rat liver treated chronically with 10 nM TCDD included as an external control for real-time RT-PCR analysis.

Section 3.2.4 qRT-PCR probe/ primer efficiency

In order to accurately measure the levels of mRNA in qRT-PCR, it is essential to validate the use of Pfaffl's method, which is derived from the $\Delta\Delta C_t$ method and corrects for efficiency, by determining the amplification efficiency (E) for each gene and demonstrating equal efficiency between the target and the reference genes.

Standard curves for human and rat *CYP1A1*, β -actin and *AhR* genes were determined by amplifying 5-fold serial dilutions of cDNA from H4-II-E and MCF-7 cells. Figure 3.12 shows concentrations of the template versus the C_t (threshold cycle). A least mean squares curve fitting algorithm is used to generate the standard curves displayed. Curves are displayed for each gene. Efficiency, slope and regression (RSq) of the standard curve fits for rat and human β -actin, *CYP1A1* and *AhR* genes are listed in Table 3.4 and Table 3.5 respectively.

Standard curves for all six genes had a regression coefficient close to 1, with real-time PCR efficiency of >100% (Table 3.4 and Table 3.5), with a slope close to 1, for which applied $E = (10^{-1/\text{slope}})$. An ideal PCR reaction will have an amplification efficiency of 100 (+/- 10%). The ef-

efficiencies determined from the standard were not significantly different from this range, and they were not significantly different from each other, except for human *β -actin*, where the PCR efficiency was 125%. However, since the PCR efficiency for the all genes was less than 140%, that was considered acceptable (<http://www.dddmag.com/reliability-of-qPCR-data.aspx>).

Therefore, the Pfaffl's method can be applied and *β -actin* reference gene was used for normalisation. Gene copy number will be calculated from the efficiencies determined for each set of TaqMan primers/probes as described in Materials and Methods (Section 2.2.13.2).

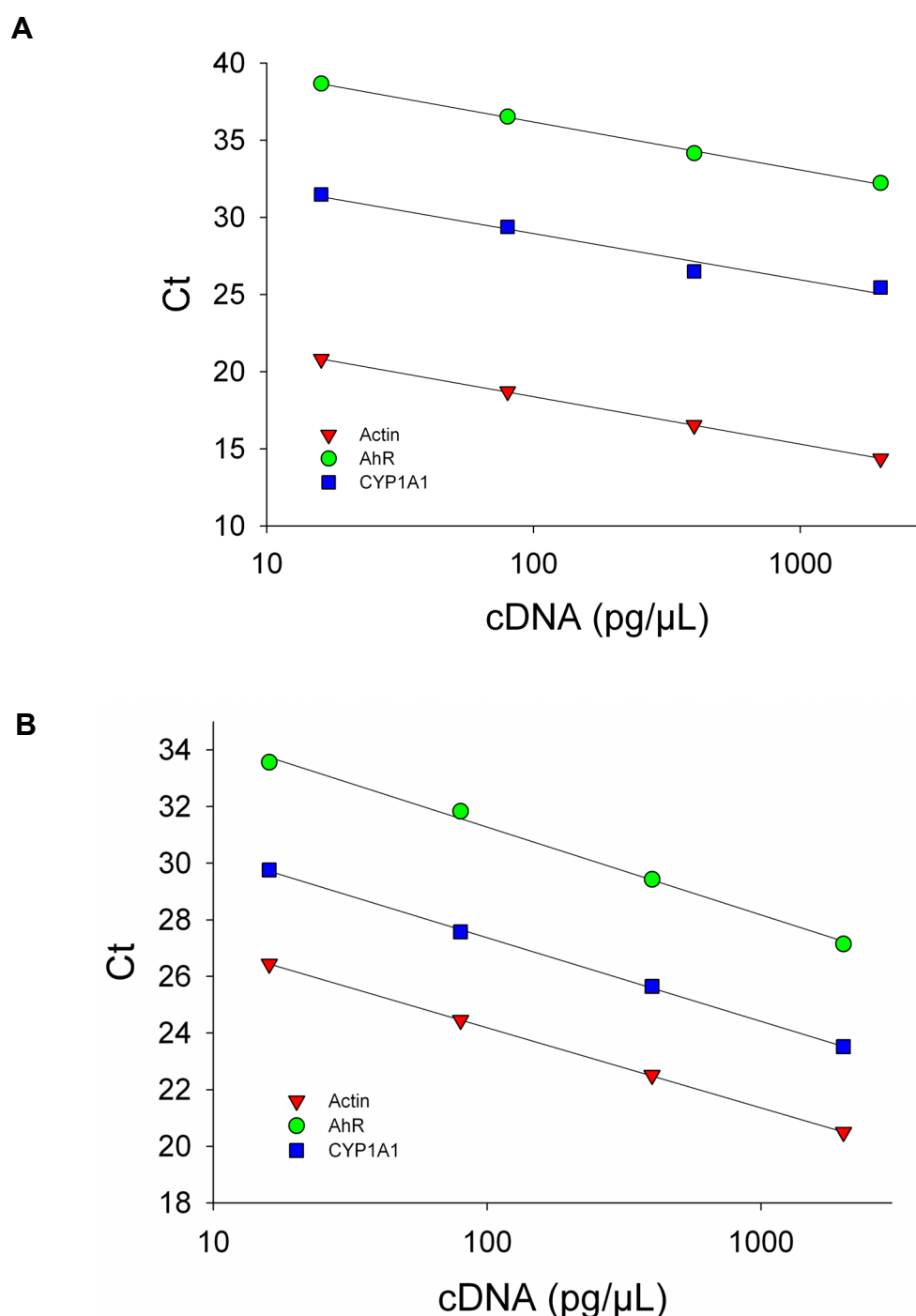


Figure 3.12 Amplification efficiencies for *CYP1A1*, β -actin and *AhR*. The cDNA from H4-II-E (A) and MCF-7 cells (B) was serially diluted and amplified with β -actin (*ROX*) (red triangles), *CYP1A1* (*FAM*) (blue squares) and *AhR* (*HEX*) primers (green circles) and detected with TaqMan probe with real-time RT-PCR. After 4-h incubation with TCDD (10 nM), cells were washed with 1x PBS, trypsinized then RNA isolated and reverse transcribed into cDNA. Serial dilutions of cDNA were amplified with qRT-PCR reaction for three genes β -actin, *CYP1A1* and *AhR* as described in Materials and Methods (Section 2.2.13.4). Standard curves were generated by using the least mean squares curve fitting algorithm by Mx4000 from individual experiments. Each point represents the average of mean for duplicate samples obtained from one experiment. Ordinates: Ct values. Abscissae: concentrations of cDNA (pg/ μ L).

Gene	Slope (Ct x pg ⁻¹ x µl ⁻¹)	Efficiency (%)	Regression
<i>CYP1A1</i>	-2.9	119	0.988
<i>β-actin</i>	-3.1	109	0.994
<i>AhR</i>	-3	114	0.996

Table 3.4 Quantitation data of qRT-PCR for rat genes. Slope, efficiencies and regression of *CYP1A1*, *β-actin* and *AhR*. Efficiencies are derived as percentages. The R Squared (RSq) or regression (Pearson's correlation coefficient) value was determined for each standard from the equation of the line. The slope is directly related to the average amplification efficiency throughout the cycling reaction. The amplification efficiency of the reaction is derived from the slope according to Pfaffl [162]: PCR efficiency = $10^{(-1/\text{slope})}$. The quantification data was generated by MX4000 Software using the least mean squares curve fitting as described under Materials and Methods Section 2.2.13.4

Gene	Slope (Ct x pg ⁻¹ x µl ⁻¹)	Efficiency (%)	Regression
<i>CYP1A1</i>	-2.95	118	0.996
<i>β-actin</i>	-2.83	125	0.997
<i>AhR</i>	-3.1	110	0.982

Table 3.5 Quantitation data of qRT-PCR for human genes. Slope, efficiencies and regression of *CYP1A1*, *β-actin* and *AhR*. Efficiencies are derived as percentages. The R Squared (RSq) or regression (Pearson's correlation coefficient) value was determined for each standard from the equation of the line. The slope is directly related to the average amplification efficiency throughout the cycling reaction. The amplification efficiency of the reaction is derived from the slope according to Pfaffl [162]: PCR efficiency = $10^{(-1/\text{slope})}$. The quantification data was generated by MX4000 Software using the least mean squares curve fitting as described under Materials and Methods Section 2.2.13.4.

Section 3.2.5 *CYP1A1* induction assay in H4-II-E cells

Section 3.2.5.1 Effect of confluence

This experiment investigates the effect of cell density on *CYP1A1* mRNA basal expression and inducibility in response to inducer, TCDD, in H4-II-E cells and aims to select the conditions under which there is optimal induction of *CYP1A1* mRNA and the response to TCDD is linear over the time course. H4-II-E cells were plated at a density of 1×10^4 cells/well. When cells attained

either 20-30% confluence (24 h, low-density; 5.6×10^4 /well) or 90-95% confluence, (72 h, high-density; 18×10^4 /well), the cells were treated by replacing the medium in cultures with fresh medium containing either 0.5% DMSO (vehicle control) or 10 nM TCDD and then incubated for 4, 8, 12 and 24 h. RNA was extracted from the cultures, transcribed into cDNA and subjected to qRT-PCR analysis essentially as described in Materials and Methods (Section 2.2.7, Section 2.2.8, Section 2.2.10, Section 2.2.13.2 and Section 2.2.13.3).

The measurements of mRNA use normalization against β -actin mRNA to correct for loading differences, so it was essential to test that β -actin mRNA expression is not affected by any treatment at any time of the induction. An additional reference gene used in this study was the *AhR* mRNA.

Figure 3.13 D and Figure 3.13 E show β -actin and *AhR*/ β -actin mRNA ratios relative to vehicle control at 4 h. The results show that the β -actin mRNA levels and *AhR*/ β -actin mRNA ratios were stable after all treatments, except for the β -actin mRNA for DMSO-treated cultures at 8 and 12 h, where the decreased levels were found to be significantly different from control at 4 h. However, this result may be due to insufficient input of cDNA in these samples, which was a consistent problem in low-density cultures. β -actin mRNA and the *AhR*/ β -actin mRNA ratios were more stable in high-density cultures. Thus, in high-density cultures, they are suitable to use as a reference genes. This finding proves that the induction of *CYP1A1* mRNA relative to controls was not due to sample variability as there was no corresponding change in the two control genes. The stable expression of reference genes over time and treatments, makes the analysis for *CYP1A1* mRNA more robust.

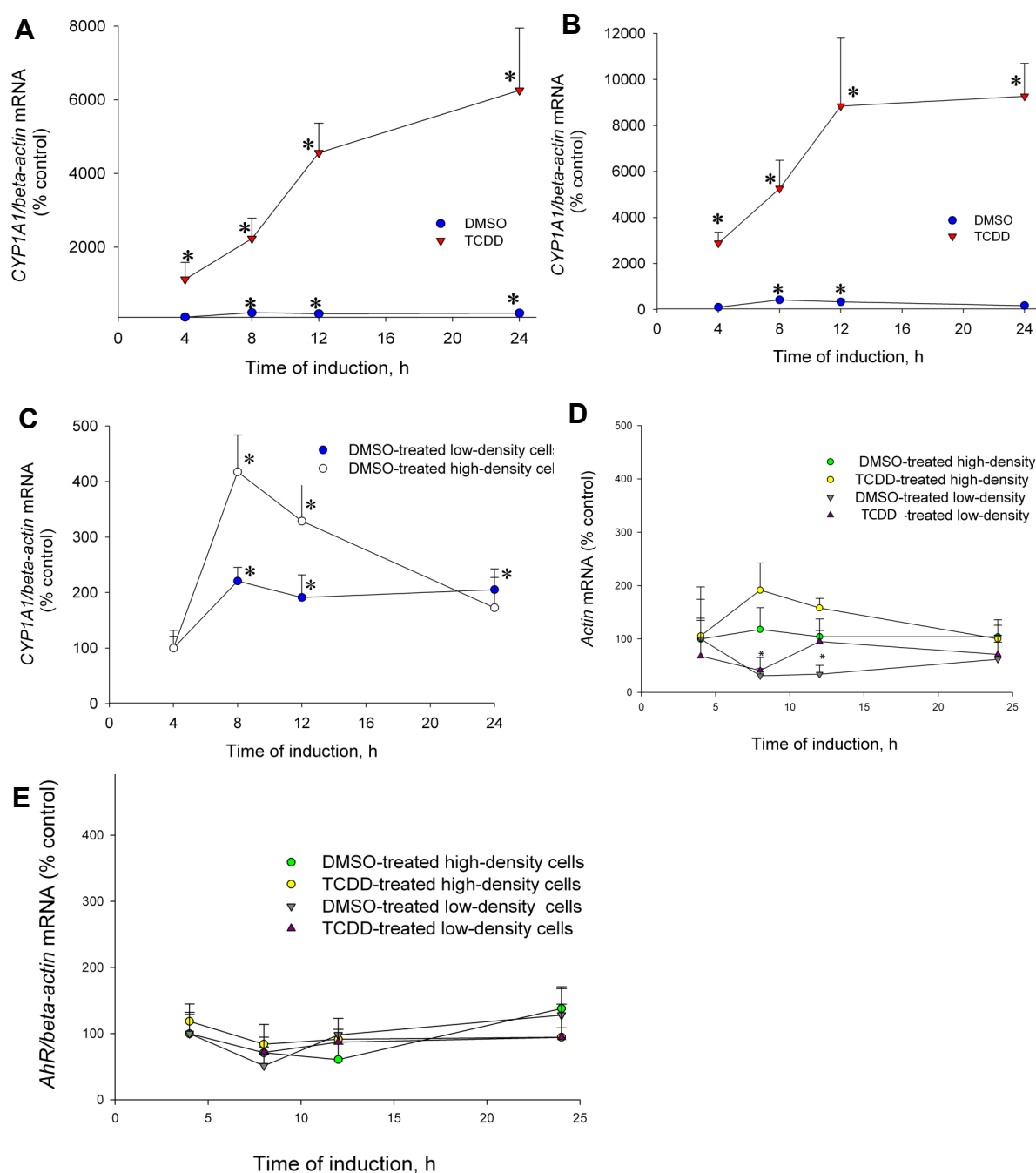


Figure 3.13 Effect of cell density on *CYP1A1* mRNA in H4-II-E cells over time course. **A.** Low- (5.6×10^4 cells/well) and **B.** high- (18×10^4 cells/well) density cultures were incubated with fresh medium containing 10 nM TCDD or 0.5% DMSO for 0, 4, 8, 12 and 24 h at 37°C, then harvested at the specified time. Total RNA was extracted and reverse-transcribed. 2 ng cDNA was amplified and Ct levels of *CYP1A1* and β -actin were determined by RT-PCR. The relative gene expression levels were normalized to those of β -actin and calculated from $E^{-\Delta\Delta C_t}$, as described in Material and Methods (Section 2.2.13.2). Each point represents the average of mean \pm S.D of four replicate determinations and is representative of results obtained from two experiments. Each qRT-PCR reaction was performed twice. In ordinates: (A, B and C) *CYP1A1*/ β -actin mRNA ratios relative to vehicle control at 4 h, (D) β -actin mRNA relative to vehicle control at 4 h, (E): *AhR*/ β -actin mRNA ratios relative to vehicle control at 4 h. The figure (E) is missing one data point, the DMSO-treated low-density cells at 4 h. (*, asterisks; $p < 0.05$, t -test, $n=4$, comparison of TCDD-treated cultures at each time point with vehicle controls at corresponding time points). β -actin mRNA and *AhR*/ β -actin mRNA ratios at different time points for each treatment were not significantly different from vehicle-treated cultures at 4 h ($p > 0.05$, one-way ANOVA analysis followed by Dunnett's Multiple Comparison test), except for β -actin mRNA for DMSO-treated low-density cells at 8 and 12 h (*) ($p < 0.05$, one-way ANOVA analysis followed by Dunnett's Multiple Comparison test).

It was important to examine *CYP1A1* mRNA levels in the control cultures, and determine if these were perturbed. Figure 3.13 C shows the results for DMSO-treated cultures displayed in Figure 3.13 A and B, but on a different scale. Figure 3.13 C shows that *CYP1A1*/ β -*actin* mRNA ratios were increased in vehicle controls in low-density cells at all time points relative to 4 h ($p < 0.05$, $n = 4$; one way-ANOVA analysis followed by Dunnett's Multiple Comparison test). In high-density cells, *CYP1A1*/ β -*actin* mRNA ratios are induced at 8 and 12 h ($p < 0.05$, $n = 4$; one way-ANOVA analysis followed by Dunnett's Multiple Comparison test) but decreased at 24 h ($p > 0.05$, $n = 4$; one way-ANOVA analysis followed by Dunnett's Multiple Comparison test) treatment relative to 4 h levels (Figure 3.13 C). This is in agreement with findings reported by Kocarek et al (1993) [172], where the *P450 1A1* RNA levels were increased 1 to 2 h after a medium change, reached maximum level at 6 h and declined to baseline by 24 h.

Figure 3.13 A and Figure 3.13 B reveal that the increase in *CYP1A1* mRNA levels by TCDD was observed as early as 4 h in both low- and high-density cells (4 h, $p < 0.01$, t -test, $n = 4$, compared to vehicle controls at 4 h). In high- and low-density cells, maximal levels of induced *CYP1A1* mRNA were achieved from 12 h and were maintained until 24 h. The mean and S.D for *CYP1A1*/ β -*actin* mRNA (% vehicle control at 4 h) induced by TCDD in high density cells at 8 and 12 h were, 5300 ± 1200 and 9000 ± 3000 respectively). Whereas, the mean and S.D for *CYP1A1*/ β -*actin* mRNA ratios (% vehicle control at 4 h) by TCDD in low-density cells, at 8 and 12 h were, 2200 ± 560 and 5000 ± 800 respectively. The maximal induced levels were 90-fold and 60-fold above controls for high- and low-confluent H4-II-E cells respectively. These results confirmed inducibility of the *CYP1A1* mRNA in low-(Figure 3.13 A) and high-(Figure 3.13 B) density H4-II-E cells by TCDD as previously reported [173] [58] [174] [175] [176] with 3-fold greater induction observed in high-compared with low-density cells ($p < 0.05$, t -test; $n = 4$, for TCDD-treated high density cultures over TCDD-treated low-density cultures at each time

point). In high and low density cells, the *CYP1A1/β-actin* mRNA ratios in response to TCDD, were still increasing till 12 h. Thus, working at early time points, such as 4 h, insures linearity of the response which deviates from linearity at 12 h and onward.

Given the higher induction levels of *CYP1A1/β-actin* mRNA by TCDD in high-density cells coupled with increased RNA yield, and the more stable expression of RNA of reference genes, high-density conditions were used subsequently. Throughout all experiments, unless indicated elsewhere in the text, cultures were seeded at a density of 1×10^5 cells/ well in 96 well plates so that they reach high-density by 24 h (Figure 3.10). After 24 h, inducing compounds were added at the indicated concentrations and cultures incubated for 4 h.

Section 3.2.5.2 Effect of varying the treatment time

The *CYP1A1/β-actin* mRNA ratios increased linearly till 12 h in response to 10 nM TCDD (Figure 3.13 B). However, TCDD is resistant to metabolism [61], and it is not known whether a metabolically labile compound, such as 5F 203 [146], would show a different time-course of induction of CYP1A1. The aim is to select the time at which the *CYP1A1/β-actin* mRNA ratios prove linear for both TCDD and 5F 203. The following experiment was conducted to examine the time-course profile of the induction of *CYP1A1/β-actin* mRNA ratios by 5F 203 under the same conditions applied for TCDD on H4-II-E cultures (Section 3.2.5.1). The experiment also seeks to examine the effect of DMSO on the *CYP1A1/β-actin* mRNA ratios H4-II-E cells over time course.

H4-II-E cells were incubated with 1 μM 5F 203 for 0, 2, 4, 6 and 8 h at 37°C. In parallel, cultures were incubated with 10 nM TCDD as a positive control or 0.1% DMSO as a negative control for 4 h. All treatments were added to cultures in fresh medium. Untreated cultures were not sub

jected to medium change and were included as a negative control. *CYP1A1* mRNA induction by TCDD (10 nM), 5F 203 (1 μ M) or 0.1% DMSO at different time points is shown in Figure 3.14 A.

Figure 3.14 B shows the time-response curve for the *CYP1A1*/ β -actin ratios in response to DMSO (0.1%). A significant increase in *CYP1A1* mRNA was observed in vehicle-treated cells

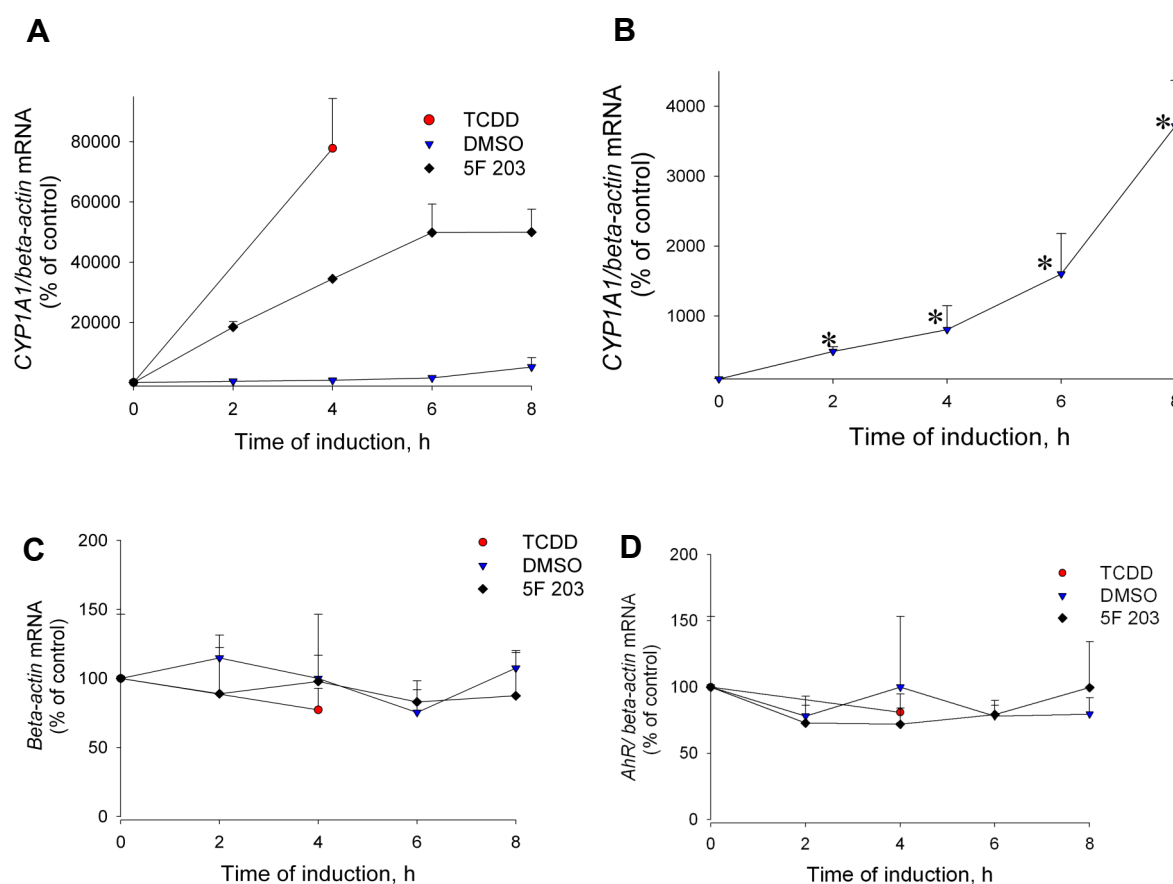


Figure 3.14 Time course of induction of *CYP1A1* mRNA by 5F 203 in H4-II-E cells. H4-II-E cultures were treated with fresh medium containing 1 μ M 5F 203 (black diamonds) or 0.1% DMSO (blue triangles) for 0, 2, 4, 6 and 8 h or TCDD (10 nM) (red circle), used as a positive control at 4 h. *CYP1A1*/ β -actin mRNA ratios were determined as described in Figure 3.13 legend. Each point represents the average of mean \pm S.D for four replicate determinations, and is representative of results obtained from two experiments. Each qRT-PCR reaction was performed twice. Ordinates: (A and B) *CYP1A1*/ β -actin mRNA ratio relative to untreated H4-II-E cells at 0 h, with (C) showing the DMSO-treated cultures displayed in (A) but on a different scale. (C) β -actin mRNA relative to untreated H4-II-E cells at 0 h, (D) *AhR*/ β -actin mRNA ratios relative to untreated H4-II-E cells at 0 h. (*, asterik, difference between means of DMSO-treated cultures at each time point and untreated cultures at 0 h were greater than two standard deviations). β -actin mRNA and *AhR*/ β -actin mRNA ratios at different time points for each treatment were not significantly different from untreated H4-II-E cells at 0 h ($p > 0.05$, one-way ANOVA analysis followed by Dunnett's Multiple Comparison test).

from 2 h up to 8 h consistent with the previous experiment (Figure 3.13 C). The increase of *CYP1A1*/ β -*actin* mRNA in DMSO-treated cultures from these results is in apparent contrast with literature reports of low basal hydroxylase activity in the H4-II-E cell line [173] [58] [177] or that DMSO at concentrations of 0.5% or less in the medium has no effect on aryl hydrocarbon hydroxylase induction in H4-II-E cell [171].

The expression of RNA in reference genes was first analysed. Figure 3.14 C and D characterize the expression of endogenous β -*actin* and *AhR* mRNA. As seen from these results, the expression of both β -*actin* and *AhR* mRNA was stable at all treatments at all time points. Thus the experiment proves that *CYP1A1*/ β -*actin* mRNA ratios do not reflect an artifact of sample loading or preparation.

A rapid and significant increase in *CYP1A1*/ β -*actin* mRNA ratio by 5F 203 was observed as early as 2 h (200-fold above 0-h untreated cells), before attaining maximal induction around 6-8 h. *CYP1A1*/ β -*actin* mRNA ratios achieved by 5F 203 were increasing over the period of 2-6 h and saturate at 6 h (Figure 3.14 A). The results confirmed that 5F 203 can induce *CYP1A1* mRNA. The relationship between *CYP1A1*/ β -*actin* mRNA ratios and time of treatment with 5F 203 was linear till 6 h. At 4 h of treatment with either TCDD or 5F 203, the induction of *CYP1A1*/ β -*actin* mRNA ratio was high enough to be measured reliably and was linear for both compounds. Therefore, further experiments will be conducted at 4 h treatment.

DMSO and inducers (TCDD and 5F 203) were added to the cell cultures by replacing the medium with fresh medium containing compound. A striking difference in the levels of *CYP1A1*/ β -*actin* mRNA in TCDD- treated cells was observed comparing the results of Figure 3.14 A with Figure 3.13 B. For example, in Figure 3.14 A, the levels of *CYP1A1* mRNA induced by TCDD after 4-h incubation were 780-fold above control (untreated cells at 0 h) as opposed to

only 30-fold above control (0.1% DMSO at 4 h) in Figure 3.13 B. It is important to note that the controls used in these two experiments are different. Figure 3.14 presents the data relative to untreated cells (negative control), which were not subjected to any medium change, whereas Figure 3.13 presents the data relative to vehicle-treated cells, which were subjected to replacement of the old medium with fresh medium containing DMSO. The magnitude of *CYP1A1* mRNA induction depends on the controls, since the data are presented relative to corresponding controls. Therefore, it was essential to control the background levels for *CYP1A1* in controls. This issue will be addressed in detail in the following experiment.

Section 3.2.5.3 Effect of medium on *CYP1A1* mRNA induction

The induction levels achieved by TCDD in the H4-II-E cells varied significantly between Figure 3.13 and Figure 3.14. Moreover, control *CYP1A1* levels were higher in Figure 3.13, than in Figure 3.14. One hypothesis is that fresh medium can induce *CYP1A1* mRNA. An alternative possibility is that DMSO caused the induction of *CYP1A1* mRNA.

To investigate these hypotheses, H4-II-E cultures were incubated for 24 h. After 24 h, high-density cultures were subjected to treatments (0.1% DMSO or 10 nM TCDD) by either:

- a) Replacing the incubation medium with pre-incubated (day-old) medium.
- b) Replacing the incubation medium with fresh medium.
- c) Adding 20 μ l of day-old medium to each well (to a final volume of 200 μ l).
- d) Adding 20 μ l of fresh medium to each well (to a final volume of 200 μ l).

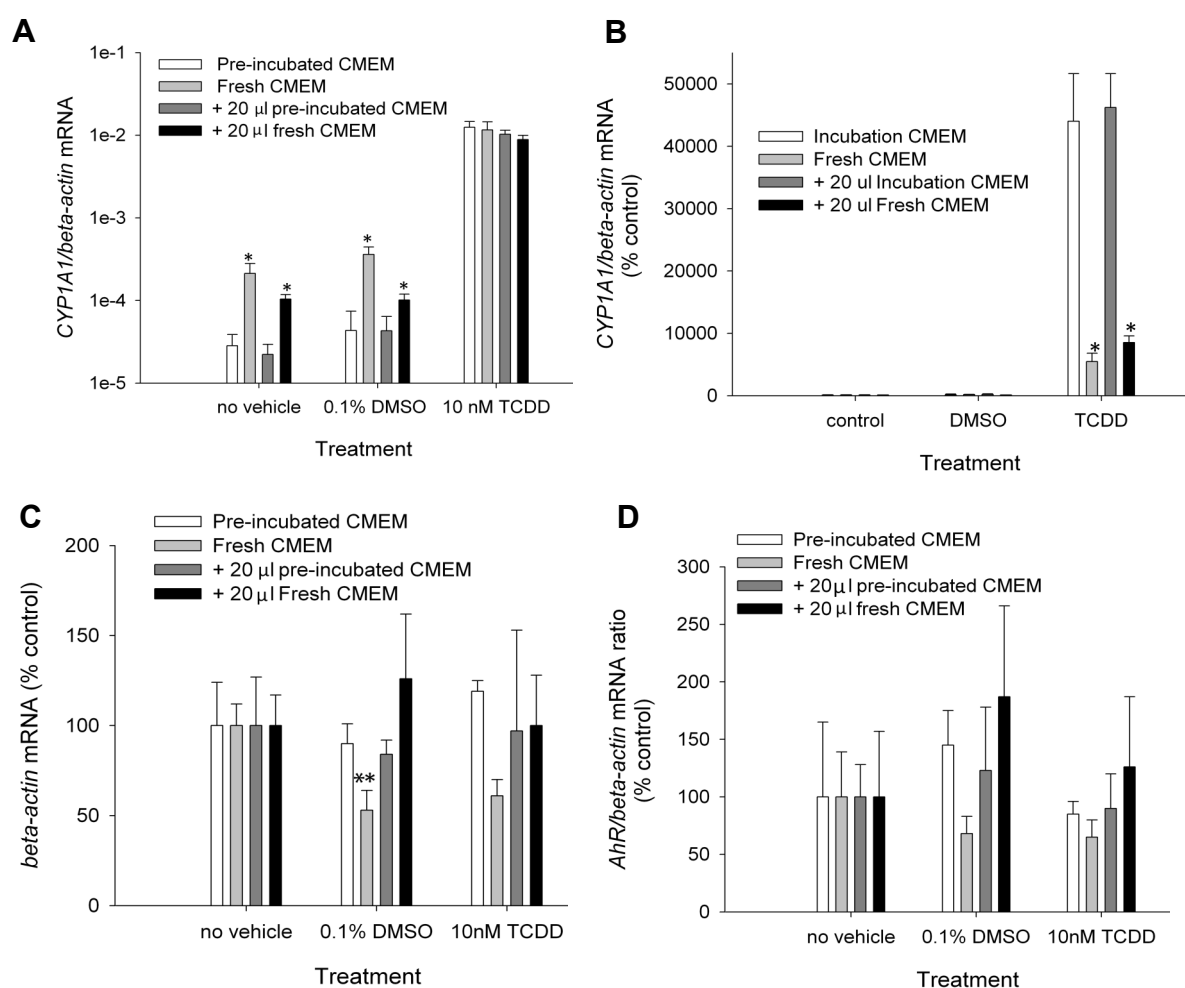


Figure 3.15 Effect of medium change on *CYP1A1* mRNA expression in H4-II-E cells: incubation medium (white bars), fresh medium (light gray bars), 20 μ l incubation medium (dark gray bars) or 20 μ l fresh medium (black bars) was added to untreated, vehicle (0.1% DMSO) or 10 nM TCDD-treated H4-II-E cultures for 4 h incubation at 37°C. *CYP1A1*/ β -actin mRNA ratios were determined as described in Figure 3.13 legend. Each bar represents the average of mean \pm S.D for triplicate samples, and is representative of results obtained from one of three experiments. Each qRT-PCR reaction was performed once. Ordinates: (A) *CYP1A1*/ β -actin mRNA ratios as absolute values on logarithmic scale, (B) *CYP1A1*/ β -actin mRNA ratios relative to no-vehicle cultures in pre-incubated medium on a linear scale, (C) β -actin mRNA relative to no-vehicle cultures, (D) *AhR*/ β -actin mRNA ratios relative to no-vehicle cultures. (*; $p < 0.01$; t -test, $n = 3$ for comparing no vehicle-, vehicle- or TCDD-treated cultures in fresh medium with those in pre-incubated medium, in parallel for comparing no vehicle-, vehicle- or TCDD-treated cultures with addition of 20 μ l fresh medium with those subjected to 20 μ l pre-incubated medium, **; $p < 0.05$; t -test, $n = 3$ for comparing DMSO-treated cultures in fresh medium with no-vehicle treated cultures in pre-incubated medium set as control).

Figure 3.15 shows the effect of medium and DMSO on *CYP1A1* mRNA basal expression and on TCDD-induced *CYP1A1* mRNA levels. The expression of β -actin mRNA and *AhR*/ β -actin-mRNA ratios are shown in Figure 3.15 C and D. The results prove that the constitutive expres

sion of the reference genes is stable after all treatments, except for β -actin in DMSO-treated cultures in fresh medium, which was found significantly different from no-vehicle treated control cultures in pre-incubated medium ($p < 0.05$, t -test, $n=3$). However, this latter result was not reproduced in other experiments. Overall, the mRNA levels for the reference genes were found to be relatively stable at all treatments, which provides reliability for the results and analysis of this experiment.

Figure 3.15 A shows the *CYP1A1*/ β -actin mRNA ratios as absolute values on a logarithmic scale, whereas in Figure 3.15 B, the data are normalised relative to vehicle control on a linear scale. Low but detectable basal levels of *CYP1A1*/ β -actin mRNA were observed in no vehicle-cultures not subjected to any fresh medium. The *CYP1A1*/ β -actin mRNA ratios were $2.8 \pm 1.0 \times 10^{-5}$ and $6 \pm 2 \times 10^{-5}$ for the no vehicle-cultures incubated with day-old medium or subjected to addition of 20 μ l of pre-incubated medium respectively. The *CYP1A1*/ β -actin mRNA ratios were $2 \pm 0.9 \times 10^{-4}$ and $1 \pm 0.1 \times 10^{-4}$ for the no vehicle-cultures incubated with fresh medium or subjected to addition of 20 μ l of fresh medium respectively. *CYP1A1*/ β -actin mRNA ratios were significantly increased when medium was replaced with fresh medium or when cultures were exposed to 20 μ l of fresh medium ($p < 0.05$, t -test, $n=3$). The level of *CYP1A1* mRNA in no-vehicle cultures incubated with fresh medium was 8-fold above no vehicle-cultures with pre-incubated medium. The level of *CYP1A1* mRNA in no vehicle-treated cultures subjected to addition of 20 μ l fresh medium were 5-fold above no vehicle-cultures subjected to 20 μ l pre-incubated medium ($p < 0.01$, t -test, $n=3$). No significant difference was observed for no vehicle-cultures subjected to addition of 20 μ l incubation medium compared to untreated cells in incubation medium. The *CYP1A1*/ β -actin mRNA levels were significantly higher in cultures treated with fresh or subjected to addition of 20 μ l fresh medium containing DMSO over vehicle-treated cultures with pre-incubated medium containing DMSO ($p < 0.05$, t -test, $n=3$). Therefore,

fresh medium is causing induction of *CYP1A1* mRNA (Figure 3.15 A). Addressing the possibility of DMSO as an inducer of *CYP1A1* mRNA, the results of Figure 3.15 A show that the addition of DMSO (0.1%) to cultures did not induce *CYP1A1*/ β -actin mRNA significantly over corresponding no vehicle-cultures ($p > 0.05$, t -test, $n=3$). This finding rules out the possibility that DMSO was an inducer of *CYP1A1* mRNA in this cell line. This is consistent with previous findings [178] [173] [179] [171].

CYP1A1/ β -actin mRNA ratios were increased by TCDD in all cultures (in pre-incubated medium, fresh medium or subjected to 20 μ l either pre-incubated medium or fresh medium) with similar absolute ratios (Figure 3.15 A). When these data were normalised to no-vehicle controls, *CYP1A1*/ β -actin mRNA ratio induced by 10 nM TCDD was 440-fold greater in cultures in pre-incubated medium compared to those with fresh medium (55-fold) ($p < 0.01$, t -test, $n=3$) (Figure 3.15 B). Similar levels of *CYP1A1*/ β -actin mRNA expression were observed in vehicle-treated cultures in pre-incubated medium and those subjected to addition of 20 μ l pre-incubated medium containing DMSO. This is also true for TCDD-treated cultures, where no difference was found in cultures in pre-incubated medium containing TCDD compared with cultures subjected to addition of 20 μ l pre-incubated medium containing TCDD (Figure 3.15 A).

To summarize, the results from Figure 3.15 A showed significant differences in the levels of *CYP1A1*/ β -actin mRNA in cells depending on the medium in which the drugs were diluted and subsequently cells were incubated. Consequently, the fold-induction of *CYP1A1*/ β -actin mRNA levels induced by TCDD was markedly affected depending on the corresponding controls (Figure 3.15 B). The results suggest that the factor that was affecting the *CYP1A1*/ β -actin mRNA background levels in the previous experiments (Figure 3.13 C and Figure 3.14 B) was the fresh medium and this problem was controlled by treating the cells with drugs diluted in a pre-incubated medium. Furthermore, these findings provide an explanation for the variability of the in-

duced levels by TCDD for the two experiments (Figure 3.13 and Figure 3.14). Thus, in subsequent experiments, cultures will be exposed to chemicals, added in 20 μ l of pre-incubated medium for a total volume of 200 μ l per well. This is consistent with earlier observations in this study (Figure 3.13 B & Figure 3.14) and provides explanation for the high background for the *CYP1A1*/ β -actin mRNA in controls (Figure 3.14 B).

Section 3.2.6 Effect of time on the dose response curves for TCDD

Figure 3.13 B showed that the induction of *CYP1A1* mRNA expression in H4-II-E cells as a function of time of exposure to TCDD was linear up to 12 h when the response starts to saturate.

It is possible that assaying dose-response relationships under non-linear conditions could displace the EC_{50} for induction of *CYP1A1* [180]. This experiment investigates the effect of time on TCDD log concentration-response curves in H4-II-E cultures, by comparing induction at linear (4 h) and non linear (24 h) response.

H4-II-E cultures were treated with TCDD for 4 and 24 h and *CYP1A1* mRNA expression was determined by qRT-PCR as described in Materials and Methods (Section 2.2.13.3).

Expression of the β -actin and *AhR* mRNA ratios was analysed in parallel to the quantitation of *CYP1A1* mRNA induction in each experiment. Figure 3.16 B and Figure 3.16 C show the expression of β -actin and *AhR*/ β -actin mRNA ratios. The results prove that the constitutive expression of the reference genes is stable after TCDD treatment at all concentrations, at both 4 and 24 h.

Figure 3.16 A shows a significant induction of *CYP1A1*/ β -actin mRNA ratios over vehicle-treated H4-II-E cells from 10 pM TCDD at 4 h ($p < 0.01$, t -test; $n=3$). The maximal levels of *CYP1A1*/ β -actin mRNA ratios were achieved by 100 pM TCDD.

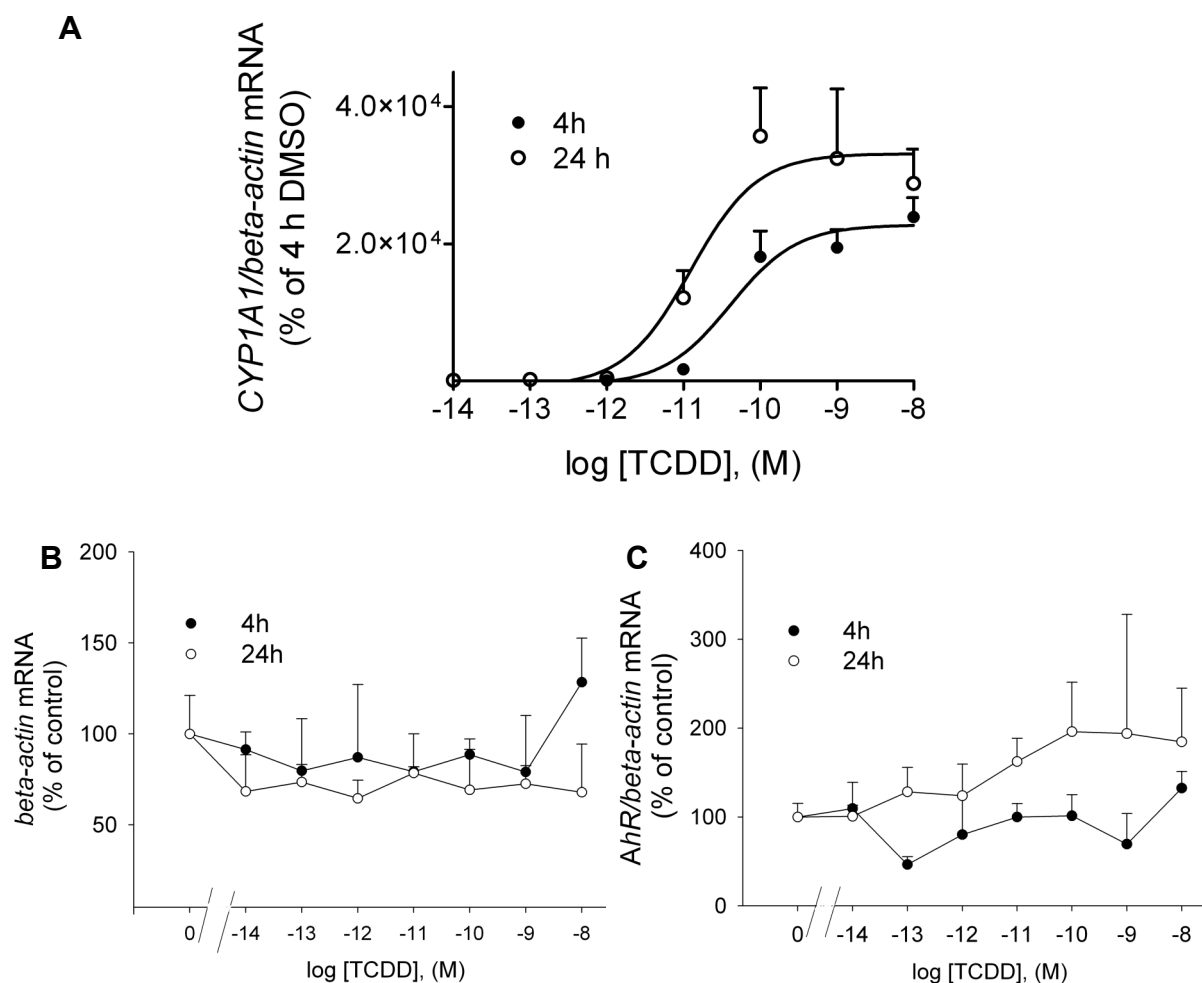


Figure 3.16 Effect of time on the concentration-response curves for *CYP1A1* mRNA induction by TCDD in H4-II-E cells. Cultures were exposed to DMSO (0.1%) or TCDD (at the indicated concentrations) for 4 h [●] and 24 h [○]. *CYP1A1*/β-actin mRNA ratios were determined as described in Figure 3.13 legend. Each point represents the mean ± S.D for triplicate samples from one experiment. Each qRT-PCR reaction was performed once. The mean and S.D for *CYP1A1*/β-actin mRNA absolute ratios for untreated and vehicle-treated H4-II-E cells were $2.2 \pm 0.7 \times 10^{-5}$ and 4.3×10^{-5} respectively. Curves were fitted using the variable slope sigmoid Hill equation (GraphPad 5.0 Software). Ordinates: (A) *CYP1A1*/β-actin mRNA ratios relative to 4 h DMSO, (B) β-actin mRNA relative to 4 h DMSO, (C) *AhR*/β-actin mRNA ratios relative to 4 h DMSO. Abscissae: logarithms of molar concentrations of TCDD. β-actin mRNA and *AhR*/β-actin mRNA ratios for vehicle-treated cultures at 4 h were represented by zero molar concentrations. β-actin mRNA and *AhR*/β-actin mRNA ratios at different time points for each treatment were not significantly different from vehicle-treated cells at 4 h ($p > 0.05$, one-way ANOVA analysis followed by Dunnett's Multiple Comparison test).

From 100 pM onward, the maximal saturated *CYP1A1*/β-actin mRNA ratios (percentage of 4 h DMSO) induced by TCDD were 23×10^3 % (95% CI, 18-27) and 33×10^3 % (95% CI, 26- 41), at 4 and 24 h respectively. TCDD's EC₅₀ values were 40 pM (95% CI, 12-140) and 13 pM (95% CI, 2.8-57) at 4 h and 24 h respectively. This experiment showed no significant difference of

time treatment (4 and 24 h) with TCDD on the EC_{50} values for induction of *CYP1A1* mRNA in H4-II-E cells (as the difference between means of EC_{50} at 4 and 24 h, were less than two standard deviations).

The effect of time on TCDD log concentration-response curves is expected to be higher than observed. However, the effect was not detected given that the 95% confidence intervals of the mean were very large (> 10 -fold) and overlapping. Based on earlier observations that the levels of *CYP1A1*/ β -actin mRNA ratios induced by TCDD at 4 h were 3-fold lower than those at 24 (Figure 3.13 B), the magnitude of the effect desired is expected to be at least 3-fold, in order to be considered significant. However, given the large size of variation, the powers of the experiment were limited and so the ability to detect a small effect as 3-fold was masked. Overall, the EC_{50} of TCDD is more likely to be affected by the time, but the experiment failed to detect it (this is called type II error). Thus, this experiment needs to be repeated in the future, including more concentrations between 10^{-12} M and 10^{-10} M, in order to reduce the 95% confidence intervals.

Section 3.2.7 Induction of *CYP1A1* mRNA by 3-methylcholanthrene (MC)

The nonhalogenated aromatic hydrocarbon, MC, exhibits similar binding to AhR as TCDD in rat [67] but is 30,000-fold less potent at inducing AHH in rat liver *in vivo* [181]. It was suggested that the reduced potency of nonhalogenated aromatic hydrocarbons is influenced by their more rapid metabolism [180] in comparison with the poorly metabolized TCDD [61]. The aim was to see whether the EC_{50} for the induction of *CYP1A1* mRNA of a compound, known to be metabolized, such as MC, can be determined under the conditions of the current assay. The ability of MC and TCDD to induce *CYP1A1* mRNA was investigated in H4-II-E cells. Cultures of H4-II-E cells were exposed to increasing concentrations of MC, the positive control TCDD or the

negative control DMSO (0.1%) for 4 h. The positive control TCDD produced maximal *CYP1A1* mRNA induction at 10 nM, which was set at 100%. The expression of β -actin mRNA and *AhR*/ β -actin mRNA ratios was examined for stability. It was essential that these reference genes proved unchanged over treatments, so that the results will be considered reliable and analysis for *CYP1A1* mRNA will be performed. As shown in Figure 3.17 B and C, generally, the expression was found stable with less than two-fold variation, thus the experiment proves that *CYP1A1*/ β -actin mRNA ratios do not reflect an artifact of sample loading or preparation. Figure 3.17 shows that TCDD and MC have similar maximal levels of *CYP1A1* mRNA induction in H4-II-E cells, as previously reported [180] [177]. The maximum *CYP1A1*/ β -actin mRNA levels attained by TCDD and MC relative to 10 nM TCDD were 117 for MC (95% CI, 109-124) and 100 for TCDD (95% CI, 94-113).

EC₅₀ values for TCDD and MC were 60 pM (95% CI, of 33-100) and 9 nM (95% CI, 7-13) respectively. The log concentration-response curves in Figure 3.17 A show that MC is ~150-fold less potent than TCDD in H4-II-E cells. These results prove the potency of MC for inducing *CYP1A1* mRNA in H4-II-E cells. This compound was found much less potent in rat liver *in vivo* [181] compared to TCDD. In the present study, MC was 150-fold more potent compared with the 30,000-fold from literature report [181]. This could be due to the possibility that, in the current assay, *CYP1A1* mRNA was measured in H4-II-E cells under conditions where metabolism of MC would be minimal (4 h by qRT-PCR) as opposed to *in vivo* at 24 h [181]. In the light of these results, the current induction assay proves useful tool to measure the EC₅₀ for the induction of *CYP1A1* mRNA for compounds prone to self-metabolism, such as phenylbenzothiazole compounds [182].

The induction assays for *CYP1A1* mRNA by TCDD in H4-II-E cells were conducted on different occasions and EC₅₀ values for TCDD are displayed in Table 3.6.

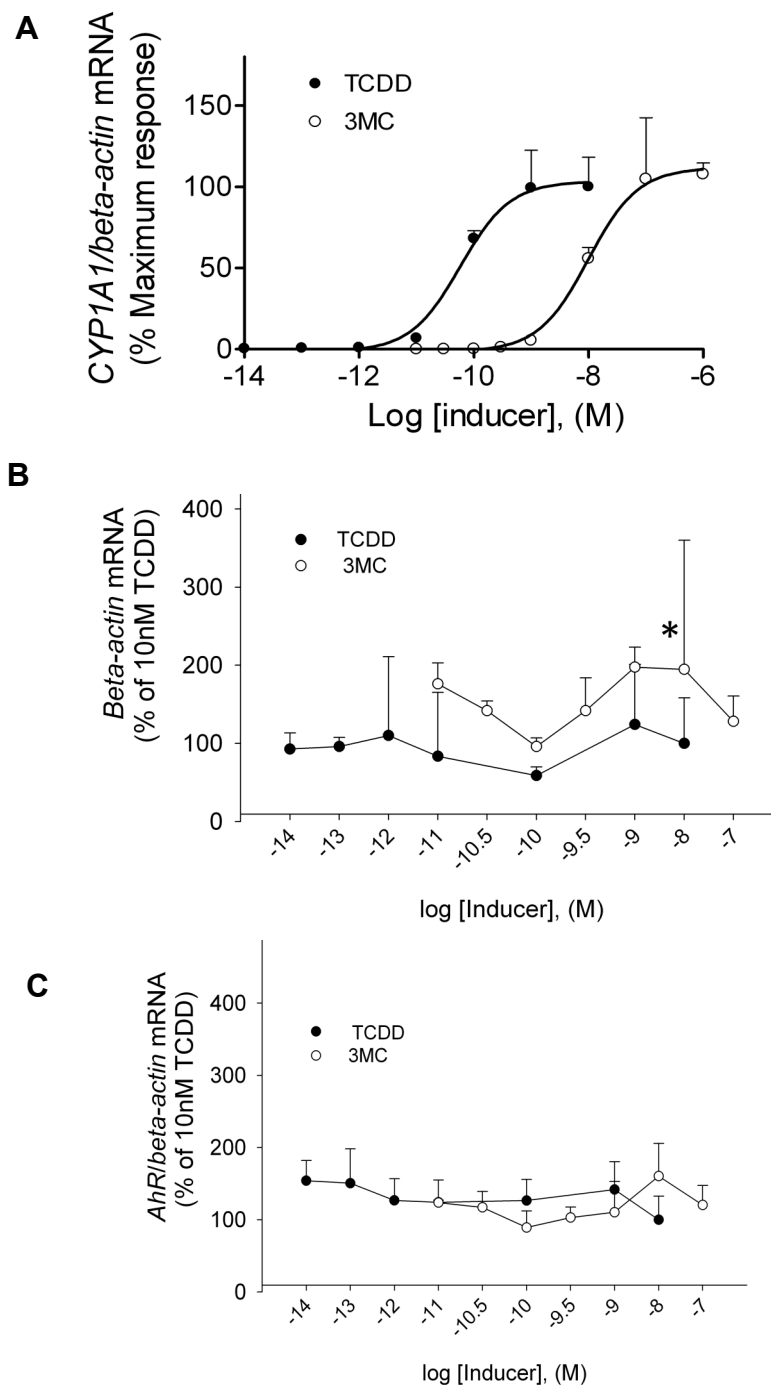


Figure 3.17 Effect of TCDD and MC on *CYP1A1* mRNA in H4-II-E cells. Cultures were treated with DMSO (0.1%), TCDD [●] or MC [○] (at the indicated concentrations) for 4 h. *CYP1A1*/ β -actin mRNA ratios were determined as described in Figure 3.13 legend. Each point represents the average of mean \pm S.D for triplicate samples, and is representative of results obtained from one of two experimental trials (for MC) and four for (TCDD). Each qRT-PCR reaction was performed once. The mean and S.D for *CYP1A1*/ β -actin basal ratios attained by untreated cultures and vehicle controls was $3.8 \pm 1.4 \times 10^{-6}$ and $1.78 \pm 1.23 \times 10^{-5}$ respectively. The mean and S.D for *CYP1A1*/ β -actin ratios for 10 nM TCDD-treated cultures was 0.15 ± 0.004 . Curves were fitted using the variable slope sigmoid Hill equation (GraphPad Prism 5.0 Software). Ordinates: (A) *CYP1A1*/ β -actin RNA ratios relative to 10 nM TCDD, (B) β -actin mRNA ratios relative to 10 nM TCDD, (C) *AhR*/ β -actin mRNA ratios relative to 10 nM TCDD. Abscissae: logarithms of molar concentrations of TCDD and MC. β -actin mRNA and *AhR*/ β -actin mRNA ratios at different time points for each treatment concentration were not significantly different from 10 nMTCDD-treated cells at 4 h ($p > 0.05$, one-way ANOVA analysis followed by Dunnett's Multiple Comparison test), except for β -actin mRNA treated with 10 nM 3MC (*, $p < 0.05$, one-way ANOVA analysis followed by Dunnett's Multiple Comparison test).

Experiments	EC ₅₀ [pM] (95% confidence intervals)
(1)	60 (33-100)
(2)	41 (12-140)
(3)	30 (5-166)
(4)	30 (2-425)
Average ± S.D	40 ± 13

Table 3.6 Summary for the EC₅₀ values of TCDD for the induction of *CYP1A1* mRNA in H4-II-E cells. EC₅₀ values were determined from log concentration-response curves using the variable slope Hill sigmoidal equation (GraphPad Prism 5.0). Each trial was conducted on a range of concentrations, each in triplicate samples. The average and S.D represent the mean and standard deviations of EC₅₀ values from four independent experiments.

These data show reproducibility of the induction assay; note that the coefficient of variation of assay EC₅₀ values is 32.5%.

Section 3.2.8 Induction of *CYP1A1* mRNA by 5F 203

5F 203 was found to be a high-affinity ligand for rat AhR (Section 3.1.8; Figure 3.9). This compound is expected to be a potent inducer of *CYP1A1* mRNA in rat H4-II-E cells. To assess the agonistic activity of 5F 203, cultures of H4-II-E cells were exposed to increasing concentrations of 5F 203. *CYP1A1* mRNA levels are expressed relative to the maximal induced level, which is arbitrarily obtained using 10 nM TCDD. The positive controls TCDD were included from another experiment (see Section 3.2.7; Figure 3.17), to compare the EC₅₀ for both compounds. It was not possible to test higher concentrations of 5F 203, because of the insolubility of the 5F 203 at concentrations higher than 30 µM. The log concentration response-curves of TCDD and 5F 203 for *CYP1A1* mRNA in H4-II-E cells are shown in Figure 3.18.

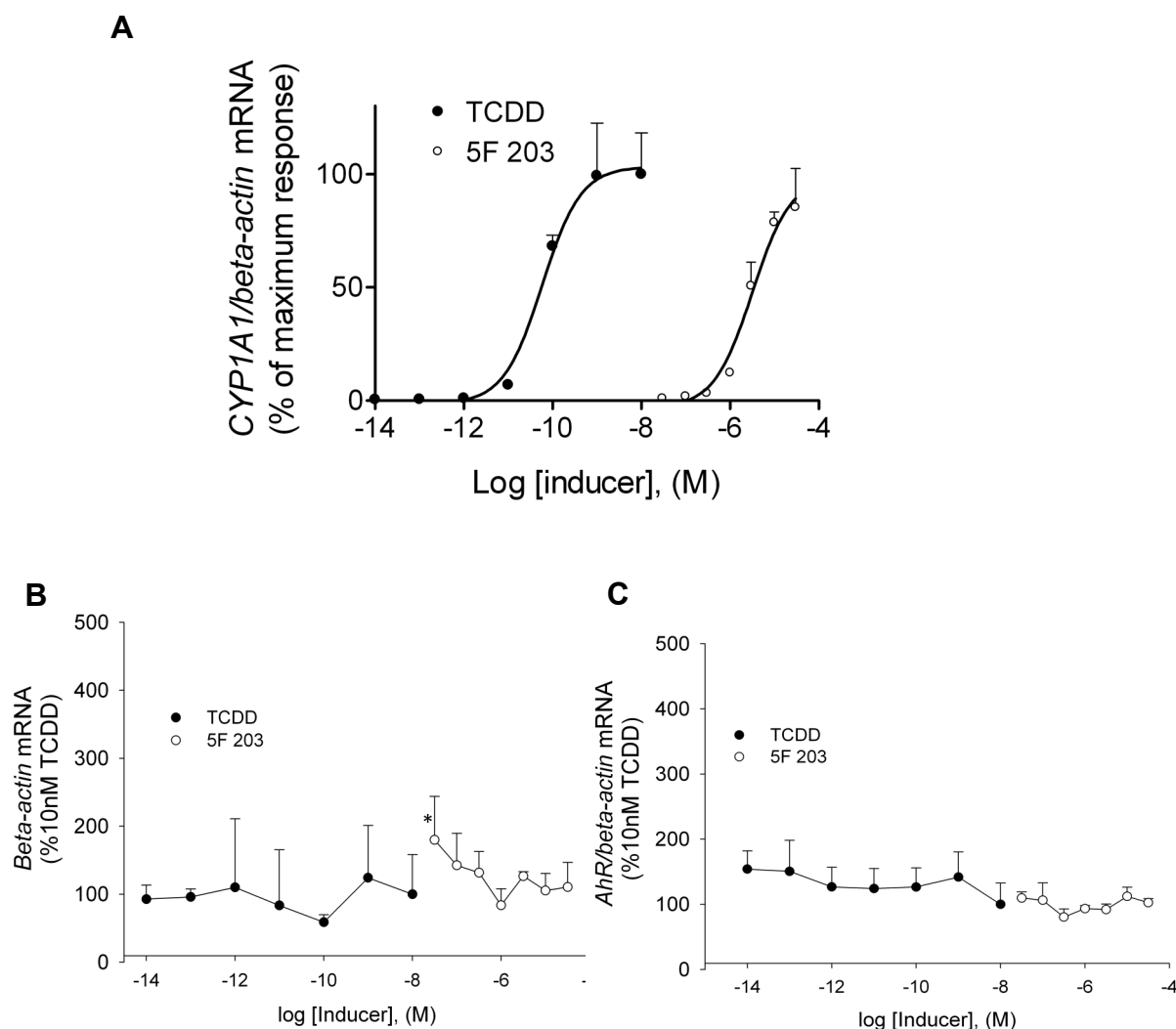


Figure 3.18 Concentration-response curves for *CYP1A1* mRNA induction by TCDD and 5F 203 in H4-II-E cells. Cultures were treated with DMSO (0.1%), 10 nM TCDD [●] or 5F 203 [○] (at the indicated concentrations) for 4 h. *CYP1A1*/ β -actin mRNA were determined as described in Figure 3.13 legend. Response curves were combined from two separate experiments. Log concentration-response curve for TCDD is the same displayed in Figure 3.17. Each point represents the average of mean \pm S.D for triplicate samples, and is representative of results obtained from one experiment (for 5F 203) and four experiments (for TCDD). Each qRT-PCR reaction was performed once. The mean and S.D for *CYP1A1*/ β -actin ratios were $1.9 \pm 1.3 \times 10^{-5}$ and $4.6 \pm 1.3 \times 10^{-5}$ for the untreated- and DMSO-treated cultures. The mean and S.D for *CYP1A1*/ β -actin ratios for 10 nM TCDD-treated cultures was 0.02 ± 0.004 . Curves were fitted using the variable slope sigmoid Hill equation (Graph-Pad Prism 5.0 Software). Ordinates: (A) *CYP1A1*/ β -actin RNA ratio relative to 10 nM TCDD, (B) β -actin mRNA relative to 10 nM TCDD, (C) *AhR*/ β -actin mRNA ratio relative to 10 nM TCDD. Abscissae: logarithms of molar concentrations of TCDD and 5F 203. β -actin mRNA and *AhR*/ β -actin mRNA ratios at different time points for each treatment concentration were not significantly different from 10 nM TCDD-treated cells at 4 h ($p > 0.05$, one-way ANOVA analysis followed by Dunnett's Multiple Comparison test), except for the β -actin mRNA treated with 30 nM 5F 203 (*, $p < 0.05$, one-way ANOVA analysis followed by Dunnett's Multiple Comparison test).

The expression β -actin mRNA and *AhR*/ β -actin mRNA ratios was examined for stability. As shown in Figure 3.18 B and C, generally, the expression was found stable within less than two

fold variation, thus the experiment proves that *CYP1A1*/ β -actin mRNA ratios do not reflect an artifact of sample loading or preparation.

As seen in Figure 3.18 A, 5F 203 increased the levels of *CYP1A1* mRNA in a concentration-dependent manner. Increased levels were observed from a concentration of 1 μ M, up to the maximum concentrations tested. The EC₅₀ for 5F 203 was 3 μ M (95% CI, 1.3-7.7) whereas EC₅₀ for TCDD was 60 pM (95% CI, 33-100). 5F 203 was able to induce *CYP1A1* mRNA but with ~50,000-fold less potency than TCDD. The 5F 203 log concentration-response curve shows that a maximal response was achieved from 10 μ M and the maximal levels of the *CYP1A1* mRNA induced by 5F 203 were 99% (95% CI, 77-120) compared with 100% by TCDD (95% CI, 94-113). These results show that 5F 203 can induce *CYP1A1* mRNA to a similar level as that seen with TCDD. Based on that, 5F 203 is a full agonist but is much less potent than TCDD.

Section 3.2.9 Induction of *CYP1A1* mRNA by IH 445, DF 203, GW 610, AW 892 and IH 318

In Section 3.1.8 (Table 3.3), DF 203, GW 610, AW 892, IH 318 and IH 445 compounds were found to be potent AhR ligands with the latter having the highest binding affinity ($K_i \approx 1$ nM). These compounds were expected to be potent inducers for *CYP1A1* mRNA in H4-II-E cells. The ability of these compounds for inducing *CYP1A1* mRNA was examined in H4-II-E cells. The induction assay was conducted essentially as described in Materials and Methods (Section 2.2.14). In Figure 3.19 are shown the log concentration-response curves for *CYP1A1* mRNA induction by DF 203, GW 610, AW 892, IH 318 and IH 445 in H4-II-E cells.

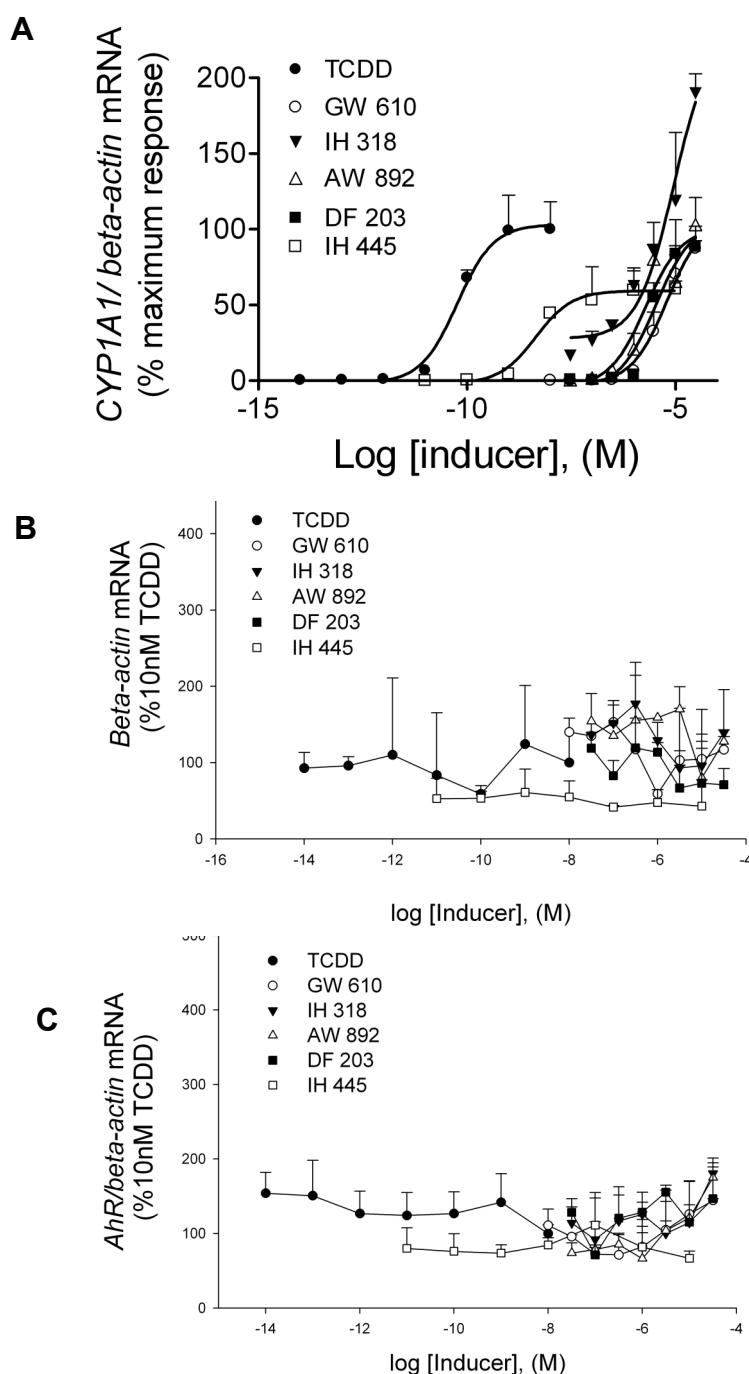


Figure 3.19 Concentration-response curves for the induction of *CYP1A1* mRNA by TCDD, IH 445, DF 203, GW 610, AW 892 and IH 318 in H4-II-E cells. Cultures were treated with DMSO (0.1%), 10 nM TCDD [●], IH 445 [□], DF 203 [■], GW 610 [○], AW 892 [△] or IH 318 [▼] (at the indicated concentrations) for 4 h. *CYP1A1*/β-actin mRNA were determined as described in Figure 3.13 legend. Response curves were combined from separate experiments. Each point represents the average of mean ± S.D for triplicate samples, and is representative of results obtained from one of two experimental trials for (IH445) and four for (TCDD). For the rest of the compounds, the results were obtained from a single experiment. Each qRT-PCR reaction was performed once. Log concentration-response curve for TCDD is the same displayed in Figure 3.17. Curves were fitted using the variable slope sigmoid Hill equation (GraphPad Prism 5.0 Software). Ordinates: (A) the *CYP1A1*/β-actin mRNA ratios relative to 10 nM TCDD, (B) β-actin mRNA relative to 10 nM TCDD, (C) AhR/β-actin mRNA ratios relative to 10 nM TCDD. Abscissae: logarithms of molar concentrations of inducers. β-actin mRNA and AhR/β-actin mRNA ratios at different time points for each treatment concentration were not significantly different from 10 nM TCDD-treated cells at 4 h ($p > 0.05$, one-way ANOVA analysis followed by Dunnett's Multiple Comparison test).

The expression of β -actin mRNA and *AhR*/ β -actin mRNA ratios was examined for stability. As shown in Figure 3.19 B and C, the expression was generally found to be stable with less than two-fold variation, thus the experiment proves that *CYP1A1*/ β -actin mRNA ratios do not reflect an artifact of sample loading or preparation.

Because the EC₅₀ and the maximal levels for *CYP1A1*/ β -actin mRNA ratios are compared between the test compounds and TCDD across experiments in some occasions, it was essential to examine whether the controls used across experiments did not change significantly. Negative (untreated- and vehicle-treated cultures) and positive control levels for *CYP1A1*/ β -actin mRNA ratios for Figure 3.19 are shown in Table 3.7. These values fall in within 2-3 fold of variability, which is acceptable, and thus the results on these test compounds were reliable.

The EC₅₀ for induction of *CYP1A1*/ β -actin mRNA by IH 445 was 4 nM (95% CI, 2-10), which is 67-fold less potent than that of TCDD (EC₅₀ = 60 pM with 95% CI, 33-100). The maximal *CYP1A1*/ β -actin mRNA ratios were 60% of that seen with 10 nM TCDD. The apparent lower maximal levels by IH 445 will be discussed further (see below Figure 3.29). Higher concentrations of IH 445 were not tested due to the insolubility of the compound in the medium. Importantly, in this assay, this compound was 800-times more potent than 5F 203.

The EC₅₀ values and maximal induced levels (as percentage of 10 nM TCDD) for the phenyl-benzothiazole compounds tested are listed in Table 3.8. From these results, the EC₅₀ values for DF 203, GW 610, AW 892 and IH 318 are all in the micromolar concentrations. DF 203 and AW 892 displayed similar potency as 5F 203 for inducing *CYP1A1* mRNA, *i.e.*, they are much less potent (>50,000-fold) than TCDD. However, GW 610 and IH 318 were 2- and 3-fold less potent than 5F 203. Importantly, the IH 318 compound elicited TCDD supermaximal levels. However, saturated levels could not be obtained because of the insolubility of the IH 318 at con

Compound	Untreated-cultures	Vehicle-treated cultures	10 nM TCDD-treated cultures
IH 445	$1.5 \pm 0.7 \times 10^{-5}$	$2.7 \pm 0.9 \times 10^{-5}$	0.024 ± 0.0028
DF 203	$5.6 \pm 1.8 \times 10^{-5}$	$6.6 \pm 2.2 \times 10^{-5}$	0.01 ± 0.002
GW 610	$2 \pm 1.3 \times 10^{-5}$	$4.6 \pm 1.3 \times 10^{-5}$	0.02 ± 0.004
AW 892	$1.6 \pm 0.7 \times 10^{-5}$	$2.8 \pm 0.9 \times 10^{-5}$	0.01 ± 0.002
IH 318	$6.4 \pm 1.6 \times 10^{-5}$	$1.4 \pm 0.5 \times 10^{-4}$	0.02 ± 0.005

Table 3.7 Control levels for *CYP1A1*/ β -actin mRNA ratios by phenylbenzothiazole compounds in H4-II-E cultures. The mean and S.D for *CYP1A1*/ β -actin ratios for untreated, vehicle or 10 nM TCDD-treated cultures were determined from triplicate measurements from separate experiments shown in Figure 3.19.

Compound	EC ₅₀ [nM] (95% confidence intervals)	Maximal levels (% 10 nM TCDD)
IH 445	4 (2-10)	60 (53-66)
DF 203	3000 (900-13000)	105 (67-144)
GW 610	6500 (3700-11000)	110 (90-130)
AW 892	2000 (300-14000)	102 (56-147)
IH 318	9000 (2500-35000)	230 (138-326)

Table 3.8 *CYP1A1* mRNA induction by IH 445, DF 203, GW 610, AW 892 and IH 318. Maximum response achieved E_{max} by inducers as well as the concentrations that produce half-maximal response EC₅₀ were obtained from log concentration-response curves for *CYP1A1* mRNA induction shown in Figure 3.19.

centrations higher than 30 μ M. Given that the response-curve for *CYP1A1* mRNA induction by IH 318 was not complete (Figure 3.19 A), the actual EC₅₀ determined was an estimation and was not considered as an accurate measurement value. However, although saturated levels by IH 318 were not achieved, it is clear that this compound is not a potent inducer for *CYP1A1* mRNA. Interestingly, all these compounds were found to be full agonists for the induction of *CYP1A1* mRNA, given that they all achieve levels of induction similar to those achieved by TCDD. Overall, under the conditions of the current *CYP1A1* induction assay, the IH 445 was classified a potent agonist whereas DF 203, GW 610, AW 892 and IH 318 were less potent agonists.

Section 3.2.10 Estimation of intrinsic efficacy and fractional receptor occupancy

The data for AhR binding affinity (Table 3.3) and potency for induction of CYP1A1 mRNA (Table 3.8) for the phenylbenzothiazole analogues tested, except for IH 445, showed significant disparity between the two measures. For a quantitative understanding of this discrepancy, it was essential to determine the intrinsic efficacy of the compounds as well as the number of receptors that have to be occupied for a given stimulus.

It is anticipated that the quantitative difference between these two measures could be due, but not limited, to the low intrinsic efficacy of the phenylbenzothiazole compounds relative to TCDD's, *i.e.*, to their inability to activate the AhR to the same extent as TCDD's, after binding. Based on the AhR binding affinities of the compounds (Table 3.3), the number of receptors (Table 3.2) from the binding studies and the additional knowledge of EC_{50} values for CYP1A1 RNA induction (Table 3.9), relative intrinsic efficacy (K_e) of AhR ligands and fractional receptor occupancy at 50% response were calculated and listed in Table 3.10 assuming same K_D and R_t as determined in rat binding system.

As seen from Table 3.10, TCDD, displays the highest intrinsic efficacy. Only ~14 % of Ah receptors have to be occupied by TCDD to elicit 50% response. The compound 1c, found to be a high-affinity AhR ligand and a potent agonist with a full induction capacity has an intrinsic efficacy which is only 2-fold lower than TCDD and has to occupy only 23% of the receptors. Compound 1c has only ~ 3-fold higher binding than induction potency. However, MC had approximately 11-fold higher binding potency than induction and requires much higher fractional receptor occupancy, 92%.

Inducer	E _{max} [% 10 nM TCDD] (95% confidence intervals)	EC ₅₀ [nM] (95% confidence intervals)	K _i [nM] (95% confidence intervals)	K _i /EC ₅₀
TCDD	100 (94-113)	0.06 (33-100)	0.37 (0.18-1)	6.2
MC	117 (109-125)	9 (7-13)	1 [§]	0.09
AZI	111 (104-118)	0.1 (0.09-0.18)	0.04 (0.01-0.1)	0.4
IH 445	60 (53-66)	4 (2-10)	0.9 (0.05-17)	0.2
5F 203	99 (77-120)	3000 (1300-7700)	2.8 (2-5)	0.00093
DF 203	100 (67-140)	3400 (900-13000)	9.9 (5-19)	0.003
GW 610	100 (89-130)	6500 (4000-12000)	6.8 (2-30)	0.001
AW 892	100 (56-147)	1900 (300-14000)	9.8 (4-22)	0.005

Table 3.9 Data for *CYP1A1* mRNA induction and AhR binding in rat. Maximum response achieved E_{max} by inducers as well as the concentrations that produce half-maximal response EC₅₀ were obtained from log concentration-response curves for *CYP1A1* mRNA induction. Inhibition dissociation constant (K_i) were obtained from the log concentration-TCDD competitive displacement curves. [§]K_i for MC was not assessed in this study but was taken from literature [67].

Compound	K _e ^a (fmol/mg)	R ₅₀ ^b (%)
TCDD	5.6	14
1c	9.2	23
MC	36.8	92
IH 445	33	82
5F 203	40	99.9
DF 203	39.9	99.7
GW 610	40	99.9
AW 892	39.8	99.5

Table 3.10 Intrinsic efficacy and fractional receptor occupancy at 50% of AhR ligands in H4-II-E cells. ^aK_e (constant of intrinsic efficacy) represents the concentration of the agonist-receptor complex that produces 50% response. ^bR₅₀ values are the fraction of receptors that must be occupied to elicit a 50% response or [A.R] / [R_t]. K_e and R₅₀ values were calculated assuming the same R_t as determined in binding assay using rat cytosols according to equation [4] (appendix).

IH 445, a potent AhR ligand and inducer, has 5-fold higher binding than the induction potency.

At 50% maximal response, 85% of the receptors have to be occupied by IH 445. 5F 203 was 1000-fold more potent for binding AhR than for inducing *CYP1A1* mRNA. Importantly, for 5F 203 to elicit the same response as TCDD at 50% response, 99.9% of the AhR have to be occupied. As seen in Table 3.10, DF 203, GW 610 and AW 892, all have similar intrinsic efficacy as 5F 203 with similar receptor occupancy levels. These compounds bind AhR avidly but are much less efficient at eliciting the response after receptor binding. So higher concentrations are required to activate the receptor and produce TCDD-response levels.

This study suggests that IH 445 is a relatively high-efficacy agonist whereas 5F 203, DF 203, GW 610 and AW 892 are low-efficacy agonists.

Section 3.2.11 Inhibition of TCDD-induced *CYP1A1* mRNA by 5F 203

Section 3.2.10 suggests that 5F 203 has a low intrinsic efficacy, with 50,000-fold lower potency than TCDD for inducing *CYP1A1* mRNA (Figure 3.18 A). Since a low-intrinsic efficacy compound has properties of both agonist and antagonist, it should exhibit a concentration-dependent inhibitory effect on the action of the high-intrinsic efficacy ligand [217]. The alternatives are that 5F 203 is metabolized or excreted. The prediction of antagonism would partially exclude the alternative possibilities resulting in lower intracellular concentrations of 5F 203. To test this prediction, the inhibitory activity of 5F 203 on TCDD was assessed by co-incubating TCDD with and without 1 μ M 5F 203 in H4-II-E cells.

The concentration of 5F 203 in mixtures with TCDD could severely affect TCDD log concentration-response, and thus TCDD potency (EC_{50}). The rationale of this experiment was based on the observation that at 1 μ M, 5F 203 increased *CYP1A1* mRNA (8% of 10 nM TCDD maximal response) (Figure 3.18 A). Below 1 μ M 5F 203, there was no detectable response. If 5F 203 has an antagonistic activity, this will be observed when working at 1 μ M, where 5F 203

induces *CYP1A1* mRNA to 8% of TCDD maximal response. At 3 μ M, 5F 203 increased the *CYP1A1*/ β -actin mRNA ratio to 50% of the maximum response. As a result, the bottom and a top levels of the log concentration-response curve obtained for these mixtures would be very close to each other, and the EC₅₀ would not be determined accurately.

It is possible to predict the EC₅₀ of TCDD in the presence of 1 μ M 5F 203 (A'), given the knowledge of the K_B (or K_i) value for 5F 203 (2.8 nM) from competitive displacement assay (Table 3.3), TCDD's K_D, TCDD's EC₅₀ in the absence of 5F 203 (A) and the concentration of 5F 203 (1 μ M). At 50% maximal response, both equations [6] and [7] (appendix) are equal, and yield an [A'] value of 22 nM, and thus the shift of TCDD response curve would be anticipated to be 360-fold to the right.

Figure 3.20 shows the log concentration-response curves for the levels of *CYP1A1* mRNA by TCDD alone (10^{-14} - 10^{-8} M) and in combination with 1 μ M 5F 203.

The effect of the treatments on the reference genes was investigated by examining β -actin mRNA and the AhR/ β -actin mRNA ratios. Figure 3.20 B and Figure 3.20 C prove that the levels of the reference genes varied within a ~ two-fold range, but no points were statistically significantly different from control (10 nM TCDD set at 100%). The results of this analysis prove that equal amounts of sample DNAs have been analysed, and that there is no significant variation in reference genes. Thus variation in *CYP1A1* levels does not reflect an artifact of sample loading or preparation.

The *CYP1A1*/ β -actin mRNA ratios (~8% of maximal response) observed below 10 pM TCDD represent levels in response to 1 μ M 5F 203 alone, as the *CYP1A1*/ β -actin mRNA ratios in response to TCDD was not detected below 10 pM TCDD (Figure 3.20 A) ($p=0.001$, t -test, $n=3$, comparing *CYP1A1*/ β -actin mRNA ratios induced by 10 pM TCDD above vehicle control lev-

els).

From the log concentration-response curves shown in Figure 3.20 A, TCDD's EC_{50} value in the absence of 1 μ M 5F 203 was 46 pM (95% CI, 13-160) whereas it was 5 nM (95% CI, 2-12) in the presence of 1 μ M 5F 203. At 1 μ M, the 5F 203 shifted the concentration-response curve for TCDD to the right by 100-fold. This is a significant effect of antagonism by 5F 203 on TCDD's potency. This is within \sim 4-fold difference from the predicted value of 360-fold, which could be due to some loss of the drug by metabolism, cellular uptake or excretion, such that the actual concentration of 5F 203 at the receptor sites is less than the concentrations added. Moreover, the effect of 5F 203 was completely reversed by TCDD (Figure 3.20 A).

Maximal levels achieved by TCDD were slightly depressed by 5F 203 though not significantly different (Figure 3.20 A; $p>0.05$; t -test comparing response by 10 nM TCDD in the presence of 1 μ M 5F 203 with TCDD alone). These results provide compelling evidence that 5F 203 inhibited TCDD-*CYP1A1* induction in H4-II-E cells. Moreover, this experiment provides powerful evidence for excluding the possibility that metabolism of the 5F 203 could be the major reason behind the large quantitative difference in potency between 5F 203 and TCDD, given its antagonistic activity on TCDD. If much of the 5F 203 were metabolized, one would expect that most of the drug would be depleted and there would be no change in potency of TCDD.

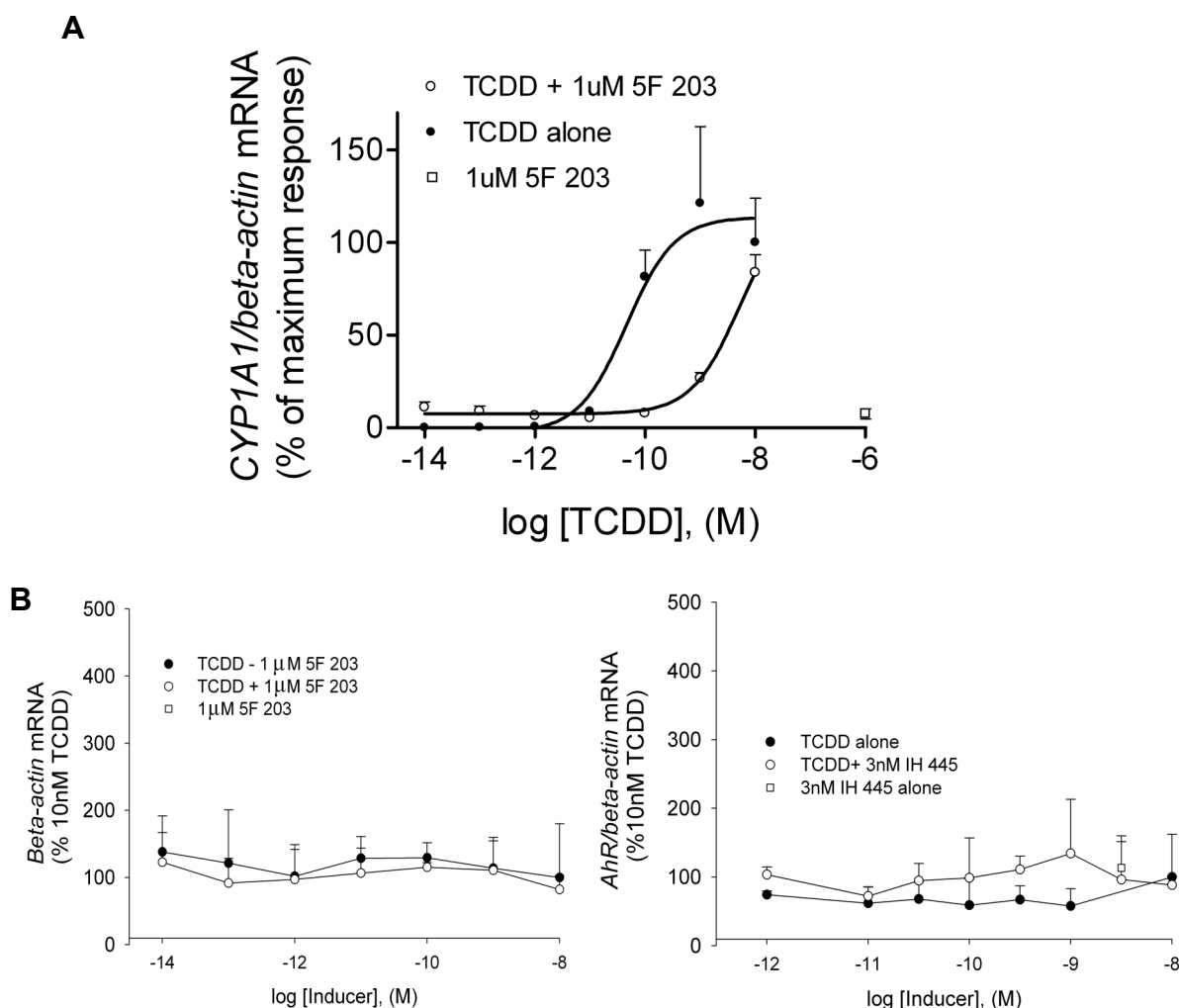


Figure 3.20 Inhibition of TCDD-induced *CYP1A1* mRNA by 5F 203 in H4-II-E cells. Cultured H4-II-E cells were exposed to a range of increasing concentrations of TCDD alone [●] or in combination with 1 μ M 5F 203 [○] for 4 h. 5F 203 (1 μ M) alone [□] was included as a positive control. *CYP1A1*/ β -actin mRNA were determined as described in Figure 3.13 legend. Each point represents the average of mean \pm S.D for triplicate samples from one experiment. Each qRT-PCR reaction was performed once. Mean and S.D for *CYP1A1*/ β -actin ratio for untreated- and vehicle treated cultures, were $1.2 \pm 8.3 \times 10^{-6}$ and $2.5 \pm 9.5 \times 10^{-6}$ respectively. Mean and S.D for *CYP1A1*/ β -actin mRNA ratios for cultures treated with 10 nM TCDD, was 0.2 ± 0.007 . The mean and S.D for induced *CYP1A1*/ β -actin mRNA ratios (% of maximal response) for cultures treated with 1 μ M 5F203 alone, was 7.5 ± 2.8 . Curves were fitted using the variable slope sigmoid Hill equation (GraphPad Prism 5.0 Software). Ordinates: (A) the *CYP1A1*/ β -actin mRNA ratios relative to 10 nM TCDD, (B) β -actin mRNA relative to 10 nM TCDD, (C) *AhR*/ β -actin mRNA ratios relative to 10 nM TCDD. Abscissae: logarithms of molar concentrations of TCDD. β -actin mRNA and *AhR*/ β -actin mRNA ratios at different time points for each treatment concentration were not significantly different from 10 nM TCDD-treated cells at 4 h ($p > 0.05$, one-way ANOVA analysis followed by Dunnett's Multiple Comparison test).

As a conclusion, the lower potency of 5F 203 for inducing *CYP1A1* mRNA in H4-II-E cells compared to TCDD, was shown to be a result of its low intrinsic efficacy and antagonistic activity and not due to metabolism of the drug.

Section 3.2.12 Competitive antagonism of 5F 203 on TCDD-induced *CYP1A1* mRNA

The results from Figure 3.20 proved that 5F 203 inhibited TCDD-induced *CYP1A1* mRNA and suggests that the nature of the inhibition is a reversible competitive antagonism. To confirm this hypothesis, the following experiment was conducted and Schild regressions (non linear and linear) analyses were performed. The aims of the Schild regressions are i) to investigate if the antagonism is competitive (if the regression proves linearity with a Schild slope of 1), ii) to determine the equilibrium dissociation constant (K_B) of the complex [antagonist-AhR] and iii) to investigate whether the system is under equilibrium.

H4-II-E cultures were treated with a range of concentrations of TCDD in the presence of three concentrations of 5F 203. The EC_{50} of TCDD for *CYP1A1* mRNA induction was measured at each concentration of 5F 203.

From the experiment in Section 3.2.11, at 50% maximal response, the K_B calculated from equations [6] and [7] (appendix) was 12 nM. Using this K_B value, $[A'] = EC_{50}$ values of TCDD in the presence of 1 μ M, 300 nM or 100 nM, were predicted to be 5, 2 and 0.6 nM respectively.

Before measuring the *CYP1A1*/ β -actin mRNA ratios induced by TCDD alone or in mixtures with different concentrations of 5F 203, it was essential to verify that the β -actin mRNA and the *AhR*/ β -actin mRNA ratios were not affected by any of the treatments. Figure 3.21 B and Figure 3.21 C prove that these ratios were within 2-fold variation, and did not change significantly throughout the different treatments (except for few individual points). Thus the *CYP1A1*/ β -actin mRNA ratios will not be affected by sample loading artifacts.

The increase of *CYP1A1*/ β -actin mRNA ratios observed at TCDD low concentrations (<10 pM) corresponds to those induced by 5F 203 alone. No increase in the *CYP1A1*/ β -actin mRNA ratios

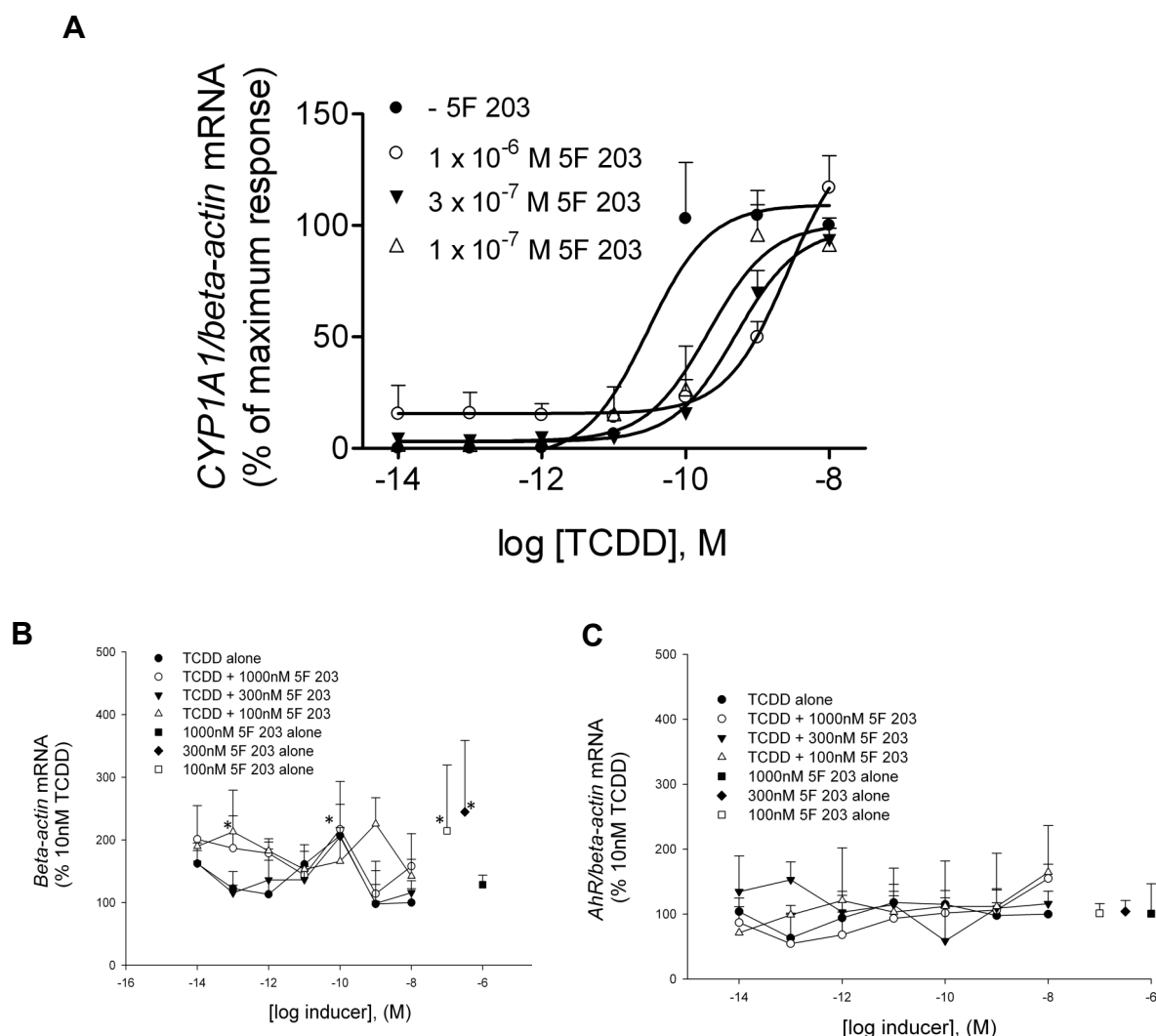


Figure 3.21 Competitive inhibition of TCDD-induced *CYP1A1* mRNA by 5F 203 in H4-II-E cells. Cultures were cotreated with varying concentrations of TCDD and 1 μ M, 300 nM or 100 nM of 5F 203. 5F 203 at 100 nM, 300 nM and 1 μ M alone were included as positive controls. *CYP1A1*/ β -actin mRNA were determined as described in Figure 3.13 legend. Each point represents the average of mean \pm S.D for triplicate samples from one experiment. Each qRT-PCR reaction was performed once. Mean and S.D for *CYP1A1*/ β -actin ratios for untreated and vehicle-treated cultures, were $7.8 \pm 1.9 \times 10^{-6}$ and $18 \pm 8.8 \times 10^{-6}$ respectively. Mean and S.D for *CYP1A1*/ β -actin mRNA ratios for cultures treated with 10 nM TCDD, was 0.02 ± 0.0006 . Mean and S.D for *CYP1A1*/ β -actin mRNA ratio (as % of maximal response) induced by 5F 203 alone at each concentration 1 μ M, 300 nM or 100 nM, were 27 ± 2.8 , 8 and 2.1 (the last two concentrations are missing one of the triplicates). Curves were fitted using the variable slope sigmoid Hill equation, (with the Hill slope of unity for all curves) (GraphPad Prism 5.0 Software). Ordinates: (A) the *CYP1A1*/ β -actin mRNA ratios relative to 10 nM TCDD, (B) β -actin mRNA relative to 10 nM TCDD, (C) AhR/ β -actin mRNA ratios relative to 10 nM TCDD. Abscissae: logarithms of molar concentrations of TCDD. β -actin mRNA and AhR/ β -actin mRNA ratios at different time points for each treatment concentration were not significantly different from 10 nM TCDD-treated cells at 4 h ($p > 0.05$, one-way ANOVA analysis followed by Dunnett's Multiple Comparison test), except for β -actin mRNA treated with (TCDD+100 nM or 300 nM 5F 203) and (100 nM or 300 nM 5F 203 alone) (*, $p < 0.05$, one-way ANOVA analysis followed by Dunnett's Multiple Comparison test).

was seen below 10 pM TCDD. The EC₅₀ for TCDD in the absence of 5F 203 was 30 pM (95% CI, 5-166), whereas in the presence of 100 nM 5F 203, the EC₅₀ was increased to 200 pM (95%

CI, 56-765). A further increase was obtained in the presence of 300 nM 5F 203, with an EC_{50} of 500 pM (95% CI, 300-700). At 1 μ M 5F 203, TCDD's EC_{50} was 3 nM (95% CI, 2-4). This latter finding is consistent with EC_{50} value of 5 nM for TCDD in the presence of 1 μ M 5F 203 (Figure 3.20 A).

Non linear Schild regressions were performed on Figure 3.21 A using a global fit analysis (with no constraints on the bottom and top, *i.e.*, these parameters are not shared among the curves). Non linear Schild regressions global analysis on the curves in Figure 3.21 A demonstrated a Schild slope of ~ 1 (95% CI, 0.5-1.8). The K_B for 5F 203 was 23 nM (95% CI, 4-139). The value of K_B was within 2-fold difference from the value calculated from the experiment in Section 3.2.11

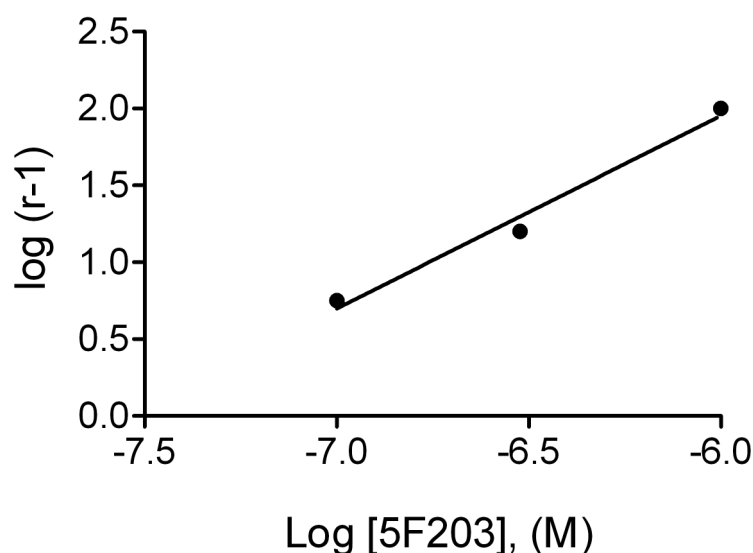


Figure 3.22 Schild regression. TCDD EC_{50} values in the presence of each concentration of 5F 203 were determined from the curves in Figure 3.21 and used for regressions. Equiactive concentration ratio r is calculated according to equation [8] (appendix). Ordinate: logarithm of $(r-1)$. Abscissa: logarithms of molar concentrations of 5F 203.

For illustration, a linear plot of the Schild regressions from the EC_{50} for TCDD at each concentrations of 5F 203 is shown in Figure 3.22. The EC_{50} concentration-ratios (cr) or (r) of TCDD was defined as $[EC_{50} \text{ in the presence of 5F 203}] / [EC_{50} \text{ in the absence of 5F 203}]$. This ratio was determined experimentally at each concentration of 5F 203 from Figure 3.21 A.

The results in Figure 3.22 prove that the regression of $\log (cr-1)$ on $\log [5F 203]$ is linear and had a slope of 1.2 ± 0.17 , which is not significantly different from 1. This furnishes further evidence that the antagonism of 5F 203 on TCDD is competitive; *i.e.*, 5F 203 and TCDD compete for the same sites of receptor. This is consistent with our previous results (Figure 3.9, Figure 3.20 A & Figure 3.21 A). Furthermore, given the slope is ~ 1 , that could imply that the system is under equilibrium.

Having found that the regression is linear and the slope is of unity, then the equilibrium dissociation constant of the antagonist-receptor complex, represented by pK_B can be estimated from the intercept with x abscissa which yields $-\log K_B$ or pK_B . The value for pK_B was 7.6, so that $K_B=25$ nM. This is consistent with the non linear regression analysis. This K_B value is within ~ 9 -fold difference from the equilibrium dissociation constant of 5F 203 derived from the radioactive competitive assay ($K_i = 2.8$ nM, Table 3.3). This difference could be due to difference in nature of the two assays. Given that this experiment was performed once, in order to ensure reproducibility of the results and validate the K_B derived for 5F 203, this experiment should be repeated in the future.

Section 3.2.13 Effect of IH 445 on TCDD-induced *CYP1A1* mRNA

The high-affinity AhR ligand IH 445 ($K_i=0.9$ nM) is a potent agonist for the induction of *CYP1A1* mRNA in H4-II-E cells (Figure 3.19). From these data, it is anticipated that IH 445 would have no any antagonistic activity on TCDD-induced *CYP1A1* mRNA in these cells. In

order to confirm this hypothesis, the following experiment was conducted.

The rationale of the experiment is based on the data obtained from the competitive binding assay (Table 3.3), where 100 nM IH 445 displaced [^3H]-TCDD specific binding by 100%. At 3 nM IH 445, 50% of [^3H]-TCDD specific binding was displaced. In order to investigate the antagonistic activity of IH 445, there is a need to work under concentrations of IH 445 at which, significant amount of TCDD will be inhibited. However, very high concentrations of IH 445 could result in a additive response, and consequently, the top and bottom levels of TCDD response will be very close, and EC_{50} could not be determined. From Figure 3.19 A, a concentration of 3 nM IH 445, offers a balance between significant competition with TCDD at the receptor sites and an induction level less than 50% of maximal response. If the IH 445 is a partial antagonist, from equations [6] and [7] (appendix), at equal responses (50% maximal response), it is expected to shift the log concentration-response of TCDD only by 4-fold when co-incubated at the concentration of 3 nM with TCDD. Whereas, if the IH 445 is a potent agonist for inducing *CYP1A1* mRNA, the EC_{50} of TCDD will not be affected.

H4-II-E cells were co-treated with a range of concentrations of TCDD \pm 3 nM IH 445 for 4 h. Figure 3.23 shows the log concentration-response curves for increasing concentrations of TCDD alone or combined with 3 nM IH 445.

The RNA ratios of the reference genes were examined to ensure stability against the various treatments. Figure 3.23 B and Figure 3.23 C show that β -actin mRNA and AhR/ β -actin mRNA ratios were unchanged by any treatment (except for one point, β -actin mRNA treated with mixtures of 300 pM TCDD and 3 nM IH 445). Consequently, the *CYP1A1*/ β -actin mRNA ratios will not be affected by sample loading artifacts.

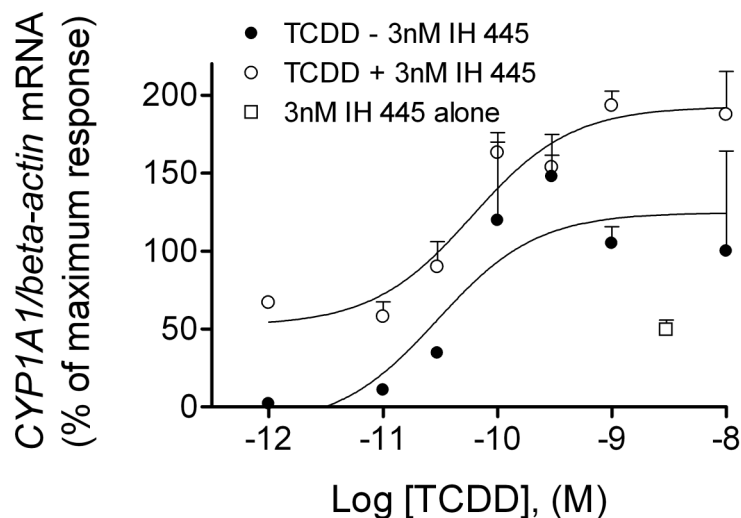
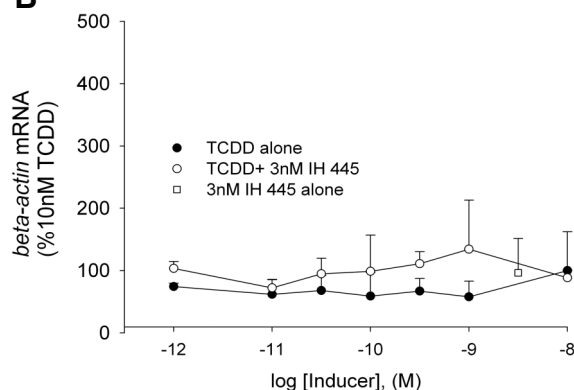
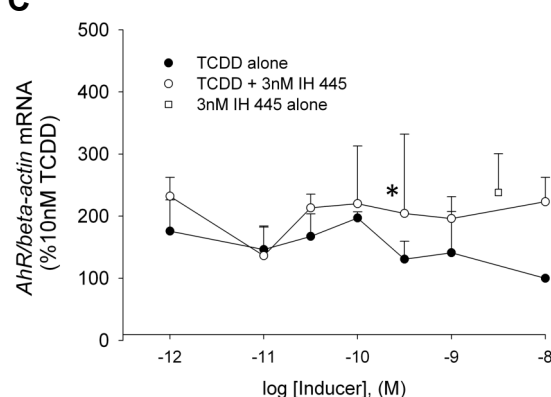
A**B****C**

Figure 3.23 Effect of IH 445 on TCDD response in H4-II-E cells. Cultured H4-II-E cells were exposed to a range of increasing concentrations of TCDD alone [○] or in combination with 3 nM IH 445 [●] for 4 h. 3 nM IH 445 alone was included as a positive control [□]. *CYP1A1*/ β -actin mRNA were determined as described in Figure 3.13 legend. Each point represents the mean \pm S.D of triplicate determinations from one experiment. Each qRT-PCR reaction was performed once. For controls, mean and S.D for *CYP1A1*/ β -actin basal ratios for untreated and vehicle-treated cultures, were $4.6 \pm 4.4 \times 10^{-5}$ and $7 \pm 5 \times 10^{-5}$ respectively. For 10 nM TCDD-treated cultures, the mean and S.D for *CYP1A1*/ β -actin mRNA ratios was $8.7 \pm 5.6 \times 10^{-5}$. The mean and S.D for the induced levels of *CYP1A1*/ β -actin mRNA ratios (% 10 nM TCDD) by 3 nM IH 445 alone was 50 ± 6.3 . Curves were fitted using the variable slope sigmoid Hill equation (GraphPad Prism 5.0 Software). Ordinates: (A) the *CYP1A1*/ β -actin mRNA ratios relative to 10 nM TCDD, (B) β -actin mRNA relative to 10 nM TCDD, (C) AhR/ β -actin mRNA ratios relative to 10 nM TCDD. Abscissae: logarithms of molar concentrations of TCDD. β -actin mRNA and AhR/ β -actin mRNA ratios at different time points for each treatment concentration were not significantly different from 10 nM TCDD-treated cells at 4 h ($p > 0.05$, one-way ANOVA analysis followed by Dunnett's Multiple Comparison test), except for β -actin mRNA treated with mixtures of 300 pM TCDD and 3 nM IH 445, which was significantly different from 10 nM TCDD-treated cells at 4 h (*, $p < 0.05$, one-way ANOVA analysis followed by Dunnett's Multiple Comparison test).

In Section 3.2.9 (Figure 3.19), IH 445 increased the *CYP1A1*/ β -actin mRNA ratio in a concen

tration-dependent manner. At 3 nM, the increased levels were ~20% those of the maximal response. However, the data from Figure 3.23 A shows that IH 445 at 3 nM (shown in the black triangle) induced ~50% of the maximal response. This difference is within ~2.5-fold between experiments. When cultures were co-exposed to increasing concentrations of TCDD, the *CYP1A1* mRNA induced levels were ~60% those of the maximal response at low TCDD concentrations (< 30 pM). These levels are due to an additive effect of IH 445 on TCDD. The top levels induced by TCDD in the absence or the presence of 3 nM IH 445 were 125% (95% CI, 71.18-178) and 193% (95% CI, 155.4 to 229.9) respectively, which was considered not statistically significant. The maximal levels induced by TCDD did not vary significantly between experiments, (given that the 95% confidence limits were overlapping). The EC₅₀ for *CYP1A1* mRNA induction by TCDD was 30 pM (95% CI, 2-400) in the absence of 3 nM IH 445, and 60 pM (95% CI, 12-294) in the presence of 3 nM IH 445. This minor effect was considered not significant given the 95% confidence limits are overlapping.

Under the conditions of the current *CYP1A1* induction assay, the results of this experiment identified IH 445 as a potent agonist for inducing *CYP1A1* mRNA with no detectable antagonistic activity on TCDD in H4-II-E cells. In the light of this finding, phenylbenzothiazole analogues showed different agonism/antagonism pattern, and thus the antagonism is a specific property of certain analogues.

Section 3.2.14 *CYP1A1* induction assay in MCF-7 cells

Section 3.2.14.1 Concentration-response curves of TCDD

CYP1A1 in MCF-7 cells is known to be inducible by TCDD [183] [11] [12]. In order to confirm that TCDD induces *CYP1A1* mRNA in MCF-7 cells and compare the induction of *CYP1A1* mRNA by TCDD in MCF-7 with H4-II-E cells, the experiment was performed essentially as

described in Section 3.2.8 under the same conditions, *i.e.*, the same cell confluence (90-95%),

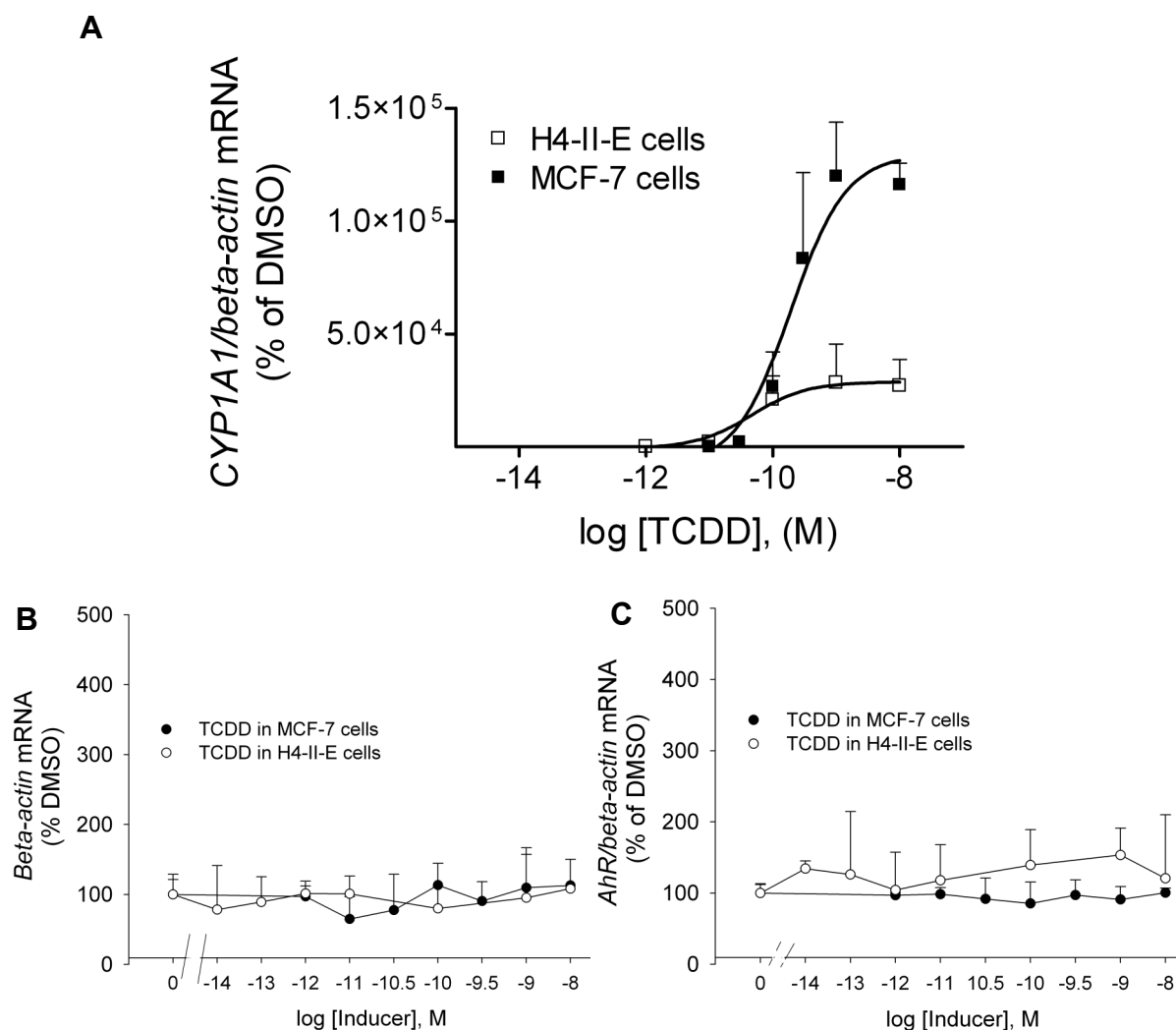


Figure 3.24 Comparison between the log concentration-response curves for *CYP1A1* mRNA induction by TCDD in H4-II-E and MCF-7 cells. Cultures were treated with DMSO (0.1%) or TCDD (at the indicated concentrations) for 4 h in H4-II-E [\square] and MCF-7 [\blacksquare] cells. *CYP1A1*/ β -actin mRNA ratios were determined as described in Figure 3.13 legend. Response curves were combined from two separate experiments. Each point represents the average of mean \pm S.D for triplicate samples, and is representative of results obtained from one of two experiments (for MCF-7 cells) and four experiments (for H4-II-E cells). Each qRT-PCR reaction was performed once. The mean \pm S.D for *CYP1A1*/ β -actin mRNA ratios for untreated and vehicle treated H4-II-E cells were 2.2×10^{-5} and 4.3×10^{-5} as absolute ratios respectively. Those in MCF-7 cells were $7 \pm 6 \times 10^{-4}$ and $8 \pm 8.6 \times 10^{-4}$, for untreated and vehicle treated cells respectively. Curves in (A) were fitted using the variable slope sigmoid Hill equation (GraphPad Prism 5.0 Software). (A) Ordinate: the *CYP1A1*/ β -Actin mRNA ratios relative to 4 h DMSO. Abscissa: logarithms of molar concentrations of TCDD. Ordinate (B): β -actin mRNA relative to 4 h DMSO, (D) *AhR*/ β -actin mRNA ratios relative to 4 h DMSO. Abscissae: logarithms of molar concentrations of TCDD. β -actin mRNA and *AhR*/ β -actin mRNA ratios for vehicle-treated cultures at 4 h were represented by zero molar concentration. β -actin mRNA and *AhR*/ β -actin mRNA ratios at different time points for each treatment concentration were not significantly different from vehicle-treated cells at 4 h ($p > 0.05$, one-way ANOVA analysis followed by Dunnett's Multiple Comparison test).

and 4 h-treatment in MCF-7 cells. The RNA levels of the reference genes were examined to en-

sure stability during the various treatments. Figure 3.24 B and Figure 3.24 C show that there was no significant difference in β -actin mRNA and AhR/ β -actin mRNA ratios during all treatments. Therefore, the *CYP1A1*/ β -actin mRNA ratios do not reflect an artifact of sample loading or preparation.

Figure 3.24 A shows the log concentration-response curves for *CYP1A1* mRNA induction by TCDD in H4-II-E and MCF-7 cells. The maximal levels for *CYP1A1* mRNA induction achieved by TCDD in MCF-7 were 4-fold higher than that in H4-II-E cells. The maximal levels for *CYP1A1* mRNA induction achieved by TCDD above vehicle controls were 14×10^4 % (95% CI, 9.8-16) and 2.9×10^4 % (95% CI, 2.5-3.2) in MCF-7 and H4-II-E cells respectively. This is in good agreement with previous findings, where maximal levels for EROD activity were found significantly lower (10-fold) in H4-II-E than MCF-7 cells [184]. The results confirm inducibility of *CYP1A1* in MCF-7 cells by TCDD. Thus, the AhR in these cells is functional and not defective.

The EC_{50} value for TCDD was 194 pM (95% CI, 65-574) in MCF-7 cells, which is ~ 3 -fold greater than that in H4-II-E cells, 60 pM (95% CI, 33-102). There was no significant difference in TCDD potency in MCF-7 and H-4-II-E cells. In Table 3.11 are summarized the EC_{50} values for TCDD for inducing *CYP1A1* mRNA in MCF-7 cells from two independent trials. The EC_{50} value for TCDD for inducing *CYP1A1* mRNA were comparable with previously reported values (Table 3.12).

Experiments	EC ₅₀ pM (95% confidence intervals)
(1)	194 (65-570)
(2)	300 (98-930)
Average	250

Table 3.11 EC₅₀ values for the induction of *CYP1A1* mRNA by TCDD in MCF-7 cells.

EC₅₀ values were determined from log concentration-response curves using the variable slope Hill sigmoidal equation (GraphPad Prism 5.0). Each trial was conducted on a range of concentrations, each in triplicate samples. The average represents the mean of EC₅₀ values from two independent experiments.

Cell line	CYP1A1 Assay	EC ₅₀ (pM)	Time of treatment	References
H4-II-E cells	EROD	0.6-1	24 hours	[175]
		10	72 hours	[183]
		6	Not specified	[184]
		96	72 hours	[185]
	AHH	150	Not specified	[184]
		230	1 hour	[186]
		50 ± 0.013*	48 hours	[187]
		80	72 hours	[185]
MCF-7 cells	EROD	400	72 hours	[183]
		30	Not specified	[184]
		94	24 hours	[13]
	AHH	100	Not specified	[184]
		380	24 hours	[13]

Table 3.12 Literature values for the EC₅₀ of TCDD for inducing ethoxyresorufin *O*-deethylase (EROD) and aryl hydrocarbon hydroxylase (AHH) at in H4-II-E and MCF-7 cells. The assays were run as described in the corresponding references and the time of the assay treatments is indicated. * EC₅₀ values ± S.D.

Section 3.2.14.2 Induction of *CYP1A1* mRNA by 5F 203

5F 203 was shown previously to induce *CYP1A1* mRNA in MCF-7 cells [182]. The aim is to determine a quantitative measurement of the potency (EC₅₀) of 5F 203 for the induction of

CYP1A1 in MCF-7 cells.

MCF-7 cells were treated with 5F 203 at a range of concentrations for 4 h and potency is compared with that of TCDD. The RNA ratios of the reference genes were examined to ensure stability under the various treatments. Figure 3.25 B and Figure 3.25 C show that β -actin mRNA and AhR/ β -actin mRNA ratios were relatively stable against all treatments, except for one point, the β -actin mRNA from cells treated with 300 pM 5F 203, which was found significantly different from the control (10 nM TCDD set as 100%). However, when repeated in another experiment, this was not reproduced. Therefore, the *CYP1A1*/ β -actin mRNA ratios do not reflect an artifact of sample loading or preparation.

From Figure 3.25 A, the positive control, TCDD, increased *CYP1A1* mRNA. The fold induction of *CYP1A1* mRNA level by 5F 203 was ~1600-fold above vehicle control compared to ~1700-fold for TCDD, though at 30-fold higher concentration (300 nM). The 5F 203 increased *CYP1A1* mRNA to a level similar to 10 nM TCDD. The log concentration-response curve of the 5F 203 showed that the levels of *CYP1A1* mRNA induced saturate approximately at 10 nM. The maximal levels induced by 5F 203 are significantly higher than those reported in literature [182].

The EC₅₀ value for TCDD was 0.2 nM (95% CI, 0.07-0.6), whereas for 5F 203, the EC₅₀ value was 2 nM (95% CI, 0.9-5). 5F 203 is only 10-fold less potent than TCDD in MCF-7 cells. Moreover, 5F 203 achieved maximal levels similar to TCDD.

Figure 3.26 illustrates the difference in the magnitude of response (displayed as percentage of vehicle control) to 5F 203 in MCF-7 and H4-II-E cells. In comparison with MCF-7 cells (Figure 3.25 A), in H4-II-E cells, maximal levels (99%) were achieved by 5F 203 at 1000-fold higher concentrations (Figure 3.18 A). 5F 203 was found to be 50,000-less potent than TCDD in H4-

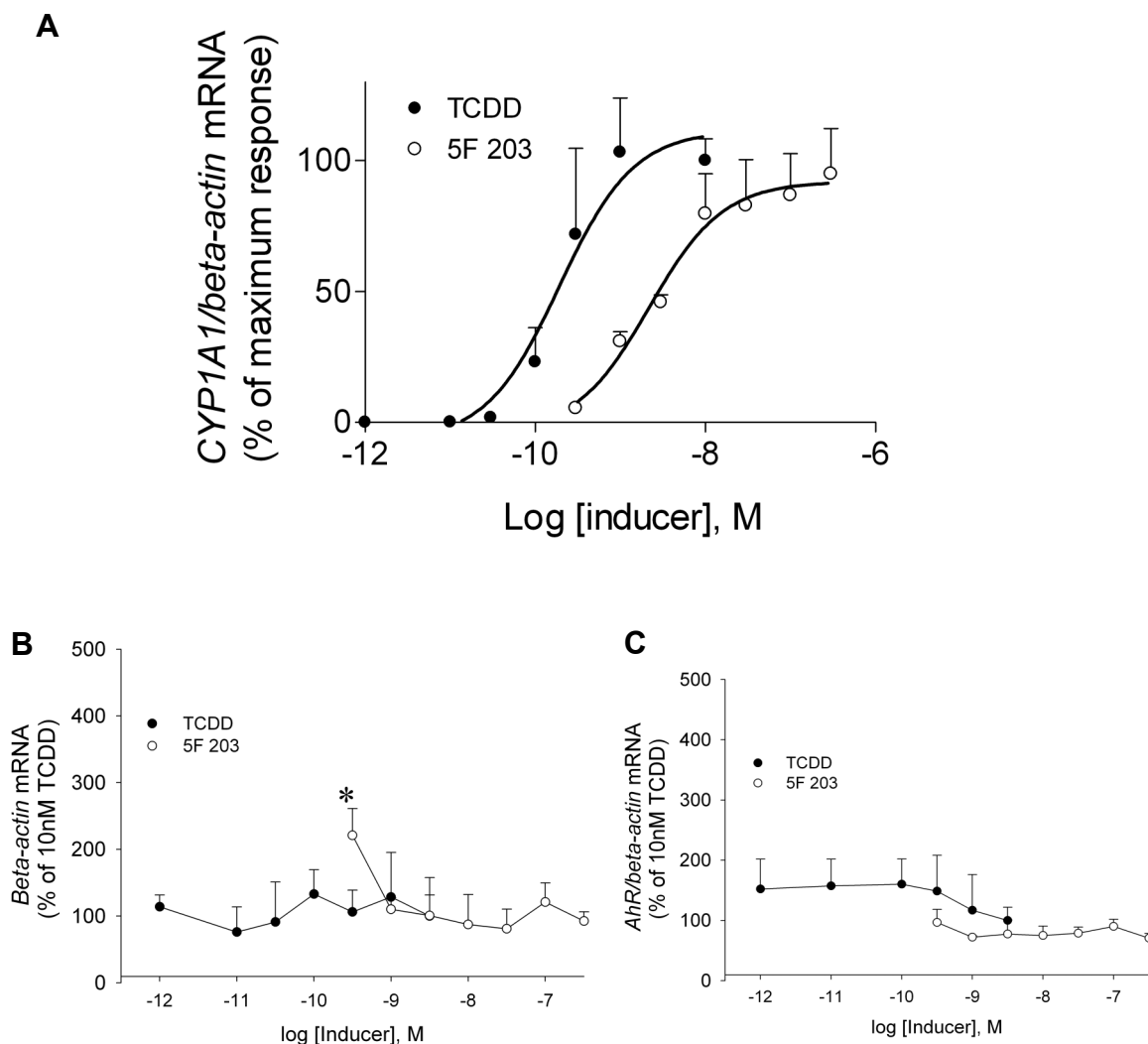


Figure 3.25 Induction of *CYP1A1* mRNA by TCDD and 5F 203 in MCF-7 cells. Cultures were treated with DMSO (0.1%), increasing concentrations of TCDD [●] or 5F 203 [○] (at the indicated concentrations) for 4 h. *CYP1A1*/ β -actin mRNA were determined as described in Figure 3.13 legend. Each point represents the average of mean \pm S.D for triplicate samples, and is representative of results obtained from one of two experiments. Each qRT-PCR reaction was performed once. TCDD log concentration-response curve is from Figure 3.24. Mean and S.D for *CYP1A1*/ β -actin ratios for untreated and vehicle-treated cultures, were 60×10^{-4} and 5×10^{-4} respectively. Mean and S.D for *CYP1A1*/ β -actin ratios for cultures treated with 10 nM TCDD was 1.3 ± 0.17 . Curves were fitted using the variable slope sigmoid Hill equation (GraphPad Prism 5.0 Software). Ordinates: (A) the *CYP1A1*/ β -actin mRNA ratios relative to 10 nM TCDD, (B) β -actin mRNA relative to 10 nM TCDD, (C) AhR/ β -actin mRNA ratios relative to 10 nM TCDD. Abscissae: logarithms of molar concentrations of TCDD and 5F 203. β -actin mRNA and AhR/ β -actin mRNA ratios at different time points for each treatment concentration were not significantly different from 10 nM TCDD-treated cells at 4 h ($p > 0.05$, one-way ANOVA analysis followed by Dunnett's Multiple Comparison test), except for the β -actin mRNA treated with 300 pM 5F 203 which was significantly different from 10 nM TCDD-treated cells at 4 h (*, $p < 0.05$, one-way ANOVA analysis followed by Dunnett's Multiple Comparison test).

II-E cells but only 10-fold less potent in MCF-7 cells. The quantitative differences (4.5-fold) for maximal levels observed for the 5F 203 (Figure 3.26) are consistent with the 4-fold difference

observed with TCDD (Figure 3.24). The results of this experiment reveal 5F 203 to be 1500-fold more potent in MCF-7 cells than in H4-II-E cells.

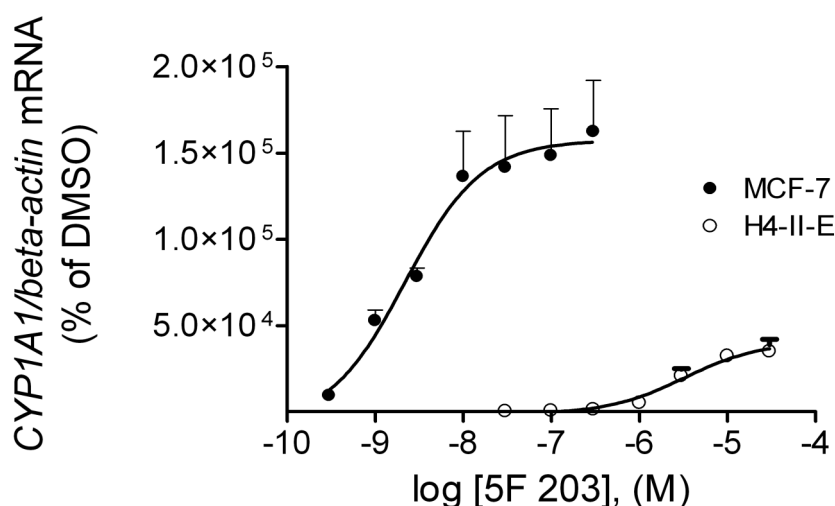


Figure 3.26 Comparison between the log concentration-response curves for *CYP1A1* mRNA induction by 5F 203 in H4-II-E and MCF-7 cells. Cultures were treated with DMSO (0.1%) or 5F 203 (at the indicated concentrations) for 4 h in H4-II-E [○] and MCF-7 [●] cells. *CYP1A1*/ β -actin mRNA ratios were determined as described in Figure 3.13 legend. Response curves were combined from two separate experiments. Each point represents the average of mean \pm S.D for triplicate samples, and is representative of results obtained from one of two experiments (for MCF-7 cells) and a single experiment (for H4-II-E cells). Each qRT-PCR reaction was performed once. Curves were fitted using the variable slope sigmoid Hill equation (GraphPad Prism 5.0 Software). Ordinate: the *CYP1A1*/ β -Actin mRNA ratio relative to 4 h DMSO. Abscissa: logarithms of molar concentrations of 5F 203.

Section 3.2.14.3 Effect of 5F 203 on TCDD-induced *CYP1A1* mRNA

5F 203 was found to be a potent agonist in MCF-7 cells (Section 3.2.14.2, Figure 3.25 A). It was anticipated that this compound would not have an antagonistic activity on TCDD in MCF-7 cells. To verify this hypothesis, the antagonistic activity of 5F 203 was investigated in MCF-7 cells by co-exposing cultures to increasing concentrations of TCDD \pm 500 pM 5F 203. The reason this concentration of 5F 203 was selected, is because this concentration offers a balance between a significant levels of *CYP1A1*/ β -actin mRNA ratios above vehicle controls ($p < 0.01$,

t-test, *n*=3, 5F 203 treatment) (Figure 3.25 A), and a significant difference between top and bottom levels of response, so that EC₅₀ would be determined accurately.

The expression of reference genes mRNAs were analysed before proceeding further with the determination of *CYP1A1*/ β -*actin* mRNA ratios and analysis of the results. Figure 3.27 B and Figure 3.27 C show that the β -*actin* mRNA and the *AhR*/ β -*actin* mRNA ratios were generally stable at all treatments (except for β -*actin* mRNA treated with mixtures of 10 pM TCDD and 500 pM 5F 203), thus the experiment proves that *CYP1A1*/ β -*actin* mRNA ratios do not reflect an artifact of sample loading or preparation.

As shown in Figure 3.27 A, at TCDD levels ≤ 30 pM, no induction of *CYP1A1* mRNA was detected. The increase in *CYP1A1*/ β -*actin* mRNA ratios was observed from 100 pM to reach maximal saturated levels at 1 nM. The increased *CYP1A1*/ β -*actin* mRNA ratios observed at TCDD concentrations below 100 pM TCDD, correspond to the levels induced by 5F 203 alone. For mixture cultures, maximal levels were not significantly different from those in TCDD-treated cultures alone.

The EC₅₀ for TCDD in the absence of 500 pM 5F 203 was 300 pM (95% CI, 98-930] whereas in the presence of 500 pM 5F 203, the EC₅₀ for TCDD was 400 pM (95% CI, 250-700), which was not significant. Under the conditions of the induction assay in this study, 5F 203 had no detectable antagonistic activity on TCDD in MCF-7 cells, and thus the 5F 203 was identified as a potent agonist.

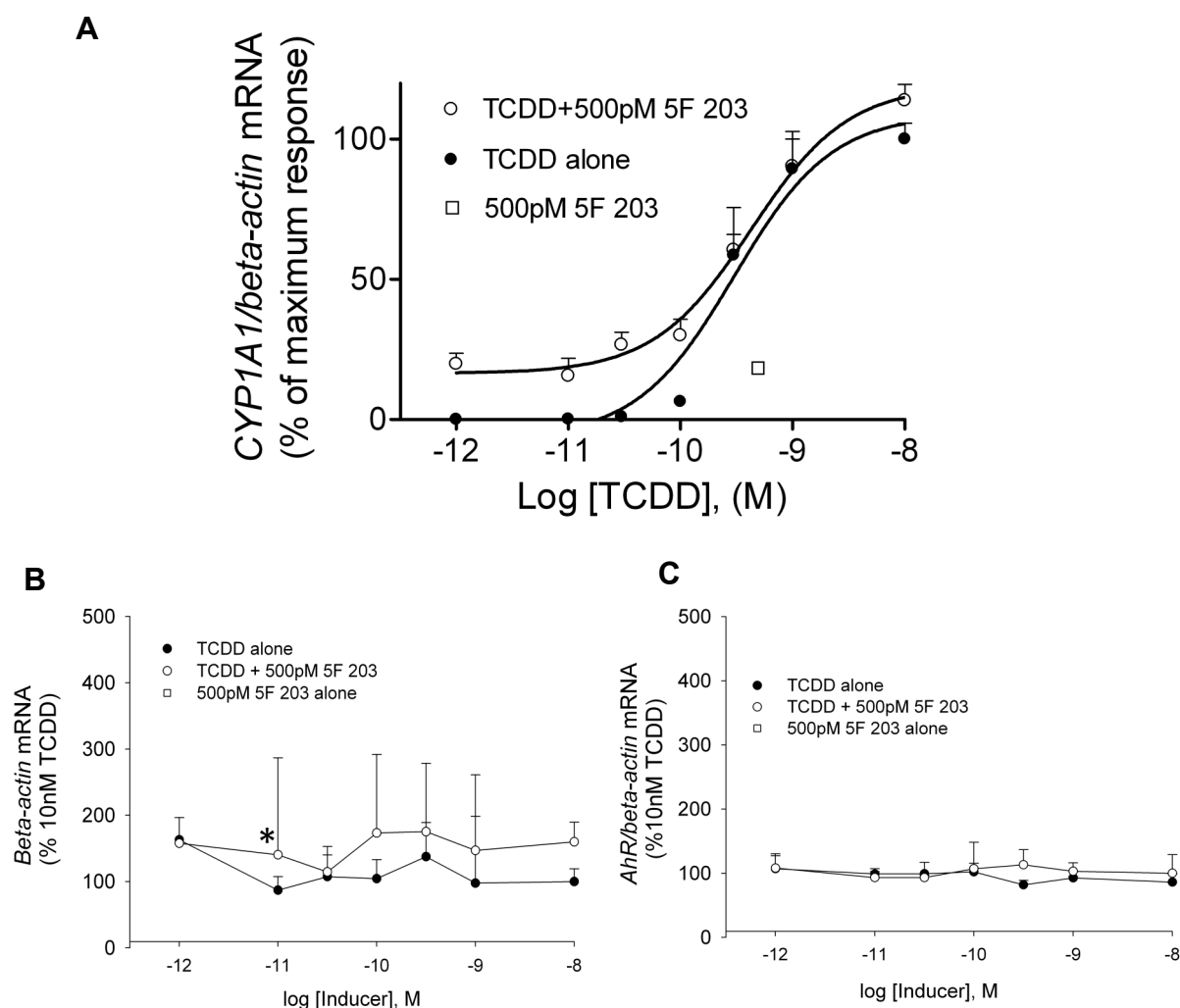


Figure 3.27 Effect of 5F 203 on TCDD response in MCF-7 cells. Cultured MCF-7 cells were exposed to a range of increasing concentrations of TCDD alone [●] or in combination with 500 pM 5F 203 [○] for 4 h. 5F 203 (500 pM) alone [□], was included as a positive control. *CYP1A1*/ β -actin mRNA were determined as described in Figure 3.13 legend. Each point represents the average of mean \pm S.D for triplicate samples, and obtained from one experiment. Each qRT-PCR reaction was performed once. For controls, mean and S.D for *CYP1A1*/ β -actin ratios for untreated and vehicle-treated cultures, were 4.9×10^{-4} and $6 \pm 3 \times 10^{-3}$ respectively. For TCDD-treated cultures, the mean and S.D for *CYP1A1*/ β -actin ratios was 1.3 ± 0.08 . Curves were fitted using the variable slope sigmoid Hill equation (GraphPad Prism 5.0 Software). Ordinates: (A) the *CYP1A1*/ β -actin mRNA ratios relative to 10 nM TCDD, (B) β -actin mRNA relative to 10 nM TCDD, (C) AhR/ β -actin mRNA ratios relative to 10 nM TCDD. Abscissae: logarithms of molar concentrations of TCDD. β -actin mRNA and AhR/ β -actin mRNA ratios at different time points for each treatment concentration were not significantly different from 10 nM TCDD-treated cells at 4 h ($p > 0.05$, one-way ANOVA analysis followed by Dunnett's Multiple Comparison test), except for β -actin mRNA treated with mixtures of 10 pM TCDD and 500 pM 5F 203, which was considered significantly different from 10 nM TCDD-treated cells at 4 h (*, $p < 0.05$, one-way ANOVA analysis followed by Dunnett's Multiple Comparison test).

Section 3.2.14.4 Induction of *CYP1A1* mRNA by CH-223191

It was reported that the (CH-223191) is an AhR pure antagonist in human hepatoma HepG2

cells [188]. This experiment aims to examine the potency of CH-223191 for the induction of *CYP1A1* mRNA in MCF-7 and verify that this compound is devoid of any agonistic activity. To assess the agonistic activity of (CH-223191) on the AhR in MCF-7, cultures were incubated with increasing concentrations of the (CH-223191) (Figure 3.28), TCDD (10 nM) as a positive control or 0.1% DMSO as a negative control for 4 h. Untreated cells were included as another negative control.

In Figure 3.28 are shown the log concentration-response curve for (CH-223191) relative to 10 nM TCDD. The log concentration-response curve for TCDD was used from a separate experiment for the sake of comparison. Up to the highest concentrations tested (30 μ M), the (CH-223191) was unable to induce *CYP1A1* mRNA in MCF-7 cells which verifies that this compound has no agonistic activity in these cells. This is consistent with previous findings where this compound failed to induce mRNA up to the highest concentration tested (10 μ M) in HepG2 cell [188].

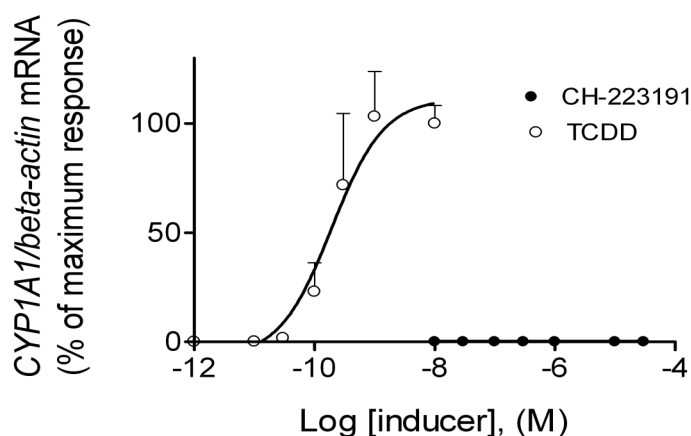


Figure 3.28 Studies on *CYP1A1* mRNA induction by CH-223191 in MCF-7 cells. Cultures were treated with DMSO (0.1%), 10 nM TCDD [○] or CH-223191 [●] (at the indicated concentrations) for 4 h. *CYP1A1*/ β -actin mRNA were determined as described in Figure 3.13 legend. Response curves were combined from two separate experiments. Each point represents the average of mean \pm S.D for triplicate samples from one of experiment. log concentration-response curve for TCDD is the same as in Figure 3.25. Each qRT-PCR reaction was performed once. For controls, mean and S.D for *CYP1A1*/ β -actin basal ratios for untreated and vehicle-treated cultures, were $55 \pm 40 \times 10^{-5}$ and $64 \pm 18 \times 10^{-5}$ respectively. For 10 nM TCDD-treated cultures, the mean and SD for *CYP1A1*/ β -actin mRNA ratios was 1.1 ± 0.052 . Curves were fitted using the variable slope sigmoid Hill equation (GraphPad Prism 5.0 Software). Ordinate: the *CYP1A1*/ β -actin mRNA ratios relative to 10 nM TCDD. Abscissa: logarithms of molar concentrations of TCDD and CH-223191.

Section 3.3 Growth inhibitory activity in H4-II-E cells

Section 3.3.1 Growth inhibitory activity of 5F 203 in H4-II-E cells

It was suggested that the activation of the AhR mediates sensitivity of MCF-7 cells to anticancer benzothiazoles [141] and that cell sensitivity to the 2-(4-aminophenyl)benzothiazoles, series (1) of benzothiazoles, seems to be CYP1A1-dependent. The model proposed for 5F 203 mechanism of action consists of activation of the AhR and subsequent induction of CYP1A1 which metabolizes the 5F 203 into reactive species that then damage DNA. In agreement with this hypothesis, CYP1A1 was not induced in resistant cells [189].

This study revealed that (5F203, DF203, GW 610, IH 318 and AW 892) had high-affinity for the AhR but had low potency for inducing *CYP1A1*, whereas IH 445 was found to be a high-affinity ligand for the AhR and a potent inducer of *CYP1A1* mRNA in H4-II-E cells. One of the aims of this project is to examine the anticancer activity of phenylbenzothiazole analogues in H4-II-E cells. Taking into consideration the hypothesis mentioned above, we addressed the question whether the rat cell line could be relatively nonresponsive to the anticancer activity of these compounds, given their lower induction potency in these cells. That was addressed by testing first the growth inhibitory activity of the 5F 203 in H4-II-E cells with the use of the cell viability assay (MTT assay). Camptothecin was used as a positive control [163]. TCDD, a potent agonist for AhR known to be relatively resistant to metabolism [61], was included to examine whether the activation of the AhR has any inhibitory activity. DMSO-treated cultures at zero time (T0) and after 72 h, were included as negative controls. Culture viability was assessed by measuring the metabolic conversion of MTT to the formazan product for each chemical treatment as described in Materials and Methods (Section 2.2.15).

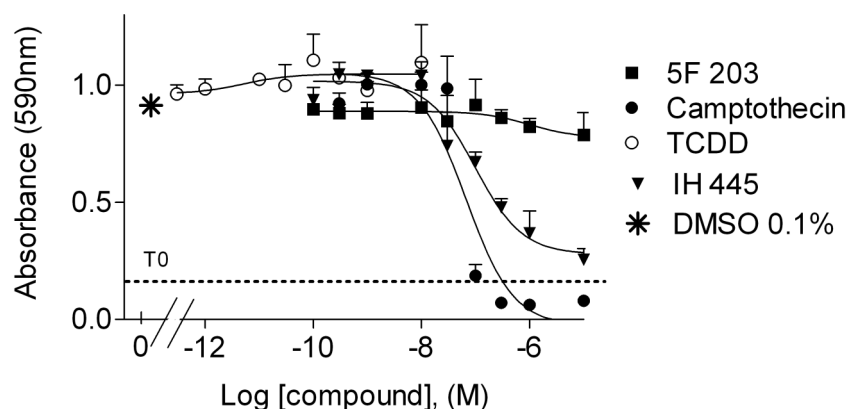


Figure 3.29 Growth inhibitory activity of 5F 203, IH 445 and TCDD in H4-II-E cells. Cells were plated at seeding densities of 5000/well and incubated for one day. The next day, cells were treated with 5F 203 [■], TCDD [○], IH 445 [▼], Camptothecin [●] (at the indicated concentrations) or 0.1% DMSO [*] for 3 days. Parallel to the addition of the drugs, MTT was added to a triplicate of cultures to assess the cell viability at the day of the treatment (T0; shown by a horizontal dashed line). After 3 days exposure, MTT was added to cells and measured using a Wallac Victor² plate reader. Each point represents the average of mean \pm S.D for triplicate samples, and is representative of results obtained from one of three experiments (5F 203), one experiment (IH 445), one experiment (Camptothecin) and two experiments (TCDD). Curves were fitted using the sigmoidal response equation (GraphPad Prism 5.0 Software). Ordinate: absorbance at 590nm. Abscissa: logarithms of molar concentrations of the compounds tested.

Figure 3.29 shows that DMSO-treated cultures at 72 h, showed high levels of cell growth. Camptothecin, at concentrations ≥ 100 nM decreased cell growth to levels below T0 control levels, and was thus found to be cytotoxic with a GI₅₀ of 67 nM (95% CI, 12-386). The use of the controls, DMSO and Camptothecin, showed that the MTT did not affect the cell growth and thus validates the assay.

As seen in Figure 3.29, TCDD did not inhibit culture viability at any concentration tested in H4-II-E cells, as cell viability in TCDD-treated cultures was not significantly different from DMSO controls. 5F 203 failed to inhibit the growth of the cells up to 10 μ M. On the other hand, this shows that the induction of *CYP1A1* by 5F 203 (Figure 3.18 A) was not affected by any cytotoxicity of this compound. In contrast, IH 445 was found to be a potent inhibitor of cell growth, with a GI₅₀ value of 100 nM (95% CI, 40-248). The cytostatic effect by IH 445 was observed from ≥ 30 nM. These data could provide explanation for the lower *CYP1A1* mRNA levels in-

duced by IH 445 (60% those of 10 nM TCDD), previously shown in Figure 3.19 A.

That TCDD showed no effect on cell viability at all concentrations tested, revealed that the activation of AhR in H4-II-E cells, without additional factors, does not result in inhibition of cell growth.

The inhibitory activity of DF 203, GW 610, AW 892 and IH 318 was assessed against H4-II-E cells by an MTT assay. The GI_{50} values, along with K_i and EC_{50} values, are summarised in Table 3.13.

Compound	K_i [nM] (95% confidence intervals)	EC_{50} [nM] (95% confidence intervals)	GI_{50} [nM] (95% confidence intervals)
TCDD	0.44 (0.18-1)	0.06 (33-100)	ND*
Camptothecin	-	-	67 (12-386)
IH 445	0.9 (0.05-16.9)	4 (2-10)	100 (40-248)
5F 203	2.8 (2-5)	3000 (1300-7700)	ND*
DF 203	9.9 (5.3-18.7)	3400 (900-13000)	ND*
GW 610	6.8 (1.5-30)	6500 (4000-12000)	1400 (450-4300)
AW 892	9.8 (4.4-22)	1900 (300-14000)	223 (133-373)
IH 318	8 (5.5-12)	ND [†]	>10000

Table 3.13 Summary for binding to AhR (rat cytosol), *CYP1A1* mRNA induction and growth inhibitory potency of compounds in H4-II-E cells. To assess growth inhibitory activity of the compounds, cultures were plated for 24 h then treated with varying concentrations of each of the compounds listed. Cell viability was assessed by MTT assay after 3 days exposure. Curves were fitted using the sigmoidal response equation (GraphPad Prism 5.0 Software) and compound concentration that inhibited the growth of cells by 50% (GI_{50}) was determined. (ND*) these compounds did not decrease the viability of the cells below the control levels (T_0) significantly. (ND[†]) the EC_{50} for IH 318 could not be accurately measured given the superinduction of *CYP1A1* mRNA and the absence of a clear plateau. (-) Camptothecin was not subjected to competitive assays nor to *CYP1A1* mRNA induction analyses. EC_{50} and K_i values are obtained from the competitive assays and the *CYP1A1* mRNA induction assays.

From Table 3.13, DF 203, GW 610 and IH 318 had weak inhibitory potency in H4-II-E cells.

Only AW 892 had a sub micromolar GI_{50} value, which reveals a relatively higher inhibitory potency. Overall, the MTT assay was validated and showed that, with the exception of the IH 445

and AW 892, all the phenylbenzothiazoles tested were devoid of anticancer activity in H4-II-E cells.

Section 3.3.2 Effect of TCDD on 5F 203 cytostatic effect in H4-II-E cells

Based on the original hypothesis for 5F 203 [182] anticancer activity that consisted of increased induction of CYP1A1 would result in more metabolism and thus cytostatic effect in MCF-7 cells. It was hypothesized that sensitising H4-II-E cells by treating with TCDD and subsequently inducing CYP1A1 enzymatic activity could enhance the anticancer activity of the compounds in H4-II-E.

H4-II-E cultures were pre-treated with 10 nM TCDD for 24 h. The following day, TCDD was removed and cells were washed with PBS without perturbing the cells, then subjected to 5F 203 treatment in an MTT assay as described under Materials and Methods Section 2.2.15. The results in Figure 3.30 showed no inhibitory activity of 5F 203 against untreated cultures for concentrations below 1 μ M. A modest inhibitory activity was observed from 1 μ M up to 10 μ M. The same effect was observed when cells were pre-treated with TCDD for 24 h, however, with a minor decrease in maximal cell growth levels. The results showed no significant difference for 5F 203 GI_{50} s between H4-II-E cultures pretreated with 10 nM TCDD, 0.6 μ M (95% CI, 0.08-4.7) and those untreated, 1.8 μ M (95% CI, 0.98-3.3). The H4-II-E cells were found relatively more responsive to 5F 203 in this experiment compared to Figure 3.29. The 5F 203 in the current experiment inhibited the cell growth by 60%, thus the GI_{50} values could not be measured accurately.

Overall, activation of AhR by TCDD (10 nM) did not significantly enhance the sensitivity of the H4-II-E cells toward the cytostatic activity of 5F 203 under the conditions of the assay. In the light of these results, it does not seem that AhR-mediated induction of *CYP1A1* is involved

in mediating the anticancer activity of 5F 203 in these cells, and thus the hypothesis previously mentioned [141] [182] does not apply in H4-II-E cells.

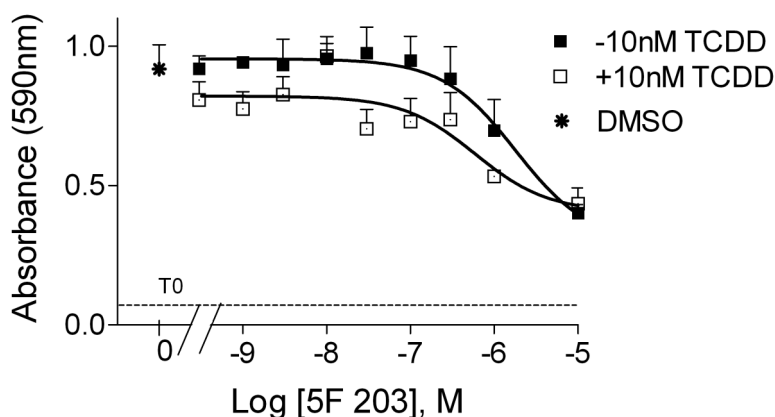


Figure 3.30 Effect of TCDD on the growth inhibitory activity of 5F 203 against H4-II-E cells. Cells were plated at seeding densities of 5000/well and incubated \pm TCDD (10 nM) for one day. The next day, medium containing TCDD was removed and replaced with a medium containing 5F 203 [□] (at the indicated concentrations). In parallel, 0.1% DMSO (*) or 5F 203 was added to cultures without 10 nM TCDD[■], for 3 days. MTT was added and cell growth determined as described in Figure 3.29 legend. Each point represents the average of mean \pm S.D for triplicate samples, and is representative of results obtained from one experiment. Curves were fitted using the sigmoidal response equation (GraphPad Prism 5.0 Software). Ordinate: absorbance at 590 nm. Abscissa: logarithms of molar concentrations of 5F 203.

Section 3.3.3 Growth inhibitory activity of 5F 203 in MCF-7 cells

The responsiveness of MCF-7 cells to phenylbenzothiazole analogues has been characterized [126] [182] [141]. This experiment seeks to address several issues: i) to verify the growth inhibitory potency of 5F 203 and thus confirm the responsiveness of the MCF-7 cell line used in this study, ii) to examine whether the activation of AhR, without the involvement of the enzymatic activity of CYP1A1, would have any inhibitory effect on cell growth by testing whether TCDD has any inhibitory activity and iii) to examine whether the inhibition of AhR, would have any inhibitory effect on cell growth by testing whether the AhR antagonist, CH-223191 has any inhibitory activity.

That was addressed by incubating cultures with varying concentrations of 5F 203, TCDD, or CH-223191 and then testing the growth inhibitory activity in MCF-7 cells with the use of the

cell viability assay (MTT assay). 0.1% DMSO-treated cultures were included as a negative control.

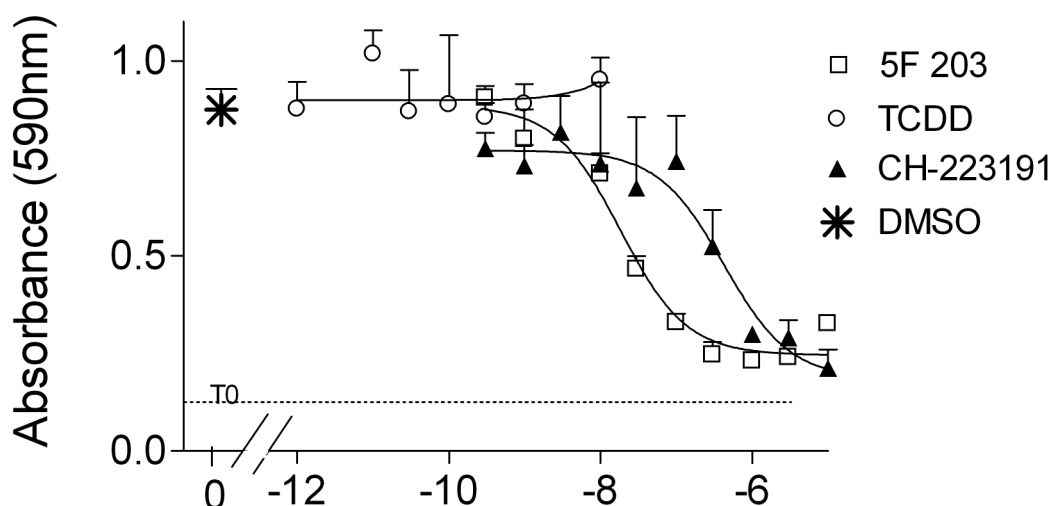


Figure 3.31 Growth inhibitory activity of 5F 203, CH-223191 and TCDD against MCF-7 cells. Cells were plated at seeding densities of 2500/well and incubated for one day. The next day, cells were treated with 5F 203 [□], TCDD [○], CH223191 [▲] (at the indicated concentrations) or 0.1% DMSO (*) for 3 days. MTT was added and cell growth determined as described in Figure 3.29 legend. Each point represents the average of mean \pm S.D for triplicate samples, and is representative of results obtained from one of four experiments (for 5F 203), one experiment (for TCDD), one experiment (for CH223191) and one experiment for the co-treatment of 5F 203 and CH223191. Curves were fitted using the sigmoidal response equation (GraphPad Prism 5.0 Software). Ordinate: absorbance at 590 nm. Abscissa: logarithms of molar concentrations of the compounds tested.

Figure 3.31 shows growth response curves in MCF-7 cells. 5F 203, decreased growth in a concentration-dependent manner, with a GI_{50} value of 18 nM (95% CI, 8.7-39], which confirms the responsiveness of the MCF-7 cell line in this study. TCDD treatment did not affect cell growth viability at any concentration. This confirms that TCDD has no inhibitory activity in MCF-7 cells. This is in good agreement with previous findings [190] [191] [192]. This finding provides evidence that the activation of the AhR by itself is not sufficient for cell growth inhibition, by the fact that TCDD, an AhR agonist, but not CYP1A1 substrate, had no effect on the growth curve.

On the other hand, the AhR pure antagonist, CH-223191 [188] also inhibited the growth of the

cells in a concentration-dependent manner, with a GI_{50} value of 420 nM (95% CI, 173-1029]. In the light of these results, we could not conclude whether the cytostatic effect observed by CH-223191 is a result of the AhR antagonism or via different mechanism of action. We went further to delineate this latter issue.

Section 3.3.4 Effect of TCDD on 5F 203 and CH-223191 growth inhibitory activity in MCF-7 cells

Figure 3.31 showed that the AhR antagonist CH-223191 had a cytostatic effect on MCF-7 cells. This experiment aims to investigate whether this cytostatic effect is AhR-mediated. It was postulated that AhR activation is important for the anticancer activity of 5F 203 in MCF-7 cells. Based on this hypothesis, this experiment also aims to investigate the involvement of AhR in mediating the activity of 5F 203. This will be addressed by confirming that the cytostatic effect of 5F 203 is not due to AhR antagonism. The rationale of this hypothesis is the following: if 5F 203 or CH-223191 inhibits the cell growth by antagonizing AhR, competition with sufficiently high TCDD concentrations will displace the compound with TCDD leading to agonism, and the inhibitory effect will be lost. This will be addressed by incubating MCF-7 cultures with increasing concentrations of TCDD \pm 500nM CH-223191 or TCDD \pm 50nM 5F 203.

The choice of 5F 203 or CH-223191 concentrations was based on the fact that, at these concentrations, ~50% cell growth inhibition was observed (Figure 3.31). CH-223191 (500 nM) and 5F 203 (50 nM) were included as positive controls.

As shown previously (Figure 3.31), TCDD did not affect the growth of MCF-7 cells at any concentration tested (Figure 3.32). CH-223191 and 5F 203 at single concentrations, inhibited cell growth by ~ 50% and 40% respectively. Addition of 500 nM CH-223191 to TCDD, resulted in a biphasic dose-response curve, where at low concentration of TCDD (< 100 pM), CH-223191

decreased cell growth to levels similar to those achieved by 500 nM CH-223191 alone. Higher TCDD concentrations (≥ 100 pM), restored some of the cell loss to a extent of $\sim 30\%$ (comparing mixtures of TCDD and CH-223191 with TCDD-treated cultures in the absence of CH-223191) (Figure 3.32).

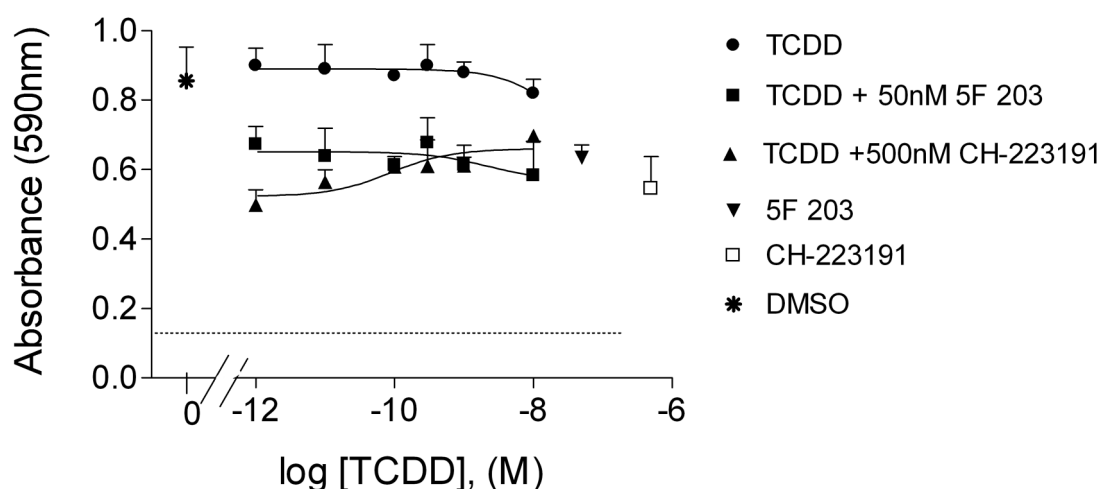


Figure 3.32 Growth inhibitory activity of TCDD \pm 5F 203 or \pm CH-223191 against MCF-7 cells. Cells were plated at seeding densities of 2500/well and incubated for one day. The next day, cells were treated with varying concentrations of TCDD alone [\circ] (at the indicated concentrations) or co-inubated with 50 nM 5F 203 [\blacksquare] or 500 nM CH-223191 [\blacktriangle]. As controls, cultures were exposed to 0.1% DMSO [$*$], 50 nM 5F 203 [\blacktriangledown] or 500 nM CH-223191 [\square] for 3 days. MTT was added and cell growth determined as described in Figure 3.29 legend. Each point represents the average of mean \pm S.D for triplicate samples from one experiment. Curves were fitted using the sigmoidal response equation (GraphPad Prism 5.0 Software). Ordinate: absorbance at 590 nm. Abscissa: logarithms of molar concentrations of the compounds tested.

This effect would be best explained by the agonistic effect of TCDD competing with CH-223191 at sufficiently high TCDD concentrations, where TCDD competes with CH-223191 for AhR and displaces it [188]. However, the addition of TCDD at high concentrations did not restore the cell growth up to control levels, but only by 30%. That could suggest that the cytostatic effect of CH-223191 is partly mediated by AhR ($\sim 30\%$). Therefore, another mechanism of growth inhibition is involved, other than AhR [188]. However, it is also possible that the CH-223191 is partly metabolically inactivated by the TCDD-induced CYP1A1 protein and other

metabolizing proteins, which could also explain the minor observed increase in cell growth.

Mixtures of 50 nM 5F 203 and a range of TCDD concentrations, had similar growth inhibition compared to 5F 203 alone and there was no significant change in cell number ($p>0.05$, t -test, $n=3$). High concentrations of TCDD did not inhibit 5F 203 inhibitory activity. If the 5F 203 is inhibiting the cell growth by antagonizing AhR, then high concentrations of TCDD would restore the cell growth to control levels. These results further confirm that the cytostatic effect of 5F 203 is not due to AhR antagonism in MCF-7 cells, and is consistent with the lack of antagonism of induction of *CYP1A1* by TCDD in these cells.

Chapter 4

Discussion

Recently, it was reported that the phenylbenzothiazole analogues induce *CYP1A1* mRNA in several cells that are sensitive to their antitumorigenic activity, *e.g.*, human breast cancer MCF-7 [182] [253]. However, there is no published data on binding of these compounds to AhR.

Quantitative comparison of ligand binding and induction potency requires data from the same species to be meaningful, and so rat was used as a model species. Such quantitative comparisons between ligand affinity for receptor and the resulting pharmacological effect, allow the application of various concepts from pharmacology.

Section 4.1 The [³H]-TCDD radioactive binding assay

Section 4.1.1 Validation of the [³H]-TCDD radioactive binding assay

AhR competitive binding assays have been established *in vitro* and have been central to investigations of direct AhR-ligand interaction, which is the initial step in AhR-mediated responses. Several techniques have been used to characterize the AhR, such as velocity sedimentation on sucrose density gradient analysis [193], hydroxyapatite [170] and charcoal adsorption using tritiated TCDD [6] [164] or 7-(¹²⁵I)iodo-2,3-dibromodibenzo-*p*-dioxin [156] as high-affinity ligands. In the present study, the use of charcoal adsorption followed by centrifugation to separate bound and free radioligand mixture was found to be a simple, quick, practical and reproducible method. These attributes enable multiple replicates and samples, and hence robust characterization of binding parameters such as K_D or B_{max} . This is in contrast to *e.g.*, density gradient centrifugation methods.

As the aim is to develop a binding assay and therefore determine the binding kinetics of TCDD to AhR, it is essential to optimise several aspects of the assay. Several factors were found to af-

fect [^3H]-TCDD specific binding and thus affect K_D value of TCDD, such as the time of incubation, the high level of non specific binding, the concentration of protein and [^3H]-TCDD, ligand depletion and finally the poor solubility of [^3H]-TCDD in aqueous solutions.

In attempts to control these factors, cytosolic protein preparations were incubated for sufficient time (16 h) at 4°C to allow equilibrium between AhR and ligands. The [^3H]-TCDD specific binding was not significantly changed from 2 h up to 16 h at 4°C (Figure 3.1), thus the (AhR-[^3H]-TCDD) complex appeared stable up to 16 h at 4°C .

The use of charcoal efficiently reduced background radioactivity. An amount of 2 mg of charcoal / mg of cytosol protein selectively stripped off nonspecifically bound [^3H]-TCDD without affecting the concentration of [^3H]-TCDD specifically bound in the rat cytosol (Figure 3.2), which reflects the high affinity of the rat hepatic AhR for TCDD [193].

Characterization of AhR ligand binding using a radioligand with a low specific radioactivity, such as [^3H]-TCDD (29.77 Ci/mmol), necessitates a sufficient amount of [^3H]-TCDD and cytosolic protein and (hence, AhR), (Figure 3.4) and (Table 3.2) to give a reliable measure of specifically bound radioactivity. However, increasing protein concentration yield increased nonspecific to specific binding ratio (Figure 3.2 & Figure 3.3), and this finding was previously reported by Bradfield and Poland (1988) [156]. In their work, Bradfield and Poland worked with 7-(^{125}I)iodo-2,3-dibromodibenzo-*p*-dioxin as a radioligand with much higher specific activity (2176 Ci/mmol) as opposed to the lower specific activity of [^3H]-TCDD (29.77-50 Ci/mmol), thus they worked at much lower protein concentrations, thereby mitigating the complications of misclassifying the free radioligand [156]. Misclassification of non-specifically bound AhR as free ligand is proposed to be the reason why the apparent K_D of TCDD from the present study along with those reported in literature is significantly greater than the theoretical K_D value of 6

pM reported by Bradfield et al. [156] by extrapolating to an infinite dilution of protein (Table 3.2). The nonspecific binding represents the noise background of the assay that ideally should remain constant at all test competitor concentrations and across experiments. The nonspecific binding of [^3H]-TCDD in the presence of test competitor was determined by co-incubating excess TCAOB with varied concentrations of test competitor. [^3H]-TCDD non specific binding was consistent at all test competitor concentrations within the same experiment and varied slightly across experiments (data not shown). This also provided evidence that the test competitor does not compete with [^3H]-TCDD for non specific sites, as it is not uncommon that drugs would compete for non specific sites at high concentrations [166].

The hydrophobic nature of TCDD is the reason for its high non specific binding. Another challenging aspect that emerges from the hydrophobic nature of TCDD is its poor solubility in aqueous solutions (Figure 3.5), which is consistent with previous findings [38]. This is particularly why binding assays using TCDD as a ligand would suffer from misclassification of free TCDD if not controlled properly. The use of centrifugation after charcoal treatment enabled the measurement of the free [^3H]-TCDD. The binding assay was optimised as to retain TCDD in solution, so that around 20% only is coming out of solution, which was considered acceptable. That was controlled by optimizing both protein concentrations (Figure 3.5) and [^3H]-TCDD concentration (Figure 3.6). More [^3H]-TCDD at 1 nM concentration is retained in solution in the presence of a concentration of 5 mg/ml cytosolic protein. [^3H]-TCDD starts to come out of solution at ≥ 2 nM; but numerous reports in the literature use [^3H]-TCDD in solution at ≥ 5 nM [169] [67] [170]. The aqueous solubility of TCDD could be increased by the addition of ampholytes, non-ionic detergents, or macromolecules, but it seems that each of these additions affects the measurement of the specific binding of TCDD [6].

Another potentially important parameter in binding assays is ligand depletion by binding to re-

ceptors. Since the binding of a ligand to a receptor must obey to the law of mass action, it is essential that only a small amount of ligand binds the receptors, *i.e.*, the concentration of “free” ligand approximates the concentration of “added” ligand, so that the law of mass action holds true. This parameter was controlled in the current binding assay, such that only 20% of TCDD is depleted by binding (Figure 3.4). Under these conditions, there is no need to correct for ligand depletion by binding.

The [^3H]-TCDD binding assay described in this study showed specific and saturable binding of TCDD to AhR. The binding kinetics, K_D and B_{max} , of [^3H]-TCDD to AhR determined from the standard binding assay were reproducible over three experiments (Table 3.1). Moreover, the K_D for TCDD determined from the direct binding assay was essentially similar to that determined from the competition assay using unlabelled TCDD as competitor, which validates the competitive binding assay. The binding kinetics derived from the current binding assay are consistent with previously reported values (Table 3.2). The K_D values from literature reported in Table 3.2 were determined from Scatchard plot analysis. The K_D for [^3H]-TCDD determined by Farrel and Safe (1987) using the hydroxyapatite assay followed by centrifugation [170], was within two-fold of the K_D derived in this study. The use of the charcoal alone without hydroxyapatite assay in the current binding assay gave K_D for TCDD similar to that reported by Farrel and Safe (1987) [170], which shows that the charcoal technique, without further separation steps, is equally sensitive. The K_D value determined in this study is similar to that reported by Poland et al., (1976) using cytosol from C57BL/6J mice [6]. From the data reported from literature, it seems that Wistar and Sprague-Dawley rat and C57BL/6 mice hepatic cytosol binds TCDD with high-affinity given the low K_D values. The C57BL/6 mouse seems to have slightly higher affinity [6]. The range of K_D values (0.37-1.45 nM) for Wistar rats summarised in Table 3.2 have been found to be influenced by several experimental variables, such as temperature and

duration of incubation, variable protein (AhR) concentration and high concentrations of [^3H]-TCDD. All these factors have significant impact on the amount of functional AhR in the preparations, the accurate classification of “free” [^3H]-TCDD in solution and the high non specific binding of [^3H]-TCDD.

Section 4.1.2 Characterization of the binding of phenylbenzothiazoles to AhR

Once the [^3H]-TCDD binding assay was validated, the binding affinities of the phenylbenzothiazoles were determined from competitive binding assays (Table 3.3), thereby showing that they are high-affinity ligands, with K_i values in the nanomolar range for the AhR. Of the 24 compounds tested for their binding avidity to the AhR, only two compounds bearing a hydroxyl group, the 2-(4-amino-3-methylphenyl)-6-hydroxybenzothiazole, (IH 130) and the 2-(3-hydroxy-methoxyphenyl)-5-fluorobenzothiazole (JP-2) were low-affinity ligands, with K_i value $> 1 \mu\text{M}$. The 2-(4-aminocarboxymethoxy-3-methylphenyl)-5-fluorobenzothiazole (JMB 81) had intermediate affinity for AhR.

The mechanism of action of phenylbenzothiazole analogues is still unknown. These agents induced CYP1A1 in sensitive cancer cells [141] [253], suggesting AhR as a possible target for these chemicals. Although the CYP1A1 induction is a well characterized biomarker for exposure to AhR ligands [94], it is also possible that induction of CYP1A1 could result from activation of the AhR through a non-ligand binding mechanism. This has been shown with a benzimidazole compound, omeprazole (OME) that was able to activate the AhR via a ligand-independent mechanism [194] [101], likely through a signaling transduction pathway that involved protein tyrosine kinase (PTK) [101]. Given the structural similarity between benzimidazoles and phenylbenzothiazoles (PBT), it is possible that the PBT activate the AhR without necessarily binding to the receptor. The competition assays provide evidence of direct binding

between phenylbenzothiazole analogues and AhR and so ligand-independent activation of the AhR by PBT is therefore a less likely possibility.

Historically, PBTs have been shown to induce CYP1A1. For example, a related compound, the 2-(4'-chlorophenyl)-benzothiazole (CPBT), was previously shown to bind AhR by displacing TCDD from binding sites [195]. However, the PBTs currently studied are considerably more potent than these other PBTs [195].

Section 4.1.3 Structure-Activity Relationships (SARs)

Section 4.1.3.1 Structure-activity relationships for binding AhR

Because of the lack of crystal structure for AhR, ligand structure-based methods provide an alternative way for our understanding the mode of AhR binding with dioxin and other ligands such as the benzothiazole drugs.

The results of Table 3.3 summarise the K_i values for the competitive binding affinities of the phenylbenzothiazole analogues for the rat cytosolic AhR. The magnitude of the K_i values for the phenylbenzothiazoles was dependent on the structure of substituents and varied over ~6000-fold (>3 log) from the IH 445 to the JP-2 which displayed the lowest and highest K_i values respectively.

Generally, it was observed that the presence of two hydrophobic groups or more, specifically two halogenated atoms or a halogen atom and an alkylated group, favours high-affinity binding. Three possibilities may explain this observation. First, it could be that the introduction of such groups at the 3' position in the phenyl and the 5' position in the benzothiazole moieties forces the whole molecule to become planar. However, it seems that absolute planarity is not a requirement for AhR binding as shown in this study by another compound not related to the phenyl-

benzothiazole analogues, tetachlorophenothiazine (TCPT) [196].

The second explanation is increased hydrophobicity of the molecule caused by the introduction of hydrophobic groups. Previous QSAR studies with a series of 7-substituted 2,3-dichlorodibenzo-*p*-dioxins showed that the binding affinity was linearly dependent on the lipophilicity (π) of the 7-X-group [197].

The third explanation is the steric effect of these groups. The introduction of bulky groups in the lateral positions increases the size of the molecule so it can fit the size required for binding. This seems to be in agreement with the tolerance of steric effect in the lateral positions proposed by Waller and McKinney (1995) [40]. Finally, a combination of these scenarios is also possible.

Phenylbenzothiazole analogues and TCDD have two aromatic rings but are structurally different. Comparing their SARs enables more understanding of the mode of binding to the AhR. The comparison of their SARs revealed some similar structural requirements for binding to the Ah receptor. Generally, for PCDDs, any pattern that includes chlorination at positions 2,3,7 and 8 is known to be associated with the compound's strong binding to the AhR. This is true only if one ring position is unoccupied [198]. Structure-activity relationships for binding of a series of 2-substituted 3,7,8-trichlorodibenzo-dioxins to AhR revealed that binding was dependent on substituent lipophilicity, steric effects and hydrogen bonding and that correlation between binding and CYP1A1 induction for these compounds was dependent the steric factor of substituent [199]. A major difference between the SAR of dioxins and PBTs is observed when an amino group is introduced at the 7-position of the 2,3-dichlorodibenzo-*p*-dioxin. The EC₅₀ of the 7-amino- 2,3-dichlorodibenzo-*p*-dioxin was greatly reduced in the rat hepatoma cell [197]. The binding affinities of phenylbenzothiazole analogues were considerably higher although these have an amino-group in the phenyl ring of all the analogues in series (1). But it does not seem

that the amino group is critical for binding given that replacement of an amino by a methoxy group did not affect the binding significantly (JP-1). Generally, the phenylbenzothiazole analogues tolerate structural modifications more than TCDD. For example, a cyanide group or a hydrogen atom in position 7 in the 2,3-dichlorodibenzo-*p*-dioxin, has a marked inhibitory effect on TCDD binding [197], whereas the introduction of the same groups in one of the lateral positions of the phenylbenzothiazole analogues, does not inhibit their binding to the Ah receptor. These data suggest that these compounds compete with dioxin at the same sites on the AhR, but they interact with different residues in this site.

Section 4.2 *CYP1A1* induction assay using TaqMan real-time RT-PCR

Section 4.2.1 The choice of the cell cultures

The CYP1A1 induction assay was initially conducted cultured cells to minimise metabolism. The cell line chosen to generate the log concentration-response curves for the test compounds was the rat hepatoma H4-II-E cell line. This cell line represents a useful model system because of low basal CYP1A1 activity and high inducibility of the enzyme activity in response to dioxin-like inducers [179] [173] [58] [175] [174].

Section 4.2.2 qRT-PCR analysis

The initial choice of quantitative reverse transcriptase real time PCR (qRT-PCR) and TaqMan technology for measuring messenger RNA (mRNA) levels allows measurement of AhR gene expression before any post translational/functional modifications [200] or enzymatic inhibition (EROD) [201] [202]. Furthermore, qRT-PCR is more sensitive over EROD activity in detecting CYP1A1 induction [258] [203] and northern or slot blotting for measuring RNA [258] and has the advantage of speed and throughput compared with conventional quantification methods, such as northern blot analysis, ribonuclease protection assay or competitive PCR. Finally, as op-

posed to semi-quantitative PCR, real-time PCR analysis yield more accurate results as the reaction is occurring and measurements are taken during exponential phase of PCR amplification as opposed to end point PCR, where the reaction is complete (www.stratagene.com).

In the present study, the quantitative PCR chosen consists of relative quantification since the issue is to compare the mRNA induced levels to vehicle or TCDD controls and not to determine the number of templates in the original sample as for the absolute quantification method. The relative quantification method consists of normalizing the mRNA levels to those of a housekeeping gene, whose expression must remain unchanged in response to experimental conditions and increasing drug exposure.

Section 4.2.3 Normalisation to housekeeping genes

The validation of the reference genes was performed systematically at every single experiment. *β-actin* and *AhR* gene expression was routinely found within ~ two-fold of control levels, in both rat and human cells, at all treatments and all experimental conditions performed, which provides evidence that the perturbation in *CYP1A1* RNA levels represents genuine gene-specific expression and is not a result of sample differences (RNA quantity and quality) or variation of the reference gene expression.

Housekeeping gene expression is not necessarily stable with all treatments [205] [206]. The use of one single reference gene for normalization is not optimal practice because it can give errors in normalization [207]. Therefore, to gain more accurate and reliable results, two reference genes were selected in the present study, the *β-actin* and the *AhR* genes. The rationale of the use of two reference genes is that the *AhR/β-actin* ratios should be close to 1 which reflects a high expression stability [207]. The coefficients of variation (cv) for *β-actin* mRNA and *AhR/β-actin* mRNA ratios were between 20-30%, which reflects on the low variation among the data. *β-ac-*

tin and *AhR* genes were chosen based on previous findings, that *β-actin* and *AhR* gene expression was relatively constant in response to TCDD in rats [153].

Section 4.2.4 Factors affecting *CYP1A1* RNA induction in H4-II-E cells

The induction levels achieved by TCDD in the H4-II-E cells varied significantly between experiments according to the controls used (Figure 3.13 B and Figure 3.14 A). The *CYP1A1/β-actin* mRNA ratio induced levels in Figure 3.13 B were relative to 4 h DMSO-treated cultures in fresh medium, whereas in Figure 3.14 A, the levels induced were derived relative to untreated cells (not subjected to medium change), and treatment levels were significantly higher. Basal *CYP1A1/β-actin* mRNA ratio for DMSO incubations set up as the background of *CYP1A1* mRNA expression was consistently detectable (Figure 3.13 C and Figure 3.14 B). The fresh medium was hypothesised to have an induction capacity. This hypothesis was investigated in Section 3.2.5.3. The results showed that the *CYP1A1/β-actin* mRNA ratio in DMSO-treated cells was 8-fold higher in fresh medium than in pre-incubated medium. Since the values for TCDD-induced *CYP1A1/β-actin* mRNA ratios are derived relative to DMSO-treated incubations, that resulted in an apparent lower induction observed by TCDD.

This is with good agreement with previous work reported by Kocarek et al (1993), where they found *CYP1A1* mRNA induction when primary cultures of rat hepatocytes were exposed to fresh medium [172]. Work on rainbow trout gonadal cells (TRG-2) showed that the addition of fresh medium to cells resulted in a 20-fold induction of *P4501A* mRNA over untreated cells [178]. It was suggested that the induction observed when changing medium is due to a component in the fresh medium, and Kocarek et al (1993) isolated the inducing factor as a photoactivated tryptophan derivative [172]. The oxidized product of tryptophan induces *IAI* and the results suggest that the transient nature of the *IAI* induction is due to elimination of activated tryptophan molecule at 24 h. That was also reported by Helferich and Denison (1991) [208],

where they found that ultraviolet-irradiated tryptophan bound specifically to the Ah receptor and caused DRE binding and gene transcription.

The results in Section 3.2.5.3 proved that DMSO had no effect on *CYP1A1* mRNA induction (Figure 3.15 A), which is consistent with [178].

Overall, these results provide evidence for the importance of controlling the background control levels in induction assays as, according to the results provided in this study, that can seriously affect the magnitude of the response and hence reduce the signal-to-noise ratio. The results have proved that fresh medium induced *CYP1A1* mRNA and that DMSO (0.1%) has no effect on induction.

Section 4.2.5 Validation of the induction assay in H4-II-E cells using TCDD

The use of TCDD as a positive control in induction analysis was based on two reasons: first, TCDD is very potent inducer of *CYP1A1* mRNA and second, it resists oxidation by xenobiotic metabolizing enzymes and thus produces a sustained induction (reviewed in [3]). With regard to *CYP1A1* mRNA induction, H4-II-E showed high inducibility and high sensitivity in response to TCDD, under the conditions optimised (4 h and pre-conditioned medium).

The fold-induction of *CYP1A1*/ β -actin mRNA ratios by 1-10 nM TCDD was 300-fold above vehicle controls. Significantly- induced levels of *CYP1A1* mRNA by TCDD were detected at concentrations <100 pM (Figure 3.24 A). The EC₅₀ values of TCDD for *CYP1A1* mRNA induction varied from 30 pM to 60 pM, on four different occasions, which is within two-fold variation (Table 3.6). This showed reproducibility of the induction assay. The EC₅₀ values for TCDD are comparable with literature values (Table 3.12). However, the values from the literature raise several issues: (a) low-fold induction coupled to high levels in controls, which could result in

an apparent underestimated EC_{50} value [175] [183], (b) improper definition of the top and bottom levels (plateau) for the dose-response curves, which might yield erroneous results [184], (c) the dose-response curves are not shown [186] [13] [185], or (d) most of the work has been conducted at late time points, *i.e.*, at saturation levels of the response, which could significantly affect the EC_{50} of TCDD as previously shown by [180]. Finally, most of these reports are lacking the statistical characterization of the measurements (S.D or 95% confidence intervals). Literature values for the EC_{50} for TCDD were collected from enzymatic assay rather than mRNA, given that CYP1A1 induction was mainly characterized via these assays. The induction of *CYP1A1* mRNA by TCDD in H4-II-E cells has been characterized but using few concentrations of TCDD [175] [209]. As a result, there is a need for a dose-response curve with an accurate measurement of EC_{50} .

Having established the feasibility of the *CYP1A1* mRNA induction assay, the method was used to generate the log concentration-curves and thus determine the EC_{50} of the benzothiazole analogues for the *CYP1A1* mRNA induction.

When TCDD and chemicals were tested on several occasions, EC_{50} values did not change significantly between experiments ($p > 0.05$, $n=3$, t -test, $n=3$). The slope also did not change significantly between compounds and across all experiments. The maximal level of induction varied less than 3-fold.

3-Methylcholanthrene (MC) is another potent AhR ligand, but in contrast to TCDD, MC is prone to metabolism [180]. Using the conditions of the current induction assay, the induction of *CYP1A1* mRNA by 3-methylcholanthrene (MC) was characterized and compared with that of TCDD.

TCDD and MC have similar maximal levels of *CYP1A1* mRNA induction in H4-II-E cells (Fig-

ure 3.17 A), as previously reported [180] [177] and was only ~200-fold less potent than TCDD for inducing *CYP1A1* mRNA in H4-II-E cells (Section 3.2.7; Figure 3.17 A). This difference in potency within 200-fold might be due to some of the metabolism previously shown at 4 h [180]. MC had similar affinity to TCDD (~1 nM) as a ligand for AhR in Sprague-Dawley rats [67] but is 30,000 times less potent *in vivo* rat [181] than TCDD as an inducer of AHH activity. Such discrepancy between binding to AhR and *CYP1A1* induction was attributed to the metabolic inactivation of the MC *in vitro* by the enzymatic activity of the *CYP1A1* at 24 h [6]. One study estimated the difference in *CYP1A1* mRNA induction potency between TCDD and MC to be (≥ 10 -fold) when assessed at 2 h in mouse cultured Hepa-1 cells, however, the EC₅₀ values were not adequately derived given the incomplete log concentration response curves of both compounds [180]. The present study proved MC to be a potent agonist for *CYP1A1* with a greater potency than previously reported [181].

Section 4.2.6 5F 203, DF 203, GW 610 and AW 892 but not IH 445: low potent agonists for inducing *CYP1A1* mRNA in H4-II-E cells

The phenylbenzothiazole compounds tested, 5F 203, IH 445, DF 203, GW 610 and AW 892 induced *CYP1A1* mRNA to TCDD maximal levels and can be classified as full agonists according to the definition by Jenkinson et al (1995) [210]. However, these compounds, except IH 445, had low potency in H4-I-E cells (Figure 3.19 A and Table 3.9).

The binding assay proved direct interactions between the phenylbenzothiazole compounds tested and the AhR, and suggests that the induction of the *CYP1A1* mRNA was a subsequent result from binding to the AhR. In order to show that AhR is required for induction of CYP1A1, it would be necessary to knock out the AhR and then study the induction by these agents under the same conditions of the assay. Finally, in order to confirm that the induction of *CYP1A1* mRNA by the test compounds is not a specific effect on *CYP1A1* but rather a result of a general

activation of AhR, it would be possible to screen the transcription of other AhR-dependent genes expression by real-time RT-PCR and follow this with protein expression analysis. Translocation of the AhR to the nucleus subsequent to binding could be confirmed by performing western blotting analysis.

Section 4.2.7 Interpretation of difference in potency between binding affinity and *CYP1A1* induction: partial agonism

IH 445, 5F 203, DF 203, GW 610 and AW 892 were high-affinity ligands for AhR in rat cytosol with K_i values in the nanomolar range (Table 3.3). These compounds were expected to be potent inducers of *CYP1A1*, as generally, AhR binding affinity correlates with induction of *CYP1A1* mRNA [202] [199] [197] [159]. The induction potential of the low-affinity ligands ($K_i > 1 \mu\text{M}$) could not be assessed in H4-II-E cells, because the limited solubility of these compounds ($> 30 \mu\text{M}$) prevented from generating their log concentration-response curves for *CYP1A1* mRNA induction.

The most potent AhR ligand, IH 445 was only 5-fold less potent in inducing *CYP1A1* mRNA than in its binding affinity for AhR (Table 3.9). For the rest of the phenylbenzothiazole compounds tested (5F 203, DF 203, GW 610 and AW 892), there was a poor correlation between Ah receptor binding affinities and induction potencies in H4-II-E cells. The most striking difference was observed with 5F 203 and GW 610, with 1000-fold lower induction potency than binding affinity for AhR. The binding affinity values of AW 892 and DF 203 were 200- and 300-fold lower than the corresponding EC_{50} values respectively (Table 3.9). Similar disparities between binding and potency for induction were obtained by others with other compounds, such as, the 6-substituted 3,4-benzocoumarins [211], PCBs [212] and di-ortho PCBs [213], αNF and methyltricholodibenzofuran [95] [214] [215] [97], 6-methyl-1,3,8-triCDFs [216]. There was no quantitative measure of their intrinsic efficacy for activating AhR signaling. Moreover, even

though direct measurements of some of these compounds to agonize and antagonize AhR signaling has been made, these measurements were performed by endpoint analyses, such as EROD and at late time points [217] [211], where the response versus time of induction is not linear and may be subject to posttranslational inhibition of enzymatic activity or metabolism. Other reports focused on investigating metabolic inactivation of the lower potency agonists as the most likely possibility without testing the antagonistic activity of these compounds, thereby assuming by that high intrinsic efficacy for these compounds [181] [180].

Given the poor correlation between binding of PBTs to AhR and *CYP1A1* mRNA induction in H4-II-E cells, this cell line provides a suitable system to further investigate the difference in potency between binding to and activation of AhR. So, it was necessary to elucidate what determines the potency of the benzothiazole analogues, by estimating the intrinsic efficacy of 5F 203 and IH 445 on TCDD for inducing *CYP1A1* mRNA in H4-II-E cells.

5F 203 bound with high affinity to AhR (K_i 2.8 nM), versus a K_D for TCDD of 0.37 nM. However, when tested for its capacity to induce *CYP1A1* mRNA in the rat cell line, it was found much less potent (50,000-fold less than TCDD). The 8-fold difference in binding affinities can not account for the large quantitative difference, 50,000-fold in *CYP1A1* mRNA induction potency between 5F 203 and TCDD. However, other possibilities exist, such as, (a) lower intracellular concentrations of 5F 203 caused by inefficient cellular uptake or metabolism, (b) 5F 203 and TCDD do not share the same mechanism of action and (c) low intrinsic efficacy of the compound that fails to fully activate the AhR, *i.e.*, that 5F 203 is a partial agonist. These three possibilities are discussed below.

(a) Measurements of the induction potency was conducted in cell cultures where the concentration of the drug can be affected by many factors such as sequestration of the chemical by serum

proteins and/or the inability to readily traverse the cellular membrane and clearance by metabolizing enzymes. These factors would tend to reduce the apparent potency of the chemicals. However, in the binding assay, these factors are not present and the drug in the medium can immediately gain access to the receptors. Although efforts have been made to work under conditions where drug metabolism is not the major determinant factor (by working at an early time point, 4 h), the possibility that some of the drug may still undergo some metabolic inactivation, cannot be ruled out. However, as shown for 5F 203, lower concentrations is very unlikely to be the main factor behind its low potency for two main reasons. First, as shown in Figure 3.14 A, the induction of *CYP1A1* against time was still increasing linearly till 6 h treatment suggesting that 5F 203 is not subjected to significant metabolism at an early time point (4 h) and second, co-incubation of TCDD and 5F 203 (Figure 3.20 A) revealed a significant inhibitory effect of 5F 203 (100-fold) on TCDD-induced *CYP1A1* mRNA. The strength of the effect of 5F 203 on TCDD-induced in H4-II-E cells excludes the possibility that the lower potency of 5F 203 in these cells is a result of low intracellular concentration of 5F 203. Finally, when MC, a compound known to be metabolized [180], was tested in rat cells, it was found only 200-fold less potent than TCDD for inducing *CYP1A1* mRNA as opposed to the 50,000-fold reduced potency of 5F 203.

(b) The log concentration-response curves for 5F 203 and TCDD are parallel (Figure 3.18 A) which provides indirect evidence for a common mechanism of action for the *CYP1A1* induction by Ah receptor. In Section 3.1.8, 5F 203 competitively displaced [³H]-TCDD specifically bound to the AhR, which proved direct interactions with the AhR (Figure 3.9). That proves that the induction of *CYP1A1* by 5F 203 is, like TCDD, AhR- mediated.

(c) 5F 203 was estimated to have a low intrinsic efficacy with a fraction occupancy around 100% for 50% maximal response. Mixtures of increasing concentrations of TCDD with 1 μ M

5F 203 increased TCDD's EC₅₀ by 100-fold. These results demonstrate that 5F 203 antagonized TCDD-induced *CYP1A1* mRNA in H4-II-E cell line. Thus, 5F 203 is classified as a partial antagonist in H4-II-E cells which provides explanation for its much lower potency than TCDD. 5F 203 binds AhR but fails to activate it at its binding concentrations.

In H4-II-E cells, 5F 203 behaves like many flavonoids in that it functions as an AhR antagonist at lower concentrations, while at higher concentrations it behaves as an AhR agonist [218]. This effect would be apparently exacerbated with a less sensitive assay methodology. Antagonistic effects between less potent PCBs and highly potent TCDD have been documented *in vivo* and *in vitro* (reviewed in [219]). Many ligands were reported to have dual function as AhR agonists/antagonists [98] [216] [211] but the molecular factors that determine either activity are still unknown. One study reported that AhR agonists, but not antagonists, induce conformational change in the *in vitro*-translated mouse AhR [220]. Alternatively, it could be that, like steroid receptors (androgen, oestrogen, progesterone and glucocorticoid), some hormone antagonists induce conformational changes that are different from those induced by agonists. It is possible that AhR agonists and antagonists bind to different residues in the binding pocket of the AhR, resulting in different conformational changes [221]. Assuming that cellular uptake and accessibility of 5F 203 and TCDD to the AhR is similar, the antagonism may be due to events involving ligand binding/AhR transformation/nuclear translocation/DRE binding that contribute to the ultimate difference in *CYP1A1* induction potency. There is the example of α NF that competes with TCDD for binding AhR [95] [215] [222], exhibits weak AhR agonist activity, inhibits the formation of nuclear TCDD-AhR complexes, and partially antagonizes TCDD-induced *CYP1A1* gene expression in several mammalian cells [96]. Alternatively, the 3'-methoxy-4'-nitroflavone binds AhR with high-affinity in mouse Hepa cells but cannot initiate transformation and nuclear translocation, as result, the 3'-methoxy-4'-nitroflavone bound to AhR remains in the

cytosol associated with hsp90 [222].

Overall, little is known about the mechanism of antagonism of AhR, and it would be useful to investigate the mechanism of antagonism of TCDD-induced *CYP1A1* mRNA induction by 5F 203 in H4-II-E cells. The antagonism of 5F 203 to TCDD could be for a specific response, which is the *CYP1A1* gene induction, however, to prove that the antagonism is at the AhR level, the general response would be antagonized, for example, to determine if translocation to the nucleus of TCDD-AhR complex is blocked by 5F 203 in a dose-dependent manner. So, it would be important to examine with the mean of a quantitative western blotting whether the 5F 203 alone or in mixtures with TCDD induces AhR translocation to the nucleus, and in case it does, whether the translocation correlates with its induction potency.

DF203, GW 610 and AW 892, are estimated to be low-intrinsic efficacy agonists, like 5F 203, with similar receptor occupancy levels. They all display similar binding affinity and induction potency profiles. These results give reasons to believe that these compounds are likely to be partial antagonists in the H4-II-E cells. In contrast, IH 445 was found to be potent in both binding to AhR and inducing *CYP1A1* mRNA in H4-II-E cells. This compound was estimated to occupy 82% of receptors to achieve 50% maximal response. In order to investigate whether this compound has an antagonistic activity in H4-II-E cells, TCDD was incubated with and without 3 nM IH 445, and this potent agonist did not antagonise TCDD. The 5-fold difference could be attributed to some loss of activity of the compound by metabolizing enzymes present in the *in vitro* induction assay but not in cytosol. Having found a derivative in the series (1) with high potency for inducing *CYP1A1* indicate that the partial agonism observed with 5F 203 is not a generic intrinsic characteristic of all the phenylbenzothiazoles, but is rather compound-specific. The difference in agonism/antagonism profile between 5F 203 and IH 445, suggests a different mode of binding to AhR by these compounds and/or different mode of activation of the recep-

tor. Perhaps, the most pronounced structural difference between the IH 445 and the other compounds tested, is the bulkier group at the 3' position (ethynyl group) of IH 445 compared with the methyl group at the same position for the other compounds.

Having determined the binding affinity (K_i) of these compounds and their EC_{50} for inducing *CYP1A1* mRNA in rat, interactive effects of mixtures of these compounds and TCDD could be roughly predicted by calculating the EC_{50} concentration of TCDD in the presence of the test compound [A'] from the equations [6] and [7] (appendix). The prediction that 1 μ M 5F 203 would antagonize TCDD by 360-fold was tested and experimentally, revealed 100-fold antagonism. This is a useful approach to predict whether a low efficacy compound, could be a partial agonist in a particular cell line. The choice of concentration of the test chemical in mixtures with TCDD is very important. This choice has to be based on the affinity and the induction response, so that the antagonism could be measured accurately.

Schild regression is a powerful method for drug classification. Not only does it allow an independent estimation of K_B value and determination of the slope, but it also gives an indication whether the system has reached equilibrium [264]. The Schild regressions on TCDD concentrations in combination with three different concentrations of 5F 203 proved linearity, with a Schild slope not significantly different from unity (Figure 3.21 and Figure 3.22). This result provides information that the analysis was performed under equilibrium. Another useful application of the Schild analysis, is that it allows analysis of the nature of the antagonism, *i.e.*, whether it is reversible competitive or non-competitive, as demonstrated for the reversible competitive antagonism of 5F 203 on TCDD (Figure 3.21) which validates the results of the competitive radioactive binding assays (Figure 3.9). Furthermore, Schild analysis allows the determination of the fraction of receptor occupancy for TCDD in mixtures with another compound. Based on K_B experimental value, from equation [5] (appendix), the fractional receptor occupancy at 50% re-

sponse of TCDD in the presence of 1 μ M 5F 203 was calculated to be 0.2% compared to the 14% in the absence of the antagonist 5F 203. Schild regressions on 5F203 revealed an 8-fold higher K_B in the induction assay compared to the K_D determined in the binding assay. This close agreement provides evidence that 5F 203 has reached receptor sites and that the intracellular concentrations in cells in cultures are not significantly lower than when compared to extracellular conditions, if sequestration by serum protein and some metabolism are taken into account.

In this study, it has been demonstrated that 5F 203 is a partial antagonist in H4-II-E cells which could provide explanation for the difference in potency between binding to and activation of AhR. The antagonistic effect of 5F 203 on the EC_{50} for induction of *CYP1A1* mRNA by TCDD was quantified. Quantifying the relative agonistic and antagonistic activities of anticancer phenylbenzothiazoles is important for drug assessment.

Section 4.2.8 TCDD and 5F 203: potent agonists in human MCF-7 cells

The phenylbenzothiazole analogues tested, except IH 445, had low potency for inducing CYP1A1 in H4-II-E cells, but were previously shown to induce CYP1A1 in MCF-7 cells [140] [141] [253], thus was used as a standard of comparison. Therefore, it was interesting to test the potency of one of these compounds, 5F 203, under the conditions of the current induction assay and compare with literature.

The fold-induction of *CYP1A1*/ β -actin mRNA ratios by 1-10 nM TCDD was 1300 above vehicle-controls MCF-7 cells. Induced levels were detected from 100 pM (Figure 3.24 A). Low constitutive levels of *CYP1A1*/ β -actin mRNA ratios were detected in MCF-7 cells. Although it was reported that neither activity nor expression of the P450 CYP1A1 is constitutive in MCF-7 cells [141], this difference may be attributed to the lower sensitivity of Western blotting and EROD assay, where low levels could not be easily measured, as compared to the sensitive measurement

by qRT-PCR. When run in two separate experiments, the EC₅₀ values of TCDD for *CYP1A1* mRNA induction were within two-fold (Table 3.11). These results further confirm the reproducibility of the induction assay previously shown in rat cells (Table 3.6). The EC₅₀ values for TCDD in MCF-7 are comparable with literature values (Table 3.12). However, the values from the literature are suffering from several caveats that were covered in Section 4.2.5.

5F 203 induced *CYP1A1*/ β -actin mRNA ratios to levels seen with TCDD. The EC₅₀ values of 5F 203 for *CYP1A1* mRNA induction was 2 nM (95% CI, 0.9-5) (Figure 3.25 A). 5F 203 in mixtures with TCDD, did not exhibit any antagonistic activity on TCDD-induced *CYP1A1* mRNA (Figure 3.27 A). These results identify 5F 203 as a full AhR agonist for inducing *CYP1A1* mRNA in MCF-7 cells, with no antagonistic activity relative to TCDD. Thus, 5F 203 is a potent agonist for inducing *CYP1A1* mRNA in MCF-7 cells.

The finding that 5F 203 is a potent agonist in MCF-7 cells confirms previous findings [263]. Given the low potency of the phenylbenzothiazoles tested in rat cells the next step would be to investigate the compounds for *CYP1A1* mRNA inducibility as well as for binding the AhR in the human cells (MCF-7 cells) and subsequently generate a QSAR model out of these data.

Section 4.2.9 Agonism/antagonism species-specific differences

The potency (EC₅₀s) for *CYP1A1* mRNA and the maximal levels of induction for TCDD were characterized in both H4-II-E and MCF-7 cells. The relative potency (EC₅₀s) and the maximal levels of induction for 5F 203, DF 203, IH 445, AW 892, GW 610 and IH 318 were characterized in both H4-II-E and MCF-7 cells.

Under the conditions of the current induction assay, TCDD showed similar potency in human and rat cells but lower magnitude of induction in rat compared with human as assessed by qRT-PCR at 4 h (Figure 3.24 A). This lower magnitude of induced levels in H4-II-E cells was also

manifested with 5F 203 (Figure 3.26). *CYP1A1* mRNA induction assays were consistently performed in both cell lines exactly under the same conditions, *i.e.*, cell number and confluence (90-95%), duration of treatment (4 h), same stock of each chemical and same reagents. Species-specific differences have been reported for *CYP1A1* mRNA induction for TCDD. Silkwork et al (2005) reported species-specific differences for induction of *CYP1A1* mRNA by TCDD in rat fresh hepatocytes and human HepG2 cell line (RT-PCR), however, significant variations were observed for cell lines within the same species [203]. It is noteworthy that cell-specific differential expression of CYP1A1 was reported. In humans, CYP1A1 is mainly expressed extrahepatically, whereas in rodent, it is mainly hepatic [125]. Human hepatocytes have a lower maximal induction level and EC₅₀ value for CYP1A1 induction by TCDD than Sprague-Dawley rat hepatocytes [203], whereas induction of CYP1A1 in human lymphocytes was higher than the level of induction in rodent lymphocytes [223]. A correlation between the levels of nuclear Ah receptor with the magnitude of the induction (CYP1A1) was reported [7] [224] [211], but this finding is controversial [225] [226] [211]. AhR might be differentially regulated in different cells at different steps of its signaling pathway [53], and the molecular basis for differences in levels of induced CYP1A1 across species is unknown.

These results identified 5F 203 as a potent agonist in human cells but a partial antagonist in rat cells. However, both cell lines are *CYP1A1* inducible. This difference in agonism profile could be attributed to species-specific differences. Species-specific antagonism of AhR was previously reported. Aarts et al (1995) found that 2,2',5,5'-Tetrachlorobiphenyl (PCB52) antagonized the expression of a luciferase reporter gene under transcriptional control of AhR in mouse H1L1.1c7 hepatoma cells exposed to TCDD but little to no inhibition was observed in guinea pig G16L1.1c8 intestine and human HG2L1.1c3 hepatoma cells [227]. Moreover, this compound did not show any agonistic activity in all three cells. Since PCB52 bound AhR in mouse

but not in human nor in guinea pig [227], this could explain the inability of PCB52 to antagonize TCDD in human and guinea pig. 3'-methoxy-4'-nitroflavone (MNF), was found to be a pure antagonist in mouse hepatoma Hepa cells but a partial agonist in Guinea pig adenocarcinoma cells using luciferase reporter gene. This compound can compete with TCDD to bind AhR in both cells and inhibits its nuclear uptake and transformation only in mouse cells [99] [222]. The Arg 355 residue in mouse AhR which is equivalent to Ile in guinea pig AhR and Thr in the human AhR, was identified to distinguish the agonistic versus antagonistic activity (MNF) [228]. Species-specific agonism of AhR has been reported, with the example of the benzimidazole drug omeprazole (OME). It activated AhR in human cells but not mouse cells in culture [229], but OME does not bind the human or mouse AhR [194]. None of the studies have identified a compound that is an agonist in one species but an antagonist in another.

A compound's potency depends on both affinity and efficacy [210]. The binding affinities of phenylbenzothiazoles were determined in the rat but not the human cells. Species- and tissue-specific differences have been reported in the binding properties, specificity, and physiochemical properties of the Ah receptor [230] [231] [232]. Moreover, it was reported that species-specific activity for induction of CYP1A1 correlates with species-specific binding to AhR [233] [35] [234]. In the present study, TCDD has a K_D of 0.37 nM for rat AhR (Figure 3.7). Literature values for TCDD K_D for human AhR varied from 1.6 nM [35], 10 nM [235] to 18.6 nM [236]. From these results, TCDD binds human AhR with lower affinity than the rat AhR. TCDD induced *CYP1A1* mRNA in MCF-7 cell line with only 10-fold higher potency than 5F 203 (Figure 3.25). In comparison with OME that does not bind the human, rat nor mouse AhR [194] but induced CYP1A1 in a ligand-independent pathway [101], 5F 203 binds the rat AhR (Figure 3.9 and Table 3.3). It does not seem from these preliminary data that the difference in 5F 203 potency across the rat and human cells is due to the species-specific binding. However, the com-

pounds in this study were not tested for their binding to the AhR in MCF-7 cells and it will be necessary to gain this information in the future and investigate the correlation between the binding and the activity across the rat and human cell lines.

As a conclusion, care has to be taken when classifying compounds based on their ability to induce CYP1A1. The classification depends on the tissue/species in which the measurement is made. As the present study revealed, a low-efficacy drug, namely 5F 203, can be a potent agonist or a partial antagonist depending on the species from which the cell line is derived. The expression of *CYP1A1* was not consistent between rat and human cells. This difference in gene expression needs to be taken into consideration when using cell models to assess drug efficacy and when extrapolating results from rat to humans.

Section 4.3 AhR, a target for anticancer phenylbenzothiazole analogues: mechanistic investigations

The general hypothesis of the mode of action of the anticancer phenylbenzothiazole series (1) consists of activation of AhR and subsequent metabolism by induced CYP1A1. However, how the receptor mediates their function remains to be elucidated. This hypothesis was based on several pieces of data from literature: 1) these planar compounds induced CYP1A1 in sensitive (MCF-7) but not in inherently resistant (MDA-MB-435) human breast cancer cells, where the AhR seems to be present constitutively in the nucleus [141] which raised the possibility of a role of the AhR in mediating the anticancer activity of these compounds, 2) the observation that cotreatment of MCF-7 cells with DF 203 and the AhR antagonist, α -naphthoflavone at 10 μ M abrogated the inhibitory effect of DF 203 [141], 3) comparative analysis on 5F 203 growth inhibition in wild-type MCF-7 with AhR-deficient AH^{R100} [144], derived from MCF-7 human breast epithelial cancer cells by continuous exposure to increasing concentrations of the polycyclic hydrocarbons benzo[a]pyrene [237], yield reduced anticancer efficacy of 5F 203 in the

AH^{R100} compared to full efficacy in the sensitive wild-type cell line. However, it was not clear from the work reported by Trapani et al (2003) [144] whether the AhR-mediated signaling could account for all the cytotoxic effect of the compound. The use of the AhR antagonist α -naphthoflavone was shown to inactivate cytochrome P450 enzymatic activity by competitively interacting with the substrate binding site when used at high concentrations (10 μ M) [238]. Consequently, the use of α -naphthoflavone at 10 μ M furnished evidence on the importance of the catalytic activity of CYP1A1 on the growth inhibition by DF 203 and does not necessarily prove the involvement of the AhR. Thus, the loss of cytotoxicity of DF 203 in mixtures with 10 μ M α -naphthoflavone could be due to the lack of metabolism by CYP1A1, previously suspected to be important for its anticancer activity [140].

Section 4.3.1 Correlation between SARs for binding and anticancer activity

The choice of rat over human species for developing the binding assay was based on two main reasons: first, it is not easy to get human liver for cytosol preparation and second, characterization of a binding assay in human cells is very demanding [168] [235] given the lability of the human AhR. The anticancer activity of PBT, except for 5F 203, was not assessed in MCF-7 cells, therefore the analysis for anticancer activity of PBT in MCF-7 cells was based on literature.

Although binding affinities of phenylbenzothiazoles (series 1 and 2) was conducted in rat but not in human cytosol, structure-activity relationships for the anticancer potency of these series in human MCF-7 cells seem to generally correlate with their structure-binding relationships for rat AhR. Concerning the compounds of series (1), the 5F 203 with its non-fluorinated analogue, DF 203, retained nanomolar affinity values in rat, with DF 203 being ~4-fold less potent than 5F 203 (Table 3.3). This correlated well with the anticancer activity of these compounds in

MCF-7 cells (Figure 3.31) [144] [253], where the presence of the fluorine atom at this position was not found to be essential for anticancer activity, but prevents the drug from hydroxylation by endogenous cytochrome P450 [126]. Shifting the fluorine atom from position 5 to either position 4 or 6 retained the nanomolar binding K_i values (with 5- and 10-fold decrease for the 6-fluoro and 4-fluoro regioisomers respectively) (Table 3.3). Similarly, both regioisomers retained nanomolar concentrations of GI_{50} values in MCF-7 cells [126]. In conclusion, for series (1), the fluoro-group was not essential for anticancer activity neither for binding.

The C-6 hydroxylated metabolite of DF203, 6-OH 203 (IH 130) had a K_i of $\sim 1.5 \mu M$ (Table 3.3). It was reported that this compound antagonises DF 203 anticancer activity, most probably by CYP1A1, and maybe not through the AhR signaling pathway. IH 130 is devoid of anti-tumour activity in sensitive human cells [141]. When the binding of IH 130 to AhR was characterized with a competitive binding assay, it showed low affinity. This suggests that the antagonistic activity of the 6-OH 203 on DF 203 is not AhR-mediated.

In contrast to series 1, it seems that the fluoro group was required for the anticancer activity of compounds from series 2 in MCF-7 cells [151], but not for binding to the AhR (Table 3.3). For example, the non-fluorinated analogue (AW 892), was a high-affinity ligand for the AhR (Table 3.3), but devoid of activity in MCF-7 cells [151]. This is in contrast with series 1, where the fluoro group was not essential for anticancer activity nor for binding. The fluorinated analogue 2-(3-methyl-4-methoxyphenyl)-5-fluorobenzothiazole (JP-1) has a GI_{50} value of 48 nM in MCF-7 cells [151] and a K_i value of 26 nM in rat (Table 3.3). However, replacement of one methoxy group by a hydroxyl (JP-2) or a methylenedioxy (JMB 81) yields inactive compounds and low-affinity ligands. The 4- (4F 610) and 6-fluoro regioisomer both have inhibitory activity on cell growth [151] and binding affinity (Table 3.3) in the nanomolar range. The 6-fluoro regioisomer is 27-fold less potent than GW 610 for binding AhR. This series (2) of phenylbenzo-

thiazoles tolerates structural modification poorly. So far, it seems that the mechanism of action of GW 610 is different from that of DF 203, in that it is independent of CYP1A1 induction [151]. A comparative analysis on the SARs of series (1) with series (2), revealed different SARs for binding and anticancer activity, which further supports mechanistic differences.

Importantly, the K_D for binding AhR and GI_{50} for cell growth inhibition in H4-II-E cells were markedly different for most of the compounds tested (5F 203, DF 203, GW 610, IH 318) but closer for AW 892 (20-fold) and IH 445 (100-fold). As a conclusion, binding AhR by itself does not account for anticancer activity of these compounds in H4-II-E cells.

Section 4.3.2 Correlation between SARs for inducing *CYP1A1* RNA and anticancer activity

It was reported that cell sensitivity to the anticancer activity of 5F 203 correlates with CYP1A1 inducibility in human cancer cells [126] [140] [141]. However, in the present study, 5F 203, DF 203 and GW 610 increased *CYP1A1*/ β -actin mRNA ratios with relatively low potency in H4-II-E cells (Figure 3.19 A), and these cells were resistant to the anticancer activity of 5F 203 and DF 203 and poorly responsive to the anticancer activity of GW 610 (Table 3.13). So, there was a correlation between poor potency for *CYP1A1* induction and loss of anticancer activity for DF 203 or 5F 203 in rat cells and therefore, it was suspected that the low potency could account for the low anticancer efficacy of these compounds in the rat cells. The hypothesis was that inducing CYP1A1 in H4-II-E cells would sensitize them to the anticancer activity of 5F 203. Therefore, cells were pre-treated with 10 nM TCDD for 24 h, before treating with 5F 203. The results showed that activation of the AhR failed to enhance the anticancer activity of 5F 203 (Figure 3.30). However, the possibility that the 5F 203 could be cleared by the CYP1A1 and other metabolizing proteins induced by TCDD, cannot be ruled out. These results show that the sensitivity of H4-II-E cells to the anticancer activity of 5F 203, is not simply related to CYP1A1

induction. A correlation between inducing *CYP1A1* mRNA and anticancer activity was found for IH 445 and GW 610, though not linear (Table 3.13). It is noteworthy that AW 892 induced *CYP1A1* mRNA at micromolar concentrations (2 μ M) and inhibited H4-II-E cell growth at sub micromolar concentrations (GI₅₀ 223 nM) (Table 3.13) but was found inactive in MCF-7 cells (GI₅₀ 53 μ M) [151]. In contrast, a correlation was observed for *CYP1A1* mRNA induction potency (EC₅₀, 2nM) and cytostatic effect (GI₅₀, 18 nM) of 5F 203 in MCF-7 cells (Figure 3.31 and Table 3.13).

These results reveal species/cell-specific differences in sensitivity to 5F 203, moreover, a correlation was observed between the potency of cytostatic effect of 5F 203 and *CYP1A1* induction.

Section 4.3.3 Investigating the effect of AhR agonism on cell growth

Given the relationship between induction of CYP1A1 and anticancer potency of phenylbenzothiazoles series 1 [126] [140] [141], it was of interest to investigate the effects of AhR agonism by testing the effects of TCDD on the growth of MCF-7 as well as H4-II-E cells. The present study confirmed that TCDD has no inhibitory activity of growth of both H4-II-E and MCF-7 cells as determined by MTT assay (Figure 3.29) and (Figure 3.31). These results provide direct evidence that AhR agonism is not sufficient to inhibit the growth of both cell lines. The effect of TCDD on cell growth is controversial in the literature. Wiebel et al, (1991) showed that TCDD did not inhibit the growth of H4-II-E cells as determined by assaying the increase in the amount of protein [239]. Knutson and Poland (1980) investigated the toxicity of TCDD on twenty-three cells in culture, among them are the H4-II-E cells. In all these cells, TCDD did not alter the morphology nor affected the cell growth or viability [192]. Likewise TCDD did not significantly affect the proteins or enzymes of the cell cycle [191]. This is contrast with an inhibitory effect of TCDD in MCF-7 cells reported [11]. In this latter report, cells were treated with 10 nM TCDD for 7 days and cell growth was measured fluorometrically by Hoechst. How-

ever, 10 nM TCDD inhibited cell growth by 40%, and 50 nM TCDD inhibited 60% of cell growth.

Other researchers have claimed that TCDD inhibits the growth of the cells, with the observation that in mixtures of TCDD and estradiol (E2), TCDD inhibits estrogen-induced proliferation through an inhibitory AhR-ER α cross-talk, suggesting an anti-estrogenic-like effect of TCDD in MCF-7 cells [240]. However, these conclusions seem to be controversial, since the presence of E2 seems to be the limiting factor for the estrogenic/anti-estrogenic like effect of TCDD as suggested by another recent study reported by Ohtake et al (2003) [190].

Section 4.3.4 Investigating the effect of AhR antagonism on cell growth

One of the aims of this project is to investigate the involvement of AhR in mediating the anti-cancer activity of 5F 203. That can be done by co-incubating cells with 5F 203 and a range of concentrations of the AhR antagonist CH-223191. The choice of CH-223191 as AhR antagonist over other AhR antagonists was based on several issues. First, the CH-223191 was identified as an AhR antagonist in human hepatic HepG2 cells with no agonistic activity up to a concentration of 10 μ M. The lack of agonistic activity of CH-223191 on AhR signaling was further confirmed in the present study, where CH-223191 did not increase the *CYP1A1*/ β -actin RNA levels up to a concentration of 30 μ M by qRT-PCR in MCF-7 cells (Figure 3.28). CH-223191 was shown to inhibit TCDD-induced CYP1A1 expression and CYP1A1 enzymatic activity in a dose-dependent manner by RT-PCR and Western blot assay and EROD activity [188]. Second, contrary to known AhR antagonists, flavone, resveratrol, and α -naphthoflavone, a high concentration of 10 μ M of CH-223191 did not have any agonistic activity on AhR in the absence of TCDD as assessed by luciferase activity [188]. In addition, CH-223191 was shown to have more inhibitory potency on TCDD-induced luciferase activity than flavone, resveratrol, and α -naphthoflavone [188]. Third, it showed no effect on oestrogen receptor-mediated gene activa-

tion [188], whereas flavone and resveratrol have high affinity for the oestrogen receptor [259] [241] and resveratrol stimulates the proliferation of human breast cancer cells [242]. Unexpectedly, the GI_{50} of CH-223191 was 420 nM in MCF-7 cells, so CH-223191 alone elicited a growth inhibitory activity (Figure 3.31), a finding that hampered the experiment mentioned above. Having found that the CH-223191 elicits a cytostatic effect, it was hypothesized that the AhR antagonism of CH-223191 was responsible for cell growth inhibition. This hypothesis was addressed pharmacologically by co-incubating cells with CH-223191 with a range of concentrations of TCDD. At low TCDD concentrations, 500 nM CH-223191 inhibited cell growth to levels similar to 500 nM CH-223191 alone but higher TCDD concentrations (≥ 100 pM) restored some of the cell growth but not to DMSO control levels (Figure 3.32). The results of the present study indicate that the cytostatic effect of CH-223191 is not mediated by the AhR (Figure 3.32) and that another mechanism is likely to be involved.

As mentioned above, TCDD does not inhibit the growth of MCF-7 cells. This information enables the use of TCDD as an AhR agonist in mixtures with 5F 203 to exclude the possibility that the cytostatic effect of 5F 203 could be due to AhR antagonism. MCF-7 cultures were incubated with increasing concentrations of TCDD and 50 nM 5F 203. As expected, high concentrations of TCDD did not abrogate 5F 203 cell growth inhibitory activity (Figure 3.32), excluding AhR antagonism as a mechanism for 5F 203 cell growth inhibition. Mixtures of 50 nM 5F 203 with TCDD did not enhance the cytostatic effect of 5F 203. As 5F 203 is only within 10-fold with lower potency than TCDD for inducing *CYP1A1* in MCF-7 cells (Figure 3.25 A), TCDD is unlikely to change the levels of *CYP1A1* and would not further change metabolism of 5F 203. However, although 5F 203 and TCDD bind AhR, it is possible that 5F 203 and TCDD might have different targets or trigger different effects on the same target. Thus both TCDD [209] and 5F 203 [150] induce AhR-regulated genes, such as xenobiotic metabolizing genes, *CYP1A1* and

CYP1B1, in MCF-7 cells. However, TCDD is not genotoxic and does not induce DNA damage genes [209], whereas 5F 203 induced genes associated with DNA damage in MCF-7 cells (CDKN/A (p21/Cip1), p53-induced gene-3, the apoptosis-initiating receptor TNFRSF6 (CD95/FAS) and DNA binding protein 2 [150]. Moreover, TCDD, unlike 5F 203, is resistant to metabolism [61]. Furthermore, the observation that TCDD, which is resistant to metabolism [61] did not inhibit MCF-7 cell growth, compared to 5F 203, which is known to be metabolised [146] suggests that AhR activation is not sufficient for this effect without additional factors downstream of binding AhR, presumably, metabolism.

Section 4.3.5 Mechanism of action of 5F 203: relevance of the mechanism of Genotoxicity?

Quantitative analysis from the present study on the CYP1A1 induction and the anti-proliferative activity of the 5F 203 in MCF-7 cells demonstrated that this drug inhibited 50% of the growth of the MCF-7 cells at 18 nM (Figure 3.31) and was able to induce *CYP1A1* mRNA at 2 nM (Figure 3.25). Thus the concentration at which 5F 203 induces CYP1A1 falls in at the same range of concentration at which this drug is manifesting its physiological effect on cell growth inhibition. This coincidence encourages consideration of the alternative hypothesis that genotoxicity of 5F 203 is a cause for its cytostatic effect. In this hypothesis, 5F 203 is inhibiting the cell growth by damaging DNA active metabolite/DNA adduct formation. However, DNA adducts of 5F 203 were only detectable at concentrations that exceed 0.1 μ M [146]. However, the concentration of 5F 203 at which it elicits its cytostatic effect (18 nM) is much lower than the concentration at which the DNA adducts are formed (>0.1 μ M) [146]. While the levels of exposure required for the anticancer activity of 5F 203 are in the nanomolar range (nM), the finding that a concentration 100-1000-fold higher results in DNA adducts does not provide convincing evidence that genotoxicity is responsible for the cytostatic effect seen at ~ 18 nM 5F 203.

Section 4.3.6 Relevance of partial agonism in risk assessment

The importance of the quantitative analysis of the partial agonism of AhR ligands lies in the fact that mixtures of ligands for AhR, naturally occurring dietary as well as environmental or synthetic xenobiotics, that have different intrinsic efficacy will not necessarily show additive effects in producing a stimulus (*e.g.* CYP1A1 induction or toxicity). Thus this concept potentially has significant implications for the toxic equivalency factor (TEQ) risk assessment scheme, since it relies on the concept of additivity [1] [243]. The default assumption of additivity *i.e.*, that most of AhR ligands are high-intrinsic efficacy agonists can be tested quantitatively using the methodology described herein for 5F 203.

Section 4.3.7 Concluding remarks

Pharmacological and toxicological studies are critical before the optimal concentration of a drug that yields the physiologically desirable effect can be determined. From the toxicological standpoint, at high concentrations, the drug could exhibit adverse effects. From the pharmacological standpoint, if a drug is a partial AhR agonist with a moderate induction of the *CYP1A1* at low concentrations, at high concentrations, it can act as an agonist. In this regard, quantitative data are very important and should be taken into account for preclinical drug assessment.

The results showed that the cytostatic effect of 5F 203 is not mediated by AhR antagonism. On the other hand, AhR agonism does not account for the growth inhibitory of 5F 203 either and additional factors to AhR seem to be required. The potency of the cytostatic effect of 5F 203 parallels the potency for inducing *CYP1A1* in H4-II-E and MCF-7 cells, *i.e.*, 5F 203 was found to be a potent agonist for inducing *CYP1A1* as well as for inhibiting cell growth in MCF-7 cells, whereas this compound was found to be a partial agonist in H4-II-E cells and failed to inhibit cell growth in these cells. These results indicate that there is a correlation between species-spe-

cific partial agonism of AhR and species-specific anticancer activity. But whether agonism/antagonism for the induction of *CYP1A1* mRNA is related to the anticancer effect of 5F 203 remains to be elucidated.

5F 203 was assessed for inducing *CYP1A1* mRNA in cell lines from two different species, human and rat. The results indicate species-specific differences in potency and antagonistic activity. The use of the rat cell line allowed the classification of 5F 203 as a low-intrinsic efficacy compound, a finding that would have been masked if tested only in humans where 5F 203 exhibits an apparent high potency. This study stresses the importance of assessing drug effects in several species in order to gain an accurate classification. Among the phenylbenzothiazoles tested, IH 445, was found to be a potent agonist, with no detectable antagonistic activity on TCDD-inducible *CYP1A1* mRNA in rat cells. This important finding indicates that the partial agonism observed with 5F 203 is a compound-specific and thus not an experimental artifact.

It was demonstrated in this study by means of competitive displacement analysis using [^3H]-TCDD and Schild analysis that the PBTs tested induced *CYP1A1* mRNA via a ligand-dependent activation pathway which excludes the possibility of a ligand-independent pathway. These results elucidate the mechanism of action of these compounds on AhR signaling activation.

In order to understand the mechanism of action of drugs, they should be screened in different cell lines and different species. PBTs have been previously tested and showed different patterns of activity in the NCI panel of 60 human cell lines derived from nine organ sites; the breast cancer cell line MCF-7 was highly responsive to these compounds. In this study, the PBTs were tested in rat cells and revealed species/cell-specific differences for antiproliferative activity, a finding that raises doubts about the strategy of assessing drug activity in animal model cells than extrapolating to humans. Actually, the lysylamide prodrug of 5F 203, Phortress, is in Phase I

Clinical Trial. Unravelling the target for the PBTs would be of great importance for drug development in cancer therapy.

Finally, this study extended the number of AhR agonists/antagonists in a species/cell-specific context and gives insight into the mode of interactions between PBTs and AhR. Further study of a significant number of ligands/agonists for AhR would contribute significantly to a better understanding of the AhR biology.

Prospective work

5F 203 showed species-specific differences in agonism/antagonism of the AhR. It would be interesting to investigate whether species-specific differences in AhR are responsible for these differences. Transgenesis experiments may address this issue. In such experiments, human or rat AhR genes could be translated into cells lacking AhR. Such a model is available, *e.g.*, AhR knock out mouse Hepa cells.

PBTs were found to be low potent agonists in rat cells which did not allow the development of a QSAR model. However, given the high potency of 5F 203 in MCF-7 human cells, more compounds need to be quantitatively assessed for inducing *CYP1A1* mRNA in the same cell line before QSAR can be established. The binding affinity of PBTs to rat AhR was determined but not to human AhR, therefore, it will be essential to determine the binding affinity of the PBTs to human AhR using a human recombinant AhR expressed in *Spodoptera frugiperda* (Sf9) cells. Then it would be good to compare QSARs for PBTs binding data (human AhR) and *CYP1A1* mRNA induction data in MCF-7 cells and classify the PBTs into agonists/antagonists in human cells. Finally, it would be useful to generate a full picture for the PBT's binding data for rat and human AhR as well *CYP1A1* mRNA induction in rat and human cells and classify PBTs as agonists/antagonists in each species, *i.e.*, rat and human cells.

In order to confirm that the induction of *CYP1A1* mRNA in MCF-7 cells is not a specific response of CYP1A1 alone but rather a result of AhR activation, it would be possible to screen other AhR-dependent gene expression by real-time PCR and follow that analysis with protein expression and function (western blotting analysis and EROD activity). Subsequent to binding AhR, translocation of AhR to the nucleus and binding to the XRE could be confirmed by western blotting and EMSA analyses respectively.

Finally, AhR is suspected target for mediating the anticancer activity of Phortress. MCF-7 cells have proven to be a good model to study the involvement of AhR in the anticancer activity of 5F 203. Generating knockout AhR MCF-7 cells by means of small interfering RNA (siRNA) and examining the cell growth inhibition when these cells challenged with the compounds, would be a useful tool.

Appendix - Pharmacological background

Pharmacological definitions

A receptor is any substance that recognizes chemicals and responds to that recognition.

K_D : is the equilibrium dissociation constant of the drug. It reflects the affinity of the drug to the receptor. The smaller the K_D value is, the higher is the affinity. The affinity constant K_a is the reciprocal of the K_D .

IC_{50} : is the concentration of the competing ligand that inhibits 50% binding of the radioligand.

K_i : is the inhibition constant of the drug. This value can be related to K_D and IC_{50} by the Cheng-Prusoff equation.

K_e : is the intrinsic efficacy constant, and represents the concentration of ligand-receptor complex that gives half-maximal response.

Drug properties

Affinity: is the chemical property that causes the drug to associate with the receptor.

Efficacy: is the chemical property that produces a change in the receptor to produce a stimulus.

Biochemical binding studies

In principle, a fixed concentration of radiolabelled ligand $[L^*]$ is added to the receptor preparation for a certain time sufficient for the receptor and the ligand to reach the binding equilibrium quantity of $[L^*.R]$ complex.

The binding of labelled ligand L^* to a homogenous population of receptor follows the law of

mass action. It is a simple bimolecular association reaction:

Equilibrium is reached when the rate of formation of ligand-receptor complexes equals the rate at which existing RL* dissociate.

At equilibrium, $[Ligand] \cdot [Receptor] \cdot k_{on} = [Ligand \cdot Receptor] \cdot k_{off}$.

The equilibrium dissociation constant K_D is given by equation (1):

$$\frac{[Ligand] \cdot [Receptor]}{[Ligand \cdot Receptor]} = \frac{k_{off}}{k_{on}} = K_D \quad [1]$$

Where K_D is the concentration of ligand that binds half of the receptors at equilibrium.

In other terms, the complex $[Ligand \cdot Receptor]$ is referred as to the bound ligand "B" to

the receptor and the free fraction is "F". In equation (1):

$$\frac{F \times [Receptor]}{B} = K_D \quad [2]$$

The B_{max} represents the maximal number of binding sites. It represents entirely the bound receptor:

$$B_{max} = \text{bound receptor} \quad [3]$$

Intrinsic efficacy

It is the factor relating receptor occupancy and stimulus. This proportionality factor is given the name intrinsic efficacy. It represents the stimulus per molecule receptor produced by an agonist. It also represents the concentration of agonist-receptor complex that produces 50% of response. It is a drug-related property. It can be estimated given the receptor occupancy and the K_A (or K_D) for each agonist are known.

$$[A \times R] = \frac{[A] \times [R_t]}{[A] + K_A} \quad [4]$$

An agonist would have a factor of 1 and an antagonist would have a factor of 0, whereas a partial agonist would have a factor between 0 and 1 [244].

Competitive reversible antagonism

A competitive reversible antagonism is a condition when the agonist and antagonist bind competitively and reversibly to the same sites on the receptor. This effect can be observed on agonist dose-response curves and can be quantitated using the equation derived by Gaddum [245]:

$$\frac{[A \times R]}{[R_t]} = \frac{[A]}{[A] + K_A(1 + [B]/K_B)} \quad [5]$$

Where [A] and [B] are the agonist and antagonist respectively. [A.R] represents the agonist-receptor complex, R_t represents the total receptor population and K_B is the equilibrium dissociation constant for the antagonist-receptor complex.

Equation [5] gives the fractional occupancy by an agonist $[A.R]/[R_t]$ for any given concentration of agonist and antagonist [246].

Schild regression

This gives a measurement of antagonist potency. It was introduced by Arunlakshana and Schild [247]. The model describes a simple competitive antagonism and the antagonist potency is measured by the equilibrium dissociation constant for the antagonist-receptor complex.

From equation [5], in the absence of antagonist ($[B]=0$), the receptor occupancy by [A] is given by:

$$\frac{[A \times R]}{[R_t]} = \frac{[A]}{[A] + K_A} \quad [6]$$

The concentration of agonist $[A']$ in the presence of antagonist produces an equal response, and presumably, an equal receptor occupancy, therefore, equation [5] becomes:

$$\frac{[A \times R]}{[R_t]} = \frac{[A']}{[A'] + K_A(1 + [B]/K_B)} \quad [7]$$

At the same response, equation [6] equals equation [7], and the ratio of equiactive concentrations of agonist in the presence and absence of antagonist (concentration ratio, cr) is given by $[A']/[A]$:

$$\frac{[A']}{[A]} = cr = \left(\frac{[B]}{K_B} + 1 \right) \quad [8]$$

From this equation, the magnitude of the concentration ratios depends on $[B]$ and K_B . Whereas, $[B]$ is known, cr is determined experimentally, thus K_B can be calculated. A practical representation for equation [8] uses logarithmic conversion, so it yields a straight-line regression also known as a Schild regression:

$$\log(cr - 1) = (\log[B] - \log K_B) \quad [9]$$

The regression supports a mechanism of competitive antagonism if the slope = 1, and in this case only, the intercept provides an independent estimate of K_i (or K_B in this case) [246].

References

1. Van den Berg, M., et al., *The 2005 World Health Organization reevaluation of human and Mammalian toxic equivalency factors for dioxins and dioxin-like compounds*. Toxicol Sci, 2006. **93**(2): p. 223-41.
2. Denison, M.S., et al., *Ligand binding and activation of the Ah receptor*. Chem Biol Interact, 2002. **141**(1-2): p. 3-24.
3. Whitlock, J.P., Jr., et al., *Cytochromes P450 5: induction of cytochrome P4501A1: a model for analyzing mammalian gene transcription*. Faseb J, 1996. **10**(8): p. 809-18.
4. Nebert, D.W., F.M. Goujon, and J.E. Gielen, *Aryl hydrocarbon hydroxylase induction by polycyclic hydrocarbons: simple autosomal dominant trait in the mouse*. Nat New Biol, 1972. **236**(65): p. 107-10.
5. Poland, A. and E. Glover, *Chlorinated dibenzo-p-dioxins: potent inducers of delta-aminolevulinic acid synthetase and aryl hydrocarbon hydroxylase. II. A study of the structure-activity relationship*. Mol Pharmacol, 1973. **9**(6): p. 736-47.
6. Poland, A., E. Glover, and A.S. Kende, *Stereospecific, high affinity binding of 2,3,7,8-tetrachlorodibenzo-p-dioxin by hepatic cytosol. Evidence that the binding species is receptor for induction of aryl hydrocarbon hydroxylase*. J Biol Chem, 1976. **251**(16): p. 4936-46.
7. Dolwick, K.M., et al., *Cloning and expression of a human Ah receptor cDNA*. Mol Pharmacol, 1993. **44**(5): p. 911-7.
8. Holmes, J.L. and R.S. Pollenz, *Determination of aryl hydrocarbon receptor nuclear translocator protein concentration and subcellular localization in hepatic and nonhepatic cell culture lines: development of quantitative Western blotting protocols for calculation of aryl hydrocarbon receptor and aryl hydrocarbon receptor nuclear translocator protein in total cell lysates*. Mol Pharmacol, 1997. **52**(2): p. 202-11.
9. Backlund, M. and M. Ingelman-Sundberg, *Different structural requirements of the ligand binding domain of the aryl hydrocarbon receptor for high- and low-affinity ligand binding and receptor activation*. Mol Pharmacol, 2004. **65**(2): p. 416-25.
10. Cresteil, T., A.K. Jaiswal, and H.J. Eisen, *Transcriptional control of human cytochrome P1-450 gene expression by 2,3,7,8-tetrachlorodibenzo-p-dioxin in human tissue culture cell lines*. Arch Biochem Biophys, 1987. **253**(1): p. 233-40.
11. Dohr, O., C. Vogel, and J. Abel, *Different response of 2,3,7,8-tetrachlorodibenzo-p-dioxin (TCDD)-sensitive genes in human breast cancer MCF-7 and MDA-MB 231 cells*. Arch Biochem Biophys, 1995. **321**(2): p. 405-12.
12. Zhang, S., C. Qin, and S.H. Safe, *Flavonoids as aryl hydrocarbon receptor agonists/antagonists: effects of structure and cell context*. Environ Health Perspect, 2003. **111**(16): p. 1877-82.
13. Harris, M., et al., *Structure-dependent induction of aryl hydrocarbon hydroxylase in human breast cancer cell lines and characterization of the Ah receptor*. Cancer Res, 1989. **49**(16): p. 4531-5.
14. Wormke, M., et al., *The aryl hydrocarbon receptor mediates degradation of estrogen receptor alpha through activation of proteasomes*. Mol Cell Biol, 2003. **23**(6): p. 1843-55.

15. Hahn, M.E., *Aryl hydrocarbon receptors: diversity and evolution*. Chem Biol Interact, 2002. **141**(1-2): p. 131-60.
16. Swanson, H.I. and G.H. Perdew, *Detection of the Ah receptor in rainbow trout: use of 2-azido-3-[125I]iodo-7,8-dibromodibenzo-p-dioxin in cell culture*. Toxicol Lett, 1991. **58**(1): p. 85-95.
17. Hahn, M.E., et al., *Photoaffinity labeling of the Ah receptor: phylogenetic survey of diverse vertebrate and invertebrate species*. Arch Biochem Biophys, 1994. **310**(1): p. 218-28.
18. Yasui, T., et al., *Functional characterization and evolutionary history of two aryl hydrocarbon receptor isoforms (AhR1 and AhR2) from avian species*. Toxicol Sci, 2007. **99**(1): p. 101-17.
19. Ema, M., et al., *Human arylhydrocarbon receptor: functional expression and chromosomal assignment to 7p21*. J Biochem (Tokyo), 1994. **116**(4): p. 845-51.
20. Hankinson, O., *The aryl hydrocarbon receptor complex*. Annu Rev Pharmacol Toxicol, 1995. **35**: p. 307-40.
21. Burbach, K.M., A. Poland, and C.A. Bradfield, *Cloning of the Ah-receptor cDNA reveals a distinctive ligand-activated transcription factor*. Proc Natl Acad Sci U S A, 1992. **89**(17): p. 8185-9.
22. Wang, X., et al., *Comparative properties of the nuclear aryl hydrocarbon (Ah) receptor complex from several human cell lines*. Eur J Pharmacol, 1995. **293**(3): p. 191-205.
23. Dolwick, K.M., H.I. Swanson, and C.A. Bradfield, *In vitro analysis of Ah receptor domains involved in ligand-activated DNA recognition*. Proc Natl Acad Sci U S A, 1993. **90**(18): p. 8566-70.
24. Ikuta, T., et al., *Nuclear localization and export signals of the human aryl hydrocarbon receptor*. J Biol Chem, 1998. **273**(5): p. 2895-904.
25. Berg, P. and I. Pongratz, *Differential usage of nuclear export sequences regulates intracellular localization of the dioxin (aryl hydrocarbon) receptor*. J Biol Chem, 2001. **276**(46): p. 43231-8.
26. Roberts, B.J. and M.L. Whitelaw, *Degradation of the basic helix-loop-helix/Per-ARNT-Sim homology domain dioxin receptor via the ubiquitin/proteasome pathway*. J Biol Chem, 1999. **274**(51): p. 36351-6.
27. Huang, Z.J., I. Edery, and M. Rosbash, *PAS is a dimerization domain common to Drosophila period and several transcription factors*. Nature, 1993. **364**(6434): p. 259-62.
28. Whitelaw, M., et al., *Ligand-dependent recruitment of the Arnt coregulator determines DNA recognition by the dioxin receptor*. Mol Cell Biol, 1993. **13**(4): p. 2504-14.
29. Fukunaga, B.N., et al., *Identification of functional domains of the aryl hydrocarbon receptor*. J Biol Chem, 1995. **270**(49): p. 29270-8.
30. Kronenberg, S., C. Esser, and C. Carlberg, *An aryl hydrocarbon receptor conformation acts as the functional core of nuclear dioxin signaling*. Nucleic Acids Res, 2000. **28**(12): p. 2286-91.
31. Ma, Q., L. Dong, and J.P. Whitlock, Jr., *Transcriptional activation by the mouse Ah receptor. Interplay between multiple stimulatory and inhibitory functions*. J Biol Chem, 1995. **270**(21): p. 12697-703.

32. Carver, L.A., J.B. Hogenesch, and C.A. Bradfield, *Tissue specific expression of the rat Ah-receptor and ARNT mRNAs*. Nucleic Acids Res, 1994. **22**(15): p. 3038-44.
33. Poland, A. and E. Glover, *Variation in the molecular mass of the Ah receptor among vertebrate species and strains of rats*. Biochem Biophys Res Commun, 1987. **146**(3): p. 1439-49.
34. Petrulis, J.R. and G.H. Perdew, *The role of chaperone proteins in the aryl hydrocarbon receptor core complex*. Chem Biol Interact, 2002. **141**(1-2): p. 25-40.
35. Ema, M., et al., *Dioxin binding activities of polymorphic forms of mouse and human arylhydrocarbon receptors*. J Biol Chem, 1994. **269**(44): p. 27337-43.
36. Coumailleau, P., et al., *Definition of a minimal domain of the dioxin receptor that is associated with Hsp90 and maintains wild type ligand binding affinity and specificity*. J Biol Chem, 1995. **270**(42): p. 25291-300.
37. Ramadoss, P. and G.H. Perdew, *Use of 2-azido-3-[125I]iodo-7,8-dibromodibenzo-p-dioxin as a probe to determine the relative ligand affinity of human versus mouse aryl hydrocarbon receptor in cultured cells*. Mol Pharmacol, 2004. **66**(1): p. 129-36.
38. Jiang, T., *Characterisation of Recombinant Aryl Hydrocarbon Receptor Ligand Binding Domain*, Ph.D. thesis. 2004, Nottingham University. p. 206.
39. Chan, W.K., et al., *Baculovirus expression of the Ah receptor and Ah receptor nuclear translocator. Evidence for additional dioxin responsive element-binding species and factors required for signaling*. J Biol Chem, 1994. **269**(42): p. 26464-71.
40. Waller, C.L. and J.D. McKinney, *Three-dimensional quantitative structure-activity relationships of dioxins and dioxin-like compounds: model validation and Ah receptor characterization*. Chem Res Toxicol, 1995. **8**(6): p. 847-58.
41. Gasiewicz, T.A., et al., *Analysis of structural requirements for Ah receptor antagonist activity: ellipticines, flavones, and related compounds*. Biochem Pharmacol, 1996. **52**(11): p. 1787-803.
42. Denison, M.S. and S.R. Nagy, *Activation of the aryl hydrocarbon receptor by structurally diverse exogenous and endogenous chemicals*. Annu Rev Pharmacol Toxicol, 2003. **43**: p. 309-34.
43. Perdew, G.H. and A. Poland, *Purification of the Ah receptor from C57BL/6J mouse liver*. J Biol Chem, 1988. **263**(20): p. 9848-52.
44. Ma, Q. and J.P. Whitlock, Jr., *A novel cytoplasmic protein that interacts with the Ah receptor, contains tetratricopeptide repeat motifs, and augments the transcriptional response to 2,3,7,8-tetrachlorodibenzo-p-dioxin*. J Biol Chem, 1997. **272**(14): p. 8878-84.
45. Kuzhandaivelu, N., et al., *XAP2, a novel hepatitis B virus X-associated protein that inhibits X transactivation*. Nucleic Acids Res, 1996. **24**(23): p. 4741-50.
46. Meyer, B.K., et al., *Hepatitis B virus X-associated protein 2 is a subunit of the unliganded aryl hydrocarbon receptor core complex and exhibits transcriptional enhancer activity*. Mol Cell Biol, 1998. **18**(2): p. 978-88.
47. Carver, L.A. and C.A. Bradfield, *Ligand-dependent interaction of the aryl hydrocarbon receptor with a novel immunophilin homolog in vivo*. J Biol Chem, 1997. **272**(17): p. 11452-6.

48. Kazlauskas, A., L. Poellinger, and I. Pongratz, *Evidence that the co-chaperone p23 regulates ligand responsiveness of the dioxin (Aryl hydrocarbon) receptor*. J Biol Chem, 1999. **274**(19): p. 13519-24.
49. Whitelaw, M.L., et al., *Heat shock protein hsp90 regulates dioxin receptor function in vivo*. Proc Natl Acad Sci U S A, 1995. **92**(10): p. 4437-41.
50. Bell, D.R. and A. Poland, *Binding of aryl hydrocarbon receptor (AhR) to AhR-interacting protein. The role of hsp90*. J Biol Chem, 2000. **275**(46): p. 36407-14.
51. Petrulis, J.R., et al., *The hsp90 Co-chaperone XAP2 alters importin beta recognition of the bipartite nuclear localization signal of the Ah receptor and represses transcriptional activity*. J Biol Chem, 2003. **278**(4): p. 2677-85.
52. Hoffman, E.C., et al., *Cloning of a factor required for activity of the Ah (dioxin) receptor*. Science, 1991. **252**(5008): p. 954-8.
53. Rowlands, J.C. and J.A. Gustafsson, *Aryl hydrocarbon receptor-mediated signal transduction*. Crit Rev Toxicol, 1997. **27**(2): p. 109-34.
54. Antonsson, C., et al., *Constitutive function of the basic helix-loop-helix/PAS factor Arnt. Regulation of target promoters via the E box motif*. J Biol Chem, 1995. **270**(23): p. 13968-72.
55. Jiang, B.H., et al., *Dimerization, DNA binding, and transactivation properties of hypoxia-inducible factor 1*. J Biol Chem, 1996. **271**(30): p. 17771-8.
56. Korkalainen, M., J. Tuomisto, and R. Pohjanvirta, *Identification of novel splice variants of ARNT and ARNT2 in the rat*. Biochem Biophys Res Commun, 2003. **303**(4): p. 1095-100.
57. Maltepe, E., et al., *Abnormal angiogenesis and responses to glucose and oxygen deprivation in mice lacking the protein ARNT*. Nature, 1997. **386**(6623): p. 403-7.
58. Safe, S., *Polychlorinated biphenyls (PCBs), dibenzo-p-dioxins (PCDDs), dibenzofurans (PCDFs), and related compounds: environmental and mechanistic considerations which support the development of toxic equivalency factors (TEFs)*. Crit Rev Toxicol, 1990. **21**(1): p. 51-88.
59. Poland, A. and J.C. Knutson, *2,3,7,8-tetrachlorodibenzo-p-dioxin and related halogenated aromatic hydrocarbons: examination of the mechanism of toxicity*. Annu Rev Pharmacol Toxicol, 1982. **22**: p. 517-54.
60. Henck, J.M., et al., *2,3,7,8-tetrachlorodibenzo-p-dioxin: acute oral toxicity in hamsters*. Toxicol Appl Pharmacol, 1981. **59**(2): p. 405-7.
61. Vinopal, J.H. and J.E. Casida, *Metabolic stability of 2, 3, 7, 8-tetrachlorodibenzo-P-dioxin in mammalian liver microsomal systems and in living mice*. Arch Environ Contam Toxicol, 1973. **1**(2): p. 122-32.
62. Geyer, H.J., et al., *The relevance of fat content in toxicity of lipophilic chemicals to terrestrial animals with special reference to dieldrin and 2,3,7,8-tetrachlorodibenzo-p-dioxin (TCDD)*. Ecotoxicol Environ Saf, 1993. **26**(1): p. 45-60.
63. Poland, A., W.F. Greenlee, and A.S. Kende, *Studies on the mechanism of action of the chlorinated dibenzo-p-dioxins and related compounds*. Ann N Y Acad Sci, 1979. **320**: p. 214-30.
64. IARC, *Polychlorinated Dibenzo-para-dioxins and Polychlorinated Dibenzofurans*. IARC Monographs on the Evaluation of Carcinogenic Risk of Chemicals to

- Humans. Lyon, France: International agency for reserach on Cancer., 1997. **69**: p. 666pp.
65. Taylor, J.S., et al., *Chloracne from manufacture of a new herbicide*. Arch Dermatol, 1977. **113**(5): p. 616-9.
66. Poland, A., et al., *3,4,3',4'-Tetrachloro azoxybenzene and azobenzene: potent inducers of aryl hydrocarbon hydroxylase*. Science, 1976. **194**(4265): p. 627-30.
67. Okey, A.B. and L.M. Vella, *Binding of 3-methylcholanthrene and 2,3,7,8-tetrachlorodibenzo-p-dioxin to a common Ah receptor site in mouse and rat hepatic cytosols*. Eur J Biochem, 1982. **127**(1): p. 39-47.
68. Schmidt, J.V. and C.A. Bradfield, *Ah receptor signaling pathways*. Annu Rev Cell Dev Biol, 1996. **12**: p. 55-89.
69. Ciolino, H.P., P.J. Daschner, and G.C. Yeh, *Dietary flavonols quercetin and kaempferol are ligands of the aryl hydrocarbon receptor that affect CYP1A1 transcription differentially*. Biochem J, 1999. **340** (Pt 3): p. 715-22.
70. Ashida, H., et al., *Flavones and flavonols at dietary levels inhibit a transformation of aryl hydrocarbon receptor induced by dioxin*. FEBS Lett, 2000. **476**(3): p. 213-7.
71. Gillner, M., et al., *Interactions of indolo[3,2-b]carbazoles and related polycyclic aromatic hydrocarbons with specific binding sites for 2,3,7,8-tetrachlorodibenzo-p-dioxin in rat liver*. Mol Pharmacol, 1993. **44**(2): p. 336-45.
72. Wattenberg, L.W. and W.D. Loub, *Inhibition of polycyclic aromatic hydrocarbon-induced neoplasia by naturally occurring indoles*. Cancer Res, 1978. **38**(5): p. 1410-3.
73. Adachi, J., et al., *Indirubin and indigo are potent aryl hydrocarbon receptor ligands present in human urine*. J Biol Chem, 2001. **276**(34): p. 31475-8.
74. Wei, Y.D., et al., *Rapid and transient induction of CYP1A1 gene expression in human cells by the tryptophan photoproduct 6-formylindolo[3,2-b]carbazole*. Chem Biol Interact, 1998. **110**(1-2): p. 39-55.
75. Phelan, D., et al., *Activation of the Ah receptor signal transduction pathway by bilirubin and biliverdin*. Arch Biochem Biophys, 1998. **357**(1): p. 155-63.
76. Schaldach, C.M., J. Riby, and L.F. Bjeldanes, *Lipoxin A4: a new class of ligand for the Ah receptor*. Biochemistry, 1999. **38**(23): p. 7594-600.
77. Pollenz, R.S., C.A. Sattler, and A. Poland, *The aryl hydrocarbon receptor and aryl hydrocarbon receptor nuclear translocator protein show distinct subcellular localizations in Hepa 1c1c7 cells by immunofluorescence microscopy*. Mol Pharmacol, 1994. **45**(3): p. 428-38.
78. Denison, M.S. and E.F. Yao, *Characterization of the interaction of transformed rat hepatic cytosolic Ah receptor with a dioxin responsive transcriptional enhancer*. Arch Biochem Biophys, 1991. **284**(1): p. 158-66.
79. Reyes, H., S. Reisz-Porszasz, and O. Hankinson, *Identification of the Ah receptor nuclear translocator protein (Arnt) as a component of the DNA binding form of the Ah receptor*. Science, 1992. **256**(5060): p. 1193-5.
80. Whitlock, J.P., Jr., *Genetic and molecular aspects of 2,3,7,8-tetrachlorodibenzo-p-dioxin action*. Annu Rev Pharmacol Toxicol, 1990. **30**: p. 251-77.
81. Whitlock, J.P., Jr., *Mechanistic aspects of dioxin action*. Chem Res Toxicol, 1993. **6**(6): p. 754-63.

82. Probst, M.R., et al., *Role of the aryl hydrocarbon receptor nuclear translocator protein in aryl hydrocarbon (dioxin) receptor action*. Mol Pharmacol, 1993. **44**(3): p. 511-8.
83. Berghard, A., et al., *Cross-coupling of signal transduction pathways: the dioxin receptor mediates induction of cytochrome P-450IA1 expression via a protein kinase C-dependent mechanism*. Mol Cell Biol, 1993. **13**(1): p. 677-89.
84. Liu, S., et al., *Aryl hydrocarbon receptor agonists directly activate estrogen receptor alpha in MCF-7 breast cancer cells*. Biol Chem, 2006. **387**(9): p. 1209-13.
85. Matthews, J., et al., *Aryl hydrocarbon receptor-mediated transcription: ligand-dependent recruitment of estrogen receptor alpha to 2,3,7,8-tetrachlorodibenzo-p-dioxin-responsive promoters*. Mol Cell Biol, 2005. **25**(13): p. 5317-28.
86. Durrin, L.K. and J.P. Whitlock, Jr., *2,3,7,8-Tetrachlorodibenzo-p-dioxin-inducible aryl hydrocarbon receptor-mediated change in CYP1A1 chromatin structure occurs independently of transcription*. Mol Cell Biol, 1989. **9**(12): p. 5733-7.
87. Paranjape, S.M., R.T. Kamakaka, and J.T. Kadonaga, *Role of chromatin structure in the regulation of transcription by RNA polymerase II*. Annu Rev Biochem, 1994. **63**: p. 265-97.
88. Wu, L. and J.P. Whitlock, Jr., *Mechanism of dioxin action: Ah receptor-mediated increase in promoter accessibility in vivo*. Proc Natl Acad Sci U S A, 1992. **89**(11): p. 4811-5.
89. Nebert, D.W., et al., *Role of the aromatic hydrocarbon receptor and [Ah] gene battery in the oxidative stress response, cell cycle control, and apoptosis*. Biochem Pharmacol, 2000. **59**(1): p. 65-85.
90. Whitlock, J.P., Jr., *Induction of cytochrome P450IA1*. Annu Rev Pharmacol Toxicol, 1999. **39**: p. 103-25.
91. Kolluri, S.K., et al., *p27(Kip1) induction and inhibition of proliferation by the intracellular Ah receptor in developing thymus and hepatoma cells*. Genes Dev, 1999. **13**(13): p. 1742-53.
92. Kolluri, S.K., et al., *Novel target genes of the Ah (dioxin) receptor: transcriptional induction of N-myristoyltransferase 2*. Cancer Res, 2001. **61**(23): p. 8534-9.
93. Sogawa, K., et al., *A novel induction mechanism of the rat CYP1A2 gene mediated by Ah receptor-Arnt heterodimer*. Biochem Biophys Res Commun, 2004. **318**(3): p. 746-55.
94. McDougal, A., C. Wilson, and S. Safe, *Inhibition of 7,12-dimethylbenz[a]anthracene-induced rat mammary tumor growth by aryl hydrocarbon receptor agonists*. Cancer Lett, 1997. **120**(1): p. 53-63.
95. Blank, J.A., et al., *alpha-Naphthoflavone antagonism of 2,3,7,8-tetrachlorodibenzo-p-dioxin-induced murine lymphocyte ethoxyresorufin-O-deethylase activity and immunosuppression*. Mol Pharmacol, 1987. **32**(1): p. 169-72.
96. Astroff, B., et al., *6-Methyl-1,3,8-trichlorodibenzofuran as a 2,3,7,8-tetrachlorodibenzo-p-dioxin antagonist: inhibition of the induction of rat cytochrome P-450 isozymes and related monooxygenase activities*. Mol Pharmacol, 1988. **33**(2): p. 231-6.
97. Merchant, M., et al., *Mechanism of action of aryl hydrocarbon receptor antagonists: inhibition of 2,3,7,8-tetrachlorodibenzo-p-dioxin-induced CYP1A1 gene expression*. Arch Biochem Biophys, 1992. **298**(2): p. 389-94.

98. Biegel, L., et al., *2,2',4,4',5,5'-hexachlorobiphenyl as a 2,3,7,8-tetrachlorodibenzo-p-dioxin antagonist in C57BL/6J mice*. Toxicol Appl Pharmacol, 1989. **97**(3): p. 561-71.
99. Lu, Y.F., et al., *Identification of 3'-methoxy-4'-nitroflavone as a pure aryl hydrocarbon (Ah) receptor antagonist and evidence for more than one form of the nuclear Ah receptor in MCF-7 human breast cancer cells*. Arch Biochem Biophys, 1995. **316**(1): p. 470-7.
100. Ma, Q. and J.P. Whitlock, Jr., *The aromatic hydrocarbon receptor modulates the Hepa 1c1c7 cell cycle and differentiated state independently of dioxin*. Mol Cell Biol, 1996. **16**(5): p. 2144-50.
101. Backlund, M., et al., *Signal transduction-mediated activation of the aryl hydrocarbon receptor in rat hepatoma H4IIE cells*. J Biol Chem, 1997. **272**(50): p. 31755-63.
102. Ma, Q. and K.T. Baldwin, *2,3,7,8-tetrachlorodibenzo-p-dioxin-induced degradation of aryl hydrocarbon receptor (AhR) by the ubiquitin-proteasome pathway. Role of the transcription activator and DNA binding of AhR*. J Biol Chem, 2000. **275**(12): p. 8432-8.
103. Pollenz, R.S., *The mechanism of AH receptor protein down-regulation (degradation) and its impact on AH receptor-mediated gene regulation*. Chem Biol Interact, 2002. **141**(1-2): p. 41-61.
104. Mimura, J., et al., *Identification of a novel mechanism of regulation of Ah (dioxin) receptor function*. Genes Dev, 1999. **13**(1): p. 20-5.
105. Kociba, R.J., et al., *Results of a two-year chronic toxicity and oncogenicity study of 2,3,7,8-tetrachlorodibenzo-p-dioxin in rats*. Toxicol Appl Pharmacol, 1978. **46**(2): p. 279-303.
106. Safe, S., *Molecular biology of the Ah receptor and its role in carcinogenesis*. Toxicol Lett, 2001. **120**(1-3): p. 1-7.
107. Safe, S. and M. Wormke, *Inhibitory aryl hydrocarbon receptor-estrogen receptor alpha cross-talk and mechanisms of action*. Chem Res Toxicol, 2003. **16**(7): p. 807-16.
108. Brunnberg, S., et al., *The basic helix-loop-helix-PAS protein ARNT functions as a potent coactivator of estrogen receptor-dependent transcription*. Proc Natl Acad Sci U S A, 2003. **100**(11): p. 6517-22.
109. Gradin, K., et al., *Functional interference between hypoxia and dioxin signal transduction pathways: competition for recruitment of the Arnt transcription factor*. Mol Cell Biol, 1996. **16**(10): p. 5221-31.
110. Nguyen, T.A., et al., *Interactions of nuclear receptor coactivator/corepressor proteins with the aryl hydrocarbon receptor complex*. Arch Biochem Biophys, 1999. **367**(2): p. 250-7.
111. Denison, M.S. and S. Heath-Pagliuso, *The Ah receptor: a regulator of the biochemical and toxicological actions of structurally diverse chemicals*. Bull Environ Contam Toxicol, 1998. **61**(5): p. 557-68.
112. Safe, S.H., *Modulation of gene expression and endocrine response pathways by 2,3,7,8-tetrachlorodibenzo-p-dioxin and related compounds*. Pharmacol Ther, 1995. **67**(2): p. 247-81.
113. Andersson, P., et al., *A constitutively active dioxin/aryl hydrocarbon receptor induces stomach tumors*. Proc Natl Acad Sci U S A, 2002. **99**(15): p. 9990-5.

114. Pitot, H.C., et al., *Quantitative evaluation of the promotion by 2,3,7,8-tetrachlorodibenzo-p-dioxin of hepatocarcinogenesis from diethylnitrosamine*. Cancer Res, 1980. **40**(10): p. 3616-20.
115. Huff, J.E., et al., *Long-term hazards of polychlorinated dibenzodioxins and polychlorinated dibenzofurans*. Environ Health Perspect, 1980. **36**: p. 221-40.
116. Bunger, M.K., et al., *Resistance to 2,3,7,8-tetrachlorodibenzo-p-dioxin toxicity and abnormal liver development in mice carrying a mutation in the nuclear localization sequence of the aryl hydrocarbon receptor*. J Biol Chem, 2003. **278**(20): p. 17767-74.
117. Lahvis, G.P., et al., *Portosystemic shunting and persistent fetal vascular structures in aryl hydrocarbon receptor-deficient mice*. Proc Natl Acad Sci U S A, 2000. **97**(19): p. 10442-7.
118. Lin, T.M., et al., *Role of the aryl hydrocarbon receptor in the development of control and 2,3,7,8-tetrachlorodibenzo-p-dioxin-exposed male mice*. J Toxicol Environ Health A, 2001. **64**(4): p. 327-42.
119. Walisser, J.A., et al., *Gestational exposure of Ahr and Arnt hypomorphs to dioxin rescues vascular development*. Proc Natl Acad Sci U S A, 2004. **101**(47): p. 16677-82.
120. Yoshimoto, Y., et al., *Patent ductus venosus in children: a case report and review of the literature*. J Pediatr Surg, 2004. **39**(1): p. E1-5.
121. Safe, S., et al., *Ah receptor agonists as endocrine disruptors: antiestrogenic activity and mechanisms*. Toxicol Lett, 1998. **102-103**: p. 343-7.
122. Safe, S., C. Qin, and A. McDougal, *Development of selective aryl hydrocarbon receptor modulators for treatment of breast cancer*. Expert Opin Investig Drugs, 1999. **8**(9): p. 1385-96.
123. Chen, I., S. Safe, and L. Bjeldanes, *Indole-3-carbinol and diindolylmethane as aryl hydrocarbon (Ah) receptor agonists and antagonists in T47D human breast cancer cells*. Biochem Pharmacol, 1996. **51**(8): p. 1069-76.
124. Chen, I., et al., *Aryl hydrocarbon receptor-mediated antiestrogenic and antitumorigenic activity of diindolylmethane*. Carcinogenesis, 1998. **19**(9): p. 1631-9.
125. Hasler, J.A., et al., *Pharmacogenetics of cytochromes P450*. Mol Aspects Med, 1999. **20**(1-2): p. 12-24, 25-137.
126. Hutchinson, I., et al., *Antitumor benzothiazoles. 14. Synthesis and in vitro biological properties of fluorinated 2-(4-aminophenyl)benzothiazoles*. J Med Chem, 2001. **44**(9): p. 1446-55.
127. Hutchinson, I., et al., *Antitumor benzothiazoles. 16. Synthesis and pharmaceutical properties of antitumor 2-(4-aminophenyl)benzothiazole amino acid prodrugs*. J Med Chem, 2002. **45**(3): p. 744-7.
128. Shi, D.F., et al., *Antitumor benzothiazoles. 3. Synthesis of 2-(4-aminophenyl)benzothiazoles and evaluation of their activities against breast cancer cell lines in vitro and in vivo*. J Med Chem, 1996. **39**(17): p. 3375-84.
129. Bradshaw, T.D., et al., *Influence of 2-(4-aminophenyl)benzothiazoles on growth of human ovarian carcinoma cells in vitro and in vivo*. Br J Cancer, 1998. **78**(4): p. 421-9.
130. Bradshaw, T.D., et al., *Preclinical evaluation of amino acid prodrugs of novel antitumor 2-(4-amino-3-methylphenyl)benzothiazoles*. Mol Cancer Ther, 2002. **1**(4): p. 239-46.

131. Okey, A.B., *Enzyme induction in the cytochrome P-450 system*. Pharmacol Ther, 1990. **45**(2): p. 241-98.
132. Lewis, D.F., *Evolution of P450 superfamily in: guide to cytochrome P450 structure and function*. 2001: p. 39-39.
133. Mimura, J. and Y. Fujii-Kuriyama, *Functional role of AhR in the expression of toxic effects by TCDD*. Biochim Biophys Acta, 2003. **1619**(3): p. 263-8.
134. Gonzalez, F.J. and P. Fernandez-Salguero, *The aryl hydrocarbon receptor: studies using the AHR-null mice*. Drug Metab Dispos, 1998. **26**(12): p. 1194-8.
135. Gonzalez, F.J. and S. Kimura, *Study of P450 function using gene knockout and transgenic mice*. Arch Biochem Biophys, 2003. **409**(1): p. 153-8.
136. Lewis, D.F., *Quantitative structure-activity relationships in substrates, inducers, and inhibitors of cytochrome P4501 (CYP1)*. Drug Metab Rev, 1997. **29**(3): p. 589-650.
137. Lewis, D.F., *Structural characteristics of human P450s involved in drug metabolism: QSARs and lipophilicity profiles*. Toxicology, 2000. **144**(1-3): p. 197-203.
138. DFV, L., *Substrate selectivity and metabolism in: guide to cytochromes P450 structure and function*. . 2001: p. 110-110.
139. Stevens, M.F., et al., *Structural studies on bioactive compounds. 23. Synthesis of polyhydroxylated 2-phenylbenzothiazoles and a comparison of their cytotoxicities and pharmacological properties with genistein and quercetin*. J Med Chem, 1994. **37**(11): p. 1689-95.
140. Kashiyama, E., et al., *Antitumor benzothiazoles. 8. Synthesis, metabolic formation, and biological properties of the C- and N-oxidation products of antitumor 2-(4-aminophenyl)benzothiazoles*. J Med Chem, 1999. **42**(20): p. 4172-84.
141. Chua, M.S., et al., *Role of Cyp1A1 in modulation of antitumor properties of the novel agent 2-(4-amino-3-methylphenyl)benzothiazole (DF 203, NSC 674495) in human breast cancer cells*. Cancer Res, 2000. **60**(18): p. 5196-203.
142. Spink, D.C., et al., *Differential expression of CYP1A1 and CYP1B1 in human breast epithelial cells and breast tumor cells*. Carcinogenesis, 1998. **19**(2): p. 291-8.
143. Krishnan, V., et al., *Molecular mechanism of inhibition of estrogen-induced cathepsin D gene expression by 2,3,7,8-tetrachlorodibenzo-p-dioxin (TCDD) in MCF-7 cells*. Mol Cell Biol, 1995. **15**(12): p. 6710-9.
144. Trapani, V., et al., *DNA damage and cell cycle arrest induced by 2-(4-amino-3-methylphenyl)-5-fluorobenzothiazole (5F 203, NSC 703786) is attenuated in aryl hydrocarbon receptor deficient MCF-7 cells*. Br J Cancer, 2003. **88**(4): p. 599-605.
145. Bradshaw, T.D. and A.D. Westwell, *The development of the antitumour benzothiazole prodrug, Phortress, as a clinical candidate*. Curr Med Chem, 2004. **11**(8): p. 1009-21.
146. Leong, C.O., et al., *Antitumour 2-(4-aminophenyl)benzothiazoles generate DNA adducts in sensitive tumour cells in vitro and in vivo*. Br J Cancer, 2003. **88**(3): p. 470-7.
147. Chua, M.S., et al., *Antitumor benzothiazoles. 7. Synthesis of 2-(4-acylaminophenyl)benzothiazoles and investigations into the role of acetylation in the antitumor activities of the parent amines*. J Med Chem, 1999. **42**(3): p. 381-92.
148. Bradshaw, T.D., et al., *Mechanisms of acquired resistance to 2-(4-aminophenyl)benzothiazole (CJM 126, NSC 34445)*. Br J Cancer, 2000. **83**(2): p. 270-7.

149. Brantley, E., et al., *The antitumor drug candidate 2-(4-amino-3-methylphenyl)-5-fluorobenzothiazole induces NF-kappaB activity in drug-sensitive MCF-7 cells*. *Anticancer Drugs*, 2005. **16**(2): p. 137-43.
150. Monks, A., et al., *Genotoxic profiling of MCF-7 breast cancer cell line elucidates gene expression modifications underlying toxicity of the anticancer drug 2-(4-amino-3-methylphenyl)-5-fluorobenzothiazole*. *Mol Pharmacol*, 2003. **63**(3): p. 766-72.
151. Mortimer, C.G., et al., *Antitumor benzothiazoles. 26.(1) 2-(3,4-dimethoxyphenyl)-5-fluorobenzothiazole (GW 610, NSC 721648), a simple fluorinated 2-arylbenzothiazole, shows potent and selective inhibitory activity against lung, colon, and breast cancer cell lines*. *J Med Chem*, 2006. **49**(1): p. 179-85.
152. Abbott, P.A., et al., *Fused mesoionic heterocycles: synthesis of [1,2,3]triazolo[1,5-a]quinoline, [1,2,3]triazolo[1,5-a]quinazoline, [1,2,3]triazolo[1,5-a]quinoxaline and [1,2,3]triazolo[5,1-c]benzotriazine derivatives*. *Tetrahedron*, 2002. **58**: p. 3185-3198.
153. Bell, D.R., et al., *Relationships between tissue levels of 2,3,7,8-tetrachlorodibenzo-p-dioxin (TCDD), mRNAs, and toxicity in the developing male Wistar(Han) rat*. *Toxicol Sci*, 2007. **99**(2): p. 591-604.
154. Schwetz, B.A., et al., *Toxicology of chlorinated dibenzo-p-dioxins*. *Environ Health Perspect*, 1973. **5**: p. 87-99.
155. Bradford, M.M., *A rapid and sensitive method for the quantitation of microgram quantities of protein utilizing the principle of protein-dye binding*. *Anal Biochem*, 1976. **72**: p. 248-54.
156. Bradfield, C.A., A.S. Kende, and A. Poland, *Kinetic and equilibrium studies of Ah receptor-ligand binding: use of [125I]2-iodo-7,8-dibromodibenzo-p-dioxin*. *Mol Pharmacol*, 1988. **34**(2): p. 229-37.
157. Abbott, B.D., G.H. Perdew, and L.S. Birnbaum, *Ah receptor in embryonic mouse palate and effects of TCDD on receptor expression*. *Toxicol Appl Pharmacol*, 1994. **126**(1): p. 16-25.
158. Okey, A.B., et al., *Regulatory gene product of the Ah locus. Characterization of the cytosolic inducer-receptor complex and evidence for its nuclear translocation*. *J Biol Chem*, 1979. **254**(22): p. 11636-48.
159. Bandiera, S., et al., *Competitive binding to the cytosolic 2,3,7,8-tetrachlorodibenzo-p-dioxin receptor. Effects of structure on the affinities of substituted halogenated biphenyls--a QSAR analysis*. *Biochem Pharmacol*, 1983. **32**(24): p. 3803-13.
160. Hulme, E.C. and N.J.M. Birdsall, *Strategy and tactics in receptor-binding studies in: Receptor-ligand interactions, A practical approach*. Oxford: Oxford University Press, 1992. p.117-117.
161. Cheng, Y. and W.H. Prusoff, *Relationship between the inhibition constant (K_i) and the concentration of inhibitor which causes 50 per cent inhibition (I₅₀) of an enzymatic reaction*. *Biochem Pharmacol*, 1973. **22**(23): p. 3099-108.
162. Pfaffl, M.W., *A new mathematical model for relative quantification in real-time RT-PCR*. *Nucleic Acids Res*, 2001. **29**(9): p. e45.
163. Horwitz, S.B. and M.S. Horwitz, *Effects of camptothecin on the breakage and repair of DNA during the cell cycle*. *Cancer Res*, 1973. **33**(11): p. 2834-6.

164. Bradfield, C.A. and A. Poland, *A competitive binding assay for 2,3,7,8-tetrachlorodibenzo-p-dioxin and related ligands of the Ah receptor*. Mol Pharmacol, 1988. **34**(5): p. 682-8.
165. Hulme, E.C. and N.J.M. Birdsall, *Strategy and tactics in receptor-binding studies in: Receptor-ligand interactions, A practical approach*. Oxford: Oxford University Press, 1992. p.166-166.
166. Weiland, G.A. and P.B. Molinoff, *Quantitative analysis of drug-receptor interactions: I. Determination of kinetic and equilibrium properties*. Life Sci, 1981. **29**(4): p. 313-30.
167. Bickel, M.H. and S. Muehlebach, *Pharmacokinetics and ecodisposition of polyhalogenated hydrocarbons: aspects and concepts*. Drug Metab Rev, 1980. **11**(2): p. 149-90.
168. Manchester, D.K., et al., *Ah receptor in human placenta: stabilization by molybdate and characterization of binding of 2,3,7,8-tetrachlorodibenzo-p-dioxin, 3-methylcholanthrene, and benzo(a)pyrene*. Cancer Res, 1987. **47**(18): p. 4861-8.
169. Denison, M.S., *Heterogeneity of rat hepatic Ah receptor: identification of two receptor forms which differ in their biochemical properties*. J Biochem Toxicol, 1992. **7**(4): p. 249-56.
170. Farrell, K. and S. Safe, *Absence of positive co-operativity in the binding of 2,3,7,8-tetrachlorodibenzo-p-dioxin to its cytosolic receptor protein*. Biochem J, 1987. **244**(3): p. 539-46.
171. Owens, I.S. and D.W. Nebert, *Aryl hydrocarbon hydroxylase induction in mammalian liver-derived cell cultures. Effects of various metabolic inhibitors on the enzyme activity in hepatoma cells*. Biochem Pharmacol, 1976. **25**(7): p. 805-13.
172. Kocarek, T.A., E.G. Schuetz, and P.S. Guzelian, *Transient induction of cytochrome P450 1A1 mRNA by culture medium component in primary cultures of adult rat hepatocytes*. In Vitro Cell Dev Biol, 1993. **29A**(1): p. 62-6.
173. Niwa, A., K. Kumaki, and D.W. Nebert, *Induction of Hydrocarbon Hydroxylase Activity in Various Cell Cultures by 2,3,7,8-tetrachlorodibenzo-p-dioxin*. Mol Pharmacol, 1975. **11**: p. 399-408.
174. Lai, K.P., et al., *Dioxin-like components in human breast milk collected from Hong Kong and Guangzhou*. Environ Res, 2004. **96**(1): p. 88-94.
175. Lai, K.P., M.H. Wong, and C.K. Wong, *Modulation of AhR-mediated CYP1A1 mRNA and EROD activities by 17beta-estradiol and dexamethasone in TCDD-induced H4IIE cells*. Toxicol Sci, 2004. **78**(1): p. 41-9.
176. Zeiger, M., et al., *Inducing effects of dioxin-like polychlorinated biphenyls on CYP1A in the human hepatoblastoma cell line HepG2, the rat hepatoma cell line H4IIE, and rat primary hepatocytes: comparison of relative potencies*. Toxicol Sci, 2001. **63**(1): p. 65-73.
177. Houser, W.H., A. Raha, and M. Vickers, *Induction of CYP1A1 gene expression in H4-II-E rat hepatoma cells by benzo[e]pyrene*. Mol Carcinog, 1992. **5**(3): p. 232-7.
178. Zabel, T.R., R. Pollenz, and R.E. Peterson, *Relative Potencies Of Individual Polychlorinated Dibenzo-p-dioxin, Dibenzofuran, and Biphenyl Congeners and Congeners Mixtures Based On Induction Of Cytochrome 0451A mRNA In A Rainbow Trout Gonadal Cell Line (RTG-2)*. Environmental Toxicology and Chemistry, 1996. **15**(12): p. 2310-2318.

179. Owens, I.S. and D.W. Nebert, *Aryl hydrocarbon hydroxylase induction in mammalian liver-derived cell cultures. Stimulation of "cytochrome P1-450-associated" enzyme activity by many inducing compounds*. Mol Pharmacol, 1975. **11**(1): p. 94-104.
180. Riddick, D.S., et al., *2,3,7,8-Tetrachlorodibenzo-p-dioxin versus 3-methylcholanthrene: comparative studies of Ah receptor binding, transformation, and induction of CYP1A1*. J Biol Chem, 1994. **269**(16): p. 12118-28.
181. Poland, A. and E. Glover, *Comparison of 2,3,7,8-tetrachlorodibenzo-p-dioxin, a potent inducer of aryl hydrocarbon hydroxylase, with 3-methylcholanthrene*. Mol Pharmacol, 1974. **10**(2): p. 349-59.
182. Brantley, E., et al., *Fluorinated 2-(4-amino-3-methylphenyl)benzothiazoles induce CYP1A1 expression, become metabolized, and bind to macromolecules in sensitive human cancer cells*. Drug Metab Dispos, 2004. **32**(12): p. 1392-401.
183. Peters, A.K., et al., *Effects of polybrominated diphenyl ethers on basal and TCDD-induced ethoxyresorufin activity and cytochrome P450-1A1 expression in MCF-7, HepG2, and H4IIE cells*. Toxicol Sci, 2004. **82**(2): p. 488-96.
184. Vamvakas, A., J. Keller, and M. Dufresne, *In vitro induction of CYP1A1-associated activities in human and rodent cell lines by commercial and tissue-extracted halogenated aromatic hydrocarbons*. Environ. Toxicol. Chem, 1996. **15**: p. 814-823.
185. Sawyer, T. and S. Safe, *PCB isomers and congeners: induction of aryl hydrocarbon hydroxylase and ethoxyresorufin O-deethylase enzyme activities in rat hepatoma cells*. Toxicol Lett, 1982. **13**(1-2): p. 87-93.
186. Okey, A.B., et al., *Temperature-dependent cytosol-to-nucleus translocation of the Ah receptor for 2,3,7,8-tetrachlorodibenzo-p-dioxin in continuous cell culture lines*. J Biol Chem, 1980. **255**(23): p. 11415-22.
187. Schmitz, H.J., et al., *Potency of mixtures of polychlorinated biphenyls as inducers of dioxin receptor-regulated CYP1A activity in rat hepatocytes and H4IIE cells*. Toxicology, 1995. **99**(1-2): p. 47-54.
188. Kim, S.H., et al., *Novel compound 2-methyl-2H-pyrazole-3-carboxylic acid (2-methyl-4-o-tolylazo-phenyl)-amide (CH-223191) prevents 2,3,7,8-TCDD-induced toxicity by antagonizing the aryl hydrocarbon receptor*. Mol Pharmacol, 2006. **69**(6): p. 1871-8.
189. Brantley, E., et al., *Metabolism and subcellular binding of novel fluorinated 2-(4-amino-3-methylphenyl)benzothiazoles in human cancer cells*. Proc Am Assoc Cancer Res, 2001. **42**: p. 325.
190. Ohtake, F., et al., *Modulation of oestrogen receptor signalling by association with the activated dioxin receptor*. Nature, 2003. **423**(6939): p. 545-50.
191. Wang, W., R. Smith, 3rd, and S. Safe, *Aryl hydrocarbon receptor-mediated antiestrogenicity in MCF-7 cells: modulation of hormone-induced cell cycle enzymes*. Arch Biochem Biophys, 1998. **356**(2): p. 239-48.
192. Knutson, J.C. and A. Poland, *2,3,7,8-Tetrachlorodibenzo-p-dioxin: failure to demonstrate toxicity in twenty-three cultured cell types*. Toxicol Appl Pharmacol, 1980. **54**(3): p. 377-83.
193. Okey, A.B., L.M. Vella, and P.A. Harper, *Detection and characterization of a low affinity form of cytosolic Ah receptor in livers of mice nonresponsive to induction of cytochrome P1-450 by 3-methylcholanthrene*. Mol Pharmacol, 1989. **35**(6): p. 823-30.

194. Daujat, M., et al., *Omeprazole, an inducer of human CYP1A1 and 1A2, is not a ligand for the Ah receptor*. Biochem Biophys Res Commun, 1992. **188**(2): p. 820-5.
195. Karenlampi, S.O., et al., *2-(4'-chlorophenyl)benzothiazole is a potent inducer of cytochrome P450IA1 in a human and a mouse cell line. Anomalous correlation between protein and mRNA induction*. Eur J Biochem, 1989. **181**(1): p. 143-8.
196. Fried, K.W., et al., *Relationship between aryl hydrocarbon receptor-affinity and the induction of EROD activity by 2,3,7,8-tetrachlorinated phenothiazine and derivatives*. Toxicol Appl Pharmacol, 2007. **224**(2): p. 147-55.
197. Denomme, M.A., et al., *Effects of substituents on the cytosolic receptor-binding avidities and aryl hydrocarbon hydroxylase induction potencies of 7-substituted 2,3-dichlorodibenzo-p-dioxins. A quantitative structure-activity relationship analysis*. Mol Pharmacol, 1985. **27**(6): p. 656-61.
198. Beger, R.D., D.A. Buzatu, and J.G. Wilkes, *Combining NMR spectral and structural data to form models of polychlorinated dibenzodioxins, dibenzofurans, and biphenyls binding to the AhR*. J Comput Aided Mol Des, 2002. **16**(10): p. 727-40.
199. Romkes, M., et al., *Quantitative structure-activity relationships: analysis of interactions of 2,3,7,8-tetrachlorodibenzo-p-dioxin and 2-substituted analogues with rat, mouse, guinea pig, and hamster cytosolic receptor*. Cancer Res, 1987. **47**(19): p. 5108-11.
200. Staskal, D.F., et al., *Inhibition of human and rat CYP1A2 by TCDD and dioxin-like chemicals*. Toxicol Sci, 2005. **84**(2): p. 225-31.
201. Petrulis, J.R. and N.J. Bunce, *Competitive inhibition by inducer as a confounding factor in the use of the ethoxyresorufin-O-deethylase (EROD) assay to estimate exposure to dioxin-like compounds*. Toxicol Lett, 1999. **105**(3): p. 251-60.
202. Chen, G. and N.J. Bunce, *Polybrominated diphenyl ethers as Ah receptor agonists and antagonists*. Toxicol Sci, 2003. **76**(2): p. 310-20.
203. Silkworth, J.B., et al., *Comparison of TCDD and PCB CYP1A induction sensitivities in fresh hepatocytes from human donors, sprague-dawley rats, and rhesus monkeys and HepG2 cells*. Toxicol Sci, 2005. **87**(2): p. 508-19.
204. Livak, K.J. and T.D. Schmittgen, *Analysis of relative gene expression data using real-time quantitative PCR and the 2(-Delta Delta C(T)) Method*. Methods, 2001. **25**(4): p. 402-8.
205. Pohjanvirta, R., et al., *Evaluation of various housekeeping genes for their applicability for normalization of mRNA expression in dioxin-treated rats*. Chem Biol Interact, 2006. **160**(2): p. 134-49.
206. Schmittgen, T.D. and B.A. Zakrajsek, *Effect of experimental treatment on housekeeping gene expression: validation by real-time, quantitative RT-PCR*. J Biochem Biophys Methods, 2000. **46**(1-2): p. 69-81.
207. Vandesompele, J., et al., *Accurate normalization of real-time quantitative RT-PCR data by geometric averaging of multiple internal control genes*. Genome Biol, 2002. **3**(7): p. RESEARCH0034.
208. Helferich, W.G. and M.S. Denison, *Ultraviolet photoproducts of tryptophan can act as dioxin agonists*. Mol Pharmacol, 1991. **40**(5): p. 674-8.

209. Hockley, S.L., et al., *AHR- and DNA-damage-mediated gene expression responses induced by benzo(a)pyrene in human cell lines*. Chem Res Toxicol, 2007. **20**(12): p. 1797-810.
210. Jenkinson, D., et al., *International union of Pharmacology Comittee on Receptor Nomenclature and Drug Classification. IX. Recommendations on Terms and Symbols in Quantitative Pharmacology*. Pharmacological Reviews, 1995. **42**(2): p. 255-266.
211. Liu, H., et al., *6-substituted 3,4-benzocoumarins: a new structural class of inducers and inhibitors of CYP1A1-dependent activity*. Arch Biochem Biophys, 1993. **306**(1): p. 223-31.
212. Davis, D. and S. Safe, *Immunosuppressive activities of polychlorinated biphenyls in C57BL/6N mice: structure-activity relationships as Ah receptor agonists and partial antagonists*. Toxicology, 1990. **63**(1): p. 97-111.
213. Suh, J., et al., *Antagonism of aryl hydrocarbon receptor-dependent induction of CYP1A1 and inhibition of IgM expression by di-ortho-substituted polychlorinated biphenyls*. Toxicol Appl Pharmacol, 2003. **187**(1): p. 11-21.
214. Chen, G. and N.J. Bunce, *Interaction between halogenated aromatic compounds in the Ah receptor signal transduction pathway*. Environ Toxicol, 2004. **19**(5): p. 480-9.
215. Gasiewicz, T.A. and G. Rucci, *Alpha-naphthoflavone acts as an antagonist of 2,3,7, 8-tetrachlorodibenzo-p-dioxin by forming an inactive complex with the Ah receptor*. Mol Pharmacol, 1991. **40**(5): p. 607-12.
216. Harris, M., et al., *Partial antagonism of 2,3,7,8-tetrachlorodibenzo-p-dioxin-mediated induction of aryl hydrocarbon hydroxylase by 6-methyl-1,3,8-trichlorodibenzofuran: mechanistic studies*. Mol Pharmacol, 1989. **35**(5): p. 729-35.
217. Hestermann, E.V., J.J. Stegeman, and M.E. Hahn, *Relative contributions of affinity and intrinsic efficacy to aryl hydrocarbon receptor ligand potency*. Toxicol Appl Pharmacol, 2000. **168**(2): p. 160-72.
218. Merchant, M., V. Krishnan, and S. Safe, *Mechanism of action of alpha-naphthoflavone as an Ah receptor antagonist in MCF-7 human breast cancer cells*. Toxicol Appl Pharmacol, 1993. **120**(2): p. 179-85.
219. Safe, S., *Limitations of the toxic equivalency factor approach for risk assessment of TCDD and related compounds*. Teratog, Carcinog, and Mutag, 1998. **17**: p. 285-304.
220. Henry, E.C. and T.A. Gasiewicz, *Agonist but not antagonist ligands induce conformational change in the mouse aryl hydrocarbon receptor as detected by partial proteolysis*. Mol Pharmacol, 2003. **63**(2): p. 392-400.
221. Allan, G.F., et al., *Hormone and antihormone induce distinct conformational changes which are central to steroid receptor activation*. J Biol Chem, 1992. **267**(27): p. 19513-20.
222. Henry, E.C., et al., *Flavone antagonists bind competitively with 2,3,7, 8-tetrachlorodibenzo-p-dioxin (TCDD) to the aryl hydrocarbon receptor but inhibit nuclear uptake and transformation*. Mol Pharmacol, 1999. **55**(4): p. 716-25.
223. Nohara, K., et al., *Comparison of the 2,3,7,8-tetrachlorodibenzo-p-dioxin (TCDD)-induced CYP1A1 gene expression profile in lymphocytes from mice, rats, and humans: most potent induction in humans*. Toxicology, 2006. **225**(2-3): p. 204-13.

224. Tukey, R.H., et al., *The Ah locus: correlation of intranuclear appearance of inducer-receptor complex with induction of cytochrome P1-450 mRNA*. Cell, 1982. **31**(1): p. 275-84.
225. Harris, M., et al., *Structure-dependent induction of aryl hydrocarbon hydroxylase activity in C57BL/6 mice by 2,3,7,8-tetrachlorodibenzo-p-dioxin and related congeners: mechanistic studies*. Toxicol Appl Pharmacol, 1990. **105**(2): p. 243-53.
226. Zacharewski, T., M. Harris, and S. Safe, *Induction of cytochrome P450-dependent monooxygenase activities in rat hepatoma H-4-IIE cells in culture by 2,3,7,8-tetrachlorodibenzo-p-dioxin and related compounds: mechanistic studies using radiolabeled congeners*. Arch Biochem Biophys, 1989. **272**(2): p. 344-55.
227. Aarts, J.M., et al., *Species-specific antagonism of Ah receptor action by 2,2',5,5'-tetrachloro- and 2,2',3,3',4,4'-hexachlorobiphenyl*. Eur J Pharmacol, 1995. **293**(4): p. 463-74.
228. Henry, E.C. and T.A. Gasiewicz, *Molecular determinants of species-specific agonist and antagonist activity of a substituted flavone towards the aryl hydrocarbon receptor*. Arch Biochem Biophys, 2008.
229. Kikuchi, H., et al., *Differences in inducibility of CYP1A1-mRNA by benzimidazole compounds between human and mouse cells: evidences of a human-specific signal transduction pathway for CYP1A1 induction*. Arch Biochem Biophys, 1996. **334**(2): p. 235-40.
230. Okey, A.B., D.S. Riddick, and P.A. Harper, *The Ah receptor: mediator of the toxicity of 2,3,7,8-tetrachlorodibenzo-p-dioxin (TCDD) and related compounds*. Toxicol Lett, 1994. **70**(1): p. 1-22.
231. Bank, P.A., et al., *Species-specific binding of transformed Ah receptor to a dioxin responsive transcriptional enhancer*. Eur J Pharmacol, 1992. **228**(2-3): p. 85-94.
232. Wang, X., et al., *A comparison of the mouse versus human aryl hydrocarbon (Ah) receptor complex: effects of proteolysis*. Chem Biol Interact, 1992. **85**(1): p. 79-93.
233. Abel, J., et al., *Dose-response relationship of cytochrome P4501b1 mRNA induction by 2,3,7,8-tetrachlorodibenzo-p-dioxin in livers of C57BL/6J and DBA/2J mice*. Arch Toxicol, 1996. **70**(8): p. 510-3.
234. Poland, A. and E. Glover, *Characterization and strain distribution pattern of the murine Ah receptor specified by the Ahd and Ahb-3 alleles*. Mol Pharmacol, 1990. **38**(3): p. 306-12.
235. Harper, P.A., C.L. Golas, and A.B. Okey, *Characterization of the Ah receptor and aryl hydrocarbon hydroxylase induction by 2,3,7,8-tetrachlorodibenzo-p-dioxin and benz(a)anthracene in the human A431 squamous cell carcinoma line*. Cancer Res, 1988. **48**(9): p. 2388-95.
236. Lesca, P., et al., *The pig as a model for studying AH receptor and other PAH-binding proteins in man*. Biochem Biophys Res Commun, 1994. **200**(1): p. 475-81.
237. Yeh, G.C., et al., *Modulation of glucose-6-phosphate dehydrogenase activity and expression is associated with aryl hydrocarbon resistance in vitro*. J Biol Chem, 2001. **276**(37): p. 34708-13.
238. Lu, Y.F., et al., *Substituted flavones as aryl hydrocarbon (Ah) receptor agonists and antagonists*. Biochem Pharmacol, 1996. **51**(8): p. 1077-87.

239. Wiebel, F.J., U. Klose, and F. Kiefer, *Toxicity of 2,3,7,8-tetrachlorodibenzo-p-dioxin in vitro: H4IIEC3-derived 5L hepatoma cells as a model system*. Toxicol Lett, 1991. **55**(2): p. 161-9.
240. Safe, S., et al., *2,3,7,8-Tetrachlorodibenzo-p-dioxin (TCDD) and related compounds as antioestrogens: characterization and mechanism of action*. Pharmacol Toxicol, 1991. **69**(6): p. 400-9.
241. Suetsugi, M., et al., *Flavone and isoflavone phytoestrogens are agonists of estrogen-related receptors*. Mol Cancer Res, 2003. **1**(13): p. 981-91.
242. Schmitt, E., et al., *Hormonal and genotoxic activity of resveratrol*. Toxicol Lett, 2002. **136**(2): p. 133-42.
243. Haws, L.C., et al., *Development of a refined database of mammalian relative potency estimates for dioxin-like compounds*. Toxicol Sci, 2006. **89**(1): p. 4-30.
244. Kenakin, T., *Efficacy in: Pharmacologic analysis of drug-receptor interaction*. 1997. p. 291-292.
245. Gaddum, J., *The quantitative effects of antagonistic drugs*. J.Physiol., 1937. **89**: p. 7-9.
246. Kenakin, T., *Competitive antagonism in: Pharmacologic analysis of drug-receptor interaction*. Third edition. Philadelphia: Lippincott-Raven, 1997. p. 333-336.
247. Arunlakshana, O. and H.O. Schild, *Some quantitative uses of drug antagonists*. Br J Pharmacol Chemother, 1959. **14**(1): p. 48-58.
248. Bradshaw, T.D. and A.D. Westwell, *The development of the antitumour benzothiazole prodrug, Phortress, as a clinical candidate*. Curr Med Chem, 2004. **11**(8): p. 1009-21.
249. Reyes, H., S. Reisz-Porszasz, and O. Hankinson, *Identification of the Ah receptor nuclear translocator protein (Arnt) as a component of the DNA binding form of the Ah receptor*. Science, 1992. **256**(5060): p. 1193-5.
250. Bradshaw, T.D., et al., *In vitro evaluation of amino acid prodrugs of novel antitumour 2-(4-amino-3-methylphenyl)benzothiazoles*. Br J Cancer, 2002. **86**(8): p. 1348-54.
251. Carlstedt-Duke, J.M., *Tissue distribution of the receptor for 2,3,7,8-tetrachlorodibenzo-p-dioxin in the rat*. Cancer Res, 1979. **39**(8): p. 3172-6.
252. Fujii-Kuriyama, Y. and J. Mimura, *Molecular mechanisms of AhR functions in the regulation of cytochrome P450 genes*. Biochem Biophys Res Commun, 2005. **338**(1): p. 311-7.
253. Loaiza-Perez, A.I., Trapani, V., Hose, C., Singh, S.S., Trepel, J., Stevens, M.F.G., Bradshaw, T.D., and Sausville, E.A., *The AhR mediates sensitivity of MCF-7 breast cancer cells to the antitumor agent 2-(4-Amino-3-methylphenyl)benzothiazole*. Mol. Pharmacol, 2002. **61**: p. 13-19.
254. Fernandez-Salguero, P.M., et al., *Lesions of aryl-hydrocarbon receptor-deficient mice*. Vet Pathol, 1997. **34**(6): p. 605-14.
255. Heath-Pagliuso, S., et al., *Activation of the Ah receptor by tryptophan and tryptophan metabolites*. Biochemistry, 1998. **37**(33): p. 11508-15.
256. Barnes-Ellerbe, S., K.E. Knudsen, and A. Puga, *2,3,7,8-Tetrachlorodibenzo-p-dioxin blocks androgen-dependent cell proliferation of LNCaP cells through modulation of pRB phosphorylation*. Mol Pharmacol, 2004. **66**(3): p. 502-11.
257. Fernandez-Salguero, P.M., et al., *Aryl-hydrocarbon receptor-deficient mice are resistant to 2,3,7,8-tetrachlorodibenzo-p-dioxin-induced toxicity*. Toxicol Appl Pharmacol, 1996. **140**(1): p. 173-9.
258. Vanden Heuvel, J.P., et al., *Dioxin-responsive genes: examination of dose-response relationships using quantitative reverse transcriptase-polymerase chain reaction*. Cancer Res, 1994. **54**(1): p. 62-8.

259. de Medina, P., et al., *Synthesis and biological properties of new stilbene derivatives of resveratrol as new selective aryl hydrocarbon modulators*. J Med Chem, 2005. **48**(1): p. 287-91.
260. Pandini, A., et al., *Structural and functional characterization of the aryl hydrocarbon receptor ligand binding domain by homology modeling and mutational analysis*. Biochemistry, 2007. **46**(3): p. 696-708.
261. Hahn, M.E., et al., *Molecular evolution of two vertebrate aryl hydrocarbon (dioxin) receptors (AHR1 and AHR2) and the PAS family*. Proc Natl Acad Sci U S A, 1997. **94**(25): p. 13743-8.
262. Aiello, S., et al., *Synthesis and biological properties of benzothiazole, benzoxazole and benzpyranone analogs of the potent antitumor agent 2-(3,4-dimethoxyphenyl)-5-fluorobenzothiazole (PMX 610, NSC 721648)*. Manuscript submitted.
263. Trapani, V., *The development of Phortress: from molecule to mechanism*, Ph.D. thesis. 2002.
264. Kenakin, T., *Competitive antagonism in: Pharmacologic analysis of drug-receptor interaction*. Third edition. Philadelphia: Lippincott-Raven 1997. p. 336-336.
265. Lewis, D.F.V, *Introduction in: Guide to Cytochromes P450 : Structure and Function*. London: Taylor & Francis. 2001. p. 1-5.